

PHOTON SCIENCE 2023.

Highlights and Annual Report

Deutsches Elektronen-Synchrotron DESY
A Research Centre of the Helmholtz Association



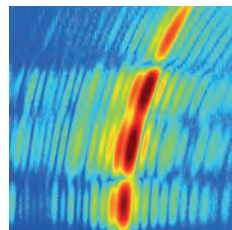


PHOTON SCIENCE 2023.

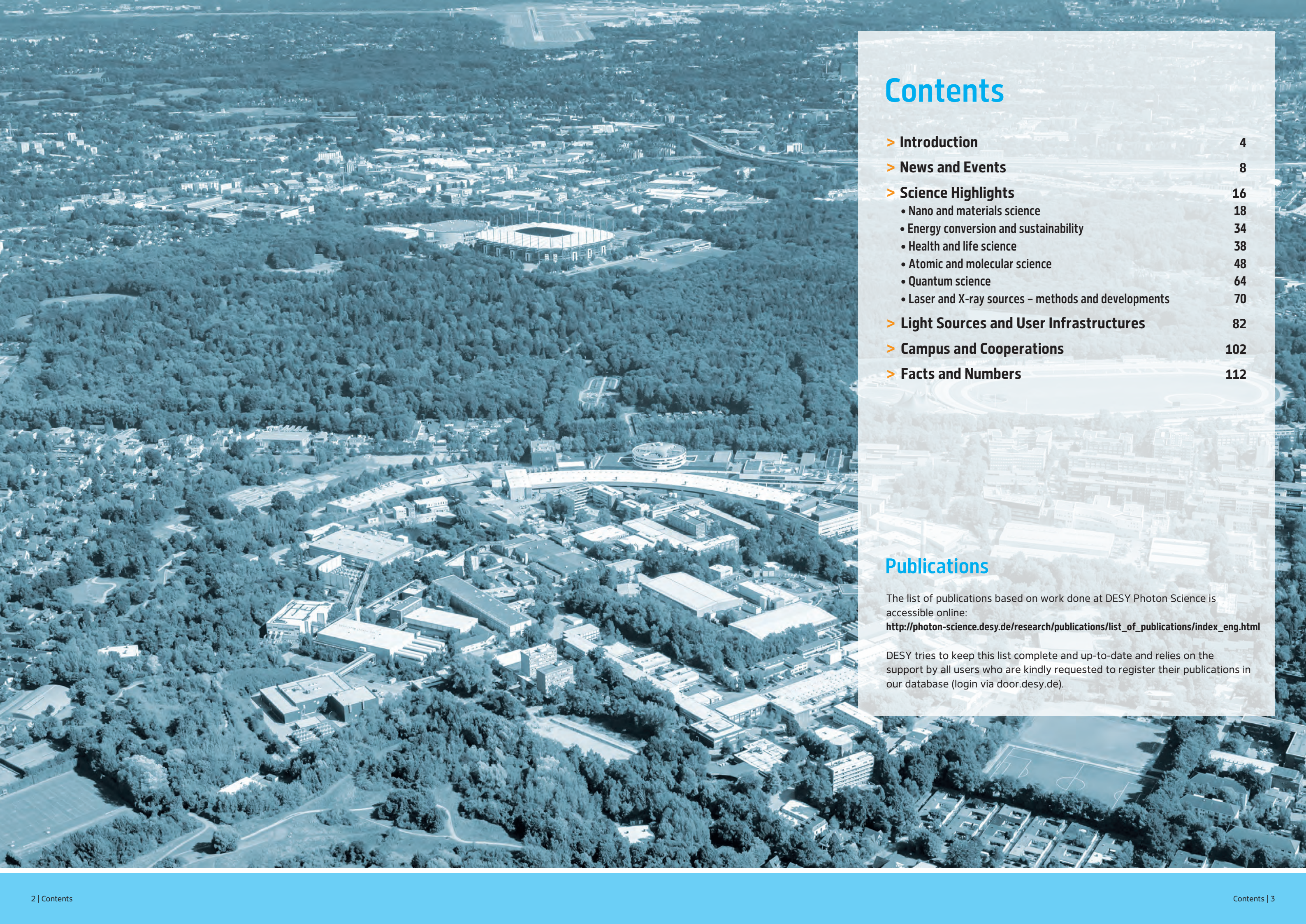
Highlights and Annual Report

Cover

The cover picture shows interference fringes observed in a single holographic scattering image used as a 3D nanoscale structural probe. The coherent X-ray surface imaging method allows, together with a sophisticated analysing tool, to visualise surface-supported and buried mesoscale structures, such as nano-electronics, quantum dots, and heterogeneous catalysts. Measured in reflection geometry, the method is sensitive to three-dimensional (3D) structures in only a single view (details see page 28).



(Original data measured at the PETRA III beamline P10)



Contents

> Introduction	4
> News and Events	8
> Science Highlights	16
• Nano and materials science	18
• Energy conversion and sustainability	34
• Health and life science	38
• Atomic and molecular science	48
• Quantum science	64
• Laser and X-ray sources – methods and developments	70
> Light Sources and User Infrastructures	82
> Campus and Cooperations	102
> Facts and Numbers	112

Publications

The list of publications based on work done at DESY Photon Science is accessible online:

http://photon-science.desy.de/research/publications/list_of_publications/index_eng.html

DESY tries to keep this list complete and up-to-date and relies on the support by all users who are kindly requested to register their publications in our database (login via door.desy.de).

The year 2023 at DESY

Chairman's foreword

Dear Colleagues and Friends of DESY,

The world is facing unprecedented challenges. The consequences of climate change are becoming increasingly evident in devastating extreme weather events. Even as the aftershocks of the SARS-COV-19 pandemic continue, we are still exposed to potential new viral and bacterial pathogens whose effects we do not know. Concurrently, the global community is shaken by geopolitical upheavals: Putin's horrifying war in Ukraine and the brutal terrorist attacks on Israel just to name a few. Now, more than ever, we must advocate for a sustainable and peaceful future, so that we do not leave a ruined world for future generations.

What role can a research centre like DESY play in contributing to a livable future in Germany, Europe and globally? How can DESY contribute to limit climate change and to preventative measures against future pandemics and other health issues. And how do we navigate international collaborations with partners from nations that challenge democratic values, such as China?

Preliminary answers to these questions can be found in our draft of the 'Strategy 2030-Loop'. Under the guiding principle 'The Decoding of Matter', DESY remains deeply

rooted in fundamental research. Our commitment as a national centre in the international CERN collaboration remains, and we continue to expand astroparticle physics. A significant move in this direction is the establishment of a German Center for Astrophysics (DZA) in the Lausitz – a political decision to which Christian Stegmann, director in charge of Astroparticle Physics at DESY, has made significant contributions. By 2024, decisions should be made regarding DESY's position within the DZA.

In recent months, we have vigorously advocated for the timely realisation of DESY's flagship project, PETRA IV. The conversion of PETRA III into a state-of-the-art 4th generation X-ray light source is essential to remain competitive worldwide. In particular, the U.S. and Asia are already heavily investing in similar research infrastructures. All the endeavors have received substantial local political backing from the Hamburg Parliament, which committed to funding 10% of the project's investment costs. This strong support continues at a national level: During the federal Budget Committee session on 16 November 2023, a decisive step was taken with the approval of 40 million Euro in seed funding for the project - highlighting the pivotal relevance of PETRA IV for future science.

Over the past months we have seen remarkable support from the high-tech and deep-tech industries. Our industrial dialogue partners recognise that they stand at the brink of profound transformation: Climate change solutions demand a shift towards sustainable materials and processes, while precision data emerges as the new currency in international competition. Those with the best databases will lead in AI-driven developments, be it in custom materials or pharmaceuticals. The current 4th generation synchrotron radiation facilities are globally recognised as vital for generating this invaluable pool of data.

The coming decade will be pivotal for our research centre. For DESY, it is crucial to ensure the swift implementation of PETRA IV and to further advance photon science, uphold DESY's leadership in plasma-based particle acceleration developments, expand new methods astroparticle physics and make a significant national contribution to the High-Luminosity Large Hadron Collider (HL-LHC) at CERN. Concurrently, we must ambitiously drive our vision of creating a dynamic research-innovation ecosystem with DESY in the core of the Science City Hamburg Bahrenfeld, incorporating innovative digital, and sustainable structures and processes.

Realising this master plan is in itself a monumental challenge. The current financial situation, with volatile energy and gas prices among other effects is leading to a rising inflation, poses significant difficulties for DESY's management. We face a new reality at DESY: Crafting a globally competitive research programme with diminishing resources, achievable only with stringent prioritisation.

The dramatic rise in the construction cost index in recent years has jeopardised several of our planned construction projects. However, we were able to successfully launch our visitor centre 'DESYUM' in Hamburg as the first major construction initiative. Fortunately, construction is progressing swiftly, making us hopeful of meeting all set milestones on time. Up next are the new accelerator centre 'CAST' which will also house the accelerator control room and the DESY Innovation Factory, a centre for start-ups. Ideally, we would like to implement these projects before PETRA IV's intensive construction phase.

DESY is held in high international regard in fundamental research. It is imperative to emphasise that our success would not be conceivable without talented researchers and engineers who consistently pioneer in developing new technologies. My special thanks therefore go to them and all DESY staff, our national and international users as well as partners for their dedicated work. This is also reflected in the numerous awards they have earned, I would like to highlight two from DESY team members here:

Franz Kärtner, founder of the deep-tech startup Cycle GmbH and professor at the Universität Hamburg, was honored by the UNIPRENEURS initiative in Berlin for his



Visualisation of the DESY visitor centre DESYUM, close to the main entrance on the DESY campus in Hamburg.

innovative entrepreneurial spirit. The UNIPRENEURS award is Germany's most prestigious recognition for outstanding engagement in scientific entrepreneurship.

The Bjørn H. Wiik Prize was awarded to DESY engineer Julien Branlard, for implementing the high-frequency control of the European XFEL. Without the system primarily developed by Branlard, stable operation of the superconducting linear accelerator would have been unattainable. His exceptional engineering achievements have gained international attention, further bolstering DESY's global reputation in accelerator development.

The crucial message: We must persistently strive to cultivate an attractive and innovative environment for the brightest minds globally or otherwise risk falling behind in the international competition – and this is not just about DESY. In challenging times, the ability to provide answers to difficult questions is needed more than ever, and this is precisely where the strength of fundamental science lies. The scientific results in this annual report are some good examples of what we can achieve when we work together for a better future!

*Yours
Helmut Dosch*

Helmut Dosch
Chairman of the DESY Board of Directors



DESY researcher Johannes Hagemann (left) shows the German Health Minister Karl Lauterbach (right) the experiments at the PETRA III beamline P06 together with Helmut Dosch (2nd from left), Science Senator Katharina Fegebank (middle), Gesa Miehe-Nordmeyer from the Federal Chancellery (2nd from right).

Photon Science at DESY

Introduction



The DESY site in Hamburg (September 2021).

Dear Colleagues and Friends of DESY Photon Science,

In a world of geopolitical turbulences that also severely influence the boundary conditions for the operation of our photon science facilities PETRA III and FLASH as well as our in-house research activities, we tried to make the best out of the present situation for our user services and research activities. The dramatic increase in electricity costs for the year 2023 could be mitigated thanks to the financial help of our funding bodies and measures implemented by the government to limit electricity costs. For this reason, we were able to fully operate our facilities the entire scheduled time in 2023. However, some consumables, such as He gas, were still in short supply or so expensive that we were forced to reduce consumption. Due to this shortage only 40% of the scheduled experiments that required He could be carried out in 2023. For the moment, the situation has slightly improved, and we also increased our efforts to recuperate lost He gas or to invest in closed-cycle cooling devices wherever possible. As far as it concerns electricity, DESY was able to secure its needs to a quite reasonable price at the stock exchange for 2024 and 2025. However,

the recent decision of the government to consolidate the federal 2024 budget will more than duplicate the grid transport cost for electricity, which will have a dramatic impact on the operation of our facilities. In addition, DESY as probably all academic and research organisations in Germany, suffers from inflation-related cost increases that are far higher than the annual increase in funding. On the longer term, this will result in a significant reduction in the service that we can provide and what we can achieve in science and technology.

Despite all these problems, the user operation at our photon science facilities was very successful in 2023. At PETRA III almost 4900 h user beamtime could be offered to the community with an availability well above 98%. In total, more than 7500 user visits were registered at PETRA III with the number of proposals still rising. Major activities towards providing new research capabilities are the 'HIKA' instrument installed and operated by KIT at P25 a new beamline for hierarchical X-ray imaging exploiting a number of contrast mechanism. At P25 a new beamline for instrument developments and industrial application is

being set up with the additional experimental techniques, fluorescence imaging and high-resolution powder diffraction. This beamline is being realised in close collaboration with the DESY's Innovation and Technology Transfer department (ITT). The design work to fill the last free undulator slot at PETRA III with a beamline dedicated to catalysis research is completed and ready to go for calls for tenders. This beamline is financed and will be operated by the FHI and the MPI for Chemical Energy Conversion. While some beamlines with standard experimental techniques at PETRA III are already highly automatised, this is not the case for more complex experiments like for *operando* studies as they are required for catalysis research. This is the main development target of the Helmholtz funded 'ROCK-IT' project which is carried out in collaboration with HZB, KIT and HZDR. For the year 2024 a rolling access scheme will be tested at five of the PETRA III beamlines. This scheme will allow to submit proposals at any time and, if successful, to obtain beamtime in a significantly shorter time than compared to the standard access mode.

Several important milestones have been achieved in 2023 within the PETRA IV project, DESY's main future project. The 'Technical Design Report' (TDR) proposal has been completed and the cost estimate was reviewed twice, first by internal experts not involved in the project and a second time by external experts from other large scale facility projects in Europe. Both reviews concluded that the PETRA IV cost review is robust and the methods applied are state-of-the-art. In 2024, work will continue towards an engineering design report with more detailed planning of the accelerator complex, the huge civil engineering tasks, and the beamlines and experimental stations. DESY together with the PETRA IV project team were very active with outreach and lobbying activities on all levels. We are very grateful to the Senate of the Free and Hanseatic City of Hamburg who decided to make its 10% share of the required external project funds available if the project is approved. There is also good news from the federal government: In its November meeting in 2023 the budget committee of the German Bundestag approved 40 M€ to continue the preparation of the PETRA IV project. Presently, we hope that the German Bundestag will follow this decision which will be extremely important to keep the momentum of the project.

User operation at FLASH was running very smoothly after the first phase of the FLASH2020+ project that was completed by end of 2022. The maximum electron energy of the FLASH linear accelerator reaches now 1.35 GeV and the newly installed laser heater allows a more stable free-

electron laser (FEL) operation. The preparation for the next phase of the upgrade scheduled for mid 2024 to mid 2025 is in full swing. During this shutdown the old fixed-gap undulators at FLASH1 will be replaced by APPLE III devices which will be tuneable in photon energy as well as in polarisation. In addition, external seeding will be implemented at FLASH1, which will lead to significantly higher spectral and temporal stability compared to the self-amplified spontaneous emission (SASE) FEL operation mode, thus enabling spectroscopic methods at the FEL that were previously not possible or only possible with lower temporal or spectral resolution. In order to increase the throughput for FEL experiments, a new operation mode will be tested in May 2024. The idea is to limit the FEL and pump laser parameters to a predefined range in order to drastically reduce setup and tuning times.

DESY scientists continue to carry out very successful experiments at the European XFEL, especially within the large user consortia SFX, HIBEF and hRIXS to which DESY is making major contributions.

The Centre for Molecular Water Science (CMWS) is an initiative to bring together scientists from all over Europe to study the peculiar properties of water from fundamental properties to all possible applications in science and technology. DESY plans together with the Helmholtz centres GFZ, Hereon, HZB and HZDR to submit a large-scale investment proposal to Helmholtz in order to establish a CMWS laboratory and office building close to the present Centre for X-ray and Nano Science (CXNS) building to foster these science activities and to provide space for outstations of collaboration partners as well as for dedicated instrumentation at the four other Helmholtz centres.

I would like to close by thanking all DESY staff, in particular all people at Photon Science, our advisory bodies and user community for their dedication and continuous support to keep the user operation at our facilities running and to carry out excellent research during these challenging times.

A handwritten signature in black ink, appearing to read 'E. Weckert', written in a cursive style.

Edgar Weckert
Director DESY Photon Science



News and Events

News and Events

A busy year 2023

January

16 January:
DESY becomes a member of the European consortium 'Laserlab Europe AISBL'

In January, DESY became a full member of the consortium Laserlab-Europe AISBL. Francesca Calegari, lead scientist for attosecond science at DESY and Professor at the Universität Hamburg, will represent DESY in the Laserlab-Europe General Assembly. AISBL is an international not-for-profit association, bringing together 46 leading laser research infrastructures in 22 European countries. Jointly, they are committed to coordinate operation and research and development efforts to facilitate the development of advanced lasers and laser-based technologies and to promote the efficient utilisation of advanced laser facilities by users from academia and industry. The majority of the members provide open access to their facilities to scientists from all over the world to perform experiments in a large variety of interdisciplinary research, covering advanced laser science and applications in most domains of research and technology.



27 January:
Great interest in the joint DESY and European XFEL Users' Meeting in Hamburg

'Finally meeting in person again!' This was one of the catchphrases on the DESY campus at this year's Users' Meeting after the meetings in the last two years had to take place in a purely virtual format due to the COVID-19 pandemic. For almost a week, more than 1100 researchers conducting research at the DESY light sources

FLASH and PETRA III or the European XFEL from over 25 countries exchanged views on the status and future of research at the Hamburg-area light sources. They met during numerous presentations, in 20 workshops and satellite meetings, at an industrial exhibition, in poster sessions and enjoyed many personal discussions.

31 January:
Meytal Landau wins EU grant to study amyloids

Structural biologist Meytal Landau has been awarded two million Euro to investigate microbial amyloid proteins. Amyloids are fibrous proteins that are of interest in various areas of medicine. Landau's ERC Consolidator Grant from the European Research Council (ERC) will last five years and will help to build a team at the Centre for Structural and Systems Biology (CSSB) on the DESY campus that will involve DESY, the Hamburg branch of the Euro-



pean Molecular Biology Laboratory (EMBL) and the University Hospital Hamburg-Eppendorf (UKE).

February

9 February:
An opportunity for students: DESY-Ukraine Winter School

22 students enrolled at Ukrainian universities worked on DESY research



projects for six weeks at the Hamburg and Zeuthen campuses. The projects enabled the students to interact with scientists and explore research areas that would be otherwise out of reach in the present situation. The students, some of whom were picked up from the Polish-Ukrainian border by DESY-organised bus transfer, arrived on campus on 31 January and stayed until 10 March.

21 February:
More than 120 scientists met for the CMWS DAYS 2023

More than 120 participants from 20 countries met online from 21-24 February for the CMWS DAYS 2023 to discuss the key challenges in molecular water research and the status and future perspectives of the Centre for Molecular Water Science (CMWS). The CMWS initiative brings together key experts to improve the

understanding of the fundamental questions about molecular processes in water and at water interfaces systematically. By now, 55 partners from different institutes around Europe and beyond have already expressed officially their interest in participating in and supporting the CMWS initiative.



March

19 March:
Start of the innovation platform HI-ACTS



The innovation platform 'Helmholtz Innovation Platform for Accelerator-Based Technologies & Solutions' HI-ACTS pursues the mission of making accelerator-based technologies specifically accessible for industrial and medical applications. HI-ACTS is jointly operated by DESY, as project coordinator, Helmholtz-Zentrum Dresden-Rossendorf (HZDR), Helmholtz-Zentrum Berlin (HZB), GSI Helmholtz Centre for Heavy Ion Research and Helmholtz-Zentrum Hereon. Accelerator technologies operated by the Helmholtz Association will be made available to industrial users in the form of a cost-effective full-service infrastructure. This means that existing research infrastructures, such as DESY's synchrotron radiation source PETRA III and its successor PETRA IV, will be more attractive for industrial users and applications.



March

27 March:
Marvin Edelmann receives the Georg-Simon-Ohm Prize 2023 from the DPG



The German Physical Society (DPG) awarded DESY PhD student Marvin Edelmann the Georg-Simon-Ohm Prize for his master thesis. With this prize, the DPG honours outstanding theses in physical engineering or related courses at universities of applied sciences. In his master thesis, done in the Ultrafast Optics and X-Rays group under the supervision of Prof. Franz Kärtner at DESY, Edelmann describes the development, the theoretical framework and the successful demonstration of three advanced and novel fiber optic technologies for pulse train generation with very low noise, approaching the fundamental constraints given by the quantum nature of light.

April

20 April:
11 million for life sciences: EU research network 'HALRIC' launched

The European Union is providing around 11 million Euro to fund the cooperation between German and southern Scandinavian research in the field of life sciences. The research network 'Hanseatic Life Science Research Infrastructure Consortium' (HALRIC) coordinates the use of unique large research facilities, such as MAX IV, DESY's PETRA III and the European XFEL, as well as other technologies to boost research and innovation. Up to 75 pilot collaborations between consortium members will be established for this purpose. The consortium is made up of universities, hospitals, research institutions, business clusters and regional governments from Germany, Sweden, Denmark and Norway, including the European Molecular Biology Laboratory, the Universität Hamburg, the University Medical Centre Hamburg-Eppendorf (UKE) and DESY.



May

10 May:
Noisy data, sharp images: Martin Burger intends to solve inverse problems at DESY



The Austrian Martin Burger is setting up the Computational Imaging group at DESY Photon Science, with which he hopes to improve the reconstruction and analysis of the scientific images recorded during the many experiments carried out at DESY and other research centres. Burger's team also forms a research unit of the Helmholtz Imaging Platform, which is operated by DESY together with the Helmholtz Centres DKFZ and MDC. Martin Burger is an expert in improving poor image data. He wants to turn noisy measurements into good pictures, obtaining as much valuable information as possible from them. Coming from the field of applied mathematics, he uses mathematical models and algorithms to facilitate the reconstruction of the images from the data.

June

16 June:
More than 100 participants at the Ultrafast X-ray Summer School

More than 100 participants from 18 countries have attended this year's Ultrafast X-ray Summer School UXSS 2023 at the Center for Free-Electron Laser Science CFEL. The five-day course allowed doctoral students and postdoctoral researchers to learn about the latest developments and opportunities in ultrafast X-ray sci-

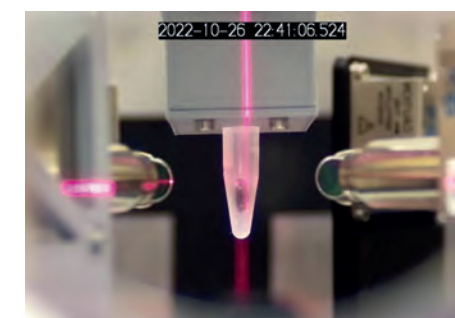
ence. Topics of the highly interdisciplinary program ranged from accelerator physics to molecular biology. In lectures by eight internationally renowned experts, the participants learned about the impact of the fast-developing ultrafast X-ray techniques on fields like structural biology, plasma physics and chemistry.



26 June:
Innovation Award awarded for breakthrough in X-ray fluorescence tracking for medical imaging

Florian Grüner, a professor at the Universität Hamburg and at the Center for Free-Electron Laser Science CFEL has been honoured for advancements in the field of *in situ* and *in vivo* tracking using advanced X-ray fluorescence imaging. His pioneering work paves the way for the precise tracking of active ingredients, immune cells, antibodies and drug carriers, enabling real-time assessment of biodistribution in the human body and providing invaluable insights for medical research. The key breakthrough achieved lies in the development of a synchrotron-based method that allows for the detection of the small-

est tumours or the tracking of drugs or cells in living organisms. This cutting-edge approach holds significant potential for pharmaceutical research, drug development and the study of biological effects of pollution with nano- or microplastics.



July

12 July:
Engjell Bebeti received the Otto-Stern Award for his master thesis

Engjell Bebeti has been honoured with the Universität Hamburg's Otto-Stern Award for his master thesis titled 'Mid-Infrared Light Phase Detection with Integrated Nanoantenna Networks', done at DESY in the Ultrafast Optics and X-Rays group under the supervision of Prof. Franz Kärtner and Felix Ritzkowsky.



20 July:
Return of the 'Summies': the summer student programme at DESY is back

The summer student program, which this year took place from 18 July to 7 September, included full-time work in established research groups, a lecture program on DESY research topics and visits to facilities operated by DESY. Some of the projects took place as well on the European XFEL campus in Schenefeld. Each of these projects gave the students in-depth hands-on experience with real-world scientific investigations, analysis, theory and experiment design, and provided networking opportunities.

September

6 September: Franz Kärtner Receives UNIPRENEURS Award

DESY researcher Franz Kärtner has been honoured by the UNIPRENEURS initiative for his entrepreneurial spirit. Kärtner heads the Ultrafast Laser and X-ray Physics group in the Center for Free-Electron Laser Science CFEL at DESY, is a professor at the Universität Hamburg and has founded a successful deep-tech start-up the Cycle GmbH. The UNIPRENEURS award is considered the highest recognition in Germany for outstanding commitment to entrepreneurship from within academia. Kärtner received the award for his developments in the field of ultra-precision synchronisation and the successful transfer of his research results into a company. Cycle GmbH develops precision time and frequency distribution systems based on femto-second lasers that help customers in science and industry to precisely control and synchronise large systems such as free-electron lasers, large ultrafast laser systems and radar telescopes.



28 September: Hamburg says yes to DESY's new X-ray light source PETRA IV

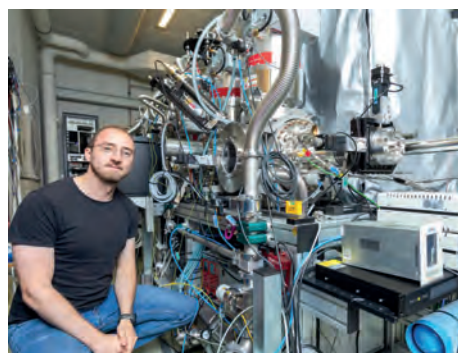
With PETRA IV, DESY is planning the most powerful X-ray light source in the world. It will revolutionise the view into the nanocosmos as well as X-ray analytics. The goal of PETRA IV is to drastically accelerate the development of new technologies – including for example new materials or drug development – by using the extremely

brilliant light to provide previously unattainable insights for scientific and technological applications. At the same time, PETRA IV will serve as a centrepiece and point of attraction in the emerging Science City Hamburg-Bahrenfeld. In its meeting on 27 September, the Hamburg City Parliament provided an important milestone for realising PETRA IV: The politicians unanimously decided that the City of Hamburg will secure its financing share of ten per cent of the total sum for the project. The total cost will be 1.54 billion Euro, to which DESY will contribute own funds of 170 million Euro.



29 September: New Humboldt Fellow at DESY and CFEL

Ivo Vinklárek works on a more detailed understanding of halogen reactions that take place in the atmosphere. Using the ultrafast imaging methods employed by Jochen Küpper's Controlled Molecule Imaging group at CFEL, he will examine small clusters that mimic short-lived agglomerations called 'collision complexes' that exist between the halogenated hydrocarbon, oxygen and water.



October

20 October: Nina Rohringer selected as APS Fellow



DESY researcher Nina Rohringer has been selected as a fellow of the American Physical Society (APS). The APS Division for Atomic, Molecular and Optical Physics (DAMOP) nominated Rohringer for her outstanding theoretical concepts in the new research area of nonlinear X-ray research and experiments at X-ray free-electron lasers. Nina Rohringer is a leading scientist at DESY and a professor at the Universität Hamburg. With her research group 'Theory of ultrafast X-ray physics' she studies the fundamental processes of the interactions of matter and ultrashort X-ray pulses of high intensity produced by free-electron lasers. This involves, e.g. the development of novel experiments at X-ray free-electron lasers as well as new types of X-ray lasers themselves.

November

2 November: Julien Branlard received the 2023 Bjørn H. Wiik Prize

Renowned for their stable, reliable and extremely precise operation, the linear accelerators European XFEL and FLASH owe their success especially to features developed by Julien Branlard and his team. For this reason, the French systems engineer was awarded this year's Bjørn H. Wiik Prize. Julien Branlard joined DESY in 2011. He moved from Fermilab (Chicago, USA) to Hamburg to work on the mega-project European XFEL and took over the low-level RF work package as team leader.



9 November: New study: DESY's light source PETRA III has created 2.25 billion Euro in added value

The study, carried out by the Fraunhofer Institute for Systems and Innovation Research, shows that DESY is not only a significant driver of scientific progress but it also has an economic impact as an employer and through the commissioning of commercial companies. Between 2010 and 2022, DESY invested some 815 million Euro in building and operating PETRA III. As a result, the research facility has produced unique scientific insights, provided essential data for innovative developments and had an economic impact far beyond the Hamburg region. Their added value amounts to more than 2.25 billion Euro.



13 November: Collaboration for the benefit of research and industry

From new imaging methods to new data formats and analyses, from screening of active agents to biomaterials: The potential that synchrotron radiation holds for applied research is enormous. Fraunhofer, DESY, Hereon and EMBL have agreed on a strategic partnership to utilise this more effectively in the future.

The aim is to establish structured collaboration between the four research institutions soon. Particular emphasis will be placed on the use of the analytical infrastructure at the DESY campus in Hamburg, for instance, the X-ray radiation source PETRA III but also the free electron lasers.



17 November: Groundbreaking decision for PETRA IV

In the meeting of the Budget Committee for the 2024 federal budget, the financing of an important preparatory project for the PETRA IV 3D X-ray microscope at DESY was decided. DESY will receive 40 million Euro as start-up financing for preparatory measures for the PETRA IV X-ray microscope including, in particular, the design and prototype of an innovative, energy-saving accelerator technology and the transformation of the business model.



Science Highlights

Nano and materials science

- > Breathing Nanoparticles 18
- > Pulling the 3D rabbit out of a 2D hat 20
- > New glass with supreme toughness 22
- > Rattling atoms in 'frozen' phase-change materials 24
- > First synthesis of the aromatic $[N_6]^{4-}$ hexazine ring 26
- > 3D view of interfacial structures in a single glance 28
- > Corrosion and catalytic reaction hand in hand 30
- > An X-ray step towards superfast nanoelectronics 32

Energy conversion and sustainability

- > Monitoring initial steps of water splitting using FLASH 34
- > Microscopic transformations of electrocatalyst surfaces 36

Health and life science

- > Darobactins: a very promising novel type of antibiotics 38
- > Effects of biodegradable implants on bone healing 40
- > To grab or not to grab? 42
- > New insights into mRNA nanoparticles 44
- > Titanium oxide for air and surface cleaning 46

Atomic and molecular science

- > A 40-year-old astrophysical riddle—literally resolved 48
- > X-rays illuminate the origin of life 50
- > Benchmarking fundamental light-matter interactions 52
- > Diamond rain and icy planets' magnetic field 54
- > 'Hot spots' of radiation damage formed around aqueous metal ions 56
- > Spatio-temporal scaling laws in a heated egg yolk 58
- > Charting the quantum landscape 60
- > Resonant X-ray excitation of the nuclear clock isomer ^{45}Sc 62

Quantum science

- > Creating chirality with nothing but light 64
- > Ultrafast tracking of an atomic-scale structural transformation 66
- > X-ray diffraction imaging of a single quantum dot 68

Laser and X-ray sources – methods and developments

- > Moulding ultrashort laser pulses 70
- > Smart data compression for the human mind 72
- > Beating the coherence time 74
- > Apochromatic X-ray lenses 76
- > Artificial intelligence for self-supervised tomographic image reconstruction 78
- > Imaging out of incoherence 80

Breathing Nanoparticles

X-ray movie of oscillating nanoparticles reveals fundamental processes of light-matter interaction

Light polarises the electron clouds of common materials. In case of metal nanoparticles, the mobile electrons experience a uniform oscillating field. This results in collective electron oscillations, quantised into quasiparticles called plasmons. The research area 'plasmon dynamics' studies the processes that happen after the driving field of light is gone. The energy stored in the plasmon is quickly transferred into highly excited electrons which are important for energy transformation, for example by photocatalysis. Their energy is dissipated by electron-electron scattering, and subsequent electron-phonon coupling excites lattice vibrations. In this process, breathing oscillations are initiated which are of special interest for applications employing nanoparticles as light concentrators and for fundamental solid-state dynamics.

These breathing oscillations are challenging to investigate experimentally due to the electron-originating contrast overshadowing other processes. The different stages of the plasmon decay are currently the subject of intense debate. Prime events are the generation of very energetic 'hot' electrons, that equilibrate their energy by electron-electron scattering into a 'warm' electron gas. This couples to the nanoparticle lattice. Recent studies suggested that the energy transfer from the warm electron gas to the nanoparticle is so efficient that the nanoparticle is heated extremely quickly [1]. In the process, the nanoparticle expands explosively, causing it to oscillate collectively, like a breathing sphere. However, direct experimental studies resolving the breathing-oscillation and its excitation mechanism

have been missing. The reported studies discuss the oscillation excitation based on periodic contrast modulations in optical experiments.

A more direct access is provided by small angle X-ray scattering which can resolve the nanoparticle size unperturbed by any electron influences. Furthermore, making use of the intense femtosecond X-ray pulses provided by X-ray free-electron lasers such as FLASH allows one to acquire scattering data in a pump-probe fashion, thus recording an X-ray movie of the nanoparticle dynamics, i.e. the nanoparticle's structural changes as a function of time. For this study, researchers from the Departments of Physics and Chemistry at Universität Hamburg and the Max Planck

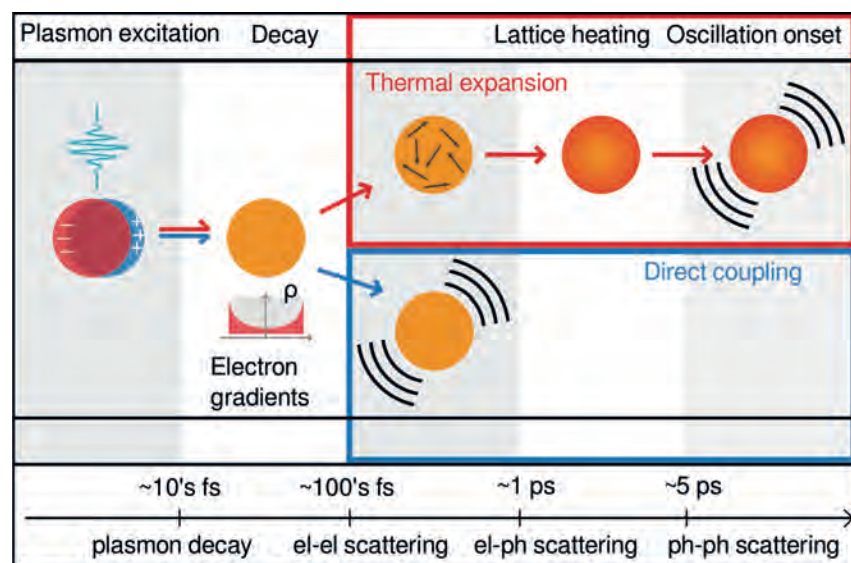
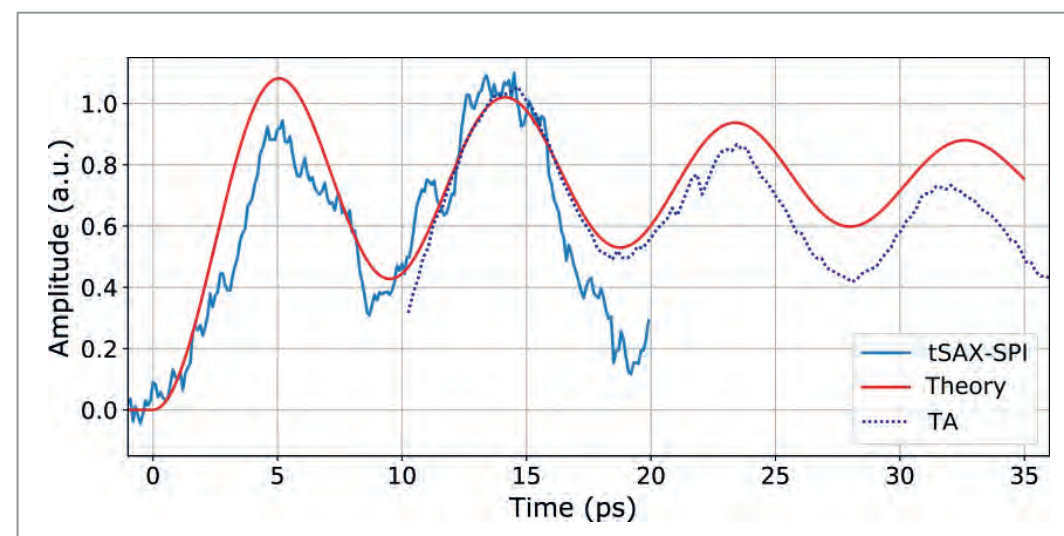


Figure 1
Scheme of the plasmon dynamics. The electron cloud is polarised periodically. Without optical excitation, plasmon damping leads to a decay into a few highly excited carriers within tenths of femtoseconds. In the established pictures these equilibrate by electron-electron scattering and dissipate their energy to the lattice, exciting breathing oscillations. In the new picture the electron density gradient directly couples to the breathing oscillations, resulting in an immediate onset.

Figure 2

Time-resolved breathing oscillation. The onset of the periodic nanoparticle size change cannot be resolved by time-resolved optical spectroscopy (transient absorption, TA) as it is overshadowed by contrast from excited electrons. Time-resolved single particle X-ray scattering (tSAX-SPI) gives a more direct access to the nanoparticle size and reveals an instant size expansion with optical excitation (at $t=0$). This effect can be explained within the new theory, including the direct coupling of the electron density to the oscillations.



Institute for the Structure and Dynamics of Matter (MPSD) conducted such an experiment at the CAMP end station of beamline BL1 at FLASH to directly resolve the onset of the breathing oscillations. Correlating the time-dependent size with the electron temperature obtained from optical spectroscopy, it was observed that the particles already expanded with the optical excitation pulse much faster than expected. In fact, by recording an X-ray movie of the lattice oscillations, a fundamentally new electron-lattice interaction mechanism was discovered.

To explain these findings, the researchers teamed up with the quantum electronics group at TU Berlin who set up a new parameter-free model. The microscopic description included all processes of the plasmon dynamics: the optical excitation, electron-electron, electron-phonon and phonon-phonon interaction. Imaged on the nanoparticle size as observable, the calculations result in a linear differential equation for the nanoparticle diameter expansion d :

$$\left(\frac{\partial^2}{\partial t^2} + 2\gamma \frac{\partial}{\partial t} - c\nabla^2\right) d(\mathbf{r}, t) = \xi(T) + \zeta \nabla \rho(\mathbf{r}, t).$$

The left-hand side of this clean equation corresponds to a damped harmonic oscillator. The right-hand side describes the sources of the breathing oscillation, namely the known thermal lattice expansion and a second source term, the spatial gradient of the electron density $\nabla \rho$. This density gradient is a direct result of the initial plasmon decay and couples immediately to the lattice without the need for electron-electron scattering (see Fig. 1). In fact, this new term is even dominant. Both sources combined, all experimental observations are well reproduced by the model (see Fig. 2). This new excitation term shows that the events of the plas-

mon decay are a lot more intertwined than assumed and that existing models on electron dynamics in metal nanoparticles must be questioned, with implications for photocatalysis [2] and other energy transformation applications. In addition, the confirmed microscopic model provides a fundamental access to the different aspects of the plasmon particle interaction and is already used in subsequent studies.

Author contact:

Holger Lange, holger.lange@uni-hamburg.de

References

- G. V. Hartland, 'Optical studies of dynamics in noble metal nanostructures', *Chem. Rev.* **111**, 3858-3887 (2011).
- U. Alam et al., 'Catalytic conversion of solar to chemical energy on plasmonic metal nanostructures', *Nature Catalysis* Vol 1, 656-665 (2018).

Original publication

'Time-Resolved Single-Particle X-ray Scattering Reveals Electron-Density Gradients As Coherent Plasmonic-Nanoparticle-Oscillation Source', *Nano Letters* **23**, 5943-5950 (2023).
DOI:10.1021/acs.nanolett.3c00920



Dominik Hoeing^{1,2}, Robert Salzwedel³, Lena Worbs^{4,5,6}, Yulong Zhuang⁷, Amit K. Samanta^{4,5}, Jannik Lübke^{1,4,5,6}, Armando D. Estillore^{4,5}, Karol Dlugolecki^{4,5}, Christopher Passow⁵, Benjamin Erk⁵, Nagitha Ekanayake⁵, Daniel Ramm⁵, Jonathan Correa⁵, Christina C. Papadopoulou⁵, Atia Tul Noor⁵, Florian Schulz⁵, Malte Selig³, Andreas Knorr³, Kartik Ayyer^{1,7}, Jochen Küpper^{1,4,5,6} and Holger Lange^{1,2}

- The Hamburg Centre for Ultrafast Imaging, Universität Hamburg, Hamburg, Germany
- Department of Chemistry, Universität Hamburg, Hamburg, Germany
- Institut für Theoretische Physik, Technische Universität Berlin, Berlin, Germany
- Center for Free-Electron Laser Science CFEL, Hamburg, Germany
- Deutsches Elektronen-Synchrotron DESY, Hamburg, Germany
- Department of Physics, Universität Hamburg, Hamburg, Germany
- Max Planck Institute for the Structure and Dynamics of Matter, Hamburg, Germany

Pulling the 3D rabbit out of a 2D hat

Ultrafast three-dimensional imaging of free-flying silver nanoclusters reveals secrets on their growth process

Assemblies of atoms or molecules in the nanometre size range, called nanoclusters, are of great scientific interest. Their peculiar and exotic properties, which often greatly differ from those of atoms and molecules on the one side and bulk matter on the other, have led to direct applications in catalysis, electronics and medicine. Nanoclusters tend to be fragile, and their behaviour is strongly affected by any interaction with the surrounding environment. Therefore, *in situ* characterisation, in particular structure determination, constitutes a great challenge. In a recent experiment, silver nanoclusters, freely flying in vacuum, were investigated at the FLASH free-electron laser using an innovative technique to obtain 3D 'snapshots' of the samples which unveiled their fascinating structures and the secrets behind their growth process.

Silver nanoclusters can be formed by aggregation in a cluster source. Here, single atoms are 'sputtered' from a solid target, start colliding and aggregating and then merge with other atoms or clusters while traveling in silver vapor to reach a size of tens of nanometres [1]. Investigating the final shapes of such clusters can reveal intriguing aspects about their formation process, in which energetic and kinetic aspects compete. The coherent soft X-ray pulses offered by FLASH are a unique tool to study such small and delicate systems in free flight and therefore to gain direct insight into the formation process [2].

Silver nanoclusters have been investigated at the CAMP end station of FLASH [3] with an imaging technique called Coherent Diffraction Imaging (CDI) [4], as exemplified in

Fig. 1a. The short-wavelength light beam is focused into a few-micrometre spot, where it interacts with and diffracts from the free-flying nanoparticles. The diffracted light forms a characteristic interference pattern that is recorded on a detector placed right after the interaction region. Due to the immense brightness of the light pulse, the sample is also highly ionised and quickly destroyed, leaving only the two-dimensional diffraction pattern as its legacy.

The pattern encodes information about the spatial distribution of the sample's electron density. This cannot be directly extracted but must be retrieved by means of suitable algorithms in the data analysis process. In typical CDI experiments, light is recorded only in a narrow range of scattering angles up to a few degrees. In such a condition,

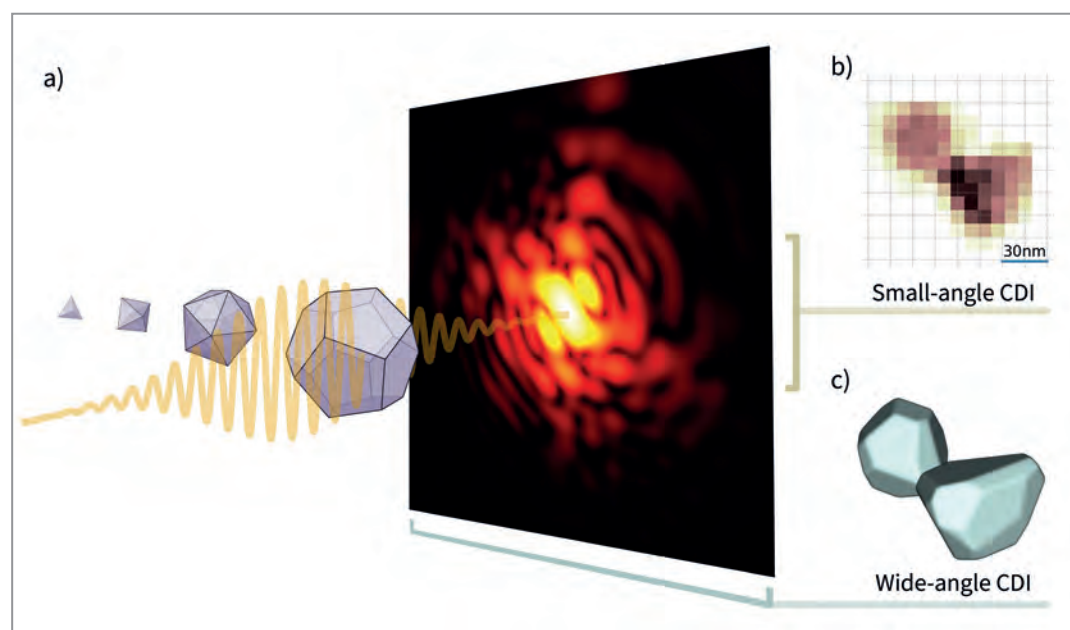


Figure 1

A typical Coherent Diffraction Imaging experiment. a) Individual samples, in this case silver nanostructures, are intercepted by the FEL light pulse. The diffraction pattern is then recorded by the scattering detector. b) A typical CDI experiment only records light at small-scattering angles which enables to reliably retrieve only a two-dimensional projection of the sample density. c) Three-dimensional reconstructions of the samples are instead successfully achieved exploiting the information provided by the diffracted light at wide scattering angles.

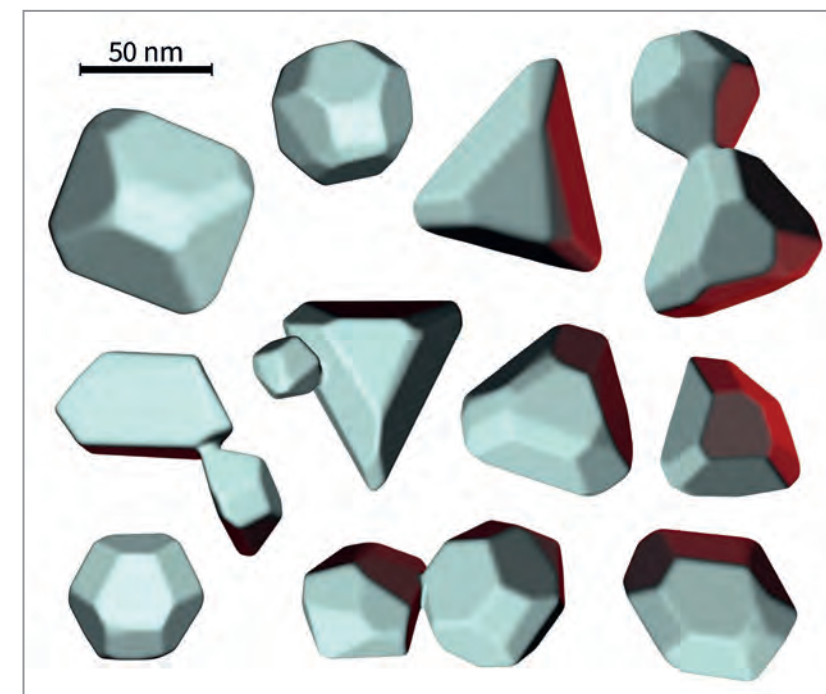


Figure 2

Examples of 3D reconstructions of individual and agglomerated silver nanoclusters. Regular architectures can be identified, as well as the presence of truncation at the tips and edges along with broken symmetries that arise from crystalline defects.

well established data analysis methods exist to recover the object, but the result is only a two-dimensional 'shadow' of the sample, or more accurately, a projection of its electron density as seen from the side of the incoming FEL pulse [4] (see Fig. 1b). For the present experiment, the light scattered by silver nanoclusters could be recorded up to a wider angle of more than 30°. In this regime, a single diffraction image also contains relevant information about the sample's depth, i.e. the direction along the incoming light. In principle, this provides access to the particle's overall three-dimensional structure [3]. However, reconstructing the three-dimensional shape of the nanocluster from a single two-dimensional scattering pattern is extremely challenging. So far, it had been an open question whether this could be done using a generic approach which is not strongly limited by crude and insufficient model shapes.

The data analysis process of this experiment thus required the development of an innovative algorithmic approach based on forward fitting to effectively retrieve the three-dimensional architecture of the silver nanoclusters, as shown in Fig. 1c. The reconstructions, some of which are shown in Fig. 2, reveal faceted shapes with unique features. Different structural motifs can be identified, from single and twinned tetrahedra to truncated octahedra and icosahedra. Even more, deviations from ideal polyhedral structures, faults such as truncated tips and edges and combinations of structural motifs and agglomerates were retrieved. Almost all these shapes are metastable, as they do not correspond to the lowest energy configurations, and they depend on the architecture of the seeds in the early stages of growth as well as the kinetics within the growth process.

This new and generic wide-angle forward fitting-based imaging approach can be extended to samples with other

morphological features. This promises new experimental possibilities by using the short light pulses of few tens of femtoseconds delivered by FLASH to get real three-dimensional movies of ultrafast light-induced dynamics at the nanoscale.

Author contact: [Alessandro Colombo](mailto:Alessandro.Colombo@phys.ethz.ch), alcolombo@phys.ethz.ch

References

1. Y. Huttel, ed., 'Gas-phase synthesis of nanoparticles', John Wiley & Sons, (2017).
2. I. Barke et al., 'The 3D-architecture of individual free silver nanoparticles captured by X-ray scattering', *Nat. Commun.* 6, 6187 (2015).
3. B. Erk et al., 'CAMP@FLASH: an end-station for imaging, electron and ion-spectroscopy, and pump-probe experiments at the FLASH free-electron laser' *J. Synchrotron Rad.* 25, 1529-1540 (2018).
4. H. N. Chapman and K. A. Nugent, 'Coherent lensless X-ray imaging', *Nat. Photonics* 4, 833-839 (2010).

Original publication

'Three-dimensional femtosecond snapshots of isolated faceted nanostructures', *Science Advances* 9, eade5839 (2023). DOI: 10.1126/sciadv.ade5839



Alessandro Colombo¹, Simon Dold², Patrice Kolb¹, Jakob Jordan³, Nils Bernhardt³, Patrick Behrens³, Jonathan Correa⁴, Stefan Düsterer⁴, Benjamin Erk⁴, Linos Hecht¹, Andrea Heilrath⁵, Robert Irsig⁵, Norman Iwe⁵, Björn Kruse⁵, Bruno Langbehn³, Bastian Manschwetus⁴, Franklin Martinez⁵, Karl-Heinz Meiwes-Broer⁵, Kevin Oldenburg⁵, Christopher Passow⁴, Christian Peltz⁵, Mario Sauppe⁴, Fabian Seel⁵, Rico Mayro P. Tanyag⁵, Rolf Treusch⁴, Anatoli Ulmer, Saida Walz³, Thomas Fennel⁵, Ingo Barke⁵, Thomas Möller⁵, Bernd von Issendorff⁶ and Daniela Rupp¹

1. Laboratory for Solid State Physics, ETH Zurich, Zurich, Switzerland
2. European XFEL, Schenefeld, Germany
3. Institute for Optics and Atomic Physics, Technical University Berlin, Berlin, Germany
4. Deutsches Elektronen-Synchrotron DESY, Hamburg, Germany
5. Institute of Physics, University of Rostock, Rostock, Germany
6. Department of Physics, University of Freiburg, Freiburg, Germany

New glass with supreme toughness

Atomic-level structure influences the boundary conditions for designing high damage-tolerant glass

Enhancing the toughness is important for the safe application of structural engineering materials, especially brittle glasses. The fracture toughness of widely commercialised glasses is less than $1.0 \text{ MPa m}^{1/2}$, limiting their applications. A well-controllable adjustment of the short-to-medium structures by paracrystallisation could be an efficient way to improve the toughness of glasses. Paracrystallisation in oxide glass was achieved by high-temperature and high-pressure annealing. These paracrystalline oxide glasses display superior toughness, reaching up to $1.99 \pm 0.06 \text{ MPa m}^{1/2}$, surpassing any other reported bulk oxide glasses.

Unlike crystalline materials, glasses are intrinsically brittle due to the absence of microstructures and a resultant lack of diverse microstructure-controlled toughening mechanisms, such as crack bridging and deflection [1,2]. Conventionally, the fracture toughness of glasses has been controlled by their chemical compositions. Multi-anion inorganic glasses (e.g. oxycarbonate, oxynitride and oxycarbonitride), into which anions of carbon or nitrogen are introduced, show ultrahigh fracture toughness (up to $1.79 \text{ MPa m}^{1/2}$). On the other hand, multi-cation oxide glasses (also known as high-entropy glasses (HEGs)) have a high

fracture toughness of $1.21\text{--}1.52 \text{ MPa m}^{1/2}$. To overcome the limitations of brittleness, considerable efforts have been devoted to design glass-based composites with nano- or microscale structures. However, this may cause the deterioration of other advantages (e.g. the transparency in oxide glasses). Furthermore, it has been shown that an enhanced degree of medium-range order (MRO) can increase the toughness and ductility of metallic glasses [3], thus providing insight into toughening glassy materials by tailoring the atomic packing order. Very recently, the discovery of the paracrystalline state of materials featuring

crystal-like MRO clusters or paracrystallites has provided a guideline to control the short-range order (SRO) to MRO structures of glasses [4].

Notably, the paracrystallites structurally resemble nuclei below the critical nucleation size during glass crystallisation. This enables us to obtain the paracrystalline state from glasses by trapping the incubation state with a high nucleation density during the initial stage of glass crystallisation. Since pressure promotes nucleation and inhibits grain growth, annealing glasses under high pressure is thus speculated to be promising for synthesising paracrystalline materials. In recent years, several studies have found that high-pressure and high-temperature (HPHT) annealing in oxide glasses can result in permanent densification accompanied by an increase in mechanical properties (e.g. elasticity, hardness and toughness) [5]. Nonetheless, densification-related structural changes and structure-property relationships remain ambiguous. Here, we report that the permanent densification by 15.7% in grossular glass by HPHT annealing treatments is contributing to the transition from amorphous to paracrystalline states. For our experiment we used high-energy X-ray diffraction to obtain the structure factors $S(Q)$ and pair distribution functions $g(r)$ of the samples, at P02.1, the powder diffraction and total scattering beamline, at PETRA III (DESY), showing that grossular glass underwent remarkable structural changes in the short and medium ranges by HPHT annealing. Furthermore, combinations of high-resolution transmission electron microscopy (HRTEM) and Raman spectra show solid evidences for the paracrystalline nature of the high-density grossular glass after HPHT annealing. From density measurements, we experimentally estimated the volume fraction of paracrystallites in the paracrystalline grossular (15 GPa–1000 °C) to be 54% which is consistent with the volume fraction of paracrystallites in the computational model. Also, the simulated density maps show a drastic density increase due to the high-volume fraction of paracrystallites which agrees well with the experimental results.

Compared with the initial glass, the paracrystalline grossular shows excellent mechanical properties, including hardness, fracture toughness and moduli (Young's modulus E , shear modulus G , and bulk modulus B). Remarkably, the paracrystalline grossular annealed at 10 GPa–1000 °C and 15 GPa–1000 °C has the highest hardness of $7.2 \pm 0.1\text{--}7.7 \pm 0.1 \text{ GPa}$ and a Young's modulus of $124.3 \pm 0.6\text{--}124.5 \pm 1.4 \text{ GPa}$ which are about 30% higher than those of the glassy grossular ($5.9 \pm 0.1 \text{ GPa}$ and $91.3 \pm 1.5 \text{ GPa}$). More surprisingly, the fracture toughness increases dramatically after paracrystallisation. Like most oxide glasses, the glassy grossular has a low fracture toughness of $0.66 \pm 0.03 \text{ MPa m}^{1/2}$. The paracrystalline grossular recovered from 15 GPa and 1000 °C exhibits a fracture toughness of $1.99 \pm 0.06 \text{ MPa m}^{1/2}$ as determined

by the indentation method. This value is three times as high as the initial glass which was further confirmed by the single-edge notched beam (SENB) method. Among the reported bulk oxide glasses the paracrystalline grossular shows the highest fracture toughness and an outstanding combination of fracture toughness and Young's modulus (Fig. 1). We attribute this exceptional toughening to the excitation of multiple shear bands, caused by a stress-induced inverse transformation from paracrystalline, to the amorphous states, revealing plastic deformation characteristics. Due to the enhanced fracture toughness, the paracrystalline grossular shows an extremely high compressive strength of $3419 \pm 353 \text{ MPa}$ and an elastic strain of $12.2 \pm 2.1\%$ which are much higher than those of the glassy grossular ($1087 \pm 59 \text{ MPa}$ and $7.0 \pm 0.8\%$). The excellent combination of mechanical and optical properties, in view of safety and lightness in structural materials, endows the paracrystalline grossular with great potential for technological applications.

Author contact: Hu Tang, hutang@jlu.edu.cn
Wenge Xiao, xiaowenge@nub.edu.cn
Howard Sheng, hsheng@gmu.edu

References

1. R. O. Ritchie, 'The conflicts between strength and toughness', *Nat. Mater.* **10**, 817–822 (2011).
2. Y. Yue, Y. Gao, W. Hu, B. Xu, J. Wang, X. Zhang, Q. Zhang, Y. Wang, B. Ge, Z. Yang, Z. Li, P. Ying, X. Liu, D. Yu, B. Wei, Z. Wang, X. F. Zhou, L. Guo, Y. Tian, 'Hierarchically structured diamond composite with exceptional toughness', *Nature* **582**, 370–374 (2020).
3. M. D. Demetriou, M. E. Launey, G. Garrett, J. P. Schramm, D. C. Hofmann, W. L. Johnson, R. O. Ritchie, 'A damage-tolerant glass', *Nat. Mater.* **10**, 123–128 (2011).
4. H. Tang, X. Yuan, Y. Cheng, H. Fei, F. Liu, T. Liang, Z. Zeng, T. Ishii, M. S. Wang, T. Katsura, H. Sheng, H. Gou, 'Synthesis of paracrystalline diamond', *Nature* **599**, 605–610 (2021).
5. T. To, S. S. Sørensen, J. F. S. Christensen, R. Christensen, L. R. Jensen, M. Bockowski, M. Bauchy, M. M. Smedskjaer, 'Bond Switching in Densified Oxide Glass Enables Record-High Fracture Toughness', *ACS Appl. Mater. Interfaces* **13**, 17753–17765 (2021).

Original publication

'Toughening oxide glasses through paracrystallisation', *Nature Materials* **22**, 1189–1195 (2023). DOI: 10.1038/s41563-023-01625-x



Hu Tang^{1,2,3}, Yong Cheng⁴, Xiaohong Yuan⁵, Kai Zhang⁶, Alexander Kurnosov¹, Zhen Chen⁴, Wenge Xiao^{7,8}, Henrik S. Jeppesen⁹, Martin Etter⁹, Tao Liang², Zhidan Zeng², Fei Wang¹, Hongzhan Fei¹⁰, Lin Wang¹, Songbai Han⁵, Ming-Sheng Wang⁴, Guang Chen⁴, Howard Sheng^{2,11} and Tomoo Katsura^{1,2}

1. Bayerisches Geoinstitut, Bayreuth, Germany
2. Center for High Pressure Science and Technology Advanced Research, Beijing, China
3. State Key Laboratory of Superhard Materials, Synergetic Extreme Condition High-Pressure Science Center, Changchun, China
4. State Key Laboratory of Physical Chemistry of Solid Surfaces, Xiamen, China
5. Academy for Advanced Interdisciplinary Studies & Shenzhen Engineering Research Center for Frontier Materials Synthesis at High Pressures, Shenzhen, China
6. National Key Laboratory of Advanced Casting Technologies, Nanjing, China
7. Institute of Light+X Science and Technology, Ningbo, China
8. State Key Lab of Modern Optical Instrumentation, Hangzhou, China
9. Deutsches Elektronen-Synchrotron DESY, Hamburg, Germany
10. School of Earth Sciences, Hangzhou, China
11. Department of Physics and Astronomy, Fairfax, VA, USA

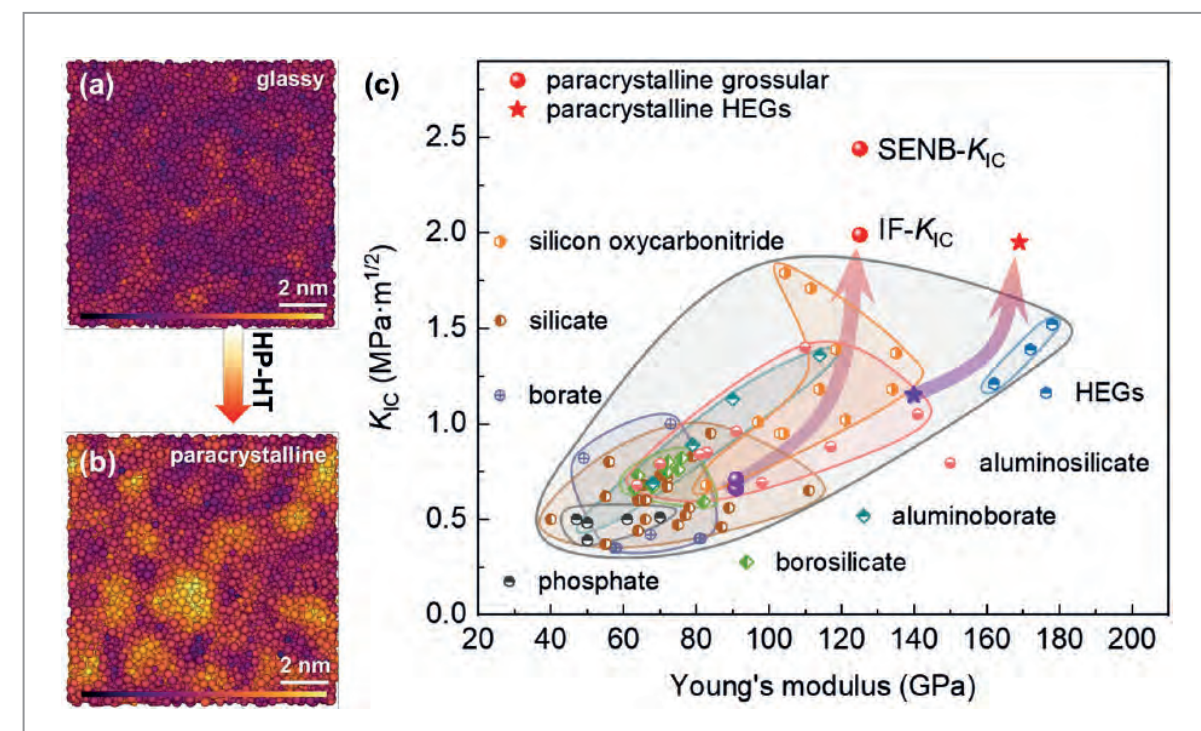


Figure 1 Structural model of b) paracrystalline grossular compared to a) its glassy state. c) Fracture toughness plotted against Young's modulus for our paracrystalline grossular, compared with other oxide glasses.

Rattling atoms in 'frozen' phase-change materials

High-mobility atoms offer new possibilities for engineering future computer memory

Phase-change materials (PCMs) are a unique class of materials that can be used to store data by encoding bits of information into their amorphous and crystalline states. PCMs are the basis of phase-change random access memory (PCRAM) technology that provides high-speed, high-capacity and non-volatile data storage capabilities. PCMs can also mimic the behaviour of neurons, constituting a building component for neuromorphic computing technology. The amorphous state of PCMs is particularly mysterious, as it has a disordered atomic arrangement and is difficult to characterise. A better understanding of the amorphous state is crucial for improving PCM-based memory and computing technologies.

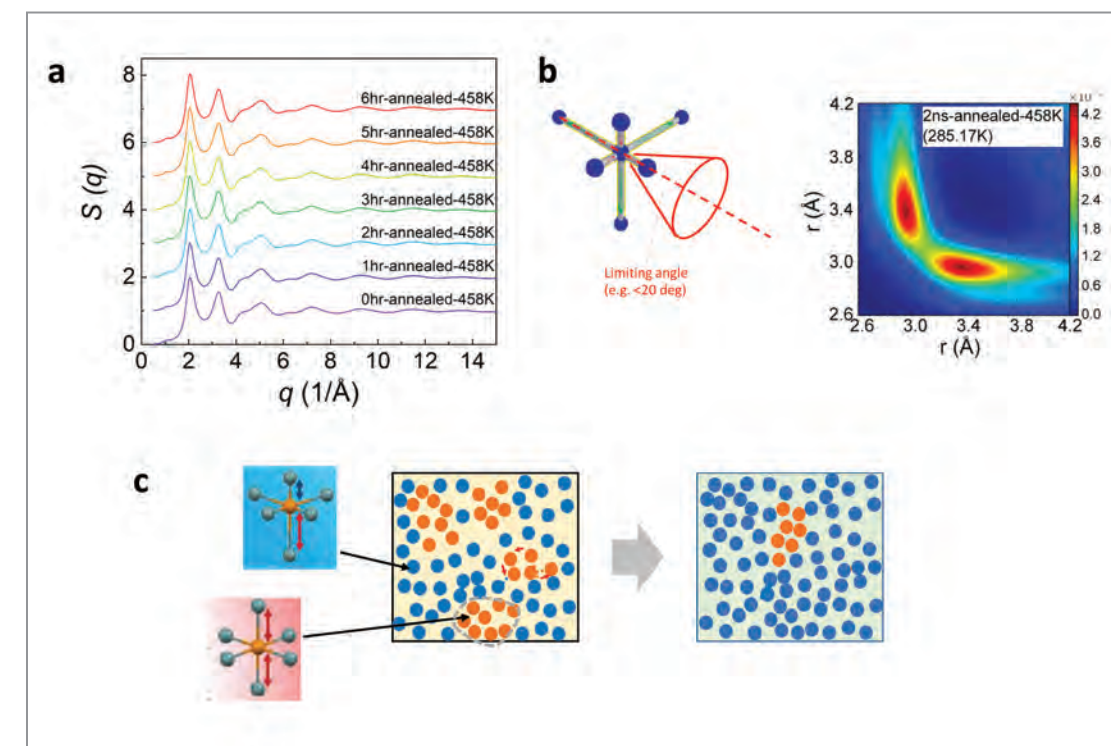
The material under current study is an alloy of germanium and antimony, namely $\text{Ge}_{15}\text{Sb}_{85}$. The amorphous phase of this material can be created by freezing the atomic rearrangement below the so-called glass transition temperature. The material is then in a 'glassy' state where the viscosity is so high that atomic motion appears to be completely frozen. However, the present study reveals that there are some 'soft spots' in this rigid amorphous matrix where fast atomic motion is still possible but restraint in local regions. The disordered atoms are arranged so inhomogeneously that some spots are softer and more loosely packed than others, like the bulbs in a frozen milk tea. The fast local atomic motions in those soft spots, so-called beta-relaxations, have been observed in various types of glasses, including molecular glasses, metallic glasses, organic glasses, polymers and even proteins. They are considered the major source of atomic mobility in glasses. The finding of beta-relaxations in amorphous PCMs offers new possibilities to control the switching between the amorphous and crystalline states. This has important implications for PCM-based computer memory and neuromorphic computing technologies because the speed of these devices depends on the switching behaviour of the PCMs.

The local high-atomic mobility within soft spots is a peculiar property of PCMs because few other covalent glasses

exhibit similar behaviours [1]. What makes it even more surprising is that, when applying some proper thermal treatment, the soft spots are quickly suppressed and eventually vanish. The high-energy high-flux PETRAIII beamline P02.1 allows for *in situ* monitoring the structural changes during thermal annealing. The X-ray is so bright that even tiny crystals can be detected if crystallisation occurs (Fig. 1a). Upon annealing, no crystal is observed while structural changes are observed in the amorphous state. The structure of the amorphous phase is spatially inhomogeneous; therefore, the structural changes within a small volume fraction of the material contribute to the changes in overall X-ray scattering signals. Modelling of *ab initio* molecular dynamics has revealed that the structural changes originate from a specific type of atomic structural distortion (Peierls-like distortions, Fig. 1b,c). The latter can be tuned by inputs of thermal energy at right timing.

The study showed that the switching behaviour from the amorphous to crystalline states is strongly affected by the suppression of the fast local atoms in the soft spots. By applying laser pulses without thermal treatment, the amorphous state is transformed into the crystalline phase on a nanosecond timescale via Joules heating. By removing these soft spots through thermal treatment, the switching speed may get ten times slower.

Figure 1
Structural changes upon annealing of amorphous phase-change materials. a) X-ray diffraction patterns upon annealing of amorphous $\text{Ge}_{15}\text{Sb}_{85}$. b) Peierls-like distortion at local octahedral structural environment. The two maxima in the contour plot of the three-body correlation functions indicate long and short bond distributions due to Peierls-like distortions. c) The schematic of structural changes upon annealing where soft and loosely packed regions become less and less via the Peierls reinforcement. The structure becomes more homogenous.



Switching of PCMs is a physical phase transformation like water being solidified to ice or vaporized. All phase changes require enough atomic mobility for the atoms to rearrange themselves to their new favourable positions. So, the atomic mobility is the limiting factor for these processes. Thanks to the soft spots, the atoms in these spots are loosely packed and are easy to move. They provide a source of high atomic mobility. Even if the mobility is rather local, it appears to be the key to make the crystallisation happen rapidly in PCMs.

How does this make an impact to real-world technologies? Technologies in memory chips rely on advanced materials properties. To design these properties, we must know the structure of the materials. This new research provides a clue on how the structure of PCMs should be engineered, even if it seems to be disordered. For example, one could either remove the soft spots to make crystallisation more gradual or increase the soft spots to accelerate crystallisations, which may help design better computer memory devices and neuromorphic applications.

Author contact: Shuai Wei, shuai.wei@chem.au.dk
Hai-Bin Yu, haibinyu@hust.edu.cn
Matthias Wuttig, wuttig@physik.rwth-aachen.de
Riccardo Mazzarello, riccardo.mazzarello@uniroma1.it

References

1. S.-X. Peng, Y. Cheng, J. Pries, S. Wei, H.-B. Yu and M. Wuttig, 'Uncovering β -relaxations in amorphous phase-change materials', *Sci. Adv.* 6, eaay6726 (2020).

Original publication

'Highly tunable β -relaxation enables the tailoring of crystallization in phase-change materials', *Nature Communications* 13, 7352 (2022). DOI: 10.1038/s41467-022-35005-x



Yudong Cheng^{1,2,9}, Qun Yang^{3,9}, Jiangjing Wang^{1,2,9}, Theodoros Dimitriadis², Mathias Schumacher², Huiru Zhang³, Maximilian J. Müller², Narges Amini⁴, Fan Yang⁵, Alexander Schoeke⁶, Julian Pries², Riccardo Mazzarello⁷, Matthias Wuttig², Hai-Bin Yu³, Shuai Wei^{4,8}

1. Center for Alloy Innovation and Design (CAID), State Key Laboratory for Mechanical Behavior of Materials, Xi'an Jiaotong University, Xi'an, China
2. Institute of Physics (IA), RWTH Aachen University, Aachen, Germany
3. Wuhan National High Magnetic Field Center and School of Physics, Huazhong University of Science and Technology, Wuhan, China
4. Department of Chemistry, Aarhus University, Aarhus, Denmark
5. Institut für Materialphysik im Weltraum, Deutsches Zentrum für Luft- und Raumfahrt (DLR), Köln, Germany
6. Deutsches Elektronen-Synchrotron DESY, Hamburg, Germany
7. Department of Physics, Sapienza University of Rome, Rome, Italy
8. iMAT Centre for Integrated Materials Research, Aarhus University, Aarhus, Denmark
9. These authors contributed equally

First synthesis of the aromatic $[N_6]^{4-}$ hexazine ring

Experiments performed at extreme pressures and temperatures reveal the stability of this long-sought-after aromatic nitrogen species

Aromaticity plays a vital role in industrial processes, chemistry and biology. In fact, aromaticity is thought to be one of the essential components of life, allowing for the existence of key hydrocarbon species. The importance of aromaticity — a peculiar electron-based feature — is due to the fact that it provides with chemical species increased stability, enabling them to persist in otherwise impossible environments [1].

Since it has been established that aromaticity is not exclusive to carbon-based species, many researchers have dedicated their studies to the discovery of new exotic aromatic units. In particular, nitrogen-only molecules have been targeted as they are known to be notoriously unstable; a fact that could be overturned by aromaticity and make them significantly more appealing for potential technological applications.

Hexaazabenzene, an N_6 ring analogous to the most well-known aromatic species, benzene, has been shortlisted as

a promising candidate. A variety of configurations and geometries have been proposed based on calculations [2], including that of the hexazine anion $[N_6]^{4-}$, but until now its experimental synthesis eluded researchers.

In an attempt to discover novel nitrogen aromatic species, potassium azide (KN_3) and molecular nitrogen (N_2) were loaded in a diamond anvil cell and compressed to an enormous pressure of 46 GPa (i.e. 460000 times atmospheric pressure) and heated to 2000°C using high power lasers.

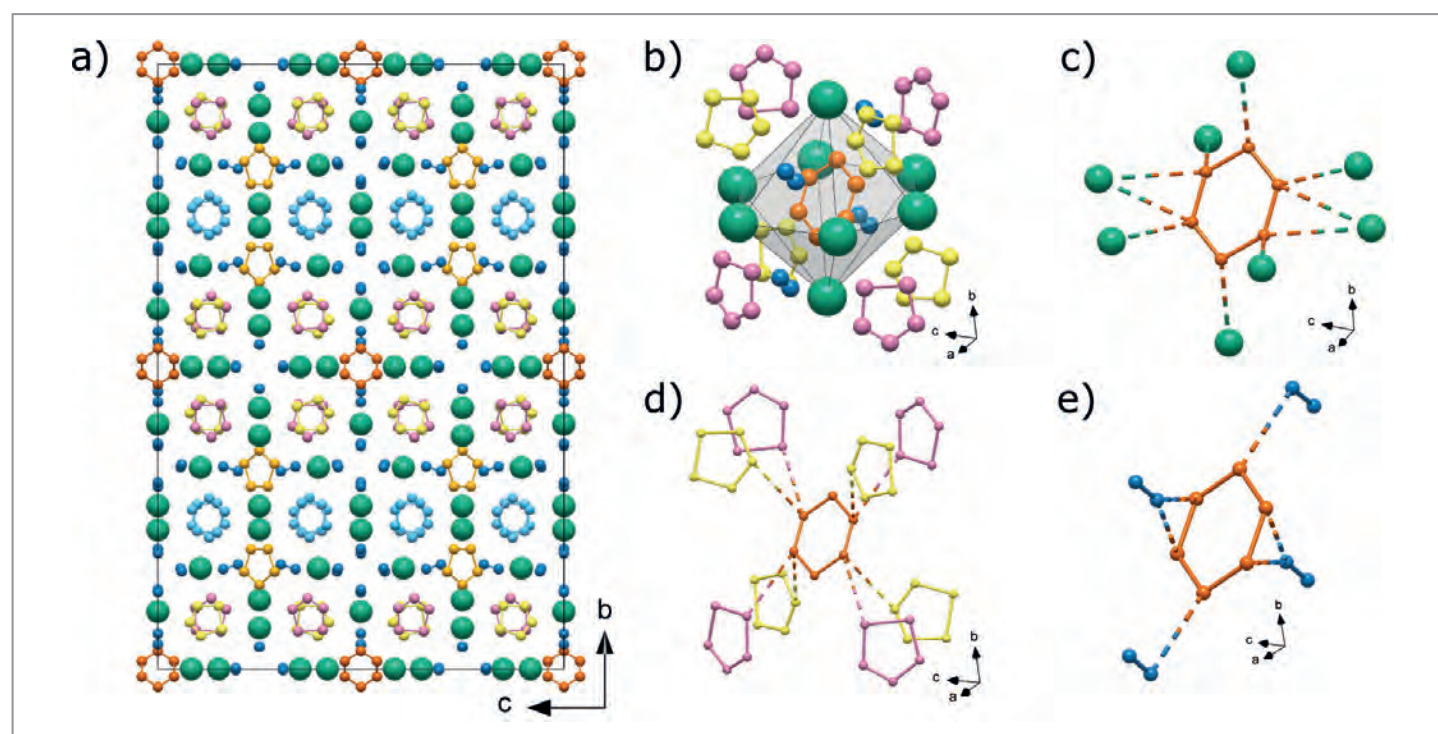


Figure 1 Experimentally determined crystal structure of the K_9N_{56} compound. a) Unit cell viewed along the a axis. b)–e) The chemical environment of the N_6 ring (b), with an emphasis on the neighbouring atoms: K atoms (c), N_5 rings (d) and N_2 dimers (e). The green spheres represent K atoms and all other spheres represent N atoms with different colours representing distinct species. (Copyright©2023 Springer Nature Limited)

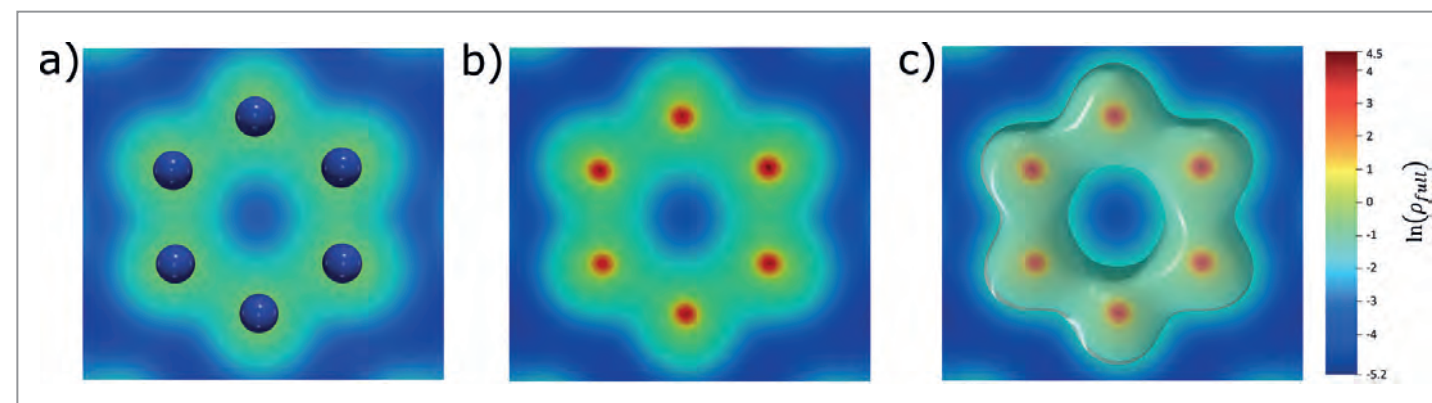


Figure 2 Visualisation of the all-electron charge density of the $[N_6]^{4-}$ ring in K_9N_{56} from DFT-based calculations. a), b) Two-dimensional slice through the all-electron charge density in the plane defined by the N_6 ring, a) with and b) without the nitrogen atoms as blue spheres. c) the same N_6 ring as in b) but with an isoelectronic surface of $0.2 e^{-\text{\AA}^{-3}}$.

To characterise the atomic arrangement adopted by the presumed newly formed compound, the pressurised samples were carried to the PETRA III beamline P02.2. The high-flux and small beam size of the hard X-ray beam of P02.2 were crucial in order to obtain sufficient high-quality single-crystal X-ray diffraction data of the submicron-sized crystallites making up the samples. With these data, a full solution of the astounding crystal structure of the K_9N_{56} compound, shown in Fig. 1, could be obtained.

The crystal structure of K_9N_{56} features a degree of complexity almost never observed for solids produced at such high pressures. The unit cell is comprised of a repeating arrangement of 520 atoms, 72 K and 448 N, and the nitrogen atoms are assembled in three distinct types of units: N_2 dimers, planar $[N_5]^-$ rings, and planar $[N_6]^{4-}$ rings. The latter, i.e. a hexazine anion, is a previously unknown nitrogen species and of particular interest. Indeed, being planar, cyclic and featuring a 10π -electron system, it fulfils Hückel's rule — the basic rule for aromaticity. Its aromaticity was also verified through density functional theory (DFT) calculations using more advanced criteria. Indeed, another characteristic of aromaticity is to have a homogeneous electronic distribution across the planar ring. As evidenced through the DFT calculations, and shown in Fig. 2, the $[N_6]^{4-}$ anion of the K_9N_{56} compound was also found to have this feature.

The stability of the K_9N_{56} compound was studied upon progressive pressure release. Powder X-ray diffraction data was collected down to a pressure of 22 GPa. Between pressures of 32 and 22 GPa, the diffraction signal of the K_9N_{56} solid disappears, suggesting its decomposition. It is hypothesised that the K_9N_{56} compound breaks down due to the loosely van der Waals-bonded neutral N_2 dimers being able to flow out of the material easily rather than due to the lack of stability of the hexazine anion.

These results emphasise that single-crystal X-ray diffraction of polycrystalline aggregates performed with the extreme-brilliance radiation of synchrotrons is crucial for solving very complex structures of solids at high pressures. This study also provides a striking example contradicting the trope of structural simplicity at high densities. The synthesis of the novel $[N_6]^{4-}$ aromatic hexazine anion should stimulate further exploration of nitrogen chemistry in the search for novel nitrogen-based technological materials.

Author contact: Dominique Laniel, dominique.laniel@ed.ac.uk

References

1. T. M. Krygowski, 'Aromaticity: what does it mean?', *ChemTexts* 1, 1-10 (2015).
2. T.-K. Ha and M. T. H. Nguyen, 'The identity of the six nitrogen atoms (N_6) species', *Chem. Phys. Lett.* 195, 179-183 (1992).

Original publication

'Aromatic hexazine $[N_6]^{4-}$ anion featured in the complex structure of the high-pressure potassium nitrogen compound K_9N_{56} ', *Nature Chemistry* 15, 641-646 (2023). DOI: 10.1038/s41557-023-01148-7



Dominique Laniel^{1,2*}, Florian Trybel³, Yuqing Yin^{4,5}, Timofey Fedotenko¹, Saiana Khandarkhaeva⁶, Andrey Aslandukov¹, Georgios Aprilis⁶, Alexei I. Abrikosov⁷, Talha Bin Masood⁷, Carlotta Giacobbe⁶, Eleanor Lawrence Bright⁶, Konstantin Glazyrin⁸, Michael Hanfland⁶, Jonathan Wright⁶, Ingrid Hotz⁷, Igor A. Abrikosov³, Leonid Dubrovinsky⁴ and Natalia Dubrovinskaia^{1,3}

1. Material Physics and Technology at Extreme Conditions, Laboratory of Crystallography, University of Bayreuth, Bayreuth, Germany
2. Centre for Science at Extreme Conditions and School of Physics and Astronomy, University of Edinburgh, Edinburgh, United Kingdom
3. Department of Physics, Chemistry and Biology (IFM), Linköping University, Linköping, Sweden
4. State Key Laboratory of Crystal Materials, Shandong University, China
5. Bayerisches Geoinstitut, University of Bayreuth, Bayreuth, Germany
6. European Synchrotron Radiation Facility, Grenoble, France
7. Department of Science and Technology (ITN), Linköping University, Norrköping, Sweden
8. Deutsches Elektronen-Synchrotron DESY, Hamburg, Germany

3D view of interfacial structures in a single glance

Hard X-ray version of Lloyd's mirror as a nanoscale probe discovered

Visualising surface-supported and buried mesoscale structures, such as nanoelectronics, quantum dots and heterogeneous catalysts, often requires high-resolution X-ray imaging and scattering. However, conventional X-ray methods based on transmission geometry are less effective in probing those objects. The scientific team discovered that X-ray surface holographic imaging in reflection geometry, much resembling Lloyd's mirror, is sensitive to three-dimensional (3D) structures in a single view. The scientists developed a 3D finite-element-based multibeam-scattering analysis to decode the complex scattering and resolve the surface features with nanometer resolutions, paving the way for high-resolution surface characterisation *in situ* or *operando*.

One of the most powerful and versatile imaging techniques developed in recent years for materials and biological science is X-ray coherent diffraction imaging, a lensless technique that can probe nanoscale and mesoscopic structures using diffraction patterns from highly coherent X-ray beams but is commonly performed in transmission geometry. The reconstruction of the samples is done with iterative phase-retrieval algorithms based on Fourier transform. Reconstructing 3D surface structures supported by thick substrates, however, has proved daunting due to strong substrate absorption in transmission geometry [1]. The strong reflective scattering from the supporting substrates or interfaces in reflection geometry can also render conventional reconstruction ineffective, requiring new analytical approaches. Researchers at Argonne National Laboratory, working with their DESY collaborator, took inspiration from a classic physics experiment to develop a

new technique for obtaining precise 3D structural information in only a single view [2]. Their work appeared in Nature Communications.

English polymath Thomas Young demonstrated how light from two different paths could create distinctive interference patterns, pointing to the wave nature of light in his famous double-slit experiment. Humphrey Lloyd extended Young's work by using a mirror to create interference patterns between a single light source and its reflection, an experiment known as 'Lloyd's mirror' [3]. Such intriguing phenomena, however, are far more difficult to demonstrate at the extremely short wavelengths of hard X-rays, thousands of times shorter than visible light.

In the current work, the investigators realised that the holographic patterns seen in hard X-ray grazing incidence reflection geometry are an analog for a more conventional Lloyd's mirror setup to provide data for high-resolution 3D reconstructions of surface and interfacial structure (Fig. 1a). The team used both simulations and imaging experiments at Beamline P10 of PETRA III (Fig. 1b) and Beamline 8-ID-I of the Advanced Photon Source (Argonne National Laboratory) to develop techniques for extracting 3D profiles of planar surface patterns at nanometer and subnanometer resolutions.

Figure 1 Hard X-ray holographic imaging of mesoscale planar surface patterns supported by a thick substrate. a) Lloyd's mirror in hard X-ray scattering version showing two-beam holographic scattering theme. b) Scattering geometry used at P10 showing the grazing incident, reflected, and scattered X-rays from the surface planar sample (inset). (Credit: Jin Wang and Miaoqi Chu)

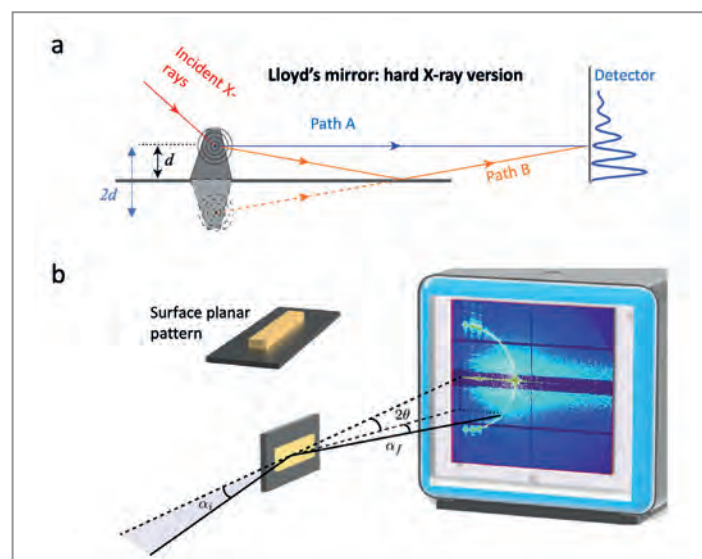
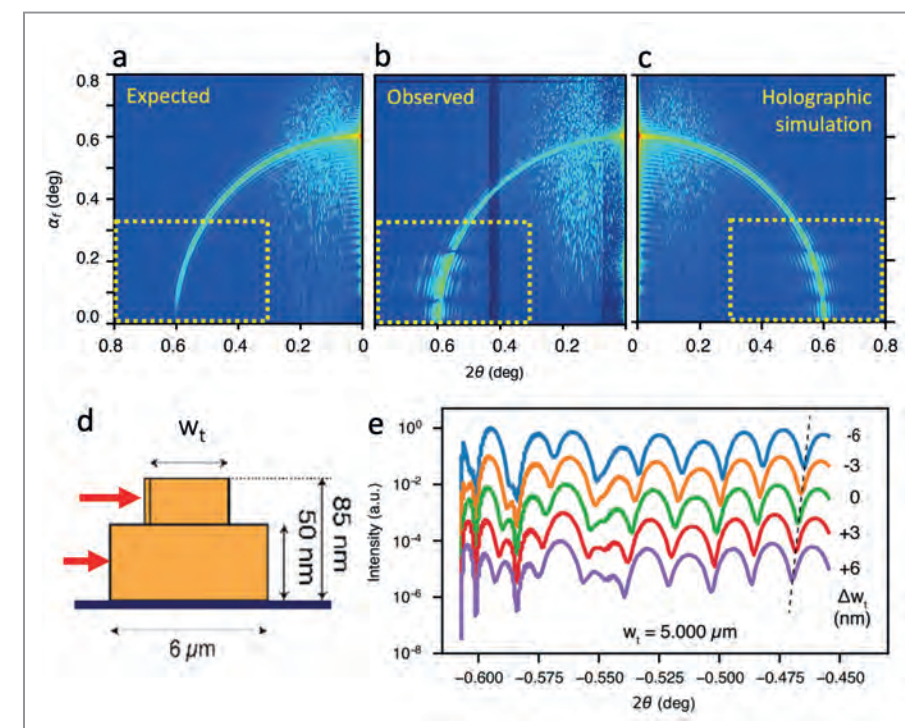


Figure 2 Simulation and validation of reflective X-ray holographic scattering imaging as a nanoscale structural probe. a) Expected scattering pattern showing prohibited low exit angle region (white box) as opposed to, b) intense scattering appeared experimentally, c) validating the holographic analyses using FE-DWBA revealing the 3D nm-resolution structural information. d) A truly 3D sample probed by the holographic scattering method, e) revealing the sensitivity of the measurement to the pattern dimension, the width of the top structure.



The great complexity and irregularity in surface scattering and speckling patterns from the grazing incidence X-ray probes, which can also include substrate and interfacial reflections, make the interpretation of morphological information quite challenging (Fig. 2a,b). One approach for dealing with these problems is known as distorted-wave Born approximation (DWBA), a strategy that the investigators adapted and extended in a new approach they call finite-element DWBA (FE-DWBA). Using a 3D grid system, it was possible to accurately compute X-ray scattering from various of heterogeneous features to generate high-resolution holographic 3D structural imaging.

To confirm and validate this approach, the experimenters conducted both extensive simulations and experimental studies. They first studied an ultrathin gold bar on a silicon substrate, designed in a simple configuration so that its features could be derived from tell-tale scattering information. However, they found that strong in-plane inhomogeneities, along with the local electron densities far different from the averaged ones at the sample surface and substrate, compromised the efficacy of the usual DWBA approach [4,5] for revealing structural features.

The research team addressed that problem with their FE-DWBA technique, in which the sample is considered not only as merely a layered structure but divided into a 3D grid both parallel and perpendicular to the substrate, which allows computations to be done based on the 3D cells. The resulting computational demands of dealing with up to five million cells in a single sample can be managed by grouping cells into stacks with the same electron profile (Fig. 2c). The team also developed a first-principles simulation and applied it to holography experiments on a more complicated and truly 3D sample with two stacked gold bars of differing

widths, provided further confirmation of the holographic Lloyd's mirror effect (Fig. 2d,e).

The extreme sensitivity and nanometer resolution of the 3D imaging that can be obtained using this 'optics-on-a-chip' approach offer a means of nondestructive visualisation of nanoscale circuit configurations and patterns without any modifications to the devices. The scientists also envision further development of this approach to achieve single-view, *in situ*, and *operando* characterisation in various other research fields in both the physical and biological sciences.

Author contact: Jin Wang, wangj@anl.gov
Miaoqi Chu, miqichu@anl.gov

References

1. T. Sun et al., 'Three-dimensional coherent X-ray surface scattering imaging near total external reflection', Nat. Photonics 6, 586–590 (2012).
2. <https://aps.anl.gov/APS-Science-Highlight/2023-11-01/a-3d-view-of-mesoscale-interfacial-structures-in-a-single-glance>, (accessed 1 Nov. 2022).
3. H. Lloyd, 'On a New Case of Interference of the Rays of Light', Transactions Royal Irish Academy 17, 171-177 (1831).
4. S. K. Sinha, E.B. Sirota and S. Garoff, 'X-ray and neutron scattering from rough surfaces', Phys. Rev. B Condens. Matter 38, 2297–2311 (1988).
5. Z. Jiang et al., 'Waveguide-enhanced grazing-incidence small-angle x-ray scattering of buried nanostructures in thin films', Phys. Rev. B 84, 075440 (2011).

Original publication

'Probing three-dimensional mesoscopic interfacial structures in a single view using multibeam X-ray coherent surface scattering and holography imaging', Nature Communications 14, 5795 (2023).
DOI: 10.1038/s41467-023-39984-3



Miaoqi Chu¹, Zhang Jiang¹, Michael Wojcik¹, Tao Sun¹, Michael Sprung² and Jin Wang¹

1. X-ray Science Division, Argonne National Laboratory, Lemont, Illinois, USA
2. Deutsches Elektronen-Synchrotron DESY, Hamburg, Germany

Corrosion and catalytic reaction hand in hand

The oxygen evolution reaction drives passivity breakdown for Ni-Cr-Mo alloys

Passivity, the key to our metal-based civilisation, refers to spontaneous formation of a protective passive film on the surface of metals such that they can be widely used in society. However, passivity breakdown can occur under corrosive conditions, leading to fast corrosion of the metal and catastrophic material's failure. Fundamental understanding of passivity breakdown is crucial for the development of advanced alloys with high corrosion resistance for uses in demanding applications. This study, published in the journal *Advanced Materials*, reveals a new corrosion mechanism, i.e. the oxygen evolution reaction drives passivity breakdown for Ni-Cr-Mo alloys. This is achieved by using multiple synchrotron X-ray techniques and electrochemical methods to study the passivity breakdown process in real time.

Metallic materials are cornerstones for our modern society. The main limiting factor of their usage is material degradation due to corrosion, resulting in global annual costs of over 3% of industrialised nations' gross domestic product [1]. Many metals/alloys exhibit a phenomenon, a so-called

passivation, i.e. the spontaneous formation of a thin passive oxide film on the surface which greatly reduces the corrosion rate such that the material can be used in corrosive environments for a long time. Corrosion resistance of alloys depends on the structure, chemistry and electronic

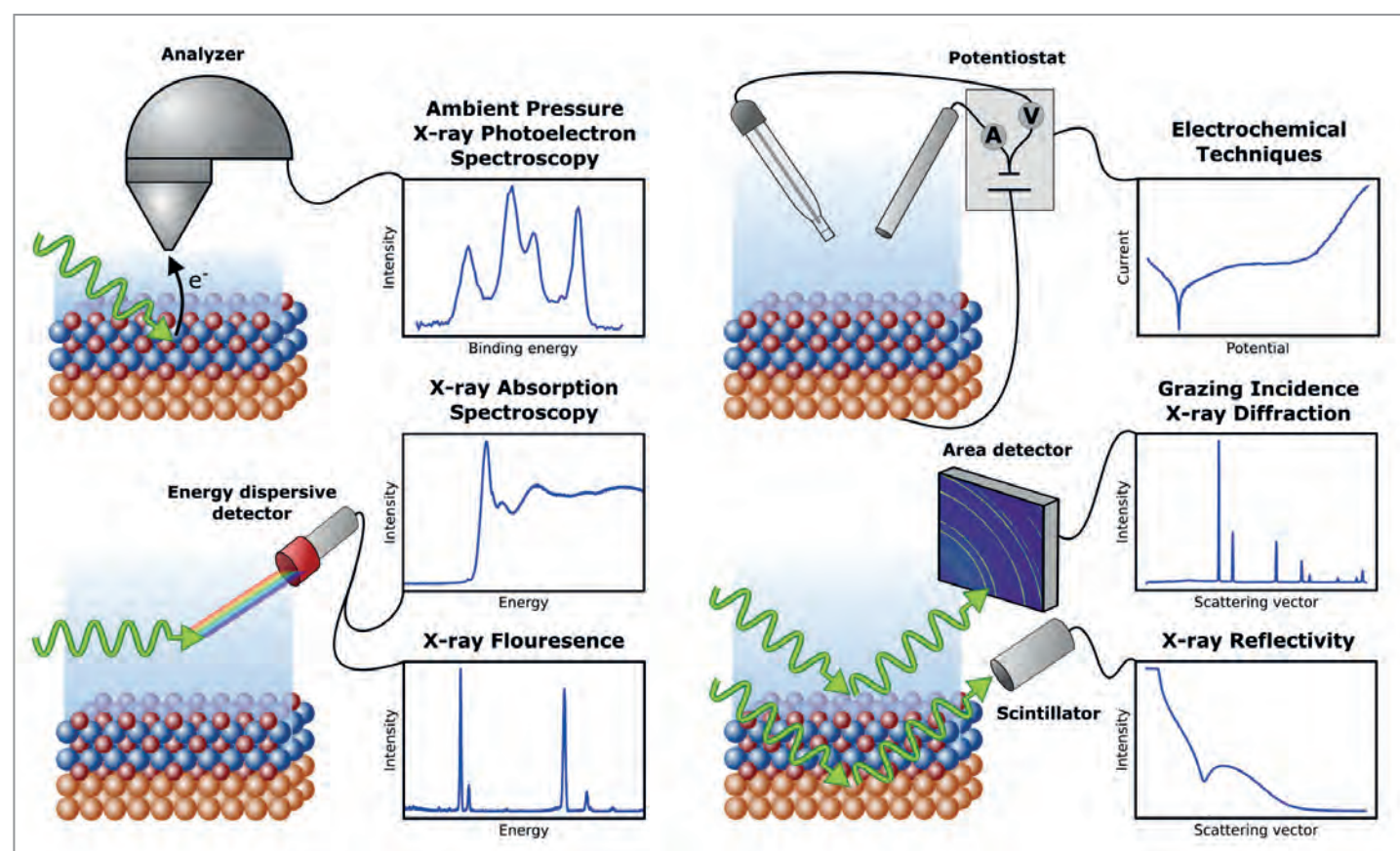


Figure 1
A schematic representation of the combination of experimental techniques used during this work. The orange atoms represent the metal, blue the metal cations and red the oxygen anions in the oxide layer. XRR, XRF and GI-XRD were integrated into one experimental setup. XANES and AP-XPS were measured in separate experiments.

properties of the passive films as well as the underlying alloy layer. A typical example is stainless steel, where the Cr added as an alloying element spontaneously forms a protective Cr-rich oxide film on the surface, acting as a kinetic barrier to further corrosion [2]. However, passivity and passive film breakdown may occur under certain corrosive conditions, leading to fast corrosion such as pitting, etc. Passivity and its breakdown involve electrochemical and chemical reactions occurring at the metal/oxide and oxide/electrolyte interfaces, the formation and dissolution of the oxides as well as ionic transport across the oxide film. A fundamental understanding of the governing mechanism is crucial for the development of high-performance alloys but it is difficult to achieve since the thin oxide films at the metal-liquid interface are notoriously challenging to study.

In harsh conditions, stainless steel may not meet the material requirements, and instead, Ni alloys containing Cr, Mo and other alloying elements are used which have excellent mechanical properties and corrosion resistance [3]. Ni alloys are less extensively studied than stainless steel, and there is a lack of understanding of the corrosion mechanisms. In this work we carried out a comprehensive *in situ* study by a combination of several synchrotron X-ray techniques to characterise the surface region of a Ni-Cr-Mo alloy immersed in NaCl electrolyte during electrochemical polarisation at stepwise increased anodic potentials. The experimental techniques are schematically shown in Fig. 1. X-ray Reflectivity (XRR), Grazing Incidence X-ray Diffraction (GI-XRD) and X-ray Fluorescence (XRF) data were collected at the PETRA III beamline P21.2, and XRR was used to investigate the thickness of the passive film. Whereas by GI-XRD the change in the metal lattice underneath the oxide film was determined, from the XRF data the concentration of dissolved elements into the electrolyte was quantified. X-ray Absorption Near Edge Structure (XANES) measurements at the PETRA III beamline P64 were used to study the chemical state of the species dissolved into the electrolyte and the chemical state of corrosion products formed on the surface. The XRR, XRF and GI-XRD were integrated into one setup, while XANES and Ambient Pressure X-ray Photoelectron Spectroscopy (AP-XPS) conducted at the HIPPIE beamline at MAX IV, Lund, Sweden to investigate the chemistry of the passive film, were measured in separate experiments. The combination of all these techniques allowed us to study the corrosion process and passivity breakdown *in situ* and to correlate to the electrochemical reactions occurring at the sample surface.

The results from the combined synchrotron and electrochemical measurements demonstrate that the Ni-Cr-Mo alloy is active for the Oxygen Evolution Reaction (OER). The alloy forms and maintains a stable passive film in the NaCl solution until the onset of OER. After the onset of OER, the passive film starts to degrade which is associated with the OER-induced mechanism where catalytically active Mo⁴⁺ oxide sites in the oxide film are further oxidised into Mo⁶⁺ complexes that are dissolved and partly redeposited

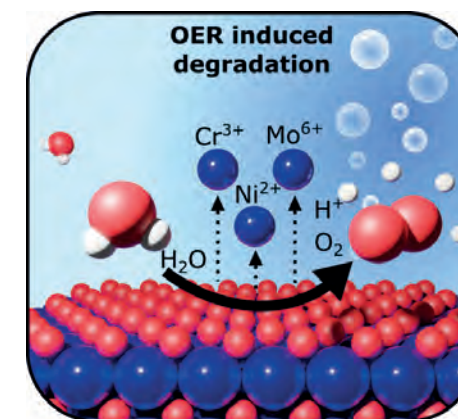


Figure 2
A schematic illustration of the new corrosion mechanism: The oxygen evolution reaction drives passivity breakdown (dissolution of Ni, Cr and Mo) for Ni-Cr-Mo alloys.

on the surface. In turn, the passivity breaks down and Ni and Cr ions are dissolved without a change in their oxidation state (Fig. 2). This is not a typical passivity breakdown mechanism like the traditional transpassive corrosion of Cr-containing alloys where Cr³⁺ is oxidised to soluble Cr⁶⁺ at sufficiently high anodic potentials. Our results provide a holistic understanding of the passivity breakdown of Ni-Cr-Mo alloys, which is associated with OER. The OER results in acidification of the solution near the surface, and the high concentration of H⁺ ions attract Cl⁻ ions which further facilitates dissolution of the protective oxide. Here, the OER plays an important role in the mechanism of passivity breakdown of Ni-Cr-Mo alloys due to their catalytic activity. This implies that the interplay between OER and material degradation must be considered in the study of corrosion of catalytically active alloys and of stability of electrode materials in catalytic processes.

Author contact: Jinshan Pan, jinshanp@kth.se
Edvin Lundgren, Edvin.Lundgren@sljus.lu.se
Alfred Larsson, alfred.larsson@sljus.lu.se

References

1. G. H. Koch, 'Cost of corrosion', Trends in oil and gas corrosion research and technologies, 3-30, A. M. El-Sherik (Ed.), Boston, Woodhead Publishing (2017).
2. P. Marcus (Ed.), 'Corrosion mechanisms in theory and practice', 3rd ed., 235-348, Boca Raton, CRC Press (2011).
3. R. Winston Revie (Ed.), 'Uhlig's corrosion handbook', 3rd ed., 837-852, John Wiley & Sons Inc., New Jersey (2011).

Original publication

'The oxygen evolution reaction drives passivity breakdown for Ni-Cr-Mo alloys', *Advanced Materials* 35, 2304621 (2023).
DOI: 10.1002/adma.202304621



Alfred Larsson¹, Andrea Grespi¹, Giuseppe Abbondanza¹, Josefin Eidhagen^{2,3}, Dorotea Gajdek⁴, Konstantin Simonov⁵, Xiaohui Yue², Ulrich Lienert⁶, Zoltan Hegedüs⁶, Arno Jeromin⁷, Thomas F. Keller^{7,8}, Mattia Scardamaglia⁹, Andrey Shavorskiy⁹, Lindsay R. Merte⁴, Jinshan Pan² and Edvin Lundgren¹

1. Lund University, Lund, Sweden
2. KTH Royal Institute of Technology, Stockholm, Sweden
3. Alleima, Sandviken, Sweden
4. Malmö University, Malmö, Sweden
5. Swerim AB, Kista, Sweden
6. Deutsches Elektronen Synchrotron DESY, Hamburg, Germany
7. Centre for X-ray and Nano Science CXNS, DESY, Hamburg, Germany
8. Universität Hamburg, Hamburg, Germany
9. MAX IV Laboratory, Lund, Sweden

An X-ray step towards superfast nanoelectronics

X-rays can demagnetise magnetic materials within femtoseconds and this can now be accurately modelled.

When a material with magnetic properties, in particular one constructed from appropriately selected layers, is illuminated by a pulse from an X-ray laser, it instantly demagnetises. This phenomenon, so far not sufficiently understood, could in the future be used in nanoelectronics to build, for example, ultrafast magnetic switches. An important step towards this goal is the new simulation tool XSPIN developed by a Polish-German-Italian team of scientists as part of a joint research project between the European XFEL, IFJ PAN and DESY.

Rapid demagnetisation in ferromagnetic materials was discovered in 1996 [1] and has since attracted the attention of many scientific teams. In the absence of bright sources capable of generating intense and short pulses in the X-ray spectral range, early research was mainly conducted using visible or infrared light. The situation changed dramatically when, in the past decade, physicists gained wider access to X-ray free-electron lasers (XFELs). This is because these unique light sources can generate X-ray pulses of very high intensity and very short duration counted in femtoseconds. Thanks to them it was discovered a few years ago that X-ray-induced demagnetisation in multilayer magnetic materials can occur significantly faster than under visible or infrared light [2]. However, a comprehensive theoretical description of the spin dynamics under the external stimulus has been lacking up to now.

In this theoretical work the newly developed computational tool XSPIN, capable of simulating ultrafast demagnetisation processes in X-ray-irradiated magnetic multilayer materials, is introduced. It treats photoinduced and electronic excitation and relaxation processes for spin-up and spin-down

electrons, also considering interlayer electron transport. It is based on an earlier simulation tool which was constructed to describe transitions in solid materials triggered by intense X-ray pulses [3]. The original model did not distinguish the orientation of the electron spin in the materials and therefore could not describe their magnetic properties. The main challenge, therefore, was to extend the core capabilities of this model tool to allow for the spin dynamics.

The correctness of the XSPIN tool was verified by comparing its predictions with experimental data collected in one of the earlier experiments conducted with the resonant magnetic small-angle X-ray scattering (mSAXS) technique at the FERMI FEL in Italy [2] (Figs. 1 and 2a). At that time, the sample was a material composed of 16 alternating layers of cobalt (Co) and platinum (Pt), each one with a thickness of just one nanometre. The photon energy was about 60 eV in the extreme ultraviolet (XUV) regime, tuned to the Co $M_{2,3}$ resonance. When interacting with the material, the X-ray light scattered and formed a diffraction ring recorded on a 2-dimensional CCD detector placed behind the sample (Fig. 1). This ring is a source of valuable

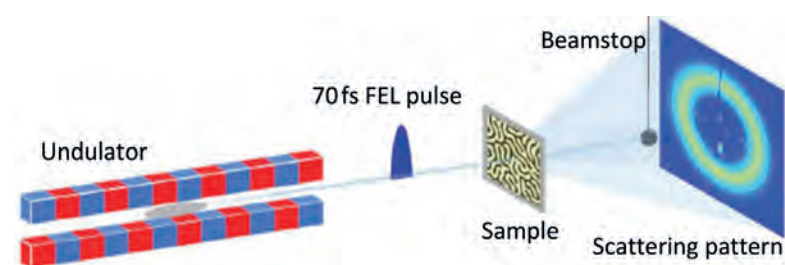


Figure 1 Principle of mSAXS measurement: An FEL pulse hits a sample of material with magnetic properties, scatters and forms a diffraction ring (figure adapted from original publication licensed under CC-BY 4.0 DEED).

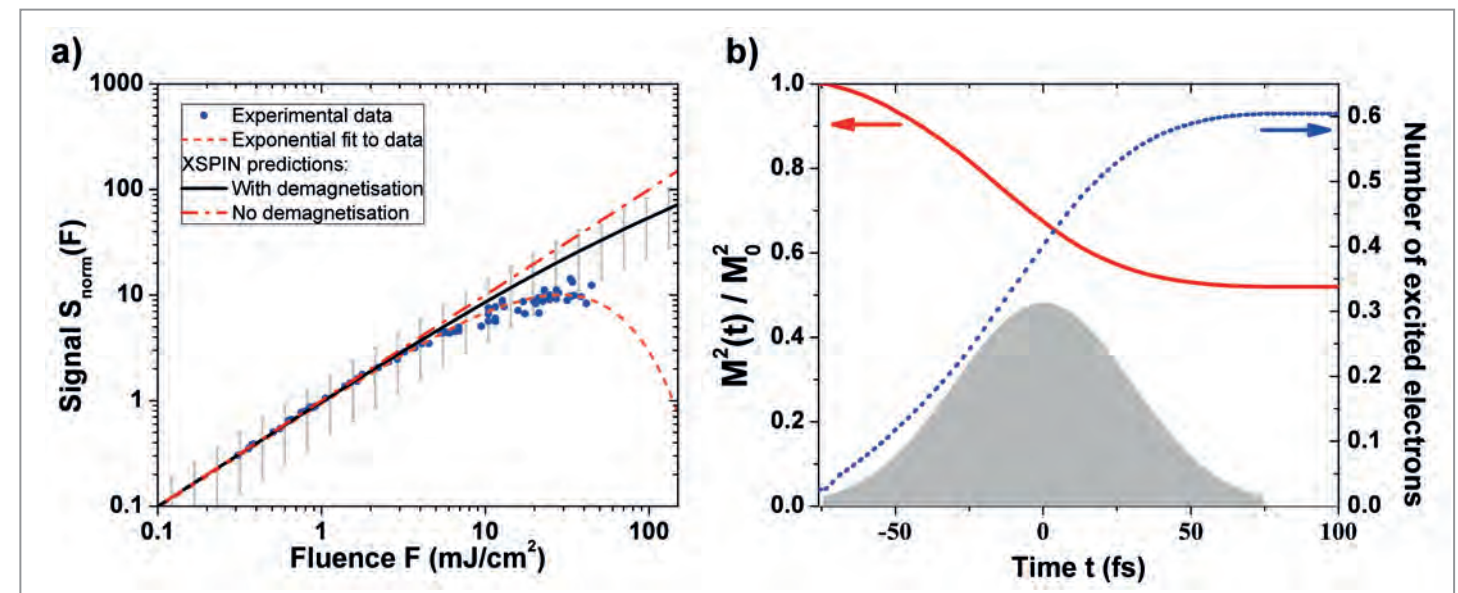


Figure 2

a) Normalised resonant magnetic scattering signal at Co M-edge shown as a function of the incoming fluence for the Co/Pt multilayer system investigated. Experimental data (blue points) are shown with the exponential fitting curve to the experimental data (orange dashed line), and with the theoretical predictions of the XSPIN code. Predictions with (black solid line) and without demagnetisation (red dash-dotted line) are shown for comparison. b) Normalised magnetisation in a single Co layer as a function of time (red solid line) and the transient number of excited electrons with energy above the Fermi level (blue dashed line) predicted by the XSPIN code for an X-ray pulse with photon energy near the Co M-edge (61.1 eV) and the fluence of $F = 13 \text{ mJ/cm}^2$, corresponding to the average absorbed dose of 0.93 eV/atom. The temporal pulse profile is schematically shown with the gray area (figure adapted from original publication licensed under CC-BY 4.0 DEED).

information—its diameter depends on the average distance between the magnetic domains in the material. So, the higher the intensity, the stronger the magnetic properties of the sample.

In that experiment the diffraction ring behaved as predicted by our model. When the XUV intensity illuminating the sample was increased, its diameter remained constant, so the arrangement of magnetic domains in the material did not change. At the same time, the higher the intensity of the incident light, the weaker the ring became due to the demagnetisation. In addition, the measured demagnetisation times were on the order of 100 femtoseconds which also agreed with our simulations. The predictions of the XSPIN code on the magnetisation change at some chosen set of X-ray parameters are shown in Fig. 2b. Due to electronic excitation and relaxation, the decrease of the magnetisation curve follows the increase of the number of excited electrons (the electrons with energy above the Fermi level) in the sample. When the electron cascading saturates, the value of magnetisation stabilises.

Up to our knowledge, the XSPIN model is the first model which couples a comprehensive quantitative description of X-ray-induced electronic damage processes with transient magnetic processes in solids. Using XSPIN, it is now possible to adjust the parameters of the X-ray laser pulses (their energy, duration and intensity) so that demagnetisation occurs on the spatial and/or temporal scale specified by the needs. Possible practical implementation of this concept will require further theoretical and experimental studies.

Author contact:

Konrad J. Kapcia, konrad.kapcia@amu.edu.pl
Victor Tkachenko, victor.tkachenko@xfel.eu
Beata Ziaja, ziaja@mail.desy.de

References

1. E. Beaurepaire, J.-C. Merle, A. Daunois and J.-Y. Bigot, 'Ultrafast spin dynamics in ferromagnetic nickel', *Phys. Rev. Lett.* **76**, 4250–4253 (1996).
2. A. Philippi-Kobs et al., 'Ultrafast demagnetization excited by extreme ultraviolet light from a free-electron laser' (2021), preprint at <https://www.researchsquare.com/article/rs-955056/v1>.
3. N. Medvedev, V. Tkachenko, V. Lipp, Z. Li and B. Ziaja, 'Various damage mechanisms in carbon and silicon materials under femtosecond x-ray irradiation', *4open* **1**, 3 (2018).

This article contains material from the IFJ PAN press release in 2022. (<https://press.ifj.edu.pl/en/news/2022/12/14/>)

Original publication

'Modeling of ultrafast X-ray induced magnetization dynamics in magnetic multilayer systems', *npj Computational Materials* **8**, 212 (2022). DOI: 10.1038/s41524-022-00895-4

K. J. Kapcia^{1,2}, V. Tkachenko^{3,4}, F. Capotondi⁵, A. Lichtenstein^{6,4}, S. Molodtsov¹, L. Müller⁷, A. Philippi-Kobs⁷, P. Piekarz³, and B. Ziaja^{1,3}

1. Center for Free-Electron Laser Science CFEL, DESY, Hamburg, Germany
2. Faculty of Physics, Adam Mickiewicz University in Poznań, Poznań, Poland
3. Institute of Nuclear Physics, Polish Academy of Sciences, Kraków, Poland
4. European XFEL, Schenefeld, Germany
5. Elettra-Sincrotrone Trieste S.C.p.A, Trieste, Basovizza, Italy
6. Universität Hamburg, Hamburg, Germany
7. Deutsches Elektronen-Synchrotron DESY, Hamburg, Germany



Monitoring initial steps of water splitting using FLASH

Free-electron laser helps to elucidate the initial reaction steps during photocatalytic water splitting in real-time.

Water is ubiquitous in nature and can heavily influence the photochemistry at environmental interfaces. This is especially true during photocatalysis, a process central to potential technology enabling the green hydrogen-based economy. To optimise these technologies, it is crucial to systematically breakdown the complex process into individual ultrafast reaction steps; something which, until recently, has been hampered by technological limitations. This study uses the free-electron laser FLASH at DESY to directly follow the photoinduced dynamics at the interface between water and a model photocatalyst during the first several picoseconds, and in doing so provides essential information relevant to a range of catalytic reactions in realistic aqueous operating conditions.

When light of appropriate energy is incident on semiconductor materials, such as titanium dioxide (TiO_2), it can lead to the generation of so-called electron hole pairs. These

are highly reactive species that can initiate a cascade of reactions at the surface to cause the evolution and breakdown of adsorbates. In addition to being one of the most promising candidates for industrially applicable photocatalysis, TiO_2 is also important for a wide range of fields spanning chemistry, biology and environmental sustainability.

Electron hole pairs are thought to be generated on an attosecond timescale (1 quintillionth of a second) with charge migration/trapping and interfacial charge transfer taking place on a femtosecond (1 quadrillionth of a second) to picosecond timescale (1 trillionth of a second). It can be said that these initial steps, particularly the interplay of recombination and mechanistic pathways such as interfacial charge transfer, govern device efficiency with the entire photocatalytic process typically hinging on how and how fast these steps take place.

X-ray photoelectron spectroscopy (XPS) is highly surface sensitive, elemental specific and chemically sensitive and therefore a powerful technique that allows one to understand the surface chemistry at catalyst surfaces. However, due to the high reactivity and short lifetimes of reaction

Figure 1
Detailed drawing of the light-induced dynamics at the interface of water molecules/titanium dioxide. (Middle figure) Time-resolved X-ray photoemission map of $\text{H}_2\text{O}/\text{TiO}_2(101)$ ($T = 160$ K) recorded during the pump-probe between -3.0 and 8.0 ps and (bottom figure) the integrated intensity as a function of delay time in which the colours (red/blue) correspond to the regions marked in the header of the X-ray photoelectron spectroscopy (XPS) map. (Credit: partly from original publication)

intermediates, an understanding of the related transient phenomena during photocatalysis cannot be obtained using traditional XPS, instead requiring techniques that can follow photoreactions on their natural time. With the advent of free-electron lasers this has become a possibility, allowing researchers to use ultrafast pulses of X-rays to follow laser-induced reactions with femtosecond resolution for the first time [1].

Capitalising on this state-of-the-art technology, a team of international scientists have combined theoretical simulations with ultrafast optical pump-X-ray probe photoemission spectroscopy at FLASH to investigate the early-stage dynamics of water splitting on the prototypical photocatalytic system of H_2O adsorbed on a single crystalline $\text{TiO}_2(101)$. Electron hole pairs are generated at the photocatalyst surface by using the pump laser of 770 nm, with subsequent X-ray pulses capturing a spectroscopic snapshot of the photoreaction. By varying the time delay between the pump and the probe lasers, researchers can acquire a 'spectroscopic movie' that allows them to follow the migration of these generated charge carriers and view fleeting reaction steps and intermediate formation in real time; information which is often lost using traditional time-averaging techniques.

The scientists were able to observe a laser-induced charge redistribution at the surface that took place within 285 fs (Fig. 1), with the formation of a new hydrogen bond between water and the surface facilitating ultrafast electron transfer to TiO_2 . Their work also highlighted the importance of the relative competition of water-water and surface-surface water interactions, with this process being suppressed as water covered the surface. Accompanying theoretical simulations, as part of a large collaboration with the Bremen Center for Computational Materials Science at the University of Bremen and the Max Planck Institute for the Structure and Dynamics of Matter in Hamburg, fully corroborated the experimental observations (Fig. 2).

A detailed understanding of transient bond formation and intermediate species, reaction mechanisms and the time scale thereof are crucial for further developments of photocatalysts. This study highlights the unique possibilities offered by soft X-ray free electron lasers such as FLASH to investigate and unravel the crucial elementary steps that

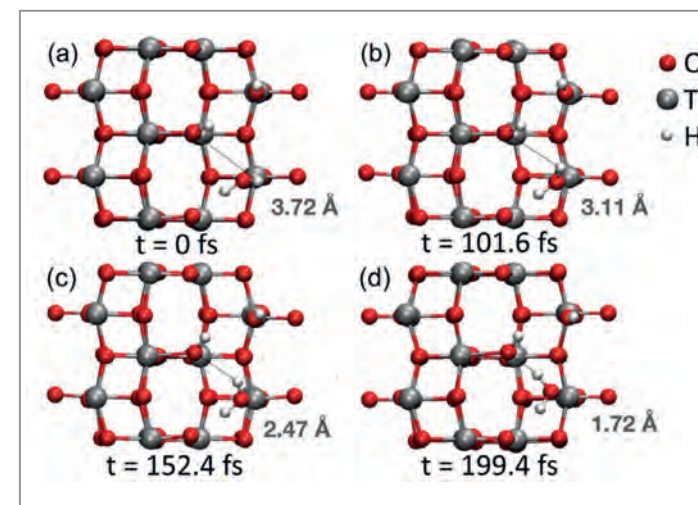


Figure 2
Dynamic evolution for H_2O adsorbed over TiO_2 and a partially hydroxylated surface. a) 0; b) 101.6; c) 152.4; d) 199.4 fs. (Credit: original publication)

take place during laser-induced photoreactions. The results unambiguously demonstrate that the activity of the photocatalyst is governed by ultrafast interfacial electron transfer from adsorbed water to the surface; in this case facilitated by new bond formation induced by charge trapping at surface sites.

Author contact: Heshmat Noei, heshmat.noei@desy.de

References

1. M. Wagstaffe, L. Wenthaus, A. Dominguez-Castro, S. Chung, G. D. Semione, St. Palutke, G. Mercurio, S. Dziarzhyski, H. Redlin, N. Klemke, Y. Yang, Th. Frauenheim, A. Dominguez, F. Kärtner, A. Rubio, W. Wurth, A. Stierle and H. Noei, 'Ultrafast Real-Time Dynamics of CO Oxidation over an Oxide Photocatalyst', *ACS Catal.* **10**, 22, 13650-13658 (2020).

Original publication

'Photoinduced Dynamics at the Water/ $\text{TiO}_2(101)$ Interface', *Physical Review Letters* **130**, 108001 (2023). DOI: 10.1103/PhysRevLett.130.108001



Michael Wagstaffe¹, Adrian Dominguez-Castro², Lukas Wenthaus³, Steffen Palutke³, Dmytro Kutnyakhov³, Michael Heber³, Federico Pressacco³, Sjarhei Dziarzhyski³, Helena Gleißner^{1,4,5}, Verena Kristin Gupta², Harald Redlin², Adriel Dominguez^{2,6,7,8}, Thomas Frauenheim^{2,6,7}, Angel Rubio^{9,10,11}, Andreas Stierle^{1,4} and Heshmat Noei^{1,5}

1. Centre for X-ray and Nanoscience CXNS, DESY, Hamburg, Germany
2. Bremen Center for Computational Material Science (BCCMS), Bremen, Germany
3. Deutsches Elektronen-Synchrotron DESY, Hamburg, Germany
4. Fachbereich Physik Universität Hamburg, Hamburg, Germany
5. The Hamburg Centre for Ultrafast Imaging, Hamburg, Germany
6. Computational Science and Applied Research Institute (CSAR), Shenzhen, China
7. Beijing Computational Science Research Center (CSRC), Beijing, China
8. Nano-Bio Spectroscopy Group, Departamento de Física de Materiales, Universidad del País Vasco, UPV/EHU- San Sebastián, Spain
9. Center for Free-Electron Laser Science, Hamburg, Germany
10. Max Planck Institute for the Structure and Dynamics of Matter, Hamburg, Germany
11. Center for Computational Quantum Physics, Flatiron Institute, New York, USA

Microscopic transformations of electrocatalyst surfaces

Operando studies reveal the surface restructuring of copper electrodes during carbon dioxide reduction

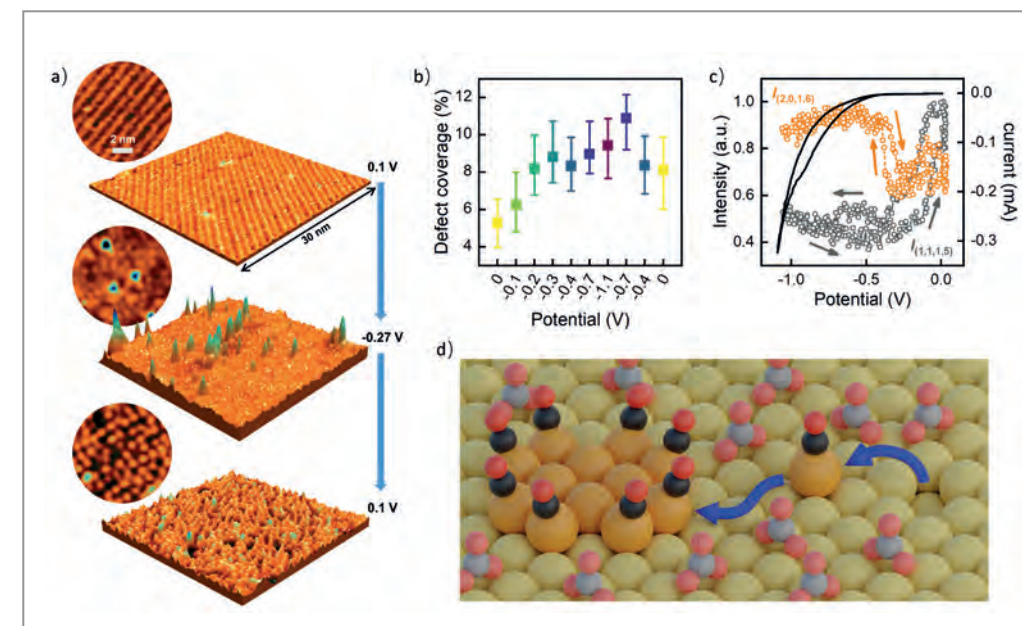
Key for the pathway towards a fully sustainable climate-neutral society is a circular economy where all materials, especially carbon, are continuously recycled. To this end, technologies have to be developed that can convert CO₂ back into synthetic fuels and base chemicals. The electrochemical reduction of CO₂ at copper electrodes allows to do so directly with electric power from renewable sources. The development of this process requires a deeper understanding of the catalyst's interface structure under operating conditions. Recent *operando* studies by surface X-ray diffraction at the PETRA III beamline P23 of DESY and complementary methods reveal highly dynamic atomic-scale changes, specifically the formation of low-coordinated Cu surface species.

Copper is an indispensable catalyst material for the CO₂ reduction reaction (CO₂RR), especially for the synthesis of particularly valuable chemicals and fuels, such as ethanol and ethylene (Fig. 1) [1]. For high selectivity towards such products it is highly favourable if the copper atoms at the surface have a strongly disordered arrangement [2]. The latter can be achieved for example by pre-oxidising the copper surface [3]. However, such disordered structures can also form spontaneously in the very initial stages of the electrocatalytic CO₂ reduction reaction, as shown in a joint study of the Institute of Experimental and Applied Physics of Kiel University (CAU) and the Department of Interface Science at the Fritz Haber Institute (FHI) of the Max Planck Society (MPG), published in the journal *Nature Catalysis*.

In our study, we focused on (100) oriented Cu electrodes, which are known to be particularly active for the formation

of multi-carbon products [1,2], and studied those in CO₂-saturated bicarbonate solutions. *In situ* scanning tunnelling microscope (STM) images (Fig. 2a) revealed an initially atomically smooth surface, covered by a well-ordered adlayer of coadsorbed carbonate anions and water molecules [4]. Upon decreasing the potential below -0.2 V (vs. the reversible hydrogen reference electrode), which corresponds to the very onset of the CO₂ reduction reaction, nanosized Cu clusters were found to emerge on the surface. *Operando* surface X-ray diffraction (SXRD) studies in a dedicated electrochemical cell at the PETRA III beamline P23 showed that these clusters formed from Cu adatoms that were extracted out of the surface layer. In particular, these measurements could be performed down to very negative potentials of -1.1 V, i.e. the technologically relevant range of the CO₂RR. Under these conditions the concomitant hydrogen evolution prohibits stable STM

Figure 2
Structural changes of Cu(100) electrode surfaces in CO₂-saturated bicarbonate solution. a) High-resolution *in situ* STM images reveal the formation of Cu nanoclusters below -0.2 V, leading to irreversible changes in the structure of the molecular adlayer on the surface. b,c) *Operando* surface X-ray diffraction at the PETRA III beamline P23 quantifies this restructuring and shows that these low-coordinated Cu surface species are present on the surface over the entire CO₂ reduction regime. d) The surface transformations can be attributed to the extraction of Cu surface atoms by the reaction intermediate CO. (Adapted from the original publication, © 2023 Springer Nature).



investigations, whereas SXRD studies are possible over time scales of hours. The latter enabled the acquisition of detailed sets of crystal truncation rods, from which quantitative data on the interface structure under reaction conditions could be obtained by fits of atomistic models. According to these studies, Cu extraction only occurs at around -0.2 V but the extracted atoms then remain on the surface over the entire CO₂RR range (Fig. 2b). This behaviour was also observed in more dynamic experiments, where the surface was monitored by SXRD during cyclic current-voltage curves (Fig. 2c). Furthermore, the SXRD measurements indicate that the coverage of formed Cu adatoms and surface vacancies was maintained at positive potentials, implying that the surface restructuring is highly irreversible. This was confirmed by complementary high-resolution STM images which revealed that despite dispersion of the Cu clusters the ordered carbonate adlayer was not recovered. Instead, a highly disordered adlayer was observed, consisting of Cu adatoms and reaction intermediates.

With the help of *operando* Raman spectroscopy, these structural transitions could be correlated with changes in the molecular interface composition. In particular, the formation of the nanoscale clusters could be linked to the generation of CO, an intermediate product of the reaction, which stabilises low-coordinated Cu atoms on the surface (Fig. 2d). Similar spectroscopic data had already been obtained in previous studies, however, the underlying complex surface restructuring processes could only be unravelled with the help of the structural results obtained by STM and synchrotron surface X-ray diffraction. These results suggest a drastic transformation of the electrode surface each time the electric current required for the CO₂ reduction is switched on. This was previously unknown but

could play an important role in catalysis. Previous work of the research team already showed that the structure of the catalyst and thus the type of formed chemical compounds can be influenced by operating the electrode with voltage pulses [3]. There, such pulses were used to periodically oxidise the copper. According to the new results, similar effects might already be obtained by simply switching the current on and off.

Author contact: Olaf M. Magnussen, magnussen@physik.uni-kiel.de

References

1. Y. Hori, 'Electrochemical CO₂ reduction on metal electrodes', *Modern aspects of electrochemistry* 42, Springer, 89-189 (2008).
2. Y. Y. Birdja, E. Pérez-Gallent, M. C. Figueiredo, A. J. Göttle, F. Calle-Vallejo and M. T. M. Koper, 'Advances and challenges in understanding the electrocatalytic conversion of carbon dioxide to fuels', *Nat. Energy* 4, 732 (2019).
3. J. Timoshenko, A. Bergmann, C. Rettenmaier, A. Herzog, R. M. Arán-Ais, H. S. Jeon, F. T. Haase, U. Hejral, P. Grosse, S. Köhl, J. Tian, O. M. Magnussen and B. Roldan Cuenya, 'Steering the structure and selectivity of electrocatalysts by potential pulses', *Nat. Catal.* 5, 259-267 (2022).
4. R. Amirbeigiab, A. Bagger, J. Tian, J. Rossmeis and O. M. Magnussen, 'Structure of the (bi)carbonate adlayer on Cu(100) electrodes', *Angew. Chem. Int. Ed.* 61, e202211360 (2022).

Original publication

'Atomic-scale surface restructuring of copper electrodes under CO₂ electroreduction conditions', *Nature Catalysis* 6, 837 (2023). DOI: 10.1038/s41929-023-01009-z



Reihaneh Amirbeigiab¹, Jing Tian², Antonia Herzog², Canrong Qiu^{1,3}, Arno Bergmann², Beatriz Roldan Cuenya² and Olaf M. Magnussen¹

1. Institute of Experimental and Applied Physics, Kiel University, Kiel, Germany
2. Department of Interface Science, Fritz-Haber Institute of the Max-Planck Society, Berlin, Germany
3. Present address: Deutsches Elektronen-Synchrotron DESY, Hamburg, Germany

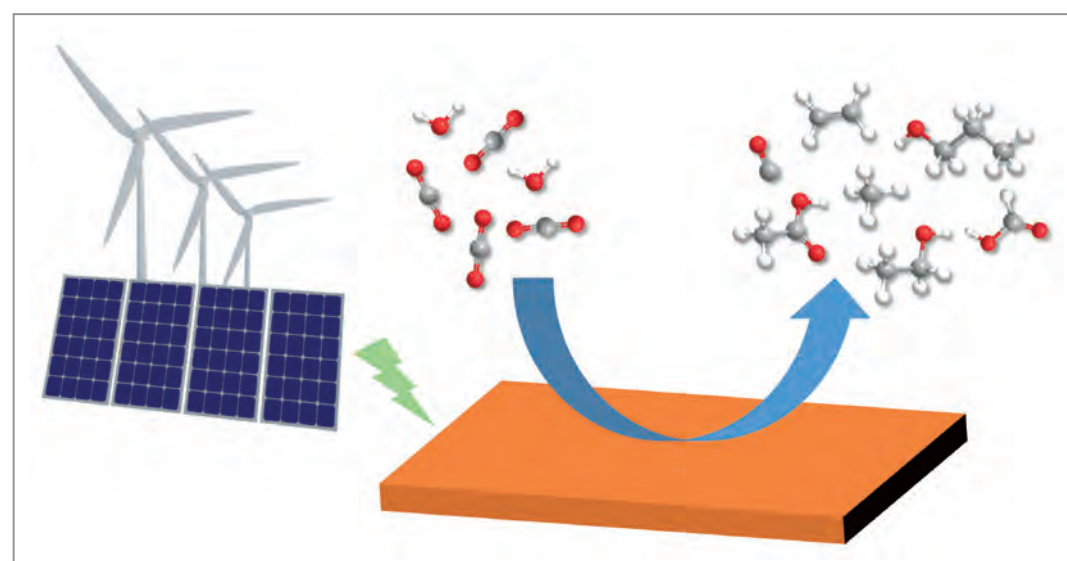


Figure 1
Carbon dioxide can be converted to valuable chemicals and fuels by electrochemical reduction in aqueous solutions using renewable energy. This process is an important component of a circular carbon economy (Credit: Jing Tian).

Darobactins: a very promising novel type of antibiotics

The new derivative D22 is highly effective against many resistant pathogens

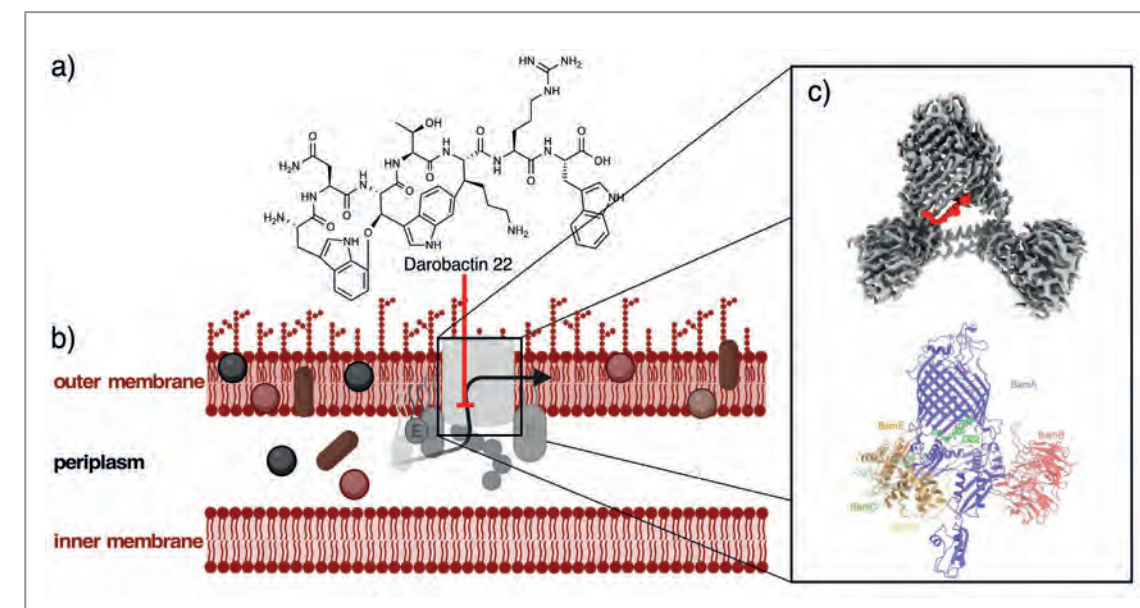
We are confronted with an escalating antibiotic crisis, primarily attributed to a slow pace of discovering and developing novel antibiotics still focusing on known compound classes attacking common targets. The severity of this issue contributed to approximately 1.27 million deaths in 2019. The Covid-19 pandemic, especially with bacterial co-infections, resulted in an alarming increase in mortality rates. Utilising cryo-electron microscopy (cryo-EM) in conjunction with a discovery pipeline for natural products, scientists at the Centre for Structural Systems Biology (CSSB) located at DESY and the Helmholtz Institute for Pharmaceutical Research Saarland (HIPS) jointly discovered darobactin D22, a novel and promising antibiotic with superior anti-microbial activity.

Darobactin is a natural antibiotic that fights off harmful Gram-negative bacteria. It is considered as a superhero in the world of antibiotics because it can defeat many difficult-to-treat antibiotic-resistant bacterial strains. What sets darobactin apart is its distinctive mechanism of action. Unlike other more traditional antibiotics, the bicyclic darobactin peptide targets the bacterial β -barrel assembly machinery (BAM), a system that is crucial for the integration and folding of many outer membrane proteins [1]. Darobactin mimics and occupies the binding site for signal sequences

for outer membrane protein integration essential for bacterial viability. As a consequence, darobactin prevents further bacterial growth including many pathogenic superbugs that cannot be killed otherwise due to their multi-drug resistance.

While initially, five natural darobactins have been reported, only Darobactin A (DA) could be isolated and its antimicrobial activity measured [2]. In an effort to establish a production platform, a prerequisite for subsequent comprehensive

Figure 2
Mode of action of D22. a) The structural elucidation of D22 with an up to 128-fold increased antibacterial activity. b) Schematic drawing of the BamA/B/C/D/E (BAM) complex sitting inside bacterial outer membrane. The red line indicates where D22 inhibits substrate assembly via the BAM complex. c) Cryo-EM density map of D22 (in red) bound to the BAM complex (top panel) with the structure model fitted in the density map with coloured BamA/B/C/D/E and D22 (bottom panel).



investigation, scientists adapted the darobactin biosynthetic gene cluster (BGC) in a heterologous expression system [3]. Further optimisation using a common lab strain of *E. coli* BL21 (DE3) suitable for large-scale industrial fermentation provided not only a cost-effective avenue to produce larger quantities but also enabled the production of a range of darobactin derivatives [3]. From the 21 novel darobactin derivatives (D1-D21) obtained, D9 exhibited an 8-fold enhanced antibacterial activity compared to DA against a broad spectrum of Gram-negative pathogens of laboratory strains and clinical isolates. Compared to the original DA, D9 was characterised by a substitution of the terminal phenylalanine with tryptophan [3]. Using cryo-EM, we were able to resolve the binding mechanism of D9 to the BAM complex. Based on these findings, we aimed to further improve the antibiotic by rational derivatisation and antimicrobial activity measurements.

Using this structure-activity-relationship approach, we determined the influence of amino acid substitution on antibacterial activity of position 4, 5, 6 and 7 and discovered D22 (Fig. 1). Compared to D9, the newly engineered D22 binds more tightly to the BamA and exhibits a 32-fold increased antimicrobial efficacy against several resistant bacterial strains, including clinical isolates of carbapenem-resistant *Acinetobacter baumannii*. Cryo-EM investigations provided important insights at the atomic level into the interaction between D22 and its target molecule, the BAM complex (Fig. 2). This observation is crucial in unravelling the precise mode of interaction, potentially leading to even further improvements in the future. Remarkably, in laboratory tests assessing antibacterial efficiency, D22 demonstrated no adverse effects on human cell lines *in vitro*; and *in vivo* experiments using a zebrafish larvae model revealed no detectable toxicity, raising optimism for eventual use in the medical treatment of humans.

The study underscores the potential of our structure-activity-relationship approach in advancing the development of novel antibiotics, offering a promising avenue in the ongoing efforts to combat antibiotic resistance.

Author contact:

Carsten Seyfert, carsten.seyfert@helmholtz-hips.de

Biao Yuan, biao.yuan@desy.de

References

1. H. Kaur, R. P. Jakob, J. K. Marzinek, R. Green, Y. Imai et al., 'The antibiotic darobactin mimics a β -strand to inhibit outer membrane insertase', *Nature* 593, 125–129 (2021).
2. Y. Imai, K. J. Meyer, A. Iinishi, Q. Favre-Godal, R. Green et al., 'A new antibiotic selectively kills Gram-negative pathogens', *Nature* 576, 459–464 (2019).
3. S. Groß, F. Panter, D. Pogorevc, C. E. Seyfert, S. Deckarm et al., 'Improved broad-spectrum antibiotics against Gram-negative pathogens via darobactin biosynthetic pathway engineering', *Chemical Science* 12, 11882–11893 (2021).

Original publication

'Darobactins exhibiting superior antibiotic activity by cryo-EM structure guided biosynthetic engineering', *Angew. Chem. Int. Ed.* 62, e202214094 (2023). DOI: 10.1002/anie.202214094



Carsten E. Seyfert^{1,2,3,4}, Christoph Porten^{1,2,3,4}, Biao Yuan^{5,6}, Selina Deckarm^{1,2,3,4}, Fabian T. Panter^{1,2,3,4}, Chantal D. Bader^{1,2,3,4}, Janetta Coetzee^{1,2,3,4}, Felix Deschner^{1,2,3,4}, Kamaledin H. M. E. Tehrani^{1,2,3,4}, Paul G. Higgins^{1,2,3,4}, Harald Seifert^{8,9}, Thomas Marlovits^{5,6,7}, Jennifer Herrmann^{1,2,3,4} and Rolf Müller^{1,2,3,4}

1. Helmholtz Institute for Pharmaceutical Research Saarland (HIPS), Microbial Natural Products, Saarbrücken, Germany
2. Helmholtz Centre for Infection Research (HZI), Braunschweig, Germany
3. Department of Pharmacy, Saarland University, Saarbrücken, Germany
4. German Centre for Infection Research (DZIF), Hannover-Braunschweig, Germany
5. University Medical Center Hamburg-Eppendorf (UKE), Hamburg, Germany
6. CSSB Centre for Structural Systems Biology, c/o DESY, Hamburg, Germany
7. Deutsches Elektronen-Synchrotron DESY, Hamburg, Germany
8. Institute for Microbiology, Immunology and Hygiene, Faculty of Medicine and University Hospital Cologne, University of Cologne, Köln, Germany
9. German Center for Infection Research (DZIF), Bonn-Köln (Germany)

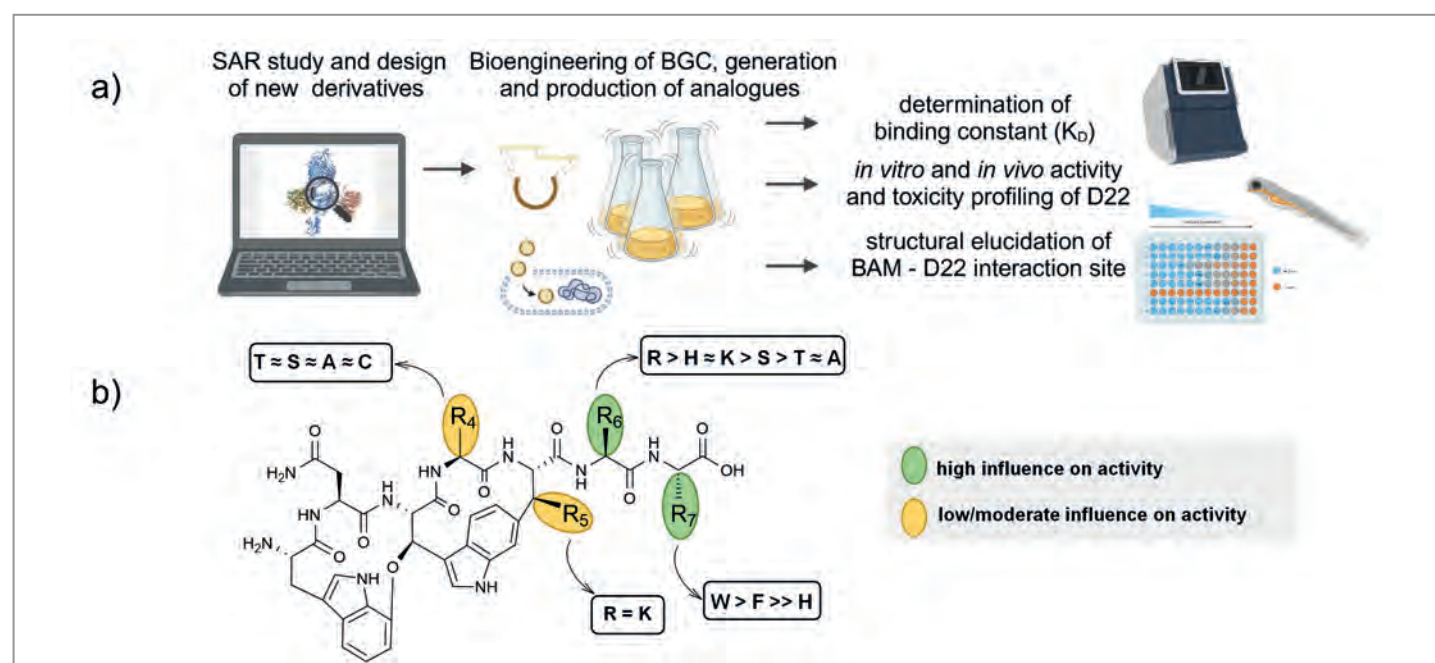


Figure 1
a) Workflow of the structure-activity-relationship (SAR) approach to generate highly active darobactin analogues. Starting by the structural determination of BamA-D9 interaction and an analysis of the docking site of darobactin at the BAM, novel derivatives were designed *in silico*, i.e. by computer simulation. Subsequently, bioengineering of the heterologous biosynthetic gene cluster (BGC) enabled the heterologous production and profiling of new derivatives, including D22.
b) D22 with exhibited positions with high or moderate/low influence on activity.

Effects of biodegradable implants on bone healing

Revealing dynamic multiscale processes in biodegradable bone implants

Bone and joint pathologies affect a growing number of people worldwide due to demographic changes towards an ageing society and increasing high-risk leisure activities. To avoid chronic pain or disabilities, adequate treatment of these pathologies is required. Magnesium-based alloys are increasingly researched as they are both biocompatible and biodegradable. As such, they can be placed into a bone for stabilisation during healing where they will degrade over time. No secondary surgery for implant removal is required. Thus, the development of new implant materials is a critical contribution to improved patient safety, reduced patient trauma and lowered costs for surgical intervention.

In contrast to titanium-based implants that are focused on longevity, magnesium-based implants are replaced with bone material over time, reducing their mechanical support continuously. Ideally, the degradation rate of biodegradable implants is tailored to match the healing rate of the bone. For this purpose, different alloying elements can be added to magnesium which modify the material's degradation dynamics [1]. A particular focus of the current research is to understand how these additives and the related changes

in material microstructure influence the degradation process. At the same time, the understanding of the bone response to the degrading implant needs to be improved. Bone is a dynamic material that undergoes continuous remodelling, depending on the mechanical and biochemical stresses exerted onto it. The cells that orchestrate the formation and removal of bone material are the osteocytes, which are housed in a connective, so-called 'lacuno-canalicular network' permeating the bone [2].

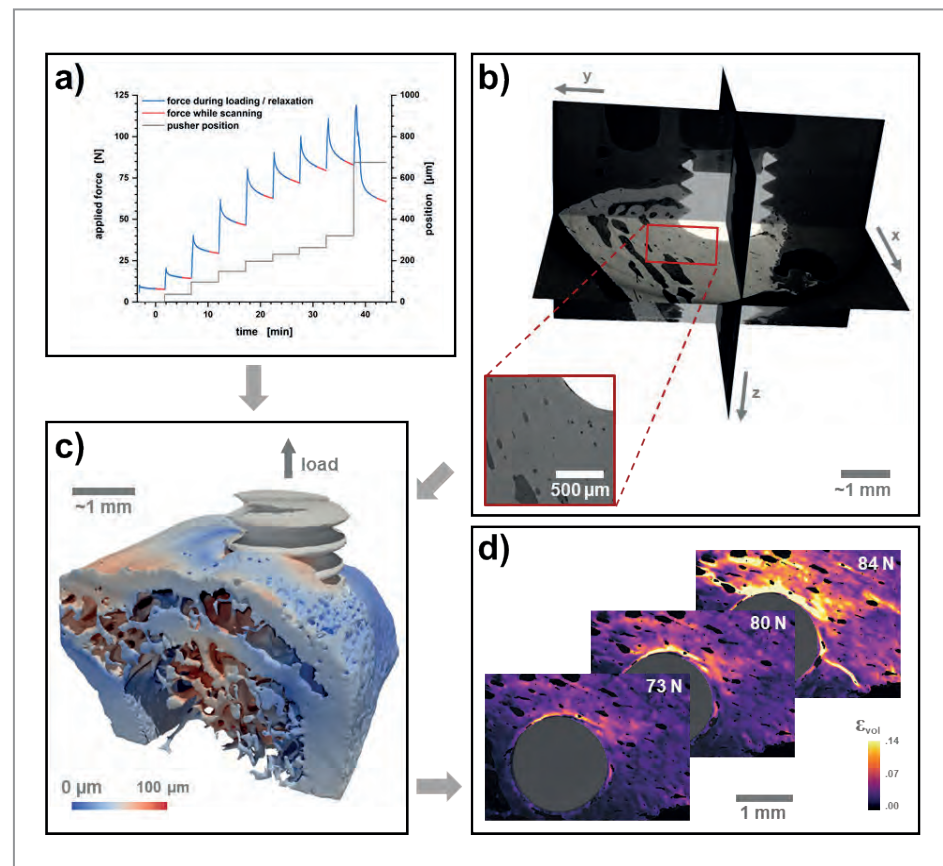
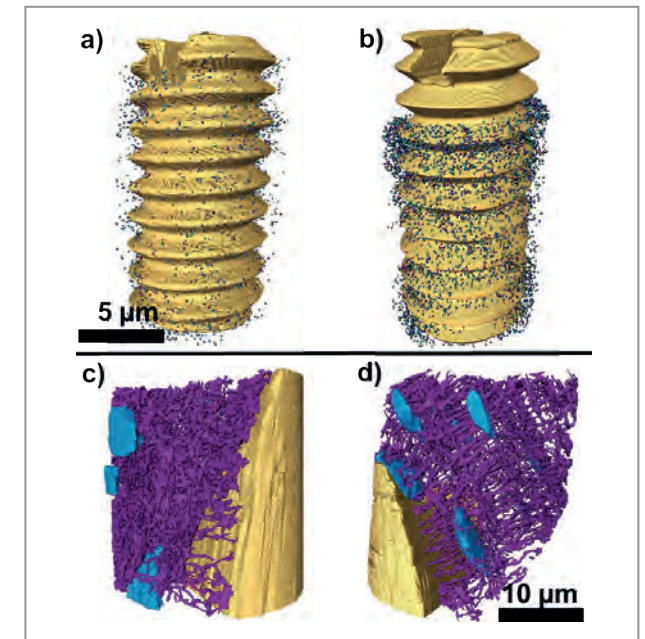


Figure 1
Illustration of the various information obtained from a push-out experiment that is combined with *in situ* μ -CT and strain analysis of a titanium bone implant by digital volume correlation. a) Applied force (blue/red line) and position of the actuator (grey line) during push-out test. b) Orthoslice view of a reconstructed bone-implant system illustrating immediate qualitative information obtained. The zoom-in shows blood vessels and osteocyte lacunae in the bone tissue. c) Rendering of the magnitude of the peri-implant bone deformation field obtained by digital volume correlation. d) Local strains and cracks in the bone are then accessible by image analysis as shown for an emerging longitudinal crack. A sequence of 2D slices displaying volumetric strain at increasing load is shown with highly strained regions, indicating fracturing, depicted in yellow. (Adapted from the original publication. Figures from the original publication are licensed under the Creative Commons Attribution 4.0 International License.)

Figure 2
a-d) Multiscale analysis: The lacunae density around the implant was lower for the a) magnesium-gadolinium alloy than for b) titanium while the morphology of the lacuno-canalicular network did not significantly differ between both (c,d). (Adapted from the original publication. Figures from the original publication are licensed under the Creative Commons Attribution 4.0 International License)



We employed synchrotron-radiation based (*in situ*) micro- and nano-computed tomography (μ /nCT) at the P05 imaging beamline at PETRA III in order to gain a more comprehensive picture of the impact of biodegradable magnesium-based implants on bone remodelling and formation.

The microstructural architecture of bone tissue in the vicinity of the implant plays a vital role in the distribution of strain energy and for implant stability. To understand this, we employed absorption contrast μ CT combined with *in situ* mechanical testing via sequential push-out tests (Fig. 1). The bone stability was quantitatively compared for different implant materials (titanium, polyetheretherketone (PEEK), biodegradable magnesium-gadolinium alloys) and healing periods (4, 8, 12 weeks). The acquired 4D load sequences were used to calculate strain maps and track bone deformations employing optical flow-based digital volume correlation (Fig. 1c,d). Bone morphological parameters are often expected to correlate with implant stability [3]. For the first time, it could be shown that these parameters vary with the implant material due to differences in the load transfer. Most evidently, with permanent implants from titanium and PEEK, bone tends to form a bulge at the implant site that is absent when biodegradable magnesium alloys were used.

Alloying magnesium with gadolinium alters the degradation rate and Young's modulus of the implant. Multi-scale imaging was used combining μ - and nCT with image-based fluid flow simulations to study the bone vascular porosity and the lacuno-canalicular network and to assess the impact of magnesium-gadolinium alloys on these in comparison to titanium implants [4]. Based on assessing the density of the lacunae, which are the pores in which the osteocytes reside, on the microscale, it could be deduced that the bone surrounding the titanium implants was more mature than that surrounding the magnesium-gadolinium implants. (Fig. 2a,b). Yet, the fluid flow dynamics within the lacuno-canalicular network remained unaffected due to a similar nanoscale morphology around both materials (Fig. 2c,d). These findings indicate that Mg-10Gd degradation affects the lacunar population rather than the lacuno-canalicular network morphology. In turn, this implies differences in bone remodelling dynamics around both materials. The results support the findings from the evaluated *in situ* mechanical tests that demonstrated that the bone-to-implant interface

of titanium implants can withstand higher loads during the early stages of bone healing in comparison to polymer-based implants or magnesium-alloys that require a longer healing period to approach comparable levels of stabilisation.

In the future, the correlation between bone maturity and implant degradation rate needs to be explored further. For this purpose, the development of computational tools based on correlative multi-scale and *in situ* imaging will be pivotal. The resulting digital twins will serve to accelerate the process of tuning material properties during development and are thus key to predicting and tailoring the biodegradation of magnesium alloys for medical applications.

Author contact: Stefan Bruns, sbruns@xnovotech.com
Sandra Sefa, sandra.sefa@hereon.de
Berit Zeller-Plumhoff, berit.zeller-plumhoff@hereon.de

References

1. N. Hort et al., 'Magnesium alloys as implant materials - Principles of property design for Mg-RE alloys', *Acta Biomater.* 6, 1714-1725 (2010).
2. L. Cardoso et al., 'Advances in assessment of bone porosity, permeability and interstitial fluid flow', *J. of Biomechanics* 46, 253-265 (2013).
3. M. Markezan et al., 'Is trabecular bone related to primary stability of miniscrews?', *Angle Orthod.* 84, 500-507 (2014).
4. S. Sefa et al., 'Multiscale morphological analysis of bone microarchitecture around Mg-10Gd implants', *Bioact. Mater.* 30, 154-168 (2023).

Original publication

'On the material dependency of peri-implant morphology and stability in healing bone', *Bioactive Materials* 28, 155-166 (2023). DOI: 10.1016/j.bioactmat.2023.05.006



Stefan Bruns¹, Diana Krüger¹, Silvia Galli², D. C. Florian Wieland¹, Jörg U. Hammel¹, Felix Beckmann¹, Ann Wennerberg³, Regine Willumeit-Römer¹, Berit Zeller-Plumhoff¹ and Julian Moosmann¹

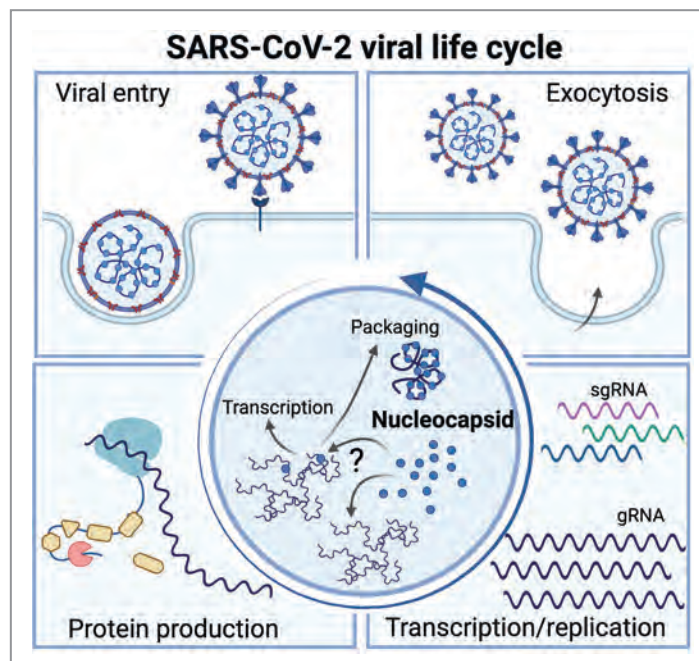
1. Helmholtz-Zentrum Hereon, Geesthacht, Germany
2. University of Malmö, Malmö, Sweden
3. University of Gothenburg, Gothenburg, Sweden

To grab or not to grab?

X-rays reveal specific recognition of own genome pieces by SARS-CoV-2

After the first cases of the Covid-19 disease outbreak in late 2019 caused by severe acute respiratory syndrome coronavirus 2 (SARS-CoV-2), coronaviruses have become the focus of worldwide attention. While seemingly new to the majority of people, coronaviruses have been part of evolution for a long time. A small number of variants have culminated in epidemics with more severe symptoms and numbers of deaths, among them the SARS-CoV crisis in the early 2000s, which appeared to be extremely lethal but much less infective than its current successor caused by SARS-CoV-2. Due to its high infectivity, the latter soon reached the rank of a pandemic with almost seven million deaths worldwide.

SARS-CoV-2 is highly transmissible (almost 800 million known infections), owing to its ability to escape immune responses and its efficient viral life cycle (Fig. 1). It enters (human) host cells by docking to cell surface receptors. Inside host cells, its large positive-sense genomic (g) ribonucleic acid (RNA) serves as a template for the immediate translation of viral proteins. Subsequently, the gRNA is replicated before new virions are assembled and released by exocytosis, being ready for the next infection cycle. A central protein involved in concerting genome translation and replication as well as the correct packaging of new genome copies into particles for viral egress is the Nucleo-



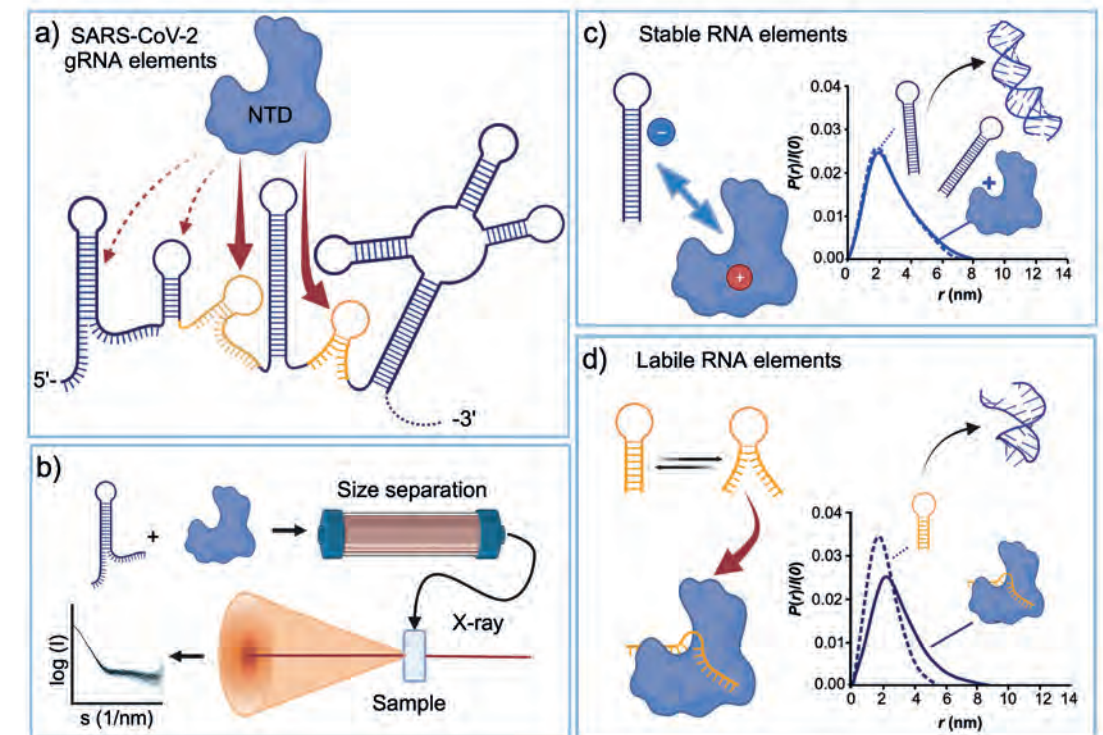
capsid protein (N) [1]. It seems plausible that N is capable of differentiating host and viral RNA, and moreover, that N can recognise specific viral genome stretches to activate distinct biological functions. Yet, the underlying mechanism remained largely unanswered despite mentionable effort and numerous N-related publications. Within coronaviruses, specific polynucleotide elements—mainly at the two ends of the genome—have evolved to act as switches or regulators for downstream processing of the RNA by viral proteins. These SARS-CoV-2 gRNA elements have been mapped precisely and rapidly by multiple labs in the world [2,3], although their role and mechanisms of action during the viral life cycle are still barely understood.

As the Nucleocapsid protein can bind to all kinds of RNAs and even DNA, researchers were left with the questions: What are the necessary elements that are recognised by N, and what are their characteristics? The authors of this study tried to reveal relevant RNA elements that might have important functions, e.g. for the correct packaging

Figure 1

The SARS-CoV-2 viral life cycle. Upon cell entry, the viral genomic (g)RNA is transcribed into subgenomic (sg)RNA and translated into the viral non-structural proteins. Subsequently, the RNA-dependent RNA-polymerase replicates gRNA before the formation of new virions and their release by exocytosis. During the viral life cycle, Nucleocapsid (N) protein plays a key role in both transcriptional regulation and genome packaging, for which the recognition of viral gRNA elements seems to be inevitable. The search for such elements at the P12 BioSAXS beamline of PETRA III revealed that N's RNA-binding domain (NTD) preferentially binds labile stem-looped viral RNAs. (Figure created using BioRender.com)

Figure 2
RNA-binding preferences of the NTD revealed by small-angle X-ray scattering (SAXS). a) Schematic representation of NTD's differential binding to SARS-CoV-2 gRNA elements. b) SEC-SAXS workflow at the P12 BioSAXS beamline. Separated, eluted fractions are subjected to the X-ray beam to obtain respective scattering profiles. c) The NTD interacts just weakly with stable RNA stem-loops, indicated by the unchanged SAXS-derived geometric parameters. d) Labile elements—existing in an opened/closed equilibrium at physiological temperature—are stably bound by the NTD and the SAXS-derived scattering pair-distance distributions, $P(r)$, confirm the selective complex formation. (Figure created using BioRender.com)



of the viral genome by N. Intending to answer these questions, they have used NMR spectroscopy applied to the most central RNA-binding domain of N called NTD, and found spectral patterns that correlate with a higher affinity among the tested gRNA elements. This enabled a robust prediction of specifically bound motifs as later proven to be elements suggested important for packaging by the lab of Nobel Prize winner J. Doudna [4].

Besides, researchers also identified novel gRNA binding elements, hitherto somewhat hidden in the genome. All elements seem to share a common characteristic: They are short RNA sequences that fold into a labile hairpin structure which can lose its structure at physiological temperature. This makes them accessible for interaction with the NTD. As the underlying dynamics and flexibility of this complex formation is challenging to capture with high-resolution structural biology techniques, researchers also used the unique strength of small-angle X-ray scattering (SAXS) applied to RNA—measured at the EMBL-P12 BioSAXS beamline on the DESY campus—to probe population-state RNA structures and viral-RNA element/N-protein complexes [5]. In combination with prior size-filtering (SEC-SAXS), protein-RNA mixtures are loaded on a chromatographic column, separating individual components from stable complexes.

In their experiments they found an unambiguous proof for selective complex formation with some of the SARS-CoV-2 regulatory RNA elements but not with others, as seen on the scale of full RNA-protein complexes under native-like conditions (Fig. 2). The N-protein thereby appears to distinguish between elements when they are provided as a mixture. Similar to the intra-viral situation, N still binds all

provided RNAs but only engages with functionally relevant ones in a stable, long-lived manner.

The findings are an important initial step to understand the atomic rules of coronaviral proteins interacting with the virus' own RNA at precise sites but not with the pre-available excess of irrelevant RNAs.

Author contact: Sophie M. Korn, smk2305@cumc.columbia.edu

References

1. Z. Bai, Y. Cao, W. Liu and J. Li, 'The SARS-CoV-2 Nucleocapsid protein and its role in viral structure, biological functions, and a potential target for drug or vaccine mitigation', *Viruses* 13, 1115 (2021).
2. A. Wacker, J. Weigand et al., 'Secondary structure determination of conserved SARS-CoV-2 RNA elements by NMR spectroscopy', *Nucleic Acids Res.* 48, 12415–12435 (2020).
3. C. Cao, Z. Cai et al., 'The architecture of the SARS-CoV-2 RNA genome inside virion', *Nat. Commun.* 12, 3917 (2021).
4. A. Syed, T. Taha, T. Tabata et al., 'Rapid assessment of SARS-CoV-2-evolved variants using virus-like particles', *Science* 374, 1626–1636 (2021).
5. J.-N. Tants and A. Schlundt, 'Advances, applications, and perspectives in small-angle X-ray scattering of RNA', *Chembiochem.* 24, e202300110 (2023).

Original publication

'The preference signature of the SARS-CoV-2 Nucleocapsid NTD for its 5'-genomic RNA elements', *Nature Communications* 14, 3331 (2023). DOI: 10.1038/s41467-023-38882-y



Sophie M. Korn^{1,2}, Karthikeyan Dhamotharan^{1,2}, Cy M. Jeffries³ and Andreas Schlundt^{1,2}

1. Institute for Molecular Biosciences, Goethe-Universität Frankfurt am Main, Frankfurt am Main, Germany
2. Center for Biomolecular Magnetic Resonance (BMRZ), Goethe-Universität Frankfurt am Main, Frankfurt am Main, Germany
3. European Molecular Biology Laboratory EMBL, c/o DESY, Hamburg, Germany

New insights into mRNA nanoparticles

A new instrument at EMBL's P12 beamline allows deeper insight into size-dependent properties of pharmaceutical nanoparticles

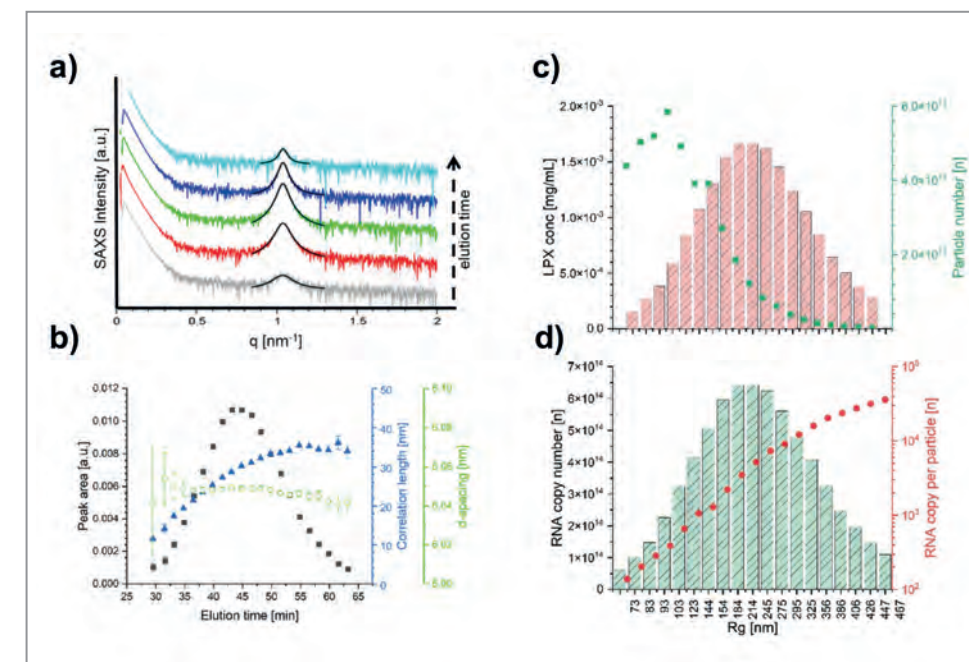
Since their successful application to combat the Covid-19 pandemic, lipid nanoparticles and messenger RNA (mRNA) have become familiar to both the scientific and public communities. Substantial activities are ongoing to develop further mRNA pharmaceuticals, spanning applications such as broader vaccination strategies and innovative approaches to cancer therapies. In all cases, the nanoparticles are essential for ensuring the effectiveness of the pharmaceutical products. At EMBL's bioSAXS beamline P12 at PETRA III [1], we have introduced a new instrument to investigate the properties of the nanoparticles in such nanomedicines, which allows better control of their quality. Other applications are in fields like toxicology or ecology where nanoparticles play a role.

Nanoparticle formulations in pharmaceutical products are used to protect the active molecules on their way to the target organs, reduce toxicity, and help to improve targeting selectivity and uptake by the right cells. While liposomes for delivery of small molecules for the treatment of cancer or fungal infections are early representatives of pharmaceutical nanoparticle systems, recently, messenger RNA (mRNA) as a pharmaceutically active molecule has gained great attention and is intended to be used for several types of pharmaceutical interventions [2]. The potential of mRNA therapeutics was underlined by its application in Covid-19 vaccines and with the Nobel Prize 2023 in medicine being awarded to Katalin Kariko and Drew Weissman for their discovery of the modified mRNA format, which was used in the vaccines. For pharmaceutical application of mRNA, which is a very large, highly charged bio-macromolecule, formulation into nanoparticles is indispensable.

One key challenge in the development of nano-pharmaceuticals is the control of the size and the size-dependent properties of the nanoparticles. These inherently exhibit a certain degree of variation in size, some can be a bit smaller, and others a bit larger than the average, a phenomenon known as 'polydispersity'. Changes in size can affect many quality characteristics of the nanoparticles, for example, how many drug molecules they contain or what their internal structure looks like. So far, it has been difficult to measure these size-dependent properties in polydisperse products. The pharmaceutical industry currently relies mostly on methods that yield only average values in their daily operations. This lack of precise control may have contributed to the limited adoption of nanoscaled products in clinical practice.

We have developed a new tool to better characterise nanoparticulate pharmaceutical products, to enable improved quality

Figure 2
Determination of quantitative size distribution profiles and derived parameters from joint analysis of different detector signals: a) SAXS patterns from the fractionated lipoplex nanoparticles at increasing elution times. Overall scattering intensity and Bragg peak characteristics were analysed. b) Lorentzian fits were used to determine the Bragg peak position (to calculate the d-spacing from Bragg's law), width (indicative for the correlation length) and area (as a measure for the amount of ordered material). c) Lipoplex concentration in mg/mL and number of particles as a function of size (using Rg from MALS). d) Total number of mRNA and mRNA copies per particle of size segment (red dots). (Credit: Figures adapted from original paper according to the Creative Commons license)



and safety assessments and foster the advancement of nanomedicines (Fig. 1). Our team has coupled a separation method, asymmetrical-flow field-flow fractionation (AF4), with small angle X-ray scattering (SAXS) measurements and used dedicated approaches for data analysis, applying our developed algorithms to match the information from the different detectors. The new instrument setup allows the quantitative determination of size-resolved structural and quality-related parameters in pharmaceutical nanoparticle products.

For proof-of-concept measurements we have chosen mRNA lipoplex nanoparticle formulations, as applicable for cancer immunotherapy [3]. With AF4, we separate free mRNA from the lipoplex nanoparticles and sort them according to their size (Fig. 1a) for investigation with the respective detection systems [4]. We use SAXS for determination of the structure and concentration of the size-separated fractions (profiles for discrete times are shown in Fig. 2a). By combining the information from X-ray (Fig. 2a-b) and light scattering (Fig. 1c), we construct new graphs (Fig 2c-d) which give the amount of material as a function of size. We also obtain the overall number of particles, the number of mRNA copies per particle, and other relevant information.

With our setup we are now able to quantitatively and comprehensively characterise all size fractions within pharmaceutical nanoparticle products. We obtain direct, quantitative size distribution profiles of the particles in combination with a number of different quality attributes, e.g. structure or drug load. Such data are highly relevant in pharmaceutical development particularly for assessing manufacturing processes and ensuring product quality. The method can be useful for setting up improved quality control procedures, evaluating manufacturing processes during develop-

ment, or investigating the comparability of products. Additionally, it finds applications in characterising nanoparticles for toxicological or environmental studies [5].

Author contact:
Melissa Gräwert, melissa.graewert@embl-hamburg.de
Heinrich Haas, haashein@uni-mainz.de
Peter Langguth, langguth@uni-mainz.de

References

- C. E. Blanchet et al., 'Versatile sample environments and automation for biological solution X-ray scattering experiments at the P12 beamline (PETRA III, DESY)', *Journal of applied crystallography* 48, 431-443 (2015).
- R. Tenchov et al., 'Lipid Nanoparticles From Liposomes to mRNA Vaccine Delivery, a Landscape of Research Diversity and Advancement', *ACS Nano* 15 (11), 16982-17015 (2021)
- L. M. Kranz et al., 'Systemic RNA delivery to dendritic cells exploits antiviral defence for cancer immunotherapy', *Nature* 534, 396-401 (2016).
- H. Haas, T. Bacic, J. Schumacher, 'Method for determining at least one parameter of a sample composition comprising nucleic acid, such as RNA, and optionally particles', WO2021009368A1 (2021).
- M. J. Huber et al., 'Physicochemical characterization and quantification of nanoparticles: applicability, limitations and complementarity of batch and fractionation methods', *Analytical and bioanalytical chemistry* 415, 3007-3031 (2023).

Original publication

'Quantitative size-resolved characterization of mRNA nanoparticles by in-line coupling of asymmetrical-flow field-flow fractionation with small angle X-ray scattering', *Scientific Reports* 13, 15764 (2023). DOI: 10.1038/s41598-023-42274-z

Melissa Ann Graewert¹, Christoph Wilhelmy², Tijana Bacic³, Jens Schumacher³, Clement Blanchet¹, Florian Meier⁴, Roland Drexel⁴, Roland Welz⁴, Bastian Kolb², Kim Bartels⁵, Thomas Nawroth², Thorsten Klein⁴, Dmitri Svergun^{1,5}, Peter Langguth² and Heinrich Haas^{2,3}

- European Molecular Biology Laboratory (EMBL), Hamburg Unit, Hamburg, Germany
- Department of Biopharmaceutics and Pharmaceutical Technology, Johannes Gutenberg-University, Mainz, Germany
- BioNTech SE, Mainz, Germany
- Postnova Analytics GmbH, Landsberg am Lech, Germany
- BIOSAXS GmbH, Hamburg, Germany

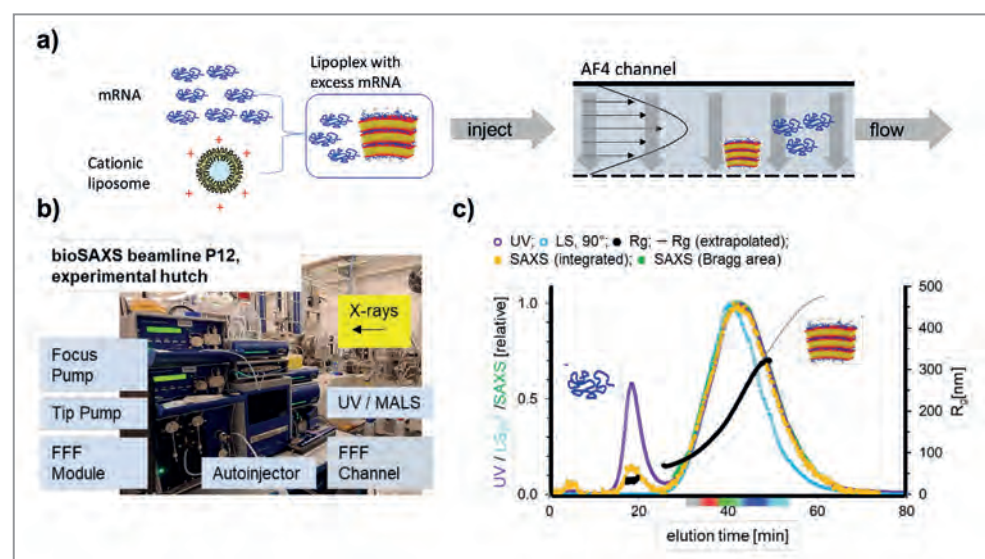


Figure 1
AF4-SAXS measurements at the bioSAXS beamline: a) Lipoplex formulations were self-assembled from cationic liposomes and excess mRNA to obtain lipoplex nanoparticles in coexistence with free mRNA [3], which were injected into the AF4 separation channel. b) Setup of the AF4 at the bioSAXS experimental station with in-line detection of ultraviolet light (UV) absorption, laser light scattering (MALS) and SAXS. c) AF4-SAXS analysis of a lipoplex formulation with an overlay of fractograms derived from UV, MALS, and SAXS including Rg values derived from MALS. Free mRNA (1st peak) and lipoplex nanoparticles (2nd peak) were successfully separated and quantified.

Titanium oxide for air and surface cleaning

A promising way to viral deactivation

Photocatalysis is widely recognised as a promising tool in the field of viral disintegration. Currently, a limiting factor for the efficient implementation of this technology are the slow reaction kinetics. Improving the efficiency of the catalyst by increasing the production of reactive oxygen species or enhancing surface adsorption via catalyst modification could be a key step. This means that fundamental surface science studies are required. This work focusses on the interaction of viruses with the catalyst surface and their subsequent photo-induced inactivation. We aim to prepare and deliver catalyst-based materials for wide-spread technological application and large-scale viral inactivation.

Among the possible transmission routes of viruses, indirect contact via contaminated surfaces of objects is a potential route. Depending on the environmental conditions, viruses can remain active on the various surfaces for minutes up to hours [1]. Therefore, design of highly efficient antiviral surface coatings using cost-effective and environmentally friendly materials for the control of surface transmission is crucial. In this applied study, we aim to tackle these challenges by chemically driven processes.

Titanium dioxide (TiO_2) has been widely used as antiviral surface or coating material and can be effectively applied in outdoor as well as indoor environments [2]. It serves as a potential catalyst for environmental applications, including air and water purification and self-cleaning materials [3]. As a photocatalyst, TiO_2 absorbs light and generates reactive oxygen species, which can inactivate microorganisms by oxidising organic compounds, converting them into harmless and non-toxic substances [3]. Notably, the efficiency of these processes can be enhanced through the surface modification of TiO_2 . It is crucial to investigate the role of the interface between the adsorbates and TiO_2 for a better understanding of the photo-reaction processes at the surface of TiO_2 .

Here, we loaded SARS-CoV-2 onto the surface of single crystalline $\text{TiO}_2(101)$ as a model system and subjected it to further inactivation using ethanol, heat and UV treatments. These surface disinfection methods deactivate the virus by the denaturation of the protein by damaging or destroying its ribonucleic acid (RNA).

To gain a deeper understanding of the molecular-scale morphology changes in adsorbed SARS-CoV-2 following the inactivation process, we utilised microscopic techniques. Our study demonstrates notable differences in the interaction of SARS-CoV-2 with $\text{TiO}_2(101)$ under UV (30 min UV irradiation, wavelength: 265 nm) and thermally (70 °C for 30 min) treated samples when compared to the sample inactivated through ethanol treatment (Fig. 1a-c). The AFM images reveal that the adsorbed viral particles were damaged by photocatalytic oxidation at the surface of TiO_2 and viral genome. The oxidation process induced changes in the morphology of the adsorbed viral particles, resulting in an increase in their diameter (Fig. 1c). Furthermore, we investigated changes in chemical composition of deactivated SARS-CoV-2 using hard X-ray photoelectron spectroscopy (HAXPES) at beamline P22 at PETRA III, DESY. These results

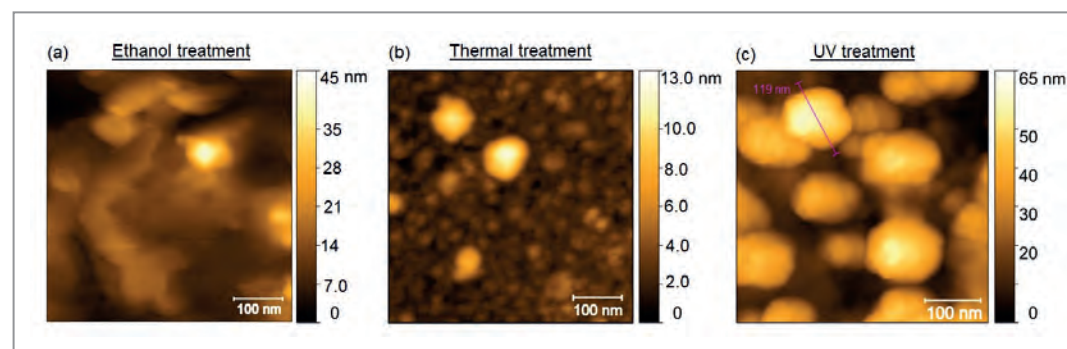
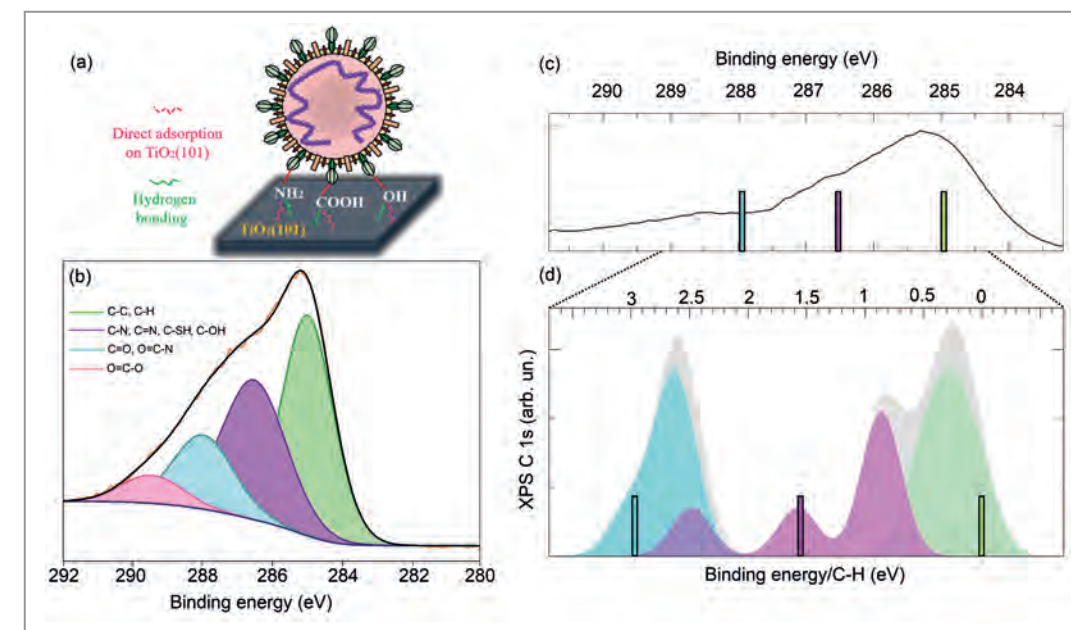


Figure 1
AFM images of adsorbed SARS-CoV-2 on the surface of $\text{TiO}_2(101)$ after a) ethanol, b) thermal and c) UV treatments.

Figure 2
a) Interaction of SARS-CoV-2 with the surface of $\text{TiO}_2(101)$.
b) C1s spectrum of adsorbed virus on the surface using HAXPES at P22 beamline at PETRA III.
c) Experimental C1s XPS spectrum and d) simulated C1s spectrum with individual components from inequivalent C atoms in virus proteins amino acids.



demonstrate that the viral proteins lose their activity due to the interaction of the amine ($-\text{NH}_2$), hydroxyl ($-\text{OH}$) and carboxylic ($-\text{COOH}$) groups in virus proteins with the surface of $\text{TiO}_2(101)$ (Fig. 2a-b). Additionally, in collaboration with researchers at Università degli Studi di Milano-Bicocca, the simulated core level spectra of C1s confirmed the interaction of viruses with the surface of $\text{TiO}_2(101)$ (Fig. 2d). Our investigations mark an important step in the development of efficient antiviral surfaces. Based on these results, we have the capability to modify the surface of the catalysts to enhance the adsorption and inactivation efficiency.

Furthermore, we studied the role of nanoparticles (NPs) in increasing the adsorption efficiency on $\text{TiO}_2(101)$. We successfully synthesised palladium (Pd) NPs with an average size of approximately 3-4 nm using physical vapor deposition in an UHV chamber at DESY NanoLab. After adsorbing SARS-CoV-2 onto the surface of this sample, we inactivated it by heating the sample to 70 °C. The AFM images recorded after annealing reveal a significant number of particles within the size range of 80-120 nm, corresponding to the viral particles. The presence of larger particles results from the interaction between the virus and Pd NPs, leading to the formation of a complex structure. We believe that the potential interaction between the spike proteins in virus and Pd NPs enhanced the adsorption efficiency of this sample when compared to the bare $\text{TiO}_2(101)$.

These results offer a deeper understanding of virus adsorption on solid materials which is crucial for designing TiO_2 -based self-cleaning materials. Nevertheless, achieving a complete oxidation of the virus at the surface is a requirement for efficient surface and air cleaning, and this aspect

is currently under investigation by researchers at the DESY NanoLab.

Author contact:

Mona Kohantorabi, mona.kohantorabi@desy.de
Heshmat Noei, heshmat.noei@desy.de

References

1. J. Hasan, A. Pyke, N. Nair, T. Yartagadda, G. Will, K. Spann and P. K. D. V. Yarlagadda, *ACS Biomater. Sci. Eng* 6, 4858–4861 (2020).
2. J. Prakash, J. Cho and Y. K. Mishra, *Micro. Nano. Eng* 14, 100100 (2022).
3. K. Hashimoto, H. Ire and A. Fujishima, *Jpn. J. Appl. Phys.* 44, 8269 (2005).

Original publication

'Adsorption and Inactivation of SARS-CoV-2 on the Surface of Anatase $\text{TiO}_2(101)$ ', *ACS Applied Materials & Interfaces* 15, 8770–8782 (2023). DOI: 10.1021/acami.2c22078



Mona Kohantorabi¹, Michael Wagstaffe¹, Marcus Creutzburg¹, Aldo Ugolotti², Satishkumar Kulkarni³, Arno Jeromin³, Tobias Krekeler³, Martin Feuerherd^{4,5}, Alexander Herrmann⁶, Gregor Ebert⁴, Ulrike Protzer⁴, Gabriela Guédez⁷, Christian Löw⁷, Roland Thuenauer^{8,9}, Christoph Schlueter¹⁰, Andrei Gloskovskij¹⁰, Thomas F. Keller¹¹, Cristiana Di Valentin², Andreas Stierle¹¹ and Heshmat Noei¹

1. Centre for X-ray and Nano Science CXNS, DESY, Hamburg, Germany
2. Dipartimento di Scienza dei Materiali, Università degli Studi di Milano-Bicocca, Milan, Italy
3. Electron Microscopy Unit, Hamburg University of Technology, Hamburg, Germany
4. Institute of Virology, Technical University of Munich/Helmholtz Munich, Munich, Germany
5. Division of Gastroenterology, Massachusetts General Hospital and Harvard Medical School, Boston, United States
6. Institute of Virology, Helmholtz Munich, Neuherberg, Germany
7. Centre for Structural Systems Biology CSSB, Deutsches Elektronen-Synchrotron DESY, EMBL Hamburg, Hamburg, Germany
8. Technology Platform Light Microscopy and Image Analysis (TPMIA), Leibniz Institute for Experimental Virology (HPI), Hamburg, Germany
9. Centre for Structural Systems Biology CSSB, Hamburg, Germany
10. Deutsches Elektronen-Synchrotron DESY, Hamburg, Germany
11. Department of Physics, University of Hamburg, Hamburg, Germany

A 40-year-old astrophysical riddle—literally resolved

X-ray lines can be confusingly broad

Very hot gases form the solar corona surround black holes and fill vast regions of space around galaxy clusters. Intense X-rays reveal their temperature, density and velocity. But for decades researchers have struggled with a problem: The measured and observed intensity ratios of some of the strongest soft X-ray spectral lines do not match those calculated, and casted doubt into the analysis of those hot plasmas. An international team led by the Max Planck Institute for Nuclear Physics in Heidelberg has solved this issue by serial experimental improvements and advanced calculations. From now on, X-ray data from space telescopes can be analysed with confirmed atomic models.

Ever since the Heidelberg scientists Bunsen and Kirchhoff invented spectral analysis in the year 1859, we have been using the light emitted by distant objects to study their composition. The colour also reveals their temperature: the hotter, the bluer. In space, most visible matter is so hot that atoms lose many of their electrons, become highly charged positive ions and emit mostly X-rays also carrying chemical fingerprints. Very strong soft X-ray lines are emitted by highly ionised iron which is abundant in the Universe. Fe¹⁶⁺ is known in astrophysics as Fe XVII (Fe I is neutral iron, Fe XVII indicates the loss of 16 out of 26 electrons) and is the brightest species over a wide range of temperatures.

In an X-ray spectrum, the positions of the lines encode both, the energies of the corresponding electronic transitions and the distance to the space sources from their redshift. The intensity ratios of line pairs allow for inferring plasma composition, temperature and density; their theoretical ratios need to be confirmed in the laboratory under specific conditions. For the prominent Fe XVII lines 3C and 3D, however, quantum mechanical calculations differed from both laboratory and astrophysical results by about 20 per cent. As this species is probably one of the most intensively observed, a theoretical problem was suspected [1].

A small but sophisticated device capable of producing very hot plasmas is the electron beam ion trap (EBIT). Its intense

beam hits atoms and ionises them. Not only that, but due to the electrons, the beam is rather negative and attracts positive ions strongly enough to trap them and allow them to be studied.

In early experiments, the spectra of Fe XVII were excited by electron collisions. The theory for this process uses approximations that physicists thought were the cause of the pesky discrepancy. Upon collisions, electrons are excited to many different high-energy electronic states from which they rain down to the ground state. An X-ray laser experiment with an EBIT at the novel free-electron laser LCLS in Stanford tried to fix this by selecting photon energies that excite only one state. The theory that predicts 'oscillator strengths', which determine how many excitations follow a given photon exposure, avoids approximations, and the 3C/3D ratio was expected to match it—but instead the results seemed to confirm the old discrepancy [2]. Analysis for unexpected influences showed that X-ray pulses from the LCLS were strong enough to distort the results. The same strength of the LCLS that made this first soft X-ray laser spectroscopy experiment possible, was also a problem. New experiments with weaker pulses were needed.

In 2020, a new attempt at the 3C/3D ratio with a compact EBIT at the P04 soft X-ray beamline (see Fig. 1) at PETRA III

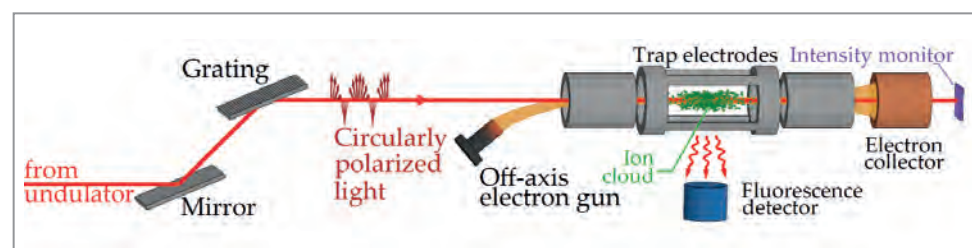


Figure 1 Experimental setup: An electron beam (orange) directed at the trap centre produces Fe XVII ions which are then excited only at very specific X-ray photon energies (red). When this happens, the ions quickly relax by re-emitting photons as fluorescence which is then registered by a silicon drift detector.

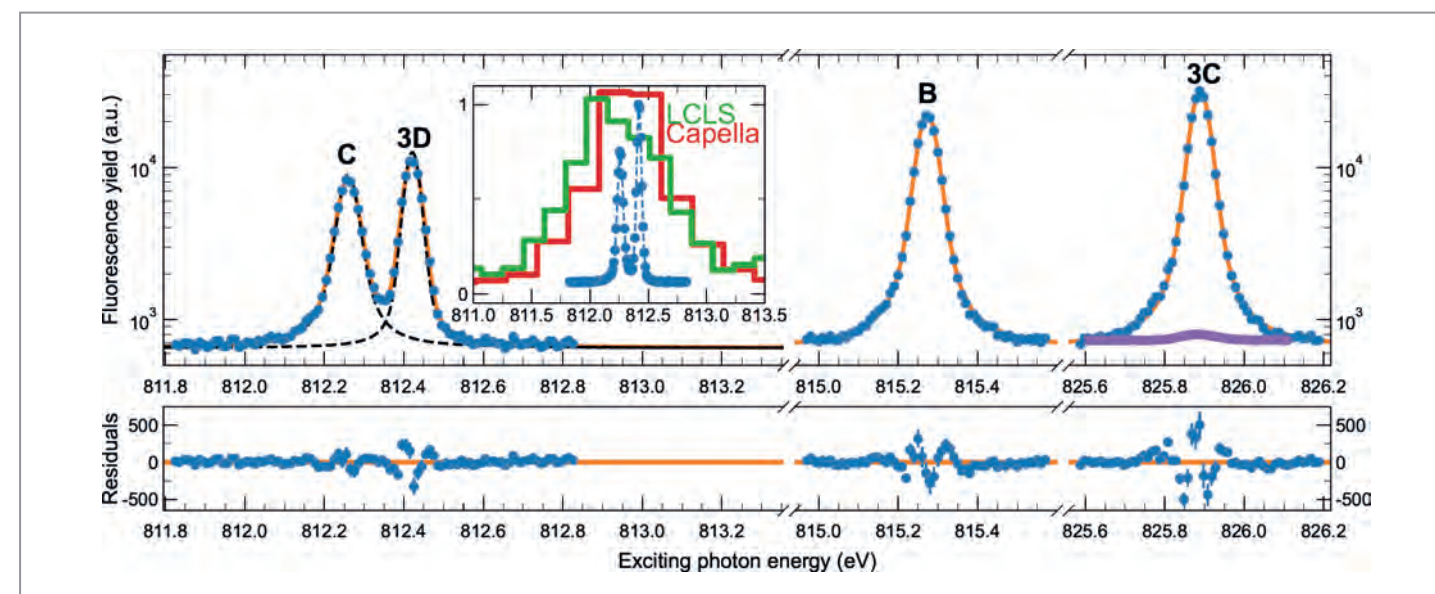


Figure 2 Fluorescence yield of the soft X-ray transitions 3C and 3D of Fe XVII and other lines of Fe XVI as a function of excitation photon energy. The greatly improved data quality compared to previous experiments (see inset and purple line) allowed us to model the natural line width and measure the correct 3C/3D intensity ratio.

brought a twenty-fold increase in spectral resolution at much weaker peak intensities of the exciting photon beam, thus eliminating the presumed cause of the problem. Alas, once again: The results moved in the right direction but the discrepancy remained while advanced calculations by the team gave much less reason to doubt the theory than in earlier work [3].

The PhD student in charge, Steffen Kühn and Chintan Shah, a postdoc, carefully prepared the next attempt. Instead of the intensity ratio, it was decided to directly measure the natural line width of each transition which depends on its oscillator strength. Since better resolution and statistics were needed, the team returned to P04 in 2022 after some homework that doubled the spectral resolution and reduced the noisy background by a factor of a thousand.

Finally, 3C and 3D now showed their natural line widths as well as their partly overlapping wide wings and subtle, unexpected diffraction effects (see Fig. 2). These previously hidden features had confused their true intensities. Now the results agreed with predictions. These were further improved to even include effects from the quantum electrodynamics of the 10-electron ion [4]. Perseverance and learning from past mistakes were the keys to success for the Heidelberg team and collaborators from NASA and the universities of Delaware and Erlangen. And the theorists of the team were beaming.

Benchmarking key calculations in the laboratory as accurately as in this work is essential before applying the theory to other species. Spectra from space telescopes can now be analysed with greater confidence. This is very good news for many astrophysicists working with the recently launched XRISM X-ray observatory and those preparing for the future international mission Athena.

Author contact: Chintan Shah, chintan.shah@mpi-hd.mpg.de
Steffen Kühn, steffen.kuehn@mpi-hd.mpg.de

References

1. G. V. Brown, 'A brief review of the intensity of lines 3C and 3D in neon-like Fe XVII', *Can. Jour. Phys.* **86**, 199–208 (2008).
2. S. Bernitt et al. 'An unexpectedly low oscillator strength as the origin of the Fe XVII emission problem', *Nature* **492**, 225–228 (2012).
3. S. Kühn et al., 'High resolution photoexcitation measurements exacerbate the long-standing Fe XVII oscillator strength problem', *Phys. Rev. Lett.* **124**, 225001 (2020).
4. S. Kühn et al., 'New measurement resolves key astrophysical Fe XVII oscillator strength problem', *Phys. Rev. Lett.* **129**, 245001(2022).

Original publication

'New measurement resolves key astrophysical Fe XVII oscillator strength problem', *Physical Review Letters* **129**, 245001 (2022).
DOI: 10.1103/PhysRevLett.129.245001



Steffen Kühn^{1,2}, Charles Cheung³, Natalia S. Oreshkina¹, René Steinbrügge⁴, Moto Togawa¹, Sonja Bernitt^{1,5,6,7}, Lukas Berger¹, Jens Buck⁸, Moritz Hoesch⁴, Jörn Seltmann⁴, Florian Trinter^{9,10}, Christoph H. Keitel¹, Mikhail G. Kozlov¹¹, Sergey G. Porsev¹², Ming Feng Gu¹², F. Scott Porter¹³, Thomas Pfeifer¹, Maurice A. Leutenegger¹³, Zoltán Harman¹, Marianna S. Safronova¹, José R. Crespo López-Urrutia¹ and Chintan Shah^{13,1}

1. Max-Planck-Institut für Kernphysik, Heidelberg, Germany
2. Heidelberg Graduate School of Fundamental Physics, Ruprecht-Karls-Universität Heidelberg, Germany
3. Department of Physics and Astronomy, University of Delaware, USA
4. Deutsches Elektronen-Synchrotron DESY, Hamburg, Germany
5. Institut für Optik und Quantenelektronik, Friedrich-Schiller-Universität Jena, Jena, Germany
6. Helmholtz-Institut Jena, Jena, Germany
7. GSI Helmholtzzentrum für Schwerionenforschung, Darmstadt, Germany
8. Institut für Experimentelle und Angewandte Physik (IEAP), Christian-Albrechts-Universität zu Kiel, Kiel, Germany
9. Institut für Kernphysik, Goethe-Universität Frankfurt am Main, Frankfurt am Main, Germany
10. Molecular Physics, Fritz-Haber-Institut der Max-Planck-Gesellschaft, Berlin, Germany
11. St. Petersburg Electrotechnical University (LETI), Saint Petersburg, Russia
12. Space Science Laboratory, University of California, Berkeley, California, USA
13. NASA/Goddard Space Flight Center, Greenbelt, Maryland, USA

X-rays illuminate the origin of life

Experiment captures ultrafast proton transfer between urea molecules in an aqueous solution

A cornerstone in theories about the emergence of life on prebiotic Earth are photoinduced reactions of urea. Through exposure to ionising radiation it is possible that urea in an aqueous solution produces malonic acid over multiple synthesis steps. In turn, this may have led to the creation of nucleobases as crucial building blocks of life [1]. Thus, the urea dimer is a key system for understanding the ultrafast chemistry at the origin of life. Here, we investigate femtosecond proton-transfer dynamics in ionised urea dimers in aqueous solution using table-top soft X-ray absorption spectroscopy with the aid of *ab initio* quantum-mechanical and molecular-mechanics (QM/MM) calculations.

In order to explore ionisation-induced dynamics of urea, we employ a pump-probe setup with a sub-micrometre-thin liquid flat jet containing an aqueous urea solution. A 400-nm pump pulse induces multiphoton ionisation in the sample, and a high-harmonics-based broadband soft X-ray pulse [2] is used to probe the sample at varying delay times.

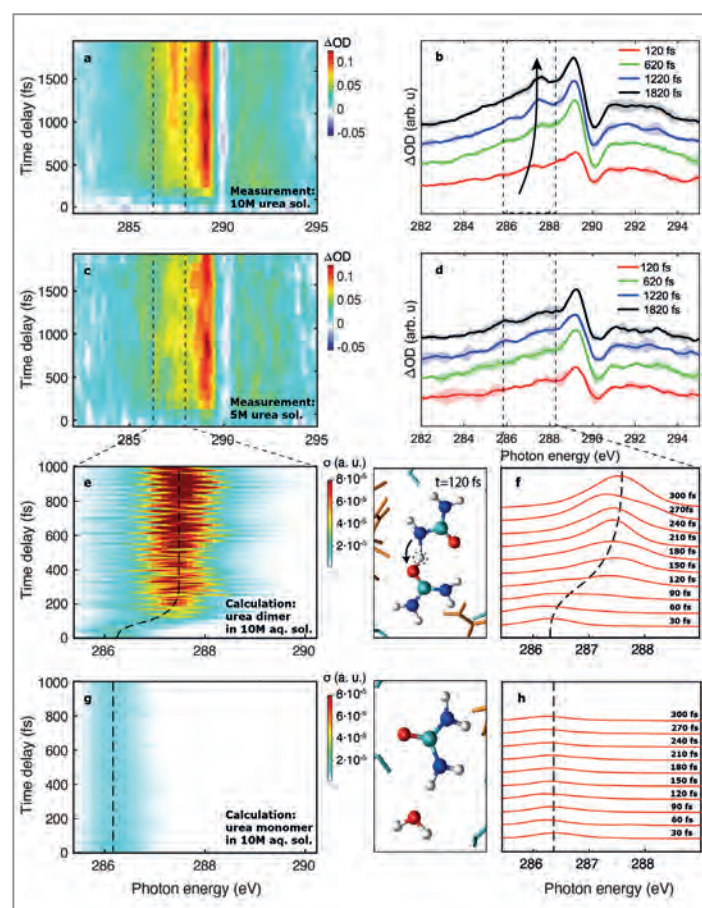


Figure 1 shows the time-resolved differences in the X-ray absorption spectra (XAS) near the carbon (C) K-edge for aqueous urea solutions with 10 M and 5 M concentrations. At both concentrations, the dominant features are a sharp depletion at 290 eV, corresponding to the $C1s \rightarrow \pi^*$ transition of the neutral urea molecule. The peak at 289 eV and the gradually increasing absorption feature from 285 eV to 289 eV are assigned to the $C1s \rightarrow \pi^*$ transition and $C1s$ to outer-valence vacancies of ionised urea molecules, respectively. The main difference between the results obtained with 10 M (Fig. 1a,b) and 5 M (Fig. 1c,d) solutions is the appearance of an additional absorption band in the 10 M data which shifts to a higher energy and simultaneously gains in intensity (arrow in Fig. 1b). The concentration dependence suggests that the additional band originates from urea molecules linked by hydrogen bonds to other urea molecules.

This feature can be identified using QM/MM calculations. To that end, the valence-ionisation dynamics of several urea monomer and dimer conformations were simulated and their time-resolved XAS spectra were calculated using the XMOLECULE toolkit [3]. After ionisation, we observe that a fraction of the trajectories representing urea dimers undergo a proton-transfer reaction, resembling the dynamics that was previously studied for a urea dimer in vacuum [4]. For the trajectories that undergo proton transfer, the calculated time-resolved XAS spectra in the region below

Figure 1 Transient carbon K-edge XAS results of 10 M or 5 M urea solutions (a–d) and a direct comparison with the QM/MM calculations after ionisation (e–h). Panels a, c, e, g show an overview of the results, and panels b, d, f, h show XAS difference spectra at selected time delays (specified in the legends).

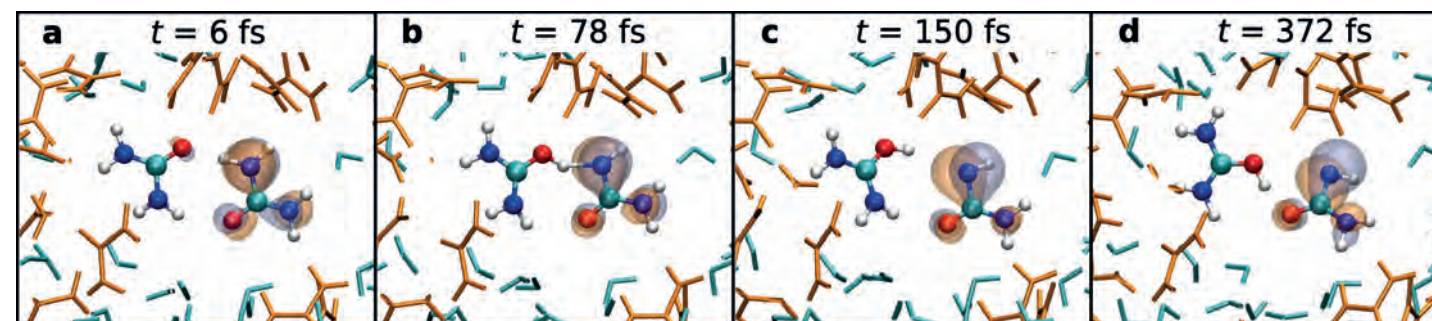


Figure 2 Snapshots from an exemplary QM/MM trajectory displaying proton transfer in the ionised urea dimer.

the pre-edge (highlighted in Fig. 1a–d by dashed lines) are shown in Fig. 1e,f, displaying both the increase of intensity and the energy shift as observed in Fig. 1b. The transient XAS spectra from trajectories that comprise a monomer with a hydrogen-bonded water molecule are shown in Fig. 1g,h. In contrast to the dimer simulations, those monomer–water simulations do not undergo proton transfer and accordingly the XAS spectra display almost no time dependence, supporting the lack of the additional feature at lower 5 M concentration in experiment (Fig. 1d). These comparisons establish proton transfer in the ionised urea dimer as the origin of the additional absorption band highlighted with the arrow in Fig. 1b.

Proton transfer is an emblematic case of strongly coupled electronic and nuclear dynamics. It is therefore interesting to explore the specific sensitivities of time-resolved XAS to such dynamics. Figure 2 presents snapshots from a QM/MM trajectory of the ionised urea dimer undergoing proton transfer. After ionisation, the electronic valence hole is localised on one of the urea molecules (Fig. 2a), which subsequently donates one of its protons to the neighbouring urea molecule (Fig. 2b), after which a rearrangement of the dimer geometry takes place (Fig. 2c,d). During this rearrangement, the valence hole, which initially has a vanishing density at the central C atom, develops a rapidly increasing amplitude near the carbon atom that maps into an increased X-ray absorption from the $C1s$ level.

Our findings reveal that ionisation of urea dimers leads to an ultrafast proton transfer from one urea molecule to its neighbour, rapidly followed by a rearrangement of the electron–hole density on the donating moiety. The produced radicals will trigger further reactions to create precursors of biomolecules. Future work can now be

envisaged to address the subsequent reaction steps to understand how nucleobases were being formed under prebiotic Earth conditions.

Author contact:

Ludger Inhester, ludger.inhester@cfel.de

Zhong Yin, yinz@tohoku.ac.jp

Jean-Pierre Wolf, jean-pierre.wolf@unige.ch

Hans Jakob Wörner, hwoerner@ethz.ch

References

1. C. M. Salván et al., 'Prebiotic origin of pre-RNA building blocks in a urea 'warm little pond' scenario', *ChemBioChem* 21, 3504–3510 (2020).
2. A. D. Smith et al., 'Femtosecond soft-x-ray absorption spectroscopy of liquids with a water-window high-harmonic source', *J. Phys. Chem. Lett.* 11, 1981–1988 (2020).
3. Y. Hao, L. Inhester, K. Hanasaki, S.-K. Son and R. Santra, 'Efficient electronic structure calculation for molecular ionization dynamics at high x-ray intensity', *Struct. Dyn.* 2, 041707 (2015).
4. Y. Shakyia, L. Inhester, C. Arnold, R. Welsch and R. Santra, 'Ultrafast time-resolved x-ray absorption spectroscopy of ionized urea and its dimer through *ab initio* nonadiabatic dynamics', *Struct. Dyn.* 8, 034102 (2021).

Original publication

'Femtosecond proton transfer in urea solutions probed by X-ray spectroscopy', *Nature* 619, 749–754 (2023).
DOI: 10.1038/s41586-023-06182-6



Zhong Yin^{1*}, Yi-Ping Chang^{2*}, Tadas Balčiūnas^{1,2*}, Yashoj Shakyia^{3,4*}, Aleksa Djorović², Geoffrey Gaulier², Giuseppe Fazio¹, Robin Santra^{3,4,5}, Ludger Inhester^{3,5}, Jean-Pierre Wolf² and Hans Jakob Wörner¹

* These authors contributed equally.

1. Laboratory of Physical Chemistry, ETH Zürich, Zurich, Switzerland
2. GAP-Biophotonics, Université de Genève, Geneva, Switzerland
3. Center for Free-Electron Laser Science CFEL, DESY, Hamburg, Germany
4. Department of Physics, Universität Hamburg, Hamburg, Germany
5. The Hamburg Centre for Ultrafast Imaging CUI, Universität Hamburg, Hamburg, Germany

Benchmarking fundamental light-matter interactions

Detailed measurement of non-linear two-photon excitations in helium

While the interaction of a single photon acting on a single electron is well understood, the problem of few photons interacting with few electrons is still an active area of research. In the process under investigation, two extreme ultraviolet (XUV) photons simultaneously excite both electrons of the helium atom. This drives the electrons into very large orbits around the positively charged nucleus; a highly correlated dance that is unstable as the electrons repel each other. Eventually, one electron escapes the atom. Measuring the angular distribution of the emitted electron provides a direct view into the highly correlated dynamics of the excited electrons.

In this process, the photons themselves transfer practically no momentum to the atom. Instead, they increase the energy of the electrons by their photon energy and transfer a discrete angular momentum. The surplus energy allows the electrons to leave the binding potential of the nucleus while the angular momentum dictates the electron's angular distribution. For the detailed measurement of this distribution, we used the reaction microscope (REMI) at the

beamline FL26 which can measure the three-dimensional momentum of each emitted electron [1]. The measurement of the momentum distribution allows us to reconstruct the dynamics of the two highly correlated electrons before ionisation.

The measurement of these non-linear events presents additional difficulties. First, a high intensity XUV light source is necessary to enable the simultaneous absorption of two photons. A sufficiently high incoming photon flux is provided by FLASH2, however, due to the way flashes of light get created at FLASH2 (the so-called SASE effect [2]), the photon energy as well as the intensity varies for each shot. This presents the second challenge: The excitation occurs only when the sum energy of the photons corresponds to the discrete excitation energy, i.e., the resonance condition is fulfilled (Fig. 1). The final obstacle is the one-photon events. Even when the FEL light is in two-photon resonance with the double excitation, this probability is still more than a hundred times smaller than that of one photon ionising the atom. Since the photon energy of the XUV light necessary for this reaction is above the helium ionisation threshold, a large background from single-photon ionisation will drown our photoemission signal.

Figure 1
a) Energy-level diagram of the two-photon process. b) Theoretical cross-section of the two-photon cross-section (blue). The insets show the calculated angular dependence of the non-linear excitation in blue compared to the linear (one-photon) one in red.

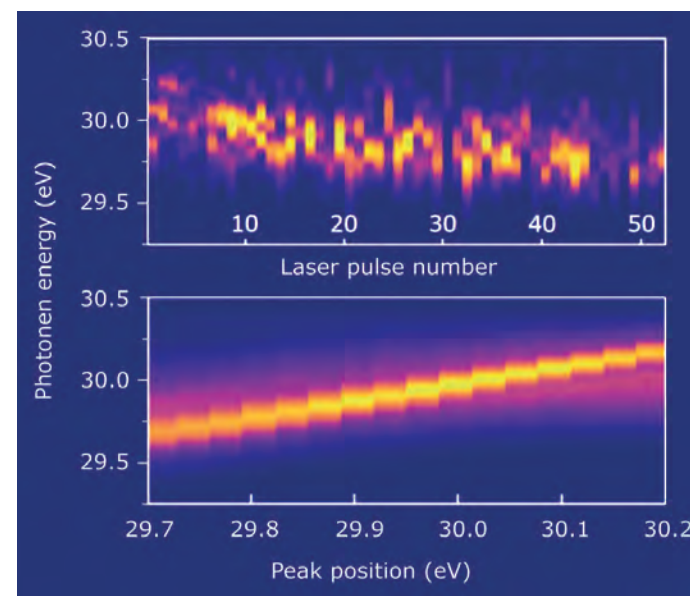
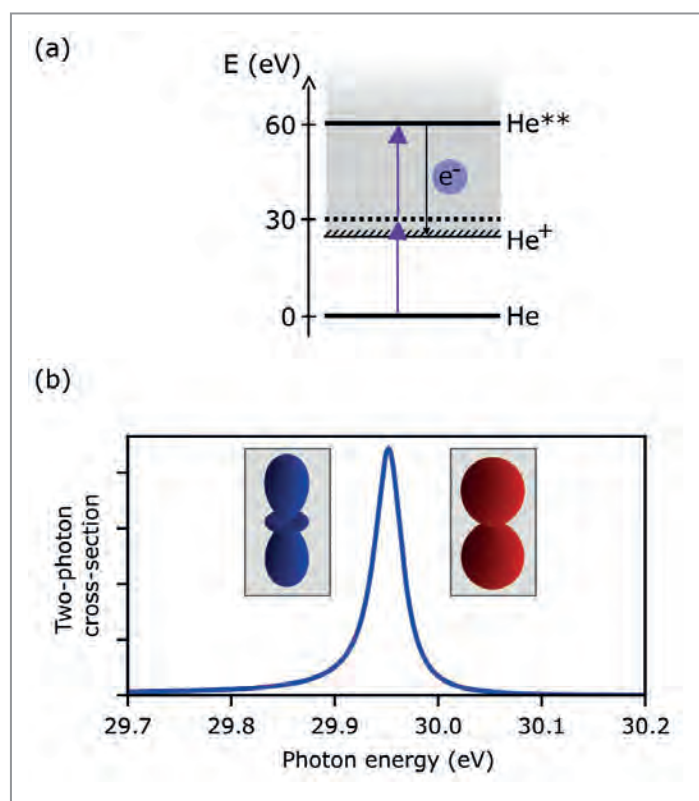


Figure 2
FEL spectra unsorted (upper panel) and sorted by their peak position (lower panel).

The challenges have been mastered by in-situ measuring the shot-by-shot FEL spectra with an online grating-based XUV photon spectrometer. This spectrometer has been specifically designed, employing the GOTTHARD detector [3] in order to be compatible with the high-repetition-rate burst-mode operation at FLASH. By sorting the FEL pulses based on the energy position of their most intense peak, we could effectively tune the FEL pulses digitally over the entire bandwidth (Fig. 2). Using this trick, a resonant and off-resonant scattering rates have been identified. Assuming that both rates have the same amount of linear one-photon events, subtracting the off-resonant background from the resonant signal results in a purely non-linear photoelectron angular distribution (Fig. 3). This detection scheme can generally be used to identify small yields of nonlinear two-photon processes in the presence of high-count rates of linear events.

In a direct comparison with state-of-the-art theory calculations [4], we found good agreement, although a slight discrepancy beyond the statistical uncertainty remained. A significant contribution may stem from the ~1% photon flux FEL second harmonic that has been present in the experiment. In principle, the single-photon ionisation has been subtracted, but an interference between the single-photon and two-photon ionisation has not been taken into account by the scheme. Considering this interaction, the calculated photoemission angular distribution significantly changes, approaching the experimental one. This creates exciting new prospects for coherent-control schemes using SASE-FEL pulses.

Author contact: Michael Straub, michael.straub@unige.ch

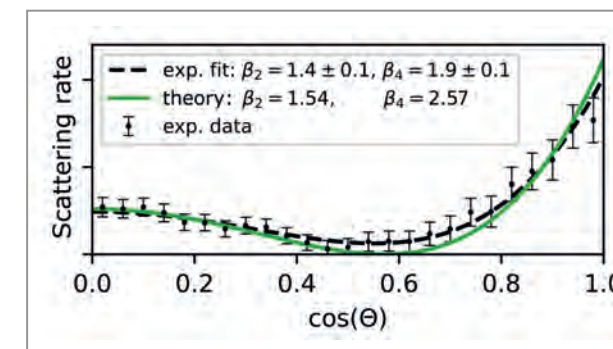


Figure 3
Comparison of theoretical and experimental angular distribution of photoelectrons. The experimental fit follows the photoemission angular distribution $\frac{d\sigma}{d\Omega} \propto 1 + \beta_2 P_2(\cos \theta) + \beta_4 P_4(\cos \theta)$ where P_n are the Legendre polynomials. The β -parameter can be directly compared to theory (plotted in green).

References

- G. Schmid, K. Schnorr, S. Augustin, S. Meister, H. Lindenblatt, F. Trost, Y. Liu, M. Braune, R. Treusch, C. D. Schröter, T. Pfeifer and R. Moshhammer, 'Reaction microscope endstation at FLASH2', *J. Synchrotron Radiat.* **26**, 854 (2019).
- T. Pfeifer, Y. Jiang, S. Düsterer, R. Moshhammer and J. Ullrich, 'Partial-coherence method to model experimental free-electron laser pulse statistics', *Opt. Lett.* **35**, 3441-3443 (2010).
- A. Mozzanica, A. Bergamaschi, R. Dinapoli, H. Graafsma, D. Greiffenberg, B. Henrich, I. Johnson, M. Lohmann, R. Valeria, B. Schmitt and S. Xintian, 'The GOTTHARD charge integrating readout detector: design and characterization', *J. Instrum.* **7**, C01019 (2012).
- Y. Wang and C. H. Greene, 'Two-photon above-threshold ionization of helium', *Phys. Rev. A* **103**, 033103 (2021).

Original publication

'Differential Measurement of Electron Ejection after Two-Photon Two-Electron Excitation of Helium', *Physical Review Letters* **129**, 183204 (2022). DOI: 10.1103/PhysRevLett.129.183204



Michael Straub¹, Thomas Ding¹, Marc Rebolz¹, Gergana D. Borisova¹, Alexander Magunia¹, Hannes Lindenblatt¹, Severin Meister¹, Florian Trost¹, Yimeng Wang², Steffen Palutke³, Markus Braune³, Stefan Düsterer³, Rolf Treusch³, Chris H. Greene², Robert Moshhammer¹, Thomas Pfeifer¹, and Christian Ott¹

- Max-Planck-Institut für Kernphysik, Heidelberg, Germany
- Department of Physics and Astronomy, Purdue University, West Lafayette, IN, USA
- Deutsches Elektronen Synchrotron DESY, Hamburg, Germany

Diamond rain and icy planets' magnetic field

Extreme conditions X-ray experiments watch for diamond formation in icy planets

At the extreme pressures and temperatures found inside icy planets, the methane found in their upper regions is converted to diamond and hydrogen. Using PETRA III beamline P02.2 and the European XFEL HED end station, an international team of scientists have made *in situ* time-resolved measurements of diamond formation from hydrocarbons. As the diamonds are denser than the surrounding ices, they will sink deeper into the planets, which provides an internal source of heating. The research sheds light on the process of 'diamond rain' occurring within these astronomical bodies, unveiling new insights into their internal dynamics and the generation of their magnetic fields.

The mantles of icy planets, such as Uranus and Neptune, consist of mixtures of small molecules, primarily water, methane and ammonia. Inside the planets, these are subject to extreme pressure and temperature and undergo remarkable changes. Under extreme conditions, water ice becomes

superionic – that is, the protons can move freely within the crystal lattice of oxygen atoms, and so it has high electrical conductivity [1]. Convection within a shell of conductive ice has been proposed as the origin of the complex magnetic fields observed for Uranus and Neptune [2].

Methane also undergoes reactions at high pressure and temperature. At milder conditions, below 10 GPa (100 kbar) or 2000K, it is converted to more complex hydrocarbons. At more extreme conditions, the hydrogen and carbon separate and diamond forms. The conditions at which this occurs are subject to disagreement between experiments using static and dynamic compression techniques.

Static compression is performed using diamond anvil cells. In these, the sample is held between the flattened tips of two diamonds which are pushed together to generate high pressure which can be maintained almost indefinitely. Diamond is observed in hydrocarbons which have been statically compressed above 10 GPa and heated over 2500 K [3]. An alternative route to extreme conditions is dynamic compression, in which a shockwave is driven into the sample. This offers access to higher pressure and temperature but only on 10 ns timescales. Diamond is observed in shocked hydrocarbons but not until much more extreme conditions above 160 GPa and 4000 K [4].

In this study, we investigated diamond formation from polystyrene, a hydrocarbon with formula $(C_8H_8)_n$. The precursor controls the ratio of carbon to hydrogen, but its chemical structure does not affect the reaction, as at high PT the bonds are short-lived and the original structure is lost prior to diamond formation [5]. The polystyrene was compressed using diamond anvil cells to pressures from 19 to 27 GPa and heated using high power X-ray pulses

from European XFEL which also served to probe the heated sample by X-ray diffraction. The unique 4.5 MHz pulse train at the EuXFEL HED instrument, with additional sample characterisation at PETRA III beamline P02.2, allowed the progression of the reaction to be followed *in situ*. A diagram of the experiment is shown in Fig. 1.

By taking a snapshot of the reaction every 220 ns, the process of diamond formation can be fully mapped, see Fig. 2. Initially, the black-body emissivity increases over about 10 μ s. This corresponds to the polystyrene breaking down into a fluid mixture of carbon and hydrogen. At later times, after 30 to 40 μ s, diamond is observed but only when the temperature is above 2500 K and only when it is sustained for at least this long. The result confirms that hydrocarbon demixing to form diamond and hydrogen occurs at lower pressure, as observed in previous laser-heated static compression studies [3] but takes at least 30 μ s to occur. As dynamic compression experiments only last 10 ns, they do not maintain the conditions for long enough for diamond formation at lower pressure.

The lower diamond formation pressure, compared to dynamic compression [4], places diamond formation at shallower depth within icy planets. The diamond formed is denser than the surrounding ice and so sinks under the influence of gravity, providing an internal heat source. The new results also place its formation above the conductive ice layer proposed to be responsible for their magnetic fields [2]. Plumes of diamond-rich material falling through these ices could play a role in driving the convection within them, which is required for the geodynamo.

Icy planets are also abundant beyond our solar system. Exoplanets with densities corresponding to icy compositions are common. The lower pressure required for diamond formation can be reached in the mantles of smaller planets, making the process more widespread. If the carbon becomes sequestered in a layer of diamond deep within them, their mantles will be carbon-depleted with implications for their formation, internal structures and potential astrobiology.

Author contact: Mungo Frost, mdfrost@slac.stanford.edu

References

- V. B. Prakapenka, N. Holtgrewe, S. S. Lobanov and A. F. Goncharov, 'Structure and properties of two superionic ice phases', *Nat. Phys.* **17**, 1233–1238 (2021).
- S. Stanley and J. Bloxham, 'Convective-region geometry as the cause of uranus' and neptune's unusual magnetic fields', *Nature* **428**, 151–153 (2004).
- H. Hirai, K. Konagai, T. Kawamura, Y. Yamamoto and T. Yagi, 'Polymerization and diamond formation from melting methane and their implications in ice layer of giant planets', *Phys. Earth Planet. Inter.* **174**, 242–246 (2009).
- D. Kraus, J. Vorberger, A. Pak, N. J. Hartley, L. B. Fletcher, S. Frydrych, E. Galtier, E. J. Gamboa, D. O. Gericke, S. H. Glenzer, E. Granados, M. J. MacDonald, A. J. MacKinnon, E. E. McBride, I. Nam, P. Neumayer, M. Roth, A. M. Saunders, A. K. Schuster, P. Sun, T. van Driel, T. Döppner and R. W. Falcone, 'Formation of diamonds in laser-compressed hydrocarbons at planetary interior conditions', *Nat. Astron.* **1**, 606–611 (2017).
- B. Cheng, S. Hamel and M. Bethkenhagen, 'Thermodynamics of diamond formation from hydrocarbon mixtures in planets', *Nat. Commun.* **14**, 1104 (2023).

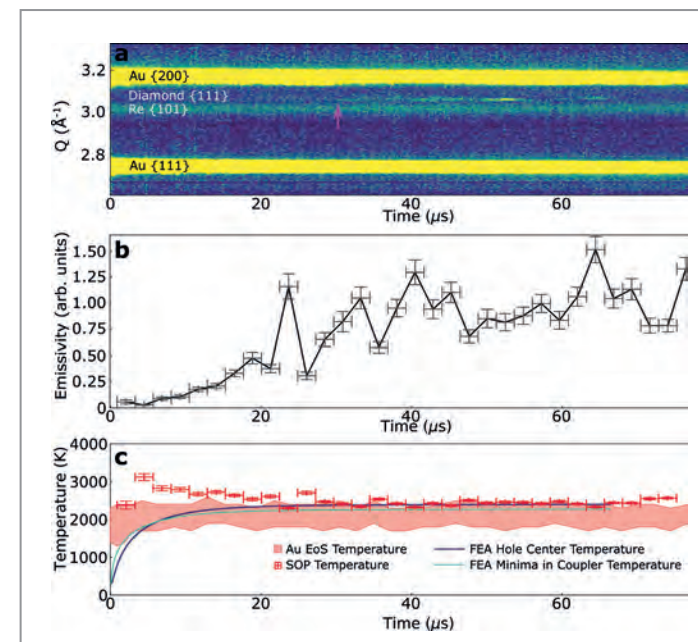


Figure 2

Time-resolved data taken on diamond formation at 20 GPa. a) Diffracted X-ray intensity in Q vs time. Yellow corresponds to high intensity. The pink arrow indicates the emergence of the diamond {111} reflection after 30 μ s. b) The relative emissivity as a function of time. The initial increase corresponds to darkening of the sample as the polystyrene breaks down into a fluid mixture of hydrogen and carbon. c) Temperature as a function of time shows reasonable agreement at 2500 K between the gold equation of state (EOS), spectrally resolved streaked optical pyrometry (SOP) and simulated finite element analysis (FEA).

Original publication

'Diamond Precipitation Dynamics from Hydrocarbons at Icy Planet Interior Conditions', *Nature Astronomy*, in press. DOI: 10.1038/s41550-023-02147-x



Mungo Frost¹, R. Stewart McWilliams², Elena Bykova³, Maxim Bykov⁴, Rachel J. Husband⁵, Leon M. Andriambariarijaona⁶, Saiana Khandarkhaeva³, Bernhard Massani², Karen Appel⁷, Carsten Baetz⁸, Orianna B. Ball², Valerio Cerantola⁷, Stella Chariton⁹, Jinhyuk Choi¹⁰, Hyunchoe Cynn¹¹, Matthew J. Duff², Anand Dwivedi⁷, Eric Edmund¹², Guillaume Fiquet⁶, Heinz Graafsma⁵, Huijeong Hwang¹³, Nicolas Jaisle¹⁴, Jaeyong Kim¹⁵, Zuzana Konôpková⁷, Torsten Laurus⁵, Yongjae Lee¹⁰, Hanns-Peter Liermann⁵, James D. McHardy², Malcolm I. McMahon², Guillaume Morard¹⁴, Motoaki Nakatsutsumi⁷, Lan Anh Nguyen¹⁵, Sandra Ninet⁶, Vitali B. Prakapenka⁵, Clemens Prescher¹⁶, Ronald Redmer¹⁷, Stephan Stern¹⁸, Cornelius Strohm⁵, Jolanta Sztuk-Dambietz⁷, Monica Turcato⁷, Zhongyan Wu¹⁵, Siegfried H. Glenzer¹ and Alexander F. Goncharov¹²

- SLAC National Accelerator Laboratory, Menlo Park, USA
- University of Edinburgh, Edinburgh, UK
- Universität Bayreuth, Bayreuth, Germany
- Universität zu Köln, Köln, Germany
- Deutsches Elektronen-Synchrotron DESY, Hamburg, Germany
- Sorbonne Université, Paris, France
- European XFEL, Schenefeld, Germany
- Helmholtz-Zentrum Dresden-Rossendorf (HZDR), Dresden, Germany
- The University of Chicago, Chicago, USA
- Yonsei University, Seoul, South Korea
- Lawrence Livermore National Laboratory, Livermore, USA
- Carnegie Institution for Science, Washington DC, USA
- Gwangju Institute of Science and Technology, Gwangju, South Korea
- Université Grenoble Alpes, Grenoble, France
- Hanyang University, Seoul, South Korea
- Albert-Ludwigs-Universität Freiburg, Freiburg, Germany
- Universität Rostock, Rostock, Germany
- X-Spectrum GmbH, Hamburg, Germany

'Hot spots' of radiation damage formed around aqueous metal ions

How X-rays cause excessive ionisation of water around metal ions

X-rays in biologically relevant systems can induce damage through direct impact or indirectly via radicals and low-energy electrons produced by water ionisation. It has been hypothesised that core-level ionisation of metal ions in solution triggers a series of ultrafast relaxation processes involving solvent molecules, ultimately leading to localised water ionisation. This study presents experimental and theoretical evidence confirming that solvated Al^{3+} ions undergo ultrafast relaxation through two-step electron-transfer-mediated decay (ETMD) processes. These processes result in the generation of slow electrons and multiple ionised water molecules in the immediate vicinity of the irradiated metal ion, forming distinct 'hot spots' of radiation damage.

As cells mostly consist of water, ionisation of water constitutes the primary source of reactive particles that indirectly damage biomolecules [1-2]. Metal ions have also been identified as key players in the process, as they have

higher photoionisation cross sections than water and are relatively abundant [3]. It is well known that the X-rays cause core ionisation of the ions, which then undergo ultrafast Auger-Meitner decay (see Fig. 1). The process leaves them with two extra positive charges, e.g., Al^{5+} is formed. This species is chemically unstable and prone to further decay. However, Al^{5+} ions cannot further decay by the Auger-Meitner process because they lack electrons in the valence shell. The ions have been suspected to decay non-locally, involving neighbouring water molecules. A complex relaxation scheme has been proposed [3] encompassing various non-local relaxation processes such as intermolecular Coulombic decay (ICD) and electron-transfer-mediated decay (ETMD) [3]. In these processes, neighbouring water molecules become ionised, and low-energy electrons can be ejected (see Fig. 1).

Using our experimental liquid-jet (photo-)electron spectroscopy setup EASI [4] at beamline P04 of DESY's synchrotron PETRA III, we searched for the spectral signatures of the decay processes, specifically for the low-energy electrons corresponding to the ETMD process for aqueous Al^{3+} ions. Our experimental setup is specialised on the detection of low-energy electrons and thus enabled to observe the rather weak ETMD features (see Fig. 2).

Figure 1

Core-ionised aluminium cations yield M^{n+2} ions which undergo a local Auger-Meitner decay and produce M^{n+1} ions. However, these ions cannot further decay locally and undergo electron-transfer-mediated decay (ETMD) involving surrounding molecules. The cascade involves two subsequent ETMD steps and leads to excessive water ionisation and formation of low-energy electrons in the vicinity of the metal ions.

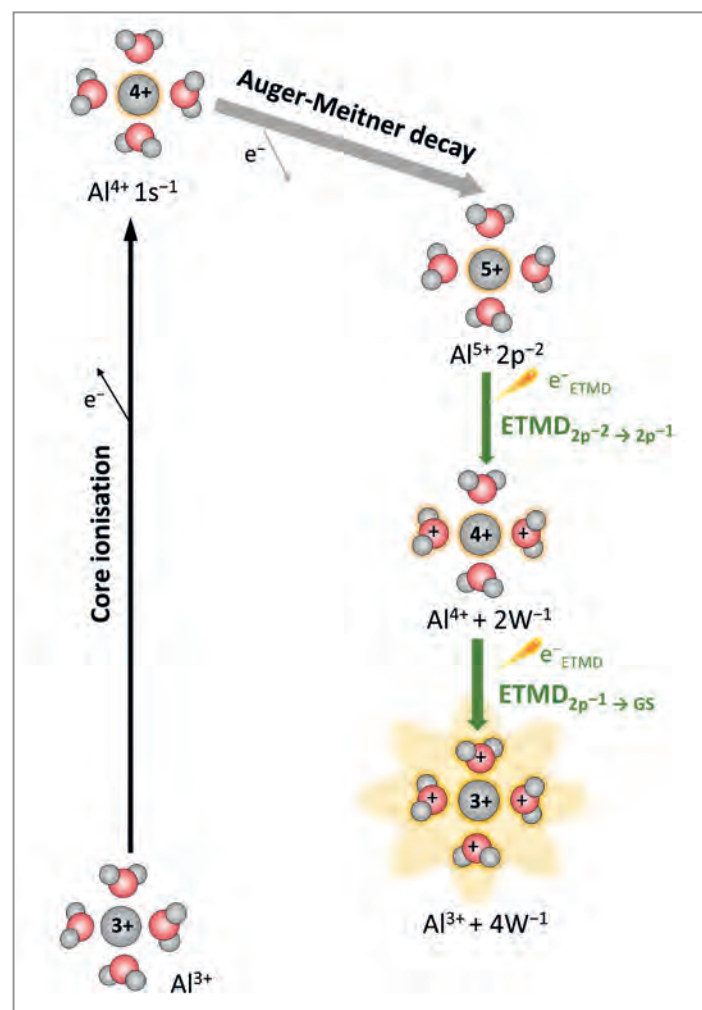
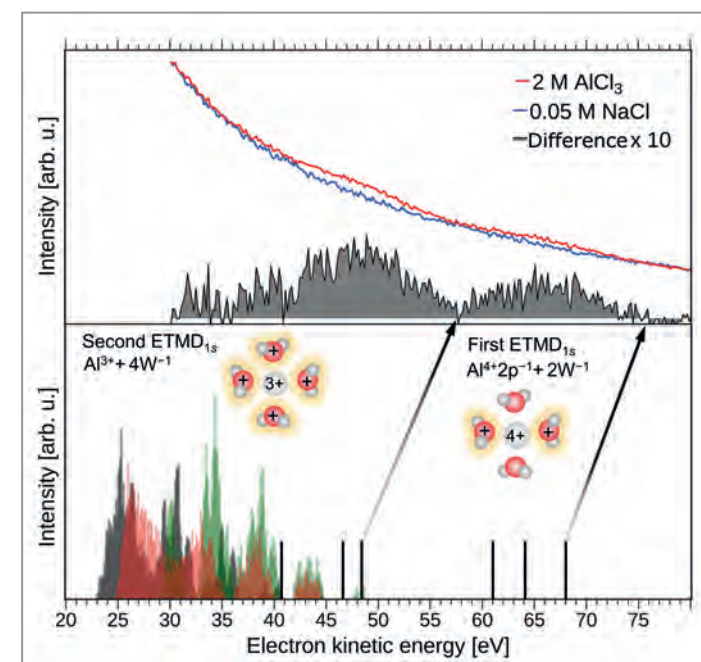


Figure 2
The upper panel shows the electron kinetic-energy spectrum of the ETMD signals of the Al^{3+} solution (red) after 1s ionisation together with the background measurement (blue) and the resulting difference spectrum (grey). The lower panel shows the histograms of calculated density of the ETMD final states for various multiplicities.



A crucial step was the measurement of a pure-water background for the comparison to a 2 M Al^{3+} aqueous solution. The difference spectrum yielded the ETMD features of the first and second decay steps.

The interpretation of the experimental data relied on the energy assignment of various electronic configurations of the Al ions. To pinpoint the specific ranges of electron kinetic energy of ETMD electrons, we performed simulations for small cluster models embedded in a polarisable environment.

By combining the experimental signals and theoretical spectra, we revealed the multiple-steps relaxation (see Fig. 1). In the beginning, the core-ionised ions relaxed via the Auger-Meitner process yielding Al^{5+} . Then a cascade of two ETMD steps followed (see Fig. 2). In the first step, Al^{4+} is formed, in the second step Al^{4+} is reduced back to the ground state Al^{3+} . In each of these two ETMD steps, up to two ionised water molecules and one low-energy electron (capable of ionising 3-5 nearby water molecules) are formed. A single core ionisation of the Al^{3+} ion may thus give rise to more than ten ionised water molecules!

Our results have important implications for the role of metal ions in radiation chemistry [3]. We show that the irradiation by X-rays does not cause arbitrary ionisation but rather an extensive and very localised water ionisation around the metal ions, e.g., we can talk about the formation of ionisation 'hot spots'. An obvious next step is to detect the formation of water ions and radicals and to quantify their production. Other important developments comprise extension of the studies to more biologically relevant ions and to deeper core levels important at higher photon

energies. It would also be highly interesting to follow the dynamics of the ETMD process on the femtosecond time scale with time-resolved spectroscopy using short-pulse light sources based on higher harmonic generation or free-electron lasers.

Author contact: Eva Muchová, muchovae@vscht.cz
Florian Trinter, trinter@fhi-berlin.mpg.de
Olle Björneholm, olle.bjorneholm@physics.uu.se.

References

1. L. Sanche, 'Beyond radical thinking' *Nature* 461, 358–359 (2009).
2. E. Alizadeh, T.M. Orlando and L. Sanche, 'Biomolecular damage induced by ionizing radiation: the direct and indirect effects of low-energy electrons on DNA', *Ann. Rev. Phys. Chem.* 66, 379–398 (2015).
3. V. Stumpf, K. Gokhberg and L.S. Cederbaum, 'The role of metal ions in X-ray-induced photochemistry', *Nat. Chem.* 8, 237–241 (2016).
4. S. Malerz et al., 'A setup for studies of photoelectron circular dichroism from chiral molecules in aqueous solution', *Rev. Sci. Instrum.* 93, 015101 (2022).

Original publication

'Radiation damage by extensive local water ionization from two-step electron-transfer-mediated decay of solvated ions', *Nature Chemistry* 15, 1408–1414 (2023).
DOI: 10.1038/s41557-023-01302-1



Geethanjali Gopakumar¹, Isaak Unger^{1,2}, Petr Slaviček³, Uwe Hergenhan⁴, Gunnar Öhrwall⁵, Sebastian Malerz⁴, Denis Céolin⁶, Florian Trinter^{4,7}, Bernd Winter⁴, Ian Wilkinson⁸, Carl Coleman^{1,9}, Eva Muchová³, Olle Björneholm¹

1. Uppsala University, Uppsala, Sweden
2. Deutsches Elektronen-Synchrotron DESY, Hamburg, Germany
3. University of Chemistry and Technology, Prague, Czech Republic
4. Fritz-Haber-Institut der Max-Planck-Gesellschaft, Berlin, Germany
5. MAX IV Laboratory, Lund, Sweden
6. Synchrotron SOLEIL, Paris, France
7. Goethe-Universität Frankfurt, Frankfurt am Main, Germany
8. Helmholtz-Zentrum Berlin für Materialien und Energie, Berlin, Germany
9. Center for Free-Electron Laser Science CFEL, DESY, Hamburg, Germany

Spatio-temporal scaling laws in a heated egg yolk

Time-temperature superposition in yolk

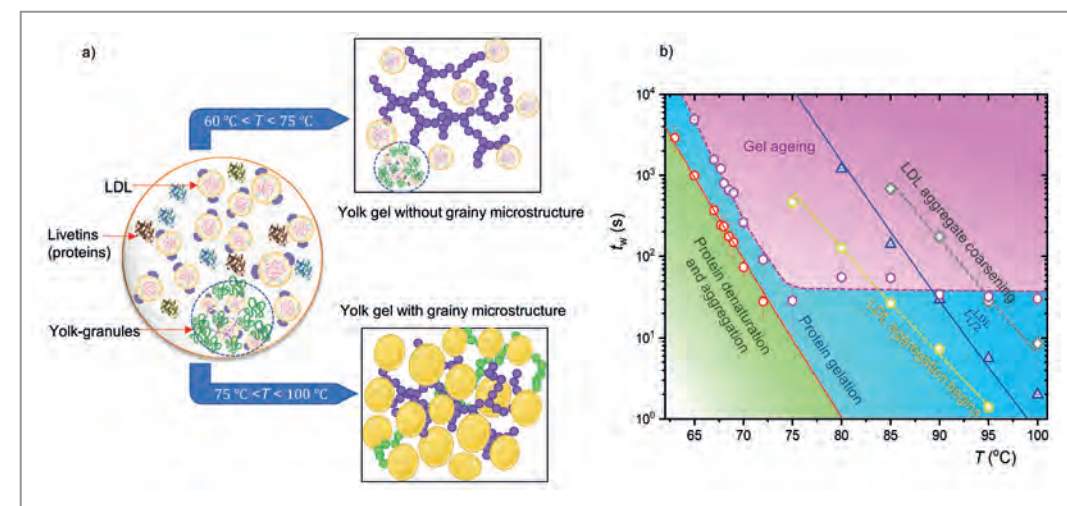
Denaturation, aggregation and gelation of proteins and lipids are biologically relevant out-of-equilibrium processes which are coupled by a hierarchy of length, time and energy scales [1,2]. Finding the characteristic scaling laws governing these processes on the relevant time and length scales is necessary to predict the changes of biomolecules to future time scales. Here, we use heated egg yolk as a model system to reveal the spatio-temporal relationships underlying these intricate processes for a wide range of time and temperature combinations.

The formation of macromolecular structures and their functionality in biological systems is a result of non-equilibrium processes driven by internal or external factors [3]. Since the structure and dynamics of non-equilibrium biological systems are continually evolving in a rather unpredictable way, the identification of universal scaling characteristics is necessary to tune and control these processes for various applications. However, the complexity of a multi-component protein sample and the need to experimentally monitor a large window of length and time scales simultaneously renders this task difficult.

To achieve this goal, we employ X-ray photon correlation spectroscopy (XPCS) in ultra-small angle X-ray scattering geometry at PETRA III beamline P10. Using XPCS, we

collect X-ray scattering movies of biomolecules in the egg yolk at low dose values for a wide length (≈ 50 nm to μm) and time scales (ms to hours). Temporal changes in the scattering patterns reveal the structural evolution of proteins and lipids in egg yolk, such as the sol-gel transition time t^* . The scattering invariant Q estimated from the scattering intensity shows two power-law regimes before and after the gelation of plasma proteins in the yolk as depicted in Fig. 1a. Simultaneously, a dynamical transition from power-law behaviour to exponential slow-down is observed with the same transition time t^* (Fig. 1b). The increase in τ by several orders of magnitude after t^* indicates the thickening of the solution to a gel phase. Similarly, at temperatures above 75 °C, the low-density lipoproteins (LDLs) in the yolk undergo a two-step

Figure 2
a) The schematic shows structural changes in egg yolk under heat induction. When heated to temperatures below 75 °C, only the proteins of the yolk plasma undergo gelation and form a protein gel network, whereas for $T > 75$ °C, fusion and aggregation of LDLs along with protein denaturation result in the formation of a grainy gel-microstructure. b) A master phase diagramme shows different non-equilibrium processes that occur when egg yolk is heated to temperatures in the range 63 – 100 °C.



aggregation process (Fig. 1c). Initially, LDLs show a reaction-limited aggregation mechanism (exponential scaling) which is followed by diffusion-limited aggregation (power-law scaling).

The scaling parameters (t^* and $t_{1/2}^{\text{LDL}}$) largely follow an Arrhenius temperature behaviour (insets in Fig. 1b,c). Thus, protein denaturation-aggregation-gelation and LDL aggregation follow Arrhenius-type time-temperature superposition (TTS) (master curves in Fig. 1). This implies identical mechanisms with temperature-dependent reaction rates.

The final microstructure of the heated yolk depends on the time-temperature combinations during heating. When the yolk is heated to temperatures below 75 °C, only the proteins of the yolk-plasma undergo gelation and form a protein gel network (Fig. 2a), whereas at higher temperatures (>75 °C), fusion and aggregation of LDLs along with protein denaturation result in the formation of a grainy gel microstructure (Fig. 2a).

Consolidating the data, a time-temperature phase diagramme of the non-equilibrium events in a thermally driven egg yolk is generated, as depicted in Fig. 2b. While the low temperature part of the phase diagramme is covered by protein denaturation-aggregation, gelation and ageing, the high temperature regime is more complex with multiple non-equilibrium events (protein gelation and LDL aggregation) occurring simultaneously. As most of the characteristic time scales are found to be temperature dependent, the onset of gel ageing time (pink hexagon in Fig. 2b) is temperature independent above 75 °C, indicating the presence of intrinsic time scales.

Our study is a good example of how *in situ* low-dose XPCS provides insight into the complexity of the processes in a

multicomponent heterogenous biological system. XPCS is thus also suitable for accessing biological molecules whose dynamics are fundamentally important for their understanding. There is plenty of scope for future studies in this area. These findings are not only relevant in food science and biomaterials but also benefit biophysics in understanding the denaturation and aggregation processes in dense protein-lipid mixtures, on lengths scales ranging from nano- to micrometres in time ranging from milliseconds to hours.

Author contact: Nimmi Das Anthuparambil, nimmi.das.anthuparambil@desy.de

References

1. R. Mezzenga et al. 'Understanding foods as soft materials', *Nat. Mater.* **410**, 729–740 (2005).
2. N. Begam et al. 'Kinetics of network formation and heterogeneous dynamics of an egg white gel revealed by coherent X-ray scattering', *Phys. Rev. Lett.* **126**, 098001 (2021).
3. X. Fang et al. 'Nonequilibrium physics in biology', *Rev. Mod. Phys.* **91**, 045004 (2019).

Original publication

'Exploring non-equilibrium processes and spatio-temporal scaling laws in heated egg yolk using coherent X-rays', *Nature Communications* **14**, 5580 (2023). DOI: 10.1038/s41467-023-41202-z



Nimmi Das Anthuparambil^{1,2}, Anita Girelli³, Sonja Timmermann², Marvin Kowalski², Mohammad Sayed Akhundzadeh², Sebastian Retzbach³, Maximilian D. Senft³, Michelle Dargasz², Dennis Guttmüller², Anusha Hiremath³, Marc Moron¹, Özgül Öztürk², Hanna-Friederike Poggemann³, Anastasia Ragulskaaya³, Nafisa Begam³, Amir Tosson², Michael Paulus⁴, Fabian Westermeier², Fajun Zhang³, Michael Sprung¹, Frank Schreiber³ and Christian Gutt²

1. Deutsches Elektronen-Synchrotron DESY, Hamburg, Germany
2. Department Physik, Universität Siegen, Siegen, Germany
3. Institut für Angewandte Physik, Universität Tübingen, Tübingen, Germany
4. Fakultät Physik/DELTA, Technische Universität Dortmund, Dortmund, Germany

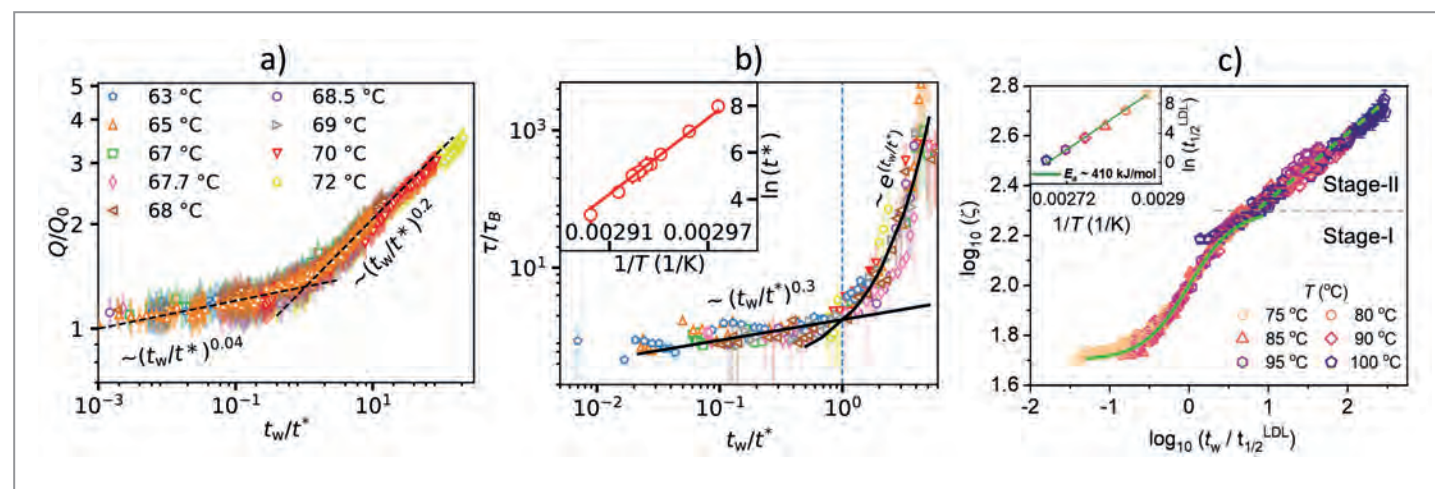


Figure 1
The normalised a) scattering invariant, Q and b) relaxation time, τ as a function of isothermal waiting time (t_w) normalised with respect to sol-gel transition time t^* . Here, Q_0 and τ_B are the scattering invariants at $t_w = 0$ and relaxation time of the system after equilibrated at the set temperature, respectively. b) has the same legends as a). The Arrhenius plot of t^* is shown in the inset of b). c) The logarithm of correlation length, ζ , of LDL aggregates as a function of t_w normalised with respect to characteristic time $t_{1/2}^{\text{LDL}}$. The green curve in stage-I and stage-II represent sigmoidal and power-law fits. The Arrhenius plot of $t_{1/2}^{\text{LDL}}$ is shown in the inset of c).

Charting the quantum landscape

European XFEL reveals exotic resonance structures of multiple-core-hole states via photon-energy scan

Understanding the interaction of intense, femtosecond X-ray pulses with heavy atoms is crucial for gaining insights into the structure and dynamics of matter. We investigated xenon atoms irradiated by high-intensity X-ray pulses, identifying exotic quantum states missing up to six electrons in their core electron shells. The unique capability of scanning the X-ray energy with high fluence over a wide range at the European XFEL combined with a dedicated computer programme for predicting X-ray-driven quantum behaviour was key to this observation. The results provide new insights into extreme light-matter interactions, which could improve the imaging of molecules or resolve unexplained observations in astrophysics.

When an atom is hit by a photon of sufficient energy, it can be ionised, leaving behind a positively charged ion with a hole in its electron shell. Depending on the photon energy, this electron originates from either a core or valence electron shell. The pulses generated by XFEL facilities are so intense that atoms or molecules can absorb more than one photon during the pulse, called 'multiphoton interaction'. The probability for this to happen increases nonlinearly with the X-ray fluence (the number of photons per unit

area). The higher the fluence, the more electrons can be ionised. In this way, it is possible to create an atom with multiple holes in its core electron shells. The X-ray photon energy and the fluence are thus the most influential parameters to define X-ray-matter interaction, and continuous tuning of the photon energy at FELs lays the groundwork for nonlinear X-ray spectroscopies at these facilities. However, scanning the photon energy while retaining a very high and stable photon fluence at FEL facilities is extremely challenging. Therefore, multiphoton light-matter interactions have only been investigated at very few selected photon energies.

In this work, we demonstrate how to overcome this bottleneck towards high-intensity nonlinear X-ray spectroscopy. Thanks to the special variable-gap undulators at the European XFEL, we could tune the photon energy over a wide range from 0.7 to 1.7 keV in the soft X-ray regime. The experiment has been performed at the 'Small Quantum Systems' SQS instrument. We irradiated xenon atoms, which have 54 electrons in their neutral state, with ultra-intense X-ray pulses leading to the ionisation of up to 41 electrons after multiphoton interaction. The resulting xenon ions were analysed via high-resolution time-of-flight spectroscopy, exhibiting an ion yield landscape as a function of charge state and photon energy (Fig. 1). We performed state-of-the-art theoretical calculations using the XATOM toolkit [1] and compared their results with the experimental data, showing good agreement. The mountains

Figure 1

Quantum landscape of highly charged xenon ions. Shown are ion charge state spectra up to Xe^{41+} recorded at photon energies between 0.7 and 1.7 keV.

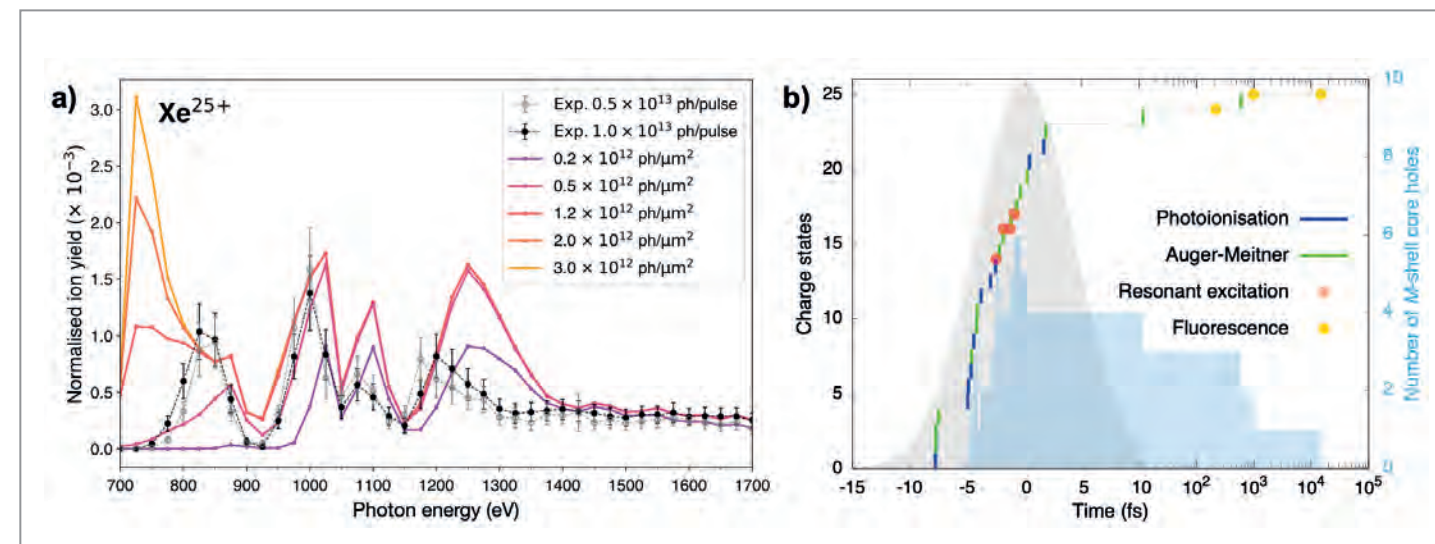
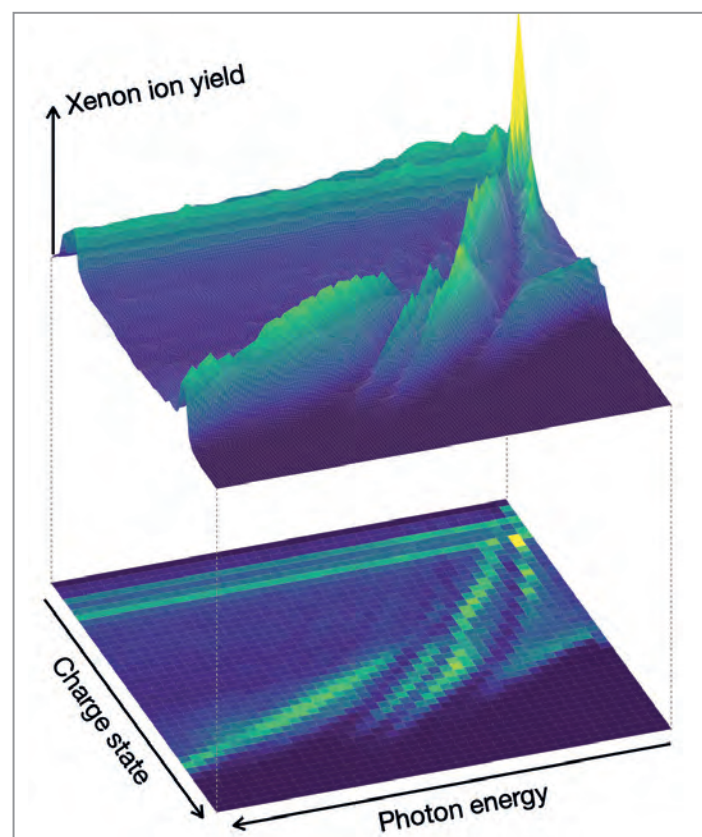


Figure 2

a) Experimental and theoretical resonance spectra for the charge state of +25 with various peak fluences. b) An exemplary ionisation pathway corresponding to the peak around 1200–1300 eV shown in a). The time evolution of the number of core holes is represented by the blue area and the x axis is on a logarithmic scale after 10 fs.

and valleys in the landscape are formed via resonance-mediated interactions that exclusively occur during intense XFEL pulses [2,3]. Moreover, our results unveil two other interesting aspects for the first time:

The first aspect is the fluence insensitivity of the spectra for a selected charge state to the peak fluence. Figure 2a shows a line cut of the resonance landscape recorded and calculated at different peak fluences for a charge state of +25. It is known that the shape of the ion yields at a fixed photon energy is sensitive to the applied peak fluence [2]. However, when the ion yields are collected at one selected charge state as a function of photon energy, their shape is no longer sensitive to the peak fluence once the fluence is high enough to saturate the production of the given charge state. This peak-fluence independence after a saturation point makes the resonance X-ray spectra, shown in Fig. 2a, robust and insensitive to small variations in experimental conditions and facilitates the unambiguous extraction of resonance features.

The second aspect is that we can observe rich structures in the landscape connected to transient resonances which are hidden in neutral atoms and only emerge during the complex charge-up process. When we have a detailed look into individual peaks, some of them are formed via massively hollow atoms [4] featuring as many as six simultaneous holes in their core electron shells. One exemplary ionisation pathway from our calculations is displayed in Fig. 2b, spotlighting the time evolution of extremely short-lived as well as unusually long-lived multiple-core-hole states.

Our study demonstrates that highly charged ions in exotic quantum states can be created and probed simultaneously with intense X-ray pulses, thus opening up new avenues

for X-ray-based techniques. For example, the unusual atomic species discovered in this study could also be formed through collisions in outer space, making them potential candidates to explain unidentified X-ray emission lines in astrophysics.

Author contact: Sang-Kil Son, sangkil.son@cfel.de
Rebecca Boll, rebecca.boll@xfel.eu
Aljoscha Rörig, aljoscha.roerig@xfel.eu

References

1. Z. Jurek, S.-K. Son, B. Ziaja and R. Santra, 'XMDYN and XATOM: versatile simulation tools for quantitative modeling of X-ray free-electron laser induced dynamics of matter', *J. Appl. Cryst.* **49**, 1048–1056 (2016).
2. B. Rudek et al., 'Relativistic and resonant effects in the ionization of heavy atoms by ultra-intense hard X-rays', *Nat. Commun.* **9**, 4200 (2018).
3. A. C. LaForge et al., 'Resonance-enhanced multiphoton ionization in the X-ray regime', *Phys. Rev. Lett.* **127**, 213202 (2021).
4. S.-K. Son, R. Boll and R. Santra, 'Breakdown of frustrated absorption in X-ray sequential multiphoton ionization', *Phys. Rev. Res.* **2**, 023053 (2020).

Original publication

'Multiple-core-hole resonance spectroscopy with ultraintense X-ray pulses', *Nature Communications* **14**, 5738 (2023). DOI: 10.1038/s41467-023-41505-1



Aljoscha Rörig^{1,2}, Sang-Kil Son³, Tommaso Mazza¹, Philipp Schmidt¹, Thomas M. Baumann¹, Benjamin Erk⁴, Markus Ilchen^{1,4,5}, Joakim Laksman¹, Valerija Music^{1,4,5}, Shashank Pathak⁶, Daniel E. Rivas¹, Daniel Rolles⁵, Svitozar Serkez¹, Sergey Usenko¹, Robin Santra^{2,3}, Michael Meyer¹ and Rebecca Boll¹

1. European XFEL, Schenefeld, Germany
2. Department of Physics, Universität Hamburg, Hamburg, Germany
3. Center for Free-Electron Laser Science CFEL, DESY, Hamburg, Germany
4. Deutsches Elektronen-Synchrotron DESY, Hamburg, Germany
5. Institut für Physik und CINSA, Universität Kassel, Kassel, Germany
6. J. R. Macdonald Laboratory, Department of Physics, Kansas State University, KS, USA

Resonant X-ray excitation of the nuclear clock isomer ^{45}Sc

Promising potential for a novel atomic clock

Using the European XFEL, an international team of researchers succeeded in exciting the sharpest atomic transition in the hard X-ray range, which is the 12.4 keV nuclear resonance of the stable isotope scandium-45. With its extremely narrow natural linewidth of 1.4 feV, it has the potential to become the most accurate nuclear clock ever. This has immediate applications for extreme metrology, in particular for research linked to the foundations of physics, such as time variations of the fundamental constants, the search for dark matter as well as probing the foundations of relativity theory.

So far, the primary timekeeping standard, also used for defining the SI unit of time, is based on an atomic transition in the well-established caesium-133 atomic clock, providing a relative uncertainty of 10^{-16} , corresponding to one second in 300 million years. The accuracy of an atomic clock is important because the smaller the error in time measurement, the smaller the error in distance measurements which enables, for example, high-precision GPS and many more applications in precision metrology.

A further increase in precision is expected from clocks that use an excited level of an atomic nucleus instead of an atomic shell transition. The atomic nucleus is about ten thousand times smaller than the electron shell and therefore much less susceptible to electromagnetic perturbations. The best-known candidate for a nuclear clock so far, the 8.3 eV level in the nuclear isomer thorium-229, exhibits such a narrow resonance line so that building a nuclear clock with an accuracy of 10^{-19} could be within the realm of possibility [1,2].

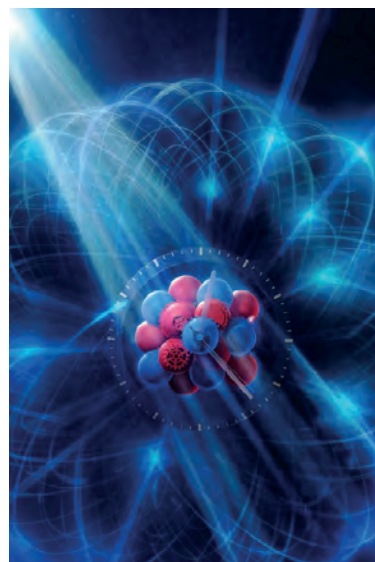


Figure 1

An artist's rendition of the excitation of the nuclear clock isomer scandium-45. X-rays from the European XFEL illuminate the nucleus to populate its 12.4 keV first excited state. In the subsequent decay the excitation energy is transferred to an electron of the K-shell, eventually leading to the emission of delayed K-fluorescence radiation as a witness of the nuclear excitation. (Credit: European XFEL/Helmholtz Institute Jena, Tobias Wüstefeld/Ralf Röhlsberger)

Along with the search for ever more precise transitions comes the challenge to find suitable radiation sources to excite such extremely narrow resonance lines. This is needed to couple the resonant transition to a light source that could then be stabilised by using the resonant signal from the clock atom. While this is comparatively easy for optical wavelengths due to the availability of powerful optical lasers, it is getting more difficult the higher the transition energy becomes. This is the case when nuclear levels are considered for atomic clocks. With the availability of self-seeded X-ray free-electron lasers (XFELs), narrow-bandwidth nuclear resonances in the regime of hard X-rays come into reach as candidates for a nuclear clock.

The most promising case is scandium-45 with a transition energy of 12.4 keV, an excited-state lifetime of 0.47 seconds and a resonance linewidth of 1.4 feV which would enable a temporal accuracy of one second in 300 billion years (10^{-19}). Scandium-45 is a stable isotope with a natural abundance of 100% which is readily available as ultrapure scandium metal foil or scandium oxide. These facts render scandium-45 superior to all other candidates for a nuclear clock.

The scientific potential of the scandium-45 resonance and proposals for its implementation were already formulated more than 30 years ago [3]. When the European XFEL recently began to operate in the so-called self-seeding mode at energies of hard X-rays [4], it could provide pulse trains of 12.4 keV X-rays with sufficiently high spectral density and a temporal pulse pattern well suited for the detection of nuclear decay products from excited scandium-45 nuclei.

In a pioneering experiment performed at the MID instrument of the European XFEL, the 12.4 keV resonance line of scandium-45 was excited (Fig. 1), witnessed by a total number of 93 delayed fluorescence photons that were detected

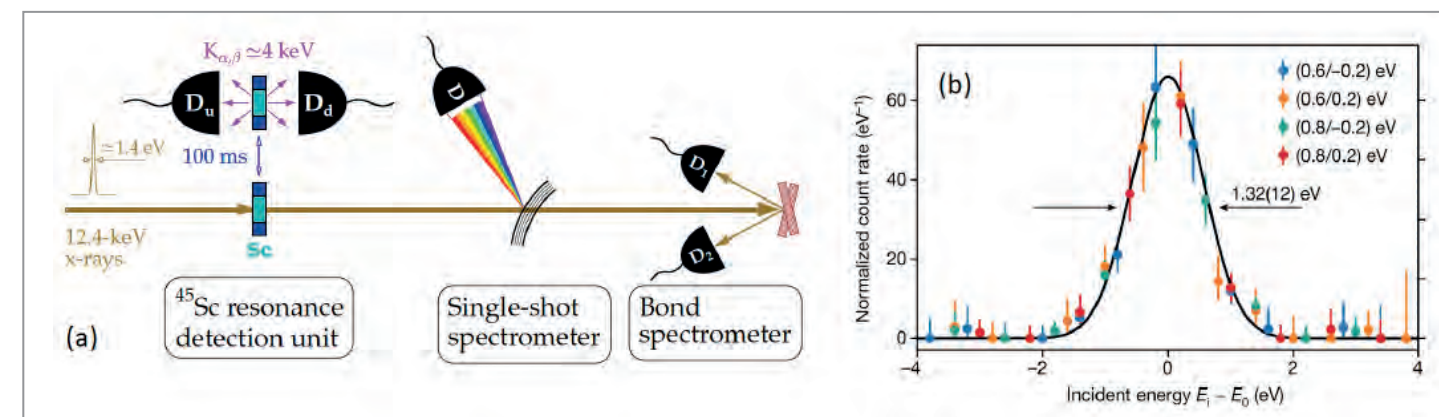


Figure 2

a) Experimental setup at the European XFEL. The Sc sample was periodically moved between the interaction zone with the X-ray beam and the position between two silicon drift detectors for the detection of the delayed 4 keV fluorescence radiation. For quick monitoring, the X-ray energy was determined with a dispersive single-shot spectrometer while a high-resolution energy analysis was performed by the Bond method using the Si(800) reflection. (b) Resonance curve recorded with delayed 4 keV K-fluorescence photons of scandium-45, witnessing the deexcitation of its 12.4 keV nuclear level. The centre of the curve marks the resonance energy that was determined to be $12,389.59 \pm 0.15$ (stat) + 0.12 (syst) eV. (Reproduced by permission of the NPG).

over 10^{20} photons in the X-ray pulses impinging on a 25- μm thin scandium metal foil. Such an efficient discrimination was possible by moving the scandium foil periodically between the interaction zone with the X-ray beam and the position between two well-shielded, low-noise silicon drift detectors for detection of the delayed 4 keV fluorescence radiation (Fig. 2a). This constituted an almost noise-free detection system for the discrimination of the fluorescence photons with a signal-to-noise ratio of 70. Employing high-resolution crystal optics for X-ray energy analysis via the Bond method [5], the value of the scandium-45 resonance energy could be determined with an accuracy 250 times higher than previously known, to a value of $12,389.59 \pm 0.15$ (stat) + 0.12 (syst) eV (Fig. 2b). The exact knowledge of this energy is of paramount importance for further steps toward realising a nuclear clock based on scandium-45. Moreover, the experiment also yielded new estimates for the nuclear resonance cross section ($\sigma_0 = 1.9(5) \times 10^{-20} \text{ cm}^2$) and the coefficients of internal conversion of this transition ($\alpha = 424$, $\alpha_K = 363$), further deepening the understanding of this remarkable nuclear transition.

The resonant excitation of the scandium-45 resonance and the precise measurement of its energy now open new avenues for applications in ultrahigh-precision X-ray spectroscopy. For example, such a high accuracy could allow the gravitational time dilation to be probed on sub-millimetre distances—this would allow studies of relativistic effects on length scales that were inaccessible so far. Moreover, this experiment demonstrates the potential of high repetition-rate narrow-band XFELs as promising platforms for studying extremely narrow nuclear resonances. Developing a nuclear clock based on scandium-45 will require further increase in resonant spectral flux, using improved narrow-band 12.4 keV X-ray sources and frequency combs stretching up to this energy.

Author contact: Ralf Röhlsberger, ralf.roehlsberger@desy.de
Yuri Shvyd'ko, shvydko@anl.gov
Jörg Evers, joerg.evers@mpi-hd.mpg.de
Olga Kocharovskaya, kochar@physics.tamu.edu

References

1. K. Beeks et al., 'The thorium-229 low-energy isomer and the nuclear clock', *Nat. Rev. Phys.* **3**, 238–248 (2021).
2. S. Kraemer et al., 'Observation of the radiative decay of the ^{229}Th nuclear clock isomer', *Nature* **617**, 706–710 (2023).
3. Yu. V. Shvyd'ko and G. V. Smirnov, 'On the direct measurement of nuclear γ -resonance parameters of long-lived (≥ 1 s) isomers', *Nucl. Instrum. Methods Phys. Res. B* **51**, 452–457 (1990).
4. S. Liu et al., 'Cascaded hard X-ray self-seeded free-electron laser at megahertz repetition rate', *Nat. Photon.* **17**, 984–991 (2023).
5. W. L. Bond, 'Precision lattice constant determination', *Acta Crystallogr.* **13**, 814–818 (1960).

Original publication

'Resonant X-ray excitation of the nuclear clock isomer ^{45}Sc ', *Nature* **633**, 471–475 (2023). DOI: 10.1038/s41586-023-06491-w



Yuri Shvyd'ko¹, Ralf Röhlsberger^{2,3,4,5}, Olga Kocharovskaya⁶, Jörg Evers⁷, Gianluca Aldo Geloni⁸, Peifan Liu¹, Deming Shu¹, Antonino Miceli¹, Brandon Stone¹, Willi Hippler^{2,3}, Berit Marx-Glowna^{2,3}, Ingo Uschmann⁴, Robert Loetzsch⁴, Olaf Leupold⁵, Hans-Christian Wille⁵, Ilya Sergeev⁵, Miriam Gerharz⁷, Xiwen Zhang⁶, Christian Grech⁵, Marc Guetg⁵, Vitali Kocharyan⁵, Naresh Kujala⁸, Shan Liu⁵, Weilun Qin⁵, Alexey Zozulya⁶, Jörg Hallmann⁸, Ulrike Boesenberg⁸, Wonhyuk Jo⁹, Johannes Möller⁸, Angel Rodriguez-Fernandez⁸, Mohamed Youssef⁸, Anders Madsen⁹ and Tomasz Kolodziej⁹

1. Argonne National Laboratory, Lemont, IL, USA
2. Helmholtz Institute Jena, Jena, Germany
3. GSI Helmholtzzentrum für Schwerionenforschung, Darmstadt, Germany
4. Friedrich-Schiller-Universität Jena, Jena, Germany
5. Deutsches Elektronen-Synchrotron DESY, Hamburg, Germany
6. Texas A&M University, College Station, TX, USA
7. Max Planck Institute for Nuclear Physics, Heidelberg, Germany
8. European XFEL, Schenefeld, Germany
9. National Synchrotron Radiation Centre SOLARIS, Kraków, Poland

Creating chirality with nothing but light

Pushing molecular chirality from a quantum racemate into a given handedness with tailored electromagnetic fields

Chiral molecules exist as pairs of mirror images known as enantiomers which cannot be superimposed by any rotation. The two enantiomers have identical physical properties; however, they can exhibit distinct optical, chemical, and biological behaviour when placed in chiral environments. To date, the origins of chirality and enantiomeric bias, as seen in phenomena like the 'homochirality of life', are still mysterious. In our recent research we demonstrate how molecular chirality can be created solely with light radiation.

Chiral molecules present in nature, such as amino acids, often exhibit 'static chirality'. Due to the insurmountable racemisation barriers, the interconversion between their two enantiomers is extremely slow at room temperature, so that they exist for a long time. If the barriers are relatively low, racemisation reactions can readily take place at room temperature. The two enantiomers then persistently form a 50:50 racemic mixture and become inseparable with conventional chemical methods. Developing methodologies to generate macroscopic chirality within such flexible, transiently chiral systems using only light radiation is thus of particular interest to us. As the dynamics of interconversion vary with the height of the barrier, we performed a systematic investigation on several model molecules.

For molecules like cyclohexylmethanol, with an intermediate racemisation barrier, the two enantiomers can rapidly interconvert at room temperature and thus cannot be separated. However, by cooling the molecules to temperatures near absolute zero (0 K), the racemisation process becomes extremely slow, making the molecules 'statically chiral'. In 2018 our research group successfully achieved the enantiomeric separation of cyclohexylmethanol by selectively exciting one enantiomer (depopulating the other enantiomer) to a specific rotational state during supersonic jet expansion ($T \sim 3$ K) [1]. If the racemisation barrier is further reduced, the enantiomers become inseparable even at absolute zero due to the quantum-mechanical effect known as tunnelling. Quantum particles can

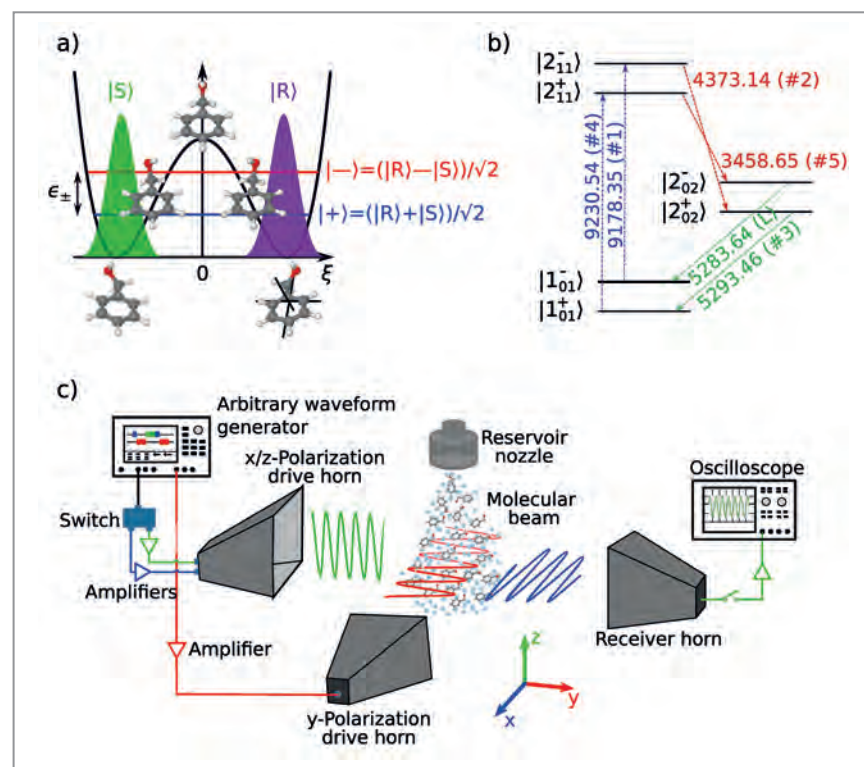
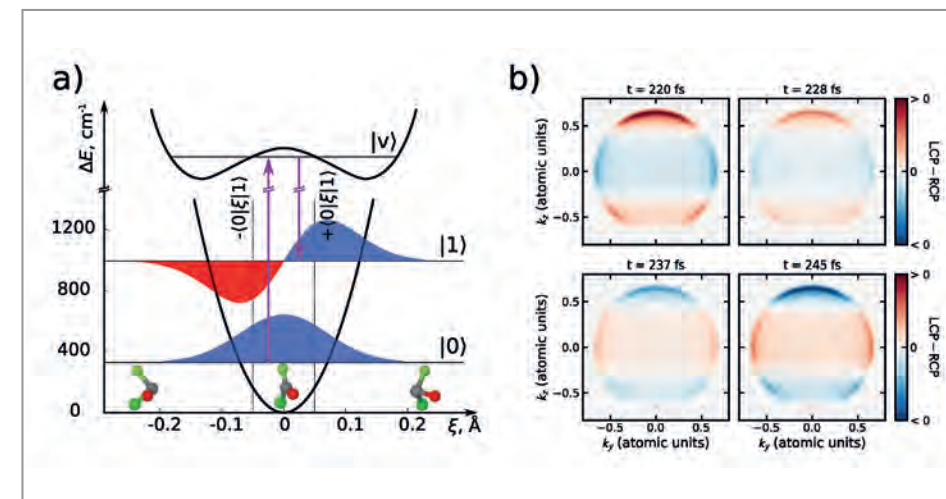


Figure 1

a) Double-well potential of the enantiomer interconversion in benzyl alcohol (BA). ξ is the large amplitude motion coordinate. b) Rotational level scheme of BA. Each rotational level is marked as $|J_{K_a K_c}^{\pm}\rangle$, where J is the total angular momentum, K_a and K_c are the projections of the angular momentum onto the molecular axes a and c , and \pm indicates the parity of the torsional state. Transitions 1-5 are associated with directly applied electric fields in the experiment, and transition 'L' indicates the 'listen' transition to be measured. c) Schematic diagram of the state-specific enantiomeric enrichment experiment. Pulses 1-5 are applied back-to-back with designated orthogonal polarisations, indicated by the color code. (Figure adapted from the original publication Sun et al.)

Figure 2

a) Raman excitation (magenta arrows) exploiting a superposition of the two lowest levels of the out-of-plane vibration via a prochiral electronically excited state with vibrational level $|v\rangle$, creating a chiral wave packet in a planar molecule, COFCI. b) Pump-probe spectroscopy of light-induced chirality using photoelectron circular dichroism (PECD). PECD refers to the forward-backward asymmetry of photoelectron angular distributions (PADs) upon ionisation of chiral molecules with left and right circularly polarised (LCP/RCP) light. The PECD signal is given as the difference between LCP/RCP velocity map images (VMI) at different pump-probe time delays. (Figure adapted from the original publication Tikhonov et al.)



'travel through the walls', and thus, enantiomers can also traverse through the potential barrier separating them. This effect leads to the emergence of two quantum states of different energies: in-phase and out-of-phase superpositions of the two enantiomers. Such a molecular system can be described as a quantum racemate that persists even at absolute zero, for instance, benzyl alcohol (Fig. 1).

As shown in Fig. 1a, the tunnelling motion in benzyl alcohol is described using a double-well energy potential. It correlates the localised wave packets of the left (S) and right (R) enantiomers with the $|\pm\rangle$ superposition quantum states which are separated by the energy difference ϵ_{\pm} . By applying a tailored set of microwave pulses, which followed the six-level rotational energy scheme in Fig. 1b), benzyl alcohol molecules are transferred, in a highly controlled way from the initial $|1_{01}^{-}\rangle$ to the final state $|2_{02}^{-}\rangle$. During this process, five different microwave pulses interact with the three electric dipole-moment components within the molecular frame while the molecules undergo the described tunnelling motion. The first three mutually orthogonal pulses are the preparation stage, creating the chiral wave packet in a specific rotational state. The second two mutually orthogonal pulses are the probing sequence, inducing a new chiral signal in the third direction (the listen signal 'L').

In a related study we investigated the special case where the racemisation barrier vanishes, such as the planar molecule COFCI (Fig. 2). Although such a molecule is inherently achiral, we developed a scheme to create a net handedness. The chirality can be induced upon excitation of an out-of-plane vibration mode. The resulting racemate can be coherently disrupted when the vibrational motion is stimulated via a Raman transition in the presence of a static electric field. The resulting molecular ensemble exhibits an excess of one enantiomer, and this excess can be probed using ultrafast photoelectron circular dichroism

(PECD) spectroscopy. Quantum-chemical calculations predict a detectable PECD signal arising from the time-dependent net handedness, employing COFCI as a model and setting the stage for future experimental examination.

Our studies show that molecular chirality can be created in a well-controlled manner even within flexible, transiently chiral and achiral molecules solely through the interactions with light radiation. This will also facilitate further advanced chirality experiments that require the separate production of enantiomers under the same experimental conditions, such as precision experiments.

Author contact: Denis Tikhonov, denis.tikhonov@desy.de
Melanie Schnell, melanie.schnell@desy.de
Wenhao Sun, wenhao.sun@desy.de

References

1. C. Pérez, A. L. Steber, A. Krin and M. Schnell, 'State-specific enrichment of chiral conformers with microwave spectroscopy', *J. Phys. Chem. Lett.* 9, 4539-4543 (2018).

Original publications

'Inducing transient enantiomeric excess in a molecular quantum racemic mixture with microwave fields', *Nature Communications* 14, 934 (2023). DOI: 10.1038/s41467-023-36653-3

Wenhao Sun¹, Denis S. Tikhonov¹, Himanshi Singh¹, Amanda L. Steber², Cristóbal Pérez¹ and Melanie Schnell^{1,2}

'Pump-probe spectroscopy of chiral vibrational dynamics', *Science Advances* 8, eade0311 (2022). DOI: 10.1126/sciadv.ade0311

Denis S. Tikhonov¹, Alexander Blech³, Monika Leibscher³, Loren Greenman⁴, Melanie Schnell^{1,2} and Christiane P. Koch³

1. Deutsches Elektronen-Synchrotron DESY, Hamburg, Germany
2. Institute of Physical Chemistry, Christian-Albrechts-Universität zu Kiel, Kiel, Germany
3. Dahlem Center for Complex Quantum Systems and Fachbereich Physik, Freie Universität Berlin, Berlin, Germany
4. Department of Physics, Kansas State University, KS, USA

Ultrafast tracking of an atomic-scale structural transformation

Observation of a new transient state in a layered quantum material

The interaction of light and matter is of great technological relevance for future devices. Tailored functionality is promised by laser-induced phase transitions which offer a drastic and sudden change of materials properties or even promote intermediate states inaccessible in equilibrium. Understanding rapid materials transformations is the realm of ultrafast science which aims to decipher dynamics that unfold much faster than a nanosecond. A key challenge in resolving such processes lies in the development of experimental tools with high temporal resolution and structural sensitivity.

Here, we show that ultrafast nanobeam electron diffraction elucidates the rapid transformation of three-dimensional structural order in a prototypical functional material. Moreover, we discover an intermediate state with a distinct type of disorder, alongside with an optically-induced change of the effective crystalline dimensionality.

We investigate layered crystals, grown at Kiel University, of tantalum disulphide ($1T\text{-TaS}_2$), a quantum material

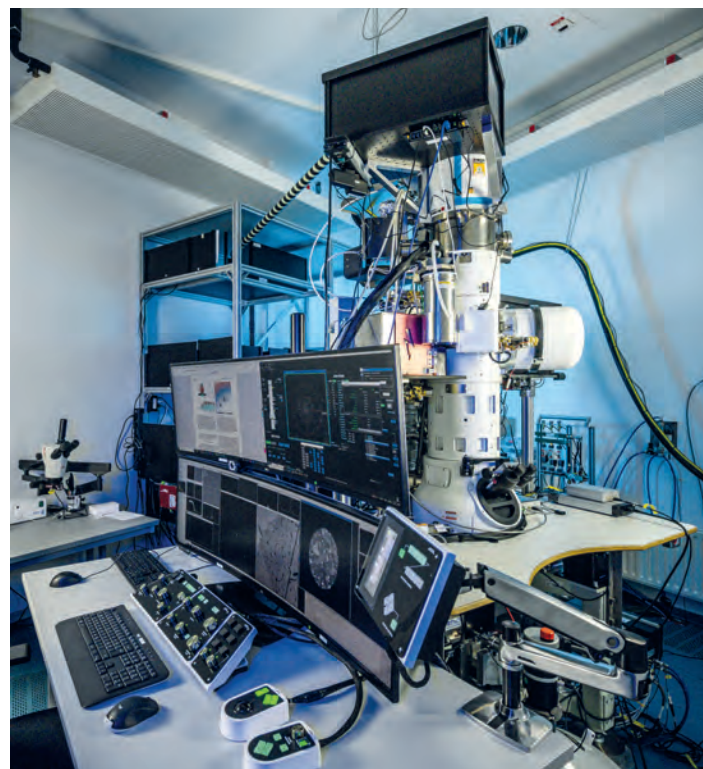


Figure 1
Göttingen Ultrafast Transmission Electron Microscope. (Credit: Irene Boettcher-Gajewski/Max Planck Institute for Multidisciplinary Sciences)

known for its sequence of phase transitions from a metallic state at high temperature to an insulating state at low temperatures. These phases are evident in electron diffractograms (Fig. 2c), each showing characteristic periodic distortions of the crystalline lattice that are coupled to the formation of a so-called charge density wave (CDW) [1,2]. The phases investigated here merely differ by a small rotation of the CDW pattern (Fig. 2a) while a switch between them involves a large increase in the material's electrical conductivity.

Distinguishing these closely related structures during the transformation is experimentally challenging due to brightness limitations of state-of-the-art ultrafast diffraction setups. In the Göttingen Ultrafast Transmission Electron Microscope (UTEM, Fig. 1), we overcome this problem by using a nanometric tip emitter for the generation of highly coherent ultrashort electron pulses [3]. The small electron source size results in exceptional electron beam properties, yielding high sensitivity and resolution. After an optical excitation of the room-temperature phase, the corresponding set of CDW-associated spots disappears within 500 fs, and the reflections from the high-temperature CDW emerge nearby, yet in an azimuthally elongated shape (Fig. 2c). The phase formation thus involves a high degree of transient disorder, previously linked to topological defects [4]. However, the microscopic mechanism, in particular how the crystal can accommodate the CDW rotation during the transition, has so far remained elusive.

In purely two-dimensional systems, melting of crystalline order is mediated by a mesoscopic rotation of the crystal axis induced by the unbinding of point defects, specifically dislocations [5]. The resulting hexatic phase possesses only orientational but no complete translational order.

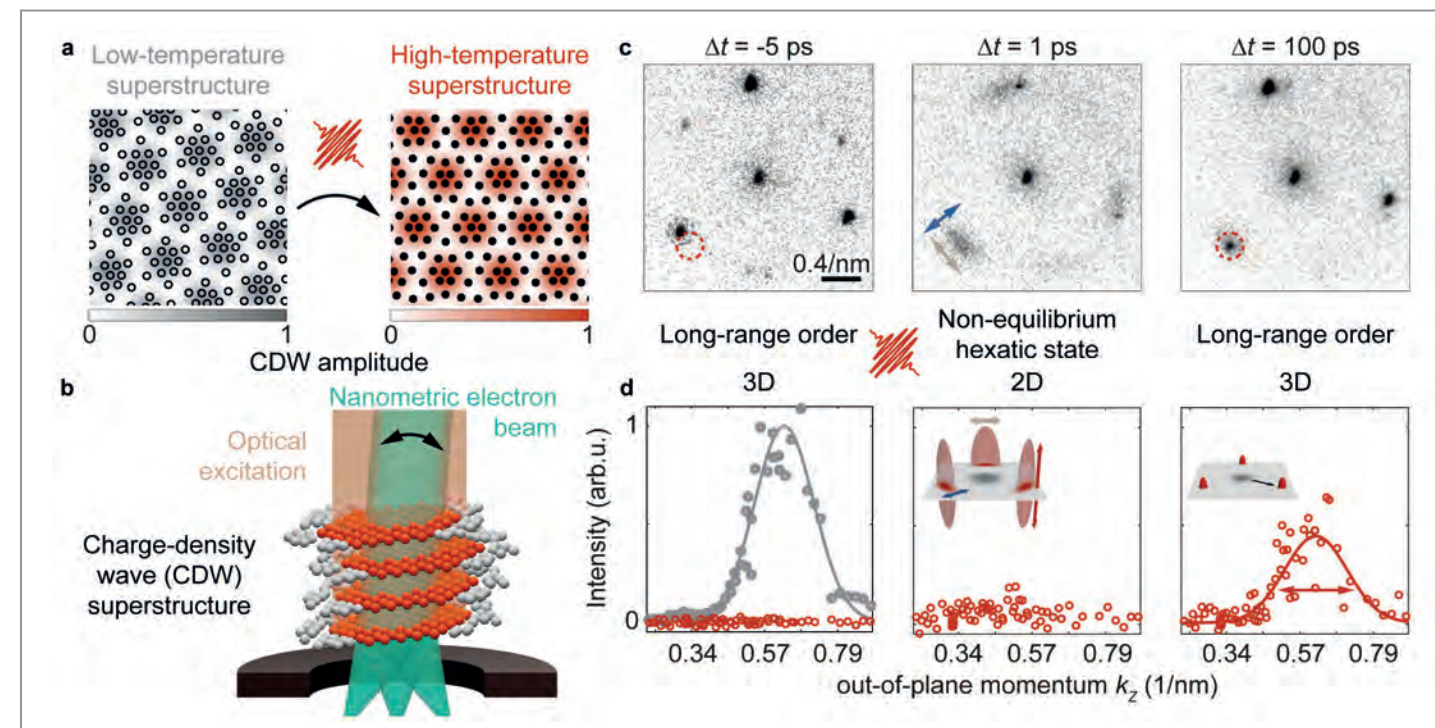


Figure 2

a) We investigate a structural transition between two charge-density wave phases. Therein, the crystal charge density is periodically modulated (coloured background), intrinsically coupled to a periodic distortion of the crystal lattice (black circles). Note the alignment of the CDW maxima in both images as both phases differ by small rotation of the CDW wave vector. b) In our experiments, we record electron diffractograms with collimated, nanometric illumination and under varying angles of incidence. c) Exemplary time series of electron diffractograms. Outer diffraction spots are indicative of the CDW phase change. While spots are sharp before and long after the optical excitation at $\Delta t=0$ ps, the early-stage dynamics are characterised by pronounced azimuthal broadening (brown arrow), indicative of a hexatic state. d) Along the material layer, we observe a similar spot elongation as the optical excitation transiently transforms the system from a three-dimensional to a two-dimensional state. Insets: schematic sketches of the three-dimensional shape of the CDW diffraction features throughout the dynamics.

Exploring the possibility of similar mechanisms in a non-equilibrium scenario, we record time series of electron diffractograms under various electron-beam angles of incidence. The tomographic reconstruction of the CDW spot resolves the three-dimensional disorder during the transition. We find that in the early stages of the dynamics the CDW spots are highly elongated, suggesting an intermediate two-dimensional character (Fig. 2d). CDW order thus emerges within the individual layers first, and neighbouring layers are decoupled. We conclude that each layer is in a transient hexatic state, and the pathway between both phases leads through a network of dislocations. This disordered state persists for 10 ps, followed by the recovery of strong interlayer correlations and the crystallisation of the final three-dimensional CDW.

Our results highlight that optical excitation can enforce low-dimensional behaviour in layered materials, shaping the transition between different structural phases. Concerning further applications of the method, highly coherent electron pulses will promote the study of ultrafast dynamics in various nanoscale systems, heterostructures and functional interfaces.

Author contact: Till Domröse, till.domroese@mpinat.mpg.de, Claus Ropers, claus.ropers@mpinat.mpg.de

References

1. K. Rossnagel, 'On the origin of charge-density waves in select layered transition-metal dichalcogenides', *J. Phys.: Condens. Matter* **23**, 213001 (2011).
2. M. Eichberger, H. Schäfer, M. Krumova, M. Beyer, J. Demsar, H. Berger, G. Moriena, G. Sciani and R. J. D. Miller, 'Snapshots of cooperative atomic motions in the optical suppression of charge density waves', *Nature* **468**, 799–802 (2010).
3. A. Feist, N. Bach, N. Rubiano da Silva, T. Danz, M. Möller, K. E. Priebe, T. Domröse, J. G. Gatzmann, S. Rost, J. Schauss, S. Strauch, R. Bormann, M. Sivis, S. Schäfer and C. Ropers, 'Ultrafast transmission electron microscopy using a laser-driven field emitter: Femtosecond resolution with a high coherence electron beam', *Ultramicroscopy* **176**, 63–73 (2017).
4. S. Vogelgesang, G. Storeck, J. G. Horstmann, T. Diekmann, M. Sivis, S. Schramm, K. Rossnagel, S. Schäfer and C. Ropers, 'Phase ordering of charge density waves traced by ultrafast low-energy electron diffraction', *Nat. Phys.* **14**, 184–190 (2018)
5. D. R. Nelson and B. I. Halperin, 'Dislocation-mediated melting in two dimensions', *Phys. Rev. B* **19**, 2457–2484 (1979).

Original publication

'Light-induced hexatic state in a layered quantum material', *Nature Materials* **22**, 1345–1351 (2023). DOI: 10.1038/s41563-023-01600-6



Till Domröse^{1,2}, Thomas Danz¹, Sophie F. Schaible², K. Rossnagel^{3,4}, Sergey V. Yalunin¹ and Claus Ropers^{1,2}

1. Department of Ultrafast Dynamics, Max Planck Institute for Multidisciplinary Sciences, Göttingen, Germany
2. 4th Physical Institute – Solids and Nanostructures, University of Göttingen, Göttingen, Germany
3. Institute of Experimental and Applied Physics, Kiel University, Kiel, Germany
4. Ruprecht Haensel Laboratory, Deutsches Elektronen-Synchrotron DESY, Hamburg, Germany

X-ray diffraction imaging of a single quantum dot

X-ray diffraction microscopy reveals anisotropic compositional loading and nanoscale chirality within a single quantum dot

Epitaxially grown self-assembled semiconductor quantum dots (QDs) offer atom-like optical properties, making them ideal for single-photon sources in quantum technologies. Selecting a QD with specific characteristics is crucial for noise-free, indistinguishable photons [1]. We developed a screening protocol to identify the best QD from a multitude of simultaneously grown dots. Our study revealed anisotropic elemental composition within single QDs, challenging existing models assuming lateral azimuthal symmetry. Additionally, we observed a progressive rotation of in-plane lattices, forming naturally occurring chiral structures. This groundbreaking discovery of nanoscale chirality within zero-dimensional QDs has profound implications for revolutionising quantum technology.

Quantum technologies comprising quantum communication, quantum computation and quantum security, are at the forefront of scientific innovation. These groundbreaking technologies rely on epitaxially grown self-assembled single quantum dots, often referred to as artificial atoms [2]. Quantum dots confine charge carriers within nanometer-sized structures and exhibit a delta-like density of states, making them ideal for use as single or entangled photon sources and qubits [3]. The production of the highest quality quantum dots involves the Stranski-Krastanov self-assembly growth mode [1], achieved through ultra-

high vacuum molecular beam epitaxy growth techniques [1-3]. However, the real challenge lies in the fact that the best quality quantum dots come in diverse sizes, shapes, compositions and strains within a single growth condition. Our results present a protocol to select the structurally most suitable quantum dot for a specific application.

Combining destructive microscopic techniques like high resolution cross-sectional transmission electron (HRXTEM) or scanning tunneling microscopy (HRXSTM) with optical measurements for selecting the best quality QDs is chal-

lenging due to complexities in interpreting results and difficulties in precisely positioning cross-sectional slices relative to the QD's centre. Using the 'Ptychographic Nano-analytical Microscope' (PtyNAMI) [4] at PETRA III beamline P06, we have developed a novel measurement protocol capable of pinpointing the most promising single QD among self-assembled dots. This method involves transmission X-ray scattering with a thinned substrate (~ 40 μm) and a nanofocused beam (~ 50 nm) with energy (28150 eV) exceeding all elemental absorption edges. Our protocol combines scanning X-ray diffraction and elemental fluorescence mapping simultaneously, as shown in Fig. 1a. We conducted the research on indium-gallium-arsenide (InGaAs) QDs grown on a GaAs substrate, utilising a 3D interferometer feedbacked piezo-stage for mesh scanning. Using this approach, we can accurately identify all the QDs through indium fluorescence mapping (Fig. 1b) with the help of a guiding marker-based correlative microscopy approach developed at the DESY NanoLab. Single quantum dots are increasingly recognised as crucial components for various emerging quantum technologies, including 'single-photon sources', 'entangled-photon-exciton sources' and 'qubits', and for fundamental science that probes 'novel light-matter interactions'.

Our investigation also led to a remarkable discovery. After analysing a few selected single QDs through compositional mapping from elemental fluorescence data (Fig. 2), we observed anisotropic elemental composition loading in different crystallographic directions. It raises a question regarding the effectiveness of the theoretical models to calculate optical properties that assume lateral azimuthal symmetry. Incorporating compositional anisotropy into theoretical models is essential for predicting single-photon source properties and optimising epitaxial growth of self-assembled quantum structures. Simultaneously, lattice mapping through diffraction revealed a progressive rotation of in-plane lattices from the base to the tip (Fig. 2), suggesting

that in a natural way, chiral QD structures can form. This chirality is driven by anisotropic elemental composition loading in different crystallographic directions during the self-assembled growth. Notably, this discovery represents the first instance of nanoscale chirality within a zero-dimensional QD structure, marking a significant advancement in the field. This discovery adds a new dimension of specific polarisation in a single photon and this realisation can potentially revolutionise our understanding of the applications with quantum technologies.

Author contact: Arka Bikash Dey, arka.bikash.dey@desy.de
Milan K. Sanyal, milank.sanyal@saha.ac.in

References

1. C. Santori, D. Fattal, J. Vučković, G. S. Solomon and Y. Yamamoto, 'Indistinguishable Photons from a Single-Photon Device', *Nature* 419, 594-597 (2002).
2. T. Walther, A. G. Cullis, D. J. Norris and M. Hopkinson, 'Nature of the Stranski-Krastanov Transition during Epitaxy of InGaAs on GaAs', *Phys. Rev. Lett.* 86, 2381-2384 (2001).
3. A. B. Dey, M. K. Sanyal, I. Farrer, K. Perumal, D. A. Ritchie, Q. Li, J. Wu and V. Dravid, 'Correlating Photoluminescence and Structural Properties of Uncapped and GaAs-Capped Epitaxial InGaAs Quantum Dots', *Sci. Rep.* 8, 7514 (2018).
4. A. Schropp et al., 'Ptychographic Nano-Analytical Microscope', *J. Appl. Crystallogr.* 53, 957-971 (2020).

Original publication

'Culling a self-assembled quantum dot as a single-photon source using X-ray microscopy', *ACS Nano* 17, 16080-16088 (2023). DOI: 10.1021/acsnano.3c04835



Arka Bikash Dey¹, Milan K. Sanyal², Andreas Schropp³, Silvio Achilles³, Thomas F. Keller^{3,4}, Ian Farrer⁵, David A. Ritchie⁶, Florian Bertram³, Christian G. Schroer³ and Oliver H. Seeck¹

1. Deutsches Elektronen-Synchrotron DESY, Hamburg, Germany
2. Surface Physics and Material Science Division, Saha Institute of Nuclear Physics, Kolkata, India
3. Center for X-ray and Nano Science CXNS, DESY, Hamburg, Germany
4. Department of Physics, Universität Hamburg, Germany
5. Department of Electronic and Electrical Engineering, University of Sheffield, Sheffield, United Kingdom
6. Cavendish Laboratory, University of Cambridge, Cambridge, United Kingdom

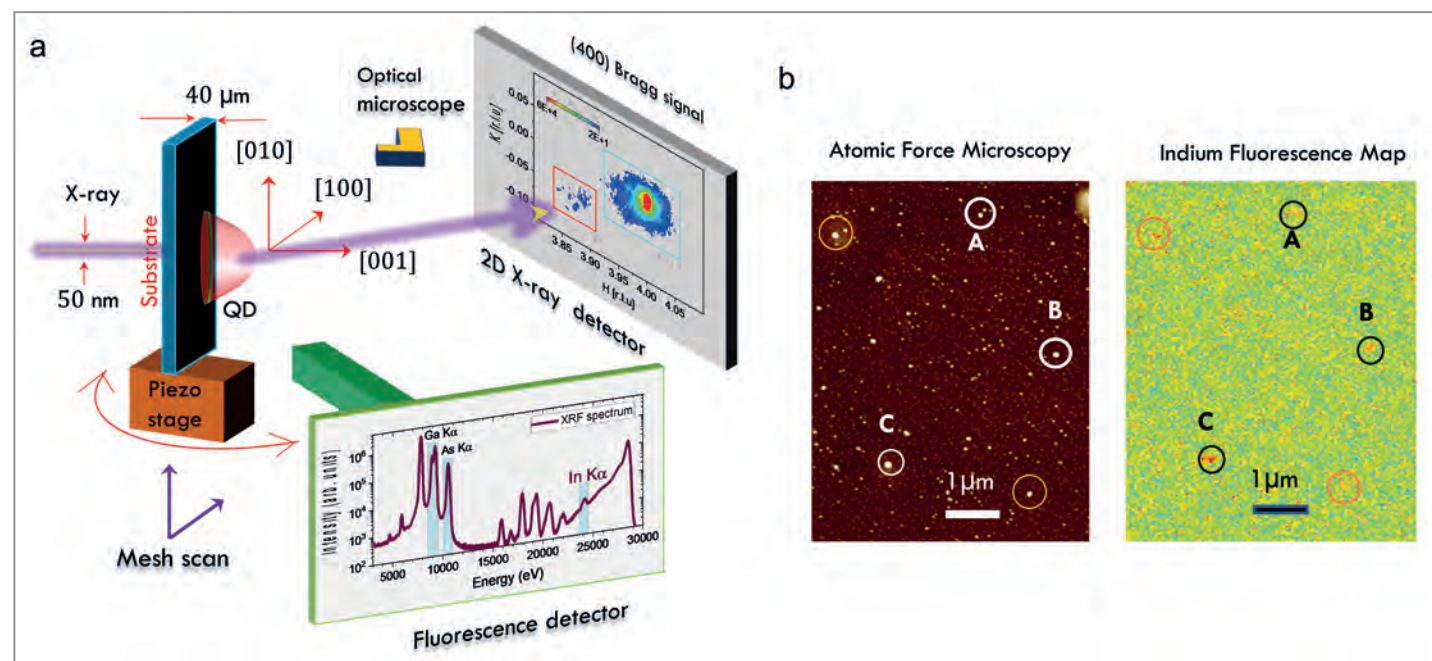
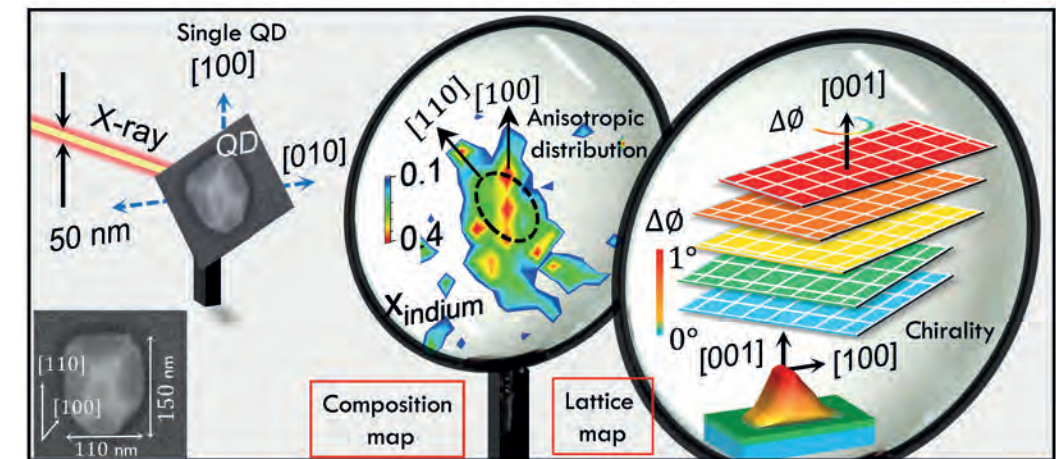


Figure 1 a) Schematic illustration of the experimental setup. b) Self-assembled epitaxial QDs of different sizes and shapes measured by atomic force microscopy. The same region is measured with indium fluorescence signal mapping with a 50 nm focused X-ray beam at the PtyNAMI set-up of PETRA III's P06 beamline.

Figure 2 Continuous mesh scans on a single QD show an anisotropic compositional distribution in different crystallographic directions (composition map) and a progressive in-plane lattice rotation from the base to the tip of the QD, making it a naturally chiral QD.



Moulding ultrashort laser pulses

Multi-pass cells release high-power lasers from gain bandwidth limitations

Conventional lasers cannot have frequencies beyond the bandwidth of their gain media. This limit dictates what colours the laser light will have and also the shortest laser pulse duration it can support. In two studies published in *Optics Letters* and *Nature Photonics*, multi-pass cells were used to break through this limitation. Multi-pass cells, composed of just two concave mirrors and a nonlinear medium, such as a noble gas or glass plates, can be used to extend the bandwidth of high-power lasers to frequencies far beyond what the gain medium could support or to even shift the frequencies completely outside the gain bandwidth.

In ultrafast optics, a wide range of frequencies are simultaneously utilised and synced to generate a very short optical pulse in the range of femtoseconds (fs, 10^{-15} seconds). A wider range of frequencies is needed to generate shorter pulses, and this range is typically limited by the laser gain medium used. Ytterbium-doped laser gain media, such as Yb:YAG, are commonly used for high-power lasers due to their advantageous gain and thermal properties, but the pulses that can be generated from them are constrained to few hundreds of femtoseconds due to the aforementioned limitation [1]. Efforts to bypass this limit require nonlinear processes to generate new frequencies.

Self-phase modulation (SPM) is a nonlinear process that occurs when very intense optical pulse interacts with

matter, inducing a temporal modulation of the material's refractive index. The temporal modulation depends directly on the temporal shape of the optical pulse intensity. In the case of a common bell-shaped intensity profile, SPM generates new frequencies on both sides of the original frequencies of the pulse. This nonlinear effect is easy to utilise as virtually any material could be used to produce this effect. The tricky part is how to use it in a controlled manner, since a large amount of SPM introduced at once will have detrimental effects on the laser beam properties. This challenge can be solved using multi-pass cells (MPCs).

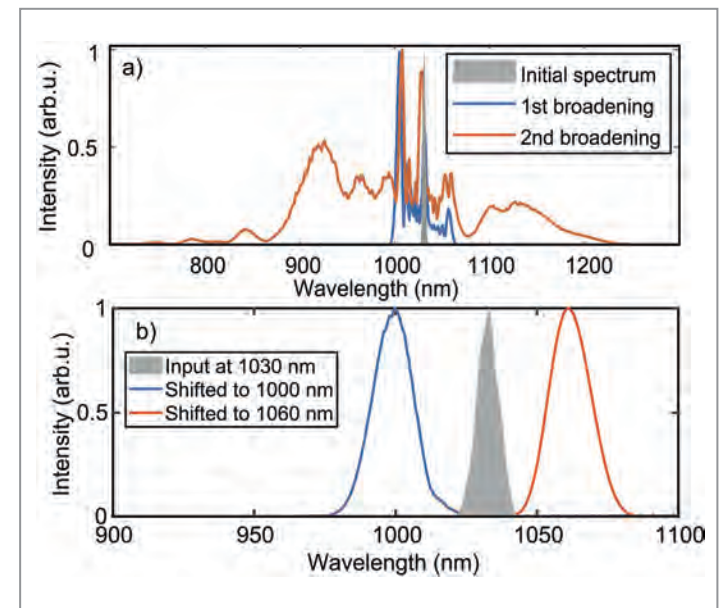
An MPC in its simplest form is just a pair of concave mirrors with a nonlinear medium in-between wherein SPM occurs (Fig. 1). The medium is typically a noble gas which has better controllable behaviour than most other gases or a transparent solid medium such as glass [2]. An input laser beam, after being formed to the right size by a telescope, enters the MPC and gets reflected back and forth by the two concave mirrors. Every time the beam passes through the MPC, it passes a small and intense focal spot where a controlled amount of SPM is introduced. The beam typically makes more than a dozen roundtrips before it is coupled out which adds up to a large amount of nonlinearity even though only a small amount is introduced each roundtrip.

In the paper in *Optics Letters* by Rajhans and Escoto et al., using two such cells in succession, were able to generate new frequencies wide enough to support a pulse of around

Figure 1
View into a multi-pass cell, showing many new optical frequencies generated through SPM. The initial beam is infrared, which is not visible, but other colours start to emerge after a few roundtrips through the multi-pass cell.



Figure 2
Measured spectral broadening and spectral shifting using multi-pass cells: The spectrum of the input laser beam (grey area) is very narrow due to the limited bandwidth of the laser gain medium. a) A first multi-pass cell enables to extend the spectral bandwidth (blue line), followed by a second cell after which a close to octave spanning spectrum is obtained (orange line). b) A multi-pass cell coupled with a pulse shaper moves the centre wavelength to 1000 nm (blue line) and to 1060 nm (orange line). The measurements are made with spectral filters to remove the remaining weak signal at the input wavelength.



7 fs, and they successfully compressed the pulse to 9.6 fs (Fig. 2a). This is an impressive result, as it was possible to convert a high-power pulse from >1000 fs to <10 fs, corresponding to a compression factor of more than 100, while maintaining the losses to be very low, ending up with 70% of the energy still within the beam even after the very large compression. This is a very promising result, in particular as it enables to use lasers with picosecond pulse durations, which are commercially available and support operation at very high average power to be used for applications that demand shorter pulse durations and higher peak powers such as laser-driven particle acceleration.

SPM is highly dependent on the temporal shape of the pulse, and the pulse can be shaped precisely to not just generate new frequencies above and below the original frequencies but also to shift the original frequencies almost entirely in one direction. This has been demonstrated in the paper in *Nature Photonics* by Balla et al., enabling to convert ultrashort laser pulses with a centre wavelength of 1030 nm to pulses with longer (1060 nm) and shorter (1000 nm) wavelength (Fig. 2b). This tunability can have wide implications, providing new parameter regimes, e.g. for nonlinear spectroscopy or for attosecond science. This again demonstrates how ultrashort laser pulses can be 'moulded' through the use of nonlinear processes controlled inside a quasi-wave guide, the MPCs.

While already enabling entirely new possibilities for ultrafast laser physics, MPC laser technology is arguably not fully mature yet, and more breakthroughs can be expected in the next few years. These two publications just provide a glimpse of what is possible, enabling enhanced peak powers, broader frequency ranges and shorter pulse durations. Other cell configurations, utilising other nonlinearities and advances in mirror coating technology, among

other things, could prospectively drive MPCs much further [2], unlocking new opportunities for ultrafast science, electron accelerators and beyond.

Author contact: Esmerando Escoto,
esmerando.escoto@desy.de

References

1. P. Russbuehler, T. Mans, G. Rotarius, J. Weitenberg, H. D. Hoffmann and R. Poprawe, '400 W Yb:YAG Innoslab fs-amplifier', *Opt. Express* 17, 12230–12245 (2009).
2. A. L. Viotti, M. Seidel, E. Escoto, S. Rajhans, W. P. Leemans, I. Hartl and C. M. Heyl, 'Multi-pass cells for post-compression of ultrashort laser pulses', *Optica* 9, 197–216 (2022).

Original publications

'Post-compression of multi-millijoule picosecond pulses to few-cycles approaching the terawatt regime', *Optics Letters* 48, 4753–4756 (2023). DOI: 10.1364/OL.498042



Supriya Rajhans^{1,2}, Esmerando Escoto¹, Nikita Khodakovskiy¹, Praveen K. Velpula³, Bonaventura Farace⁴, Uwe Grosse-Wortmann⁵, Rob J. Shalloo³, Cord L. Arnold⁴, Kristjan Pöder¹, Jens Osterhoff¹, Wim P. Leemans¹, Ingmar Hartl¹ and Christoph M. Heyl^{1,5,6}

1. Deutsches Elektronen-Synchrotron DESY, Hamburg, Germany
2. Friedrich-Schiller-Universität Jena, Jena, Germany
3. UGC-DAE Consortium for Scientific Research, Indore, India
4. Department of Physics, Lund University, Lund, Sweden
5. Helmholtz-Institute Jena, Jena, Germany
6. GSI Helmholtzzentrum für Schwerionenforschung GmbH, Darmstadt, Germany

'Ultrafast serrodyne optical frequency translator', *Nature Photonics* 17, 187–192 (2023). DOI: 10.1038/s41566-022-01121-9



Prannay Balla^{1,2,3}, Henrik Tünnermann¹, Sarper H. Salman^{1,2,3}, Mingqi Fan¹, Skirmantas Alisauskas¹, Ingmar Hartl¹ and Christoph M. Heyl^{1,2,3}

1. Deutsches Elektronen-Synchrotron DESY, Hamburg, Germany
2. Helmholtz-Institute Jena, Jena, Germany
3. GSI Helmholtzzentrum für Schwerionenforschung GmbH, Darmstadt, Germany

Smart data compression for the human mind

β -VAEs on photon diagnostics

The amount and dimensionality of scientific data is constantly increasing. In photon science this is driven by detectors with higher resolution, rising repetition rates, more diagnostics and increasingly sophisticated experiments. On the one hand, analysing this data using traditional methods becomes more challenging and, in some cases, even impossible due to the computational demands. On the other hand, online feedback from the diagnostic data as well as from the experiment would dramatically enhance the experimental environment. In our study we address this challenge by employing an unsupervised machine learning (ML) approach that compresses high-dimensional data into a form that is interpretable by the human mind.

Established data evaluation methods, such as least-square fitting, prove to be too slow when dealing with a vast amount of experimental data. Faster methods, such as principal component analysis, are strictly linear, and their components may not be readily interpretable. The desire to automatically extract the underlying core principles from high-dimensional data without a priori knowledge is common across many research fields.

The method of disentangled variational autoencoder, known as β -VAE [1], overcomes these obstacles by using a neural network to encode the high-dimensional data into a low-dimensional latent space, as shown in Fig. 1. From this compressed state, the data is reconstructed by the

decoder part of the network. In addition to the reconstruction quality, the network is also evaluated based on a so-called disentanglement criterion. It enforces that an independent variation in the raw input data is reflected in one specific component of the compressed state, resulting in an interpretable representation of the data.

In our study we employ the described technique to analyse data from the online photoionisation spectrometer, OPIS [2,3]. At the free-electron laser FLASH, ten trains with up to several hundreds of bunches are generated every second (Fig. 2a). Each photon pulse ionises a target gas in the centre of the OPIS chamber. The resulting photoelectrons traverse the flight tubes of four electron time-of-flight

spectrometers and are detected by micro-channel plate detectors. Their kinetic energy reflects the wavelength of the photon pulse and is directly correlated with their time-of-flight (Fig. 2b). Single-shot spectra exhibit a low signal-to-noise ratio and are often plagued by artefacts and random hits. Previously, this necessitated the averaging of multiple bunches for data analysis which resulted in the loss of shot-to-shot information.

The neural network is trained solely on the raw data without any a priori knowledge. It discovers representations that reveal essential information about the intensity and wavelength of a single shot, outperforming traditional methods. The reconstructed spectra are denoised, random hits are ignored (Fig. 2c) and low-intensity signatures, which are hardly visible in raw data, are revealed. Furthermore, artefacts such as baseline disturbance and a channel interleaving issue can be removed by manipulating the corresponding components in the latent space (Fig. 2d). Once trained, the application of the network is fast enough to provide online feedback to the experiment without needing large computational power.

While the presented project dealt with time-of-flight data, the β -VAE method is not only applicable to spectra [1]. In a direct follow-up project, camera images from the Polaris FEL pulse length diagnostics unit at FLASH have been used to train a network, enabling the generation of highly desired non-lasing reference images through simple manipulation of the latent space of a lasing image.

Highlighting the general applicability of the method even beyond photon science, we are currently analysing dinosaur

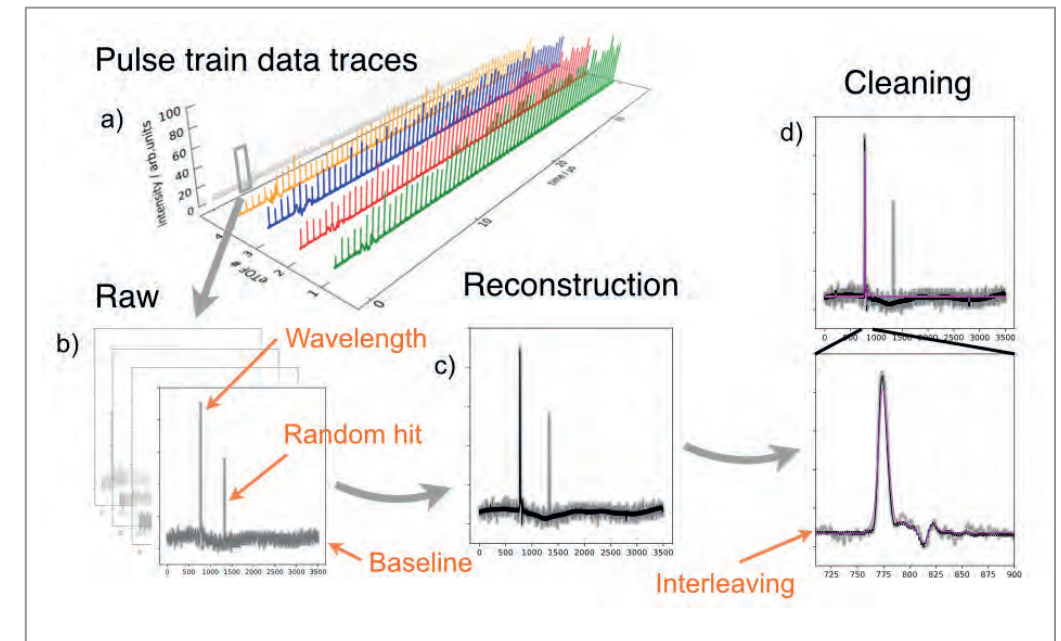


Figure 2

a) Spectra from the four-electron time-of-flight spectrometers are shown for a single bunch train, consisting of 72 single shots. b) The single-shot spectra contain the photo line, which represents the FEL wavelength, along with a number of artefacts (grey). c) The denoised reconstruction, which ignores the random hits, is plotted (black). d) Manipulating components of the latent space, that represent the artefacts, results in a cleaned reconstruction (purple).

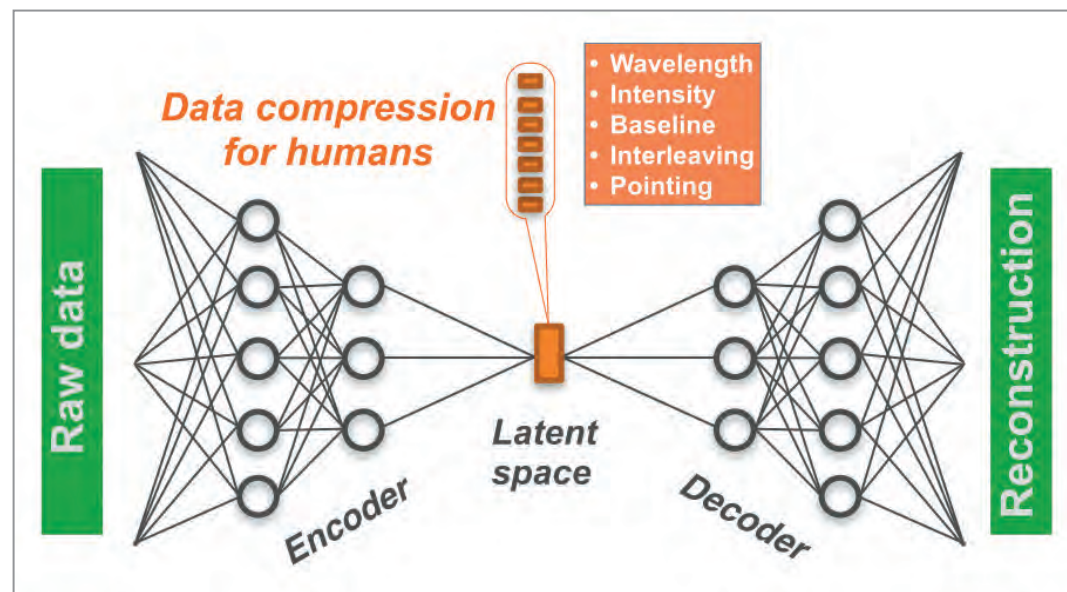


Figure 1

The architecture of the disentangled variational autoencoder is shown. In an unsupervised manner, the high-dimensional OPIS raw data is processed through a multi-dimensional bottleneck. Thanks to the disentanglement criterion, this so-called latent space reveals the underlying core principal: its components represent crucial physical parameters such as photon wavelength, beam pointing, intensity and specific detector properties like baseline disturbance and interleaving imperfections.

footprints in collaboration with the University of Edinburgh, School of GeoSciences, Stephen Brusatte et al. The β -VAE network is able to extract meaningful representations, ranging from general features like 'loading' and 'digit separation' up to very specific ones such as 'right lateral digit pachydactyly' and even reconstructs of missing toes from an incomplete fossil silhouette.

Author contact: Gregor Hartmann, gregor.hartmann@helmholtz-berlin.de

References

1. I. Higgins, L. Matthey, A. Pal, Ch. Burgess, X. Glorot, M. Botvinick, Sh. Mohamed and A. Lerchner, ' β -VAE: Learning basic visual concepts with a constrained variational framework', published as a Conference Paper at ICLR 2017.
2. M. Braune, G. Brenner, S. Dziarzhytski, P. Juranic, A. Sorokin and K. Tiedtke, 'A non-invasive online photoionization spectrometer for FLASH2', *J. Synchrotron Radiat.* 23, 10–20 (2016).
3. M. Braune, J. Buck, M. Kuhlmann, S. Grunewald, S. Düsterer, J. Viefhaus and K. Tiedtke, 'Non-invasive online wavelength measurements at FLASH2 and present benchmark', *J. Synchrotron Radiat.* 25, 3–15 (2018).

Original publication

'Unsupervised real world knowledge extraction via disentangled variational autoencoders for photon diagnostics', *Scientific Reports* 12, 20783 (2022). DOI: 10.1038/s41598-022-25249-4



Gregor Hartmann¹, Gesa Goetzke², Stefan Düsterer², Peter Feuer Forson¹, Fabiano Lever³, David Meier^{1,4}, Felix Möller¹, Luis Vera Ramirez², Markus Guehr^{2,3}, Kai Tiedtke², Jens Viefhaus¹ and Markus Braune²

1. Helmholtz-Zentrum Berlin für Materialien und Energie GmbH, Berlin, Germany
2. Deutsches Elektronen-Synchrotron DESY, Hamburg, Germany
3. Institut für Physik und Astronomie, Universität Potsdam, Potsdam-Golm, Germany
4. Intelligent Embedded Systems, Universität Kassel, Kassel, Germany

Beating the coherence time

A new method for generating ultrashort pulses in XUV and X-ray FELs has been successfully tested

Ultrashort pulses generated by free-electron lasers (FELs) have revolutionised various fields of science and technology. Scientists can now observe and control phenomena such as electron movements, chemical reactions and phase transitions with unprecedented temporal resolution. The pulse duration in short-pulse schemes for self-amplified spontaneous emission (SASE) FELs is limited by the so called FEL coherence time. However, a recently proposed concept allows one to overcome the coherence time barrier and to get much shorter pulses.

The possibilities to generate few- and sub-femtosecond pulses in extreme ultraviolet (XUV) and X-ray FELs have been studied theoretically over the last twenty years, and the successful experimental demonstration of producing sub-femtosecond FEL laser pulses was recently achieved at different facilities. For SASE FELs the shortest pulse that can typically be generated is limited by the FEL coherence time. This longitudinal coherence of the photon pulses is formed due to slippage effects in the undulators where the emitted electromagnetic wave advances the electron beam by one wavelength while the electron beam passes one undulator period. Thus, the coherence time is given by the slippage of radiation with respect to the electron beam on the scale of FEL gain length.

A method to beat the coherence time limit in SASE FELs was proposed in [1]. In a first step one can create a short lasing slice – much shorter than the FEL coherence time – within the electron bunch. Due to the SASE process in the long main undulator a microbunching, e.g. a density modulation at the resonance wavelength, is generated within that short slice. However, the radiation pulse is still much longer (on the order of the coherence time) due to the mentioned slippage in the undulator. In a second step the modulated electron bunch produces a short radiation pulse in a short radiator while the long radiation pulse from the main undulator is suppressed or separated from the short pulse. Different methods of suppression (separation) were discussed in [1], one of them is the application of an exces-

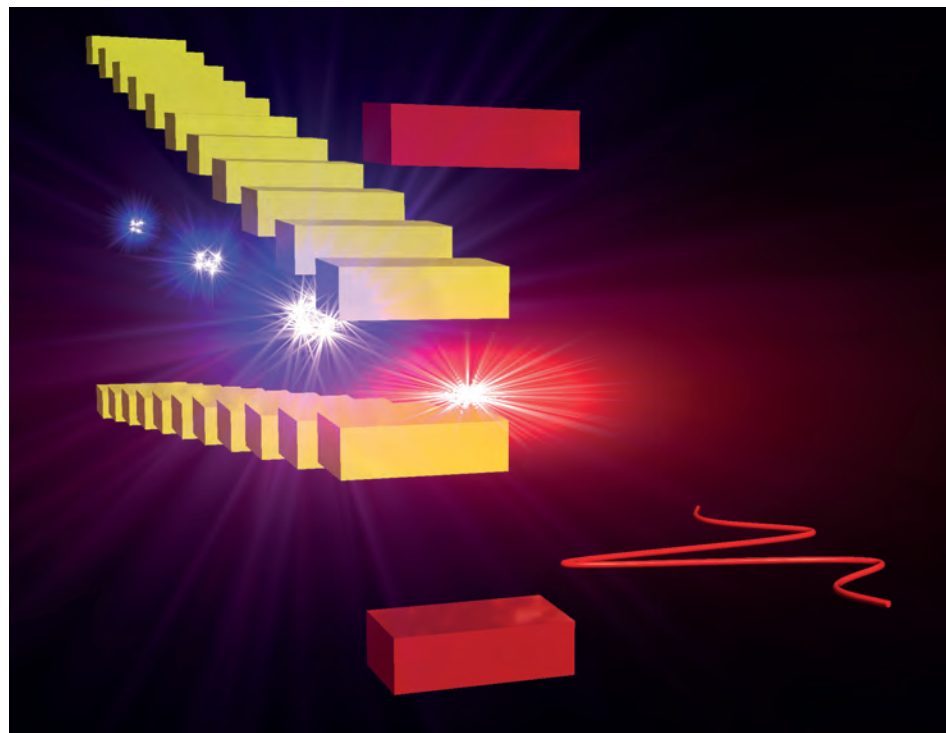


Figure 1 Schematic illustration of the new short-pulse scheme. The gaps of the magnetic segments of the undulator structure are decreasing along the undulator length, changing the resonance conditions for the SASE lasing process. By that, the long radiation pulse is suppressed while the microbunching within the electron bunch is maintained. The last undulator segment – here called radiator – is then tuned to resonance with the incoming microbunching and leads to the emission of ultrashort pulses not limited by the coherence time.

sive reverse taper in the main undulator. In fact, strong reverse undulator taper is used to suppress the radiation in the main undulator while keeping the microbunching as suggested in [2].

The scheme is shown in Fig. 1. The main undulator consists of many segments (shown in yellow) of which the gaps are decreasing along the undulator length, i.e. the undulator parameter K is increasing. The ultrashort radiation pulse is produced in a short radiator (shown in red), tuned to resonance with the incoming microbunching.

The experimental test of this concept was performed at the FLASH2 branch of the soft X-ray FEL user facility FLASH. The electron energy was 1.2 GeV and the FEL wavelength was set to 5 nm. A photoinjector laser with 1 ps duration was used to generate an electron bunch with a charge of 80 pC. Nonlinear compression was applied to the electron bunch in order to generate a short high-current leading peak for the production of ultrashort photon pulses. The gap-tunable undulator of FLASH2 consists of twelve segments. First, the so-called single-spike operation of a SASE FEL in standard configuration was established where only one longitudinal spectral mode is generated (this was validated at the FLASH2 spectrometer). Then, the following configuration was applied: The first eleven undulator segments were strongly reverse-tapered while the 12th segment played the role of the radiator. In order to effectively reduce its length (and thus the length of the radiated photon pulse), an ambient field correction coil was activated to steer the beam inside the radiator.

In order to measure the photon pulse duration, the auto-correlation method was employed. The split-and-delay unit at beamline FL24 [3] with its time resolution of 120 attoseconds was used to spatially split the incoming FEL beam into two partial beams. The two split beams were recom-

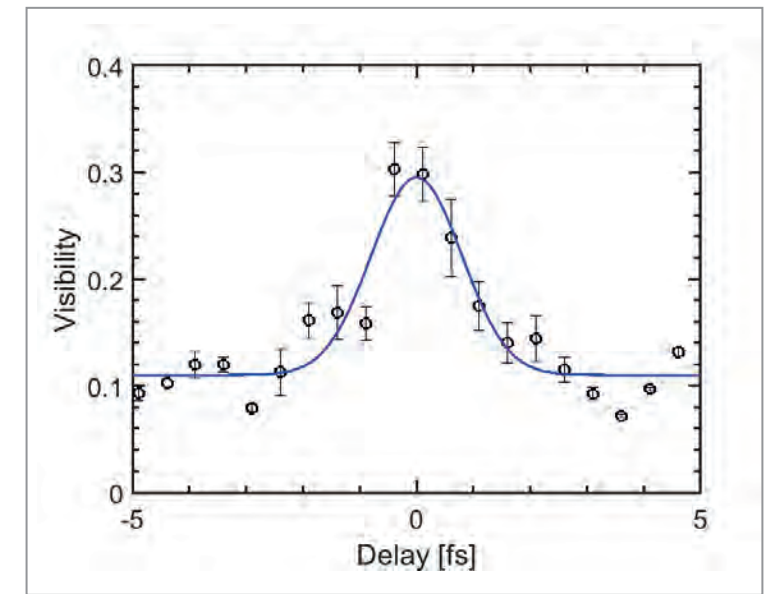


Figure 2 Field autocorrelation (AC) trace. The change of interference fringes contrasts with respect to the delay of the two overlapping photon pulses created using the split-and-delay unit at FLASH2. In case of single-spike SASE pulses, the width of the AC trace is directly related to the photon pulse duration. The conversion factor was determined by modelling and leads to a measured photon pulse duration of 1.26 ± 0.37 fs.

bined spatially and temporally on a screen at the beamline focus, creating interference fringes. By scanning the delay and measuring the visibility of the fringes, one can measure the field autocorrelation which is shown in Fig. 2.

The full width at half maximum (FWHM) of this trace is 1.88 ± 0.21 fs. Based on extensive FEL modelling of the generation process, a conversion coefficient of 0.67 to the FWHM of the pulse intensity distribution was obtained. Thus, the estimated photon pulse duration was 1.26 ± 0.37 fs and the measured pulse energy was 1.5 microjoules at the wavelength of 5 nm. This pulse duration of close to 1 fs FWHM sets a new record for FELs operating at this wavelength. The gigawatt-level short pulses with a potentially high repetition rate (up to several thousand pulses per second) can make FLASH a unique source within its wavelength range.

Author contact: Evgeny Schneidmiller, evgeny.schneidmiller@desy.de

References

1. E. A. Schneidmiller, 'Application of a modified chirp-taper scheme for generation of attosecond pulses in extreme ultraviolet and soft X-ray free electron lasers', *Phys. Rev. Accel. Beams* **25**, 010701 (2022).
2. E. A. Schneidmiller and M. V. Yurkov, 'Obtaining high degree of circular polarization at x-ray free electron lasers via a reverse undulator taper', *Phys. Rev. Spec.-Top. Accelerators and Beams* **16**, 110702 (2013).
3. M. Dreimann et al., 'The soft X-ray and XUV split-and-delay unit at beamlines FL23/24 at FLASH2', *J. Synchrotron Radiat.* **30**, 479 (2023).

Original publication

'Generation of Ultrashort Pulses in XUV and X-ray FELs via an Excessive Reverse Undulator Taper', *Photonics* **10**, 653-662 (2023). DOI: 10.3390/photonics10060653



Jakob Evgeny Schneidmiller¹, Matthias Dreimann², Marion Kuhlmann¹, Juliane Rönsch-Schulenburg¹ and Helmut Zacharias²

1. Deutsches Elektronen-Synchrotron DESY, Hamburg, Germany
2. Center for Soft Nanoscience, Westfälische Wilhelms-Universität, Münster, Germany

Apochromatic X-ray lenses

Pioneering a new X-ray focusing approach

Achromatic and apochromatic lenses, having the ability to focus multiple colours, i.e. wavelengths of light, into a single focus, have been long utilised in visible light optics. They are realised by combining individual lenses made from glass materials with different amounts of dispersion. In the X-ray regime, the realisation of achromatic and apochromatic lenses presents some unique challenges. A team of scientists from the Paul Scherrer Institut (Switzerland), the University of Basel (Switzerland) and DESY have demonstrated the first-ever realisation of apochromatic X-ray focusing by combining a Fresnel zone plate and a divergent refractive lens. The apochromatic X-ray lens was characterised by ptychographic imaging and by scanning transmission X-ray microscopy.

Refractive and diffractive lenses are broadly used in X-ray methods and high-resolution X-ray microscopy with many applications in materials science, renewable energies and biology. Nevertheless, both refractive and diffractive X-ray optics suffer from a strong chromatic aberration, that is, they focus different X-ray wavelengths at different distances along the optical axis. Consequently, many high-resolution X-ray analysis techniques are limited to the use of monochromatic X-ray beams, meaning that in many cases a large fraction of the X-ray intensity is sacrificed.

In the case of visible light, the chromatic aberration of refractive lenses was observed many centuries ago, for

example, impairing the performance of telescopes. In the mid-18th century, Chester Moor Hall tackled the chromatic aberration by stacking a convergent lens made of crown glass and a divergent lens made of flint glass to realise an achromatic doublet [1]. Due to the dispersion being stronger for flint glass than for crown glass, a tailored combination of the two lenses yields identical focal length for two separate wavelengths and low chromatic aberration for the wavelength range in between despite the pronounced chromatic aberration of each individual lens.

In the X-ray regime, the realisation of achromatic doublets presents some unique challenges, primarily due to the

inherent nature of X-ray interaction with matter and the resulting intricacies of X-ray optics fabrication. An achromatic X-ray lens can be realised by combining a weakly divergent refractive lens with a strongly converging Fresnel zone plate in close contact, as shown in Fig. 1a. Such an approach was theoretically proposed about two decades ago [2] but was only recently experimentally realised [3]. On the other hand, an alternative configuration carefully selecting the separation distance between the two individual lenses results in apochromatic X-ray focusing, as theoretically suggested in [4] and as shown in Fig. 1b. The apochromatic case offers a significantly improved chromatic aberration correction over a wider range of X-ray energies as qualitatively shown in Fig. 1c. The achromatic case has dispersion dominated by a quadratic dependence on the photon energy, while the apochromatic case shows a cubic dependence. For completeness, the dispersion of a Fresnel zone plate and refractive lens is also plotted.

The research team has now experimentally demonstrated the realisation of apochromatic X-ray focusing. The apochromatic device consisted of two independent optical elements: a divergent refractive X-ray lens produced by state-of-the-art 3D printing with submicrometre accuracy, shown in Fig 2a and b, and a Fresnel zone plate fabricated by electron beam lithography and gold electroplating. These devices were produced in-house using the clean-room and nanofabrication facilities at the Paul Scherrer Institut. The apochromatic X-ray lens was realised and characterised at the PETRA III beamline P06. The X-ray measurements consisted of scanning transmission X-ray microscopy and ptychography imaging demonstrating submicrometre apochromatic X-ray focusing for an X-ray energy range from 7 to 12 keV.

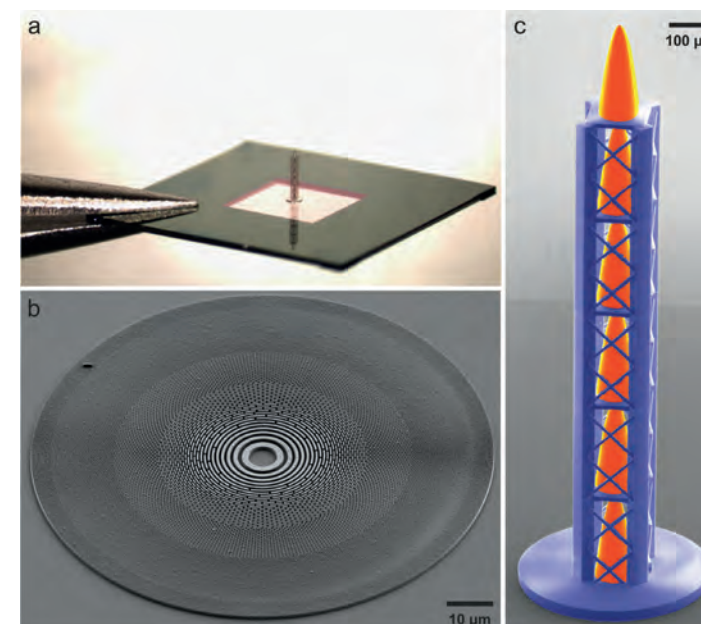


Figure 2
a) Optical microscope image of the 3D-printed diverging CRL standing on 250-nm thick silicon nitride membrane. The silicon frame is being held from the side by tweezers. b) Scanning electron microscopy image of a gold Fresnel zone plate under 45 degree tilt angle. c) Scanning electron microscopy image of the CRL showing the individual refractive lenses with high detail (in orange)

Looking ahead, apochromatic X-ray lenses have the potential of becoming a cost-effective and compact alternative to mirror-based systems, with the additional advantage of being on-axis imaging optics. They are likely to play an increasingly important role in the field of X-ray imaging and microscopy and for their scientific applications in both accelerator-based and laboratory X-ray sources.

Author contact: Joan Vila-Comamala, joan.vila-comamala@psi.ch

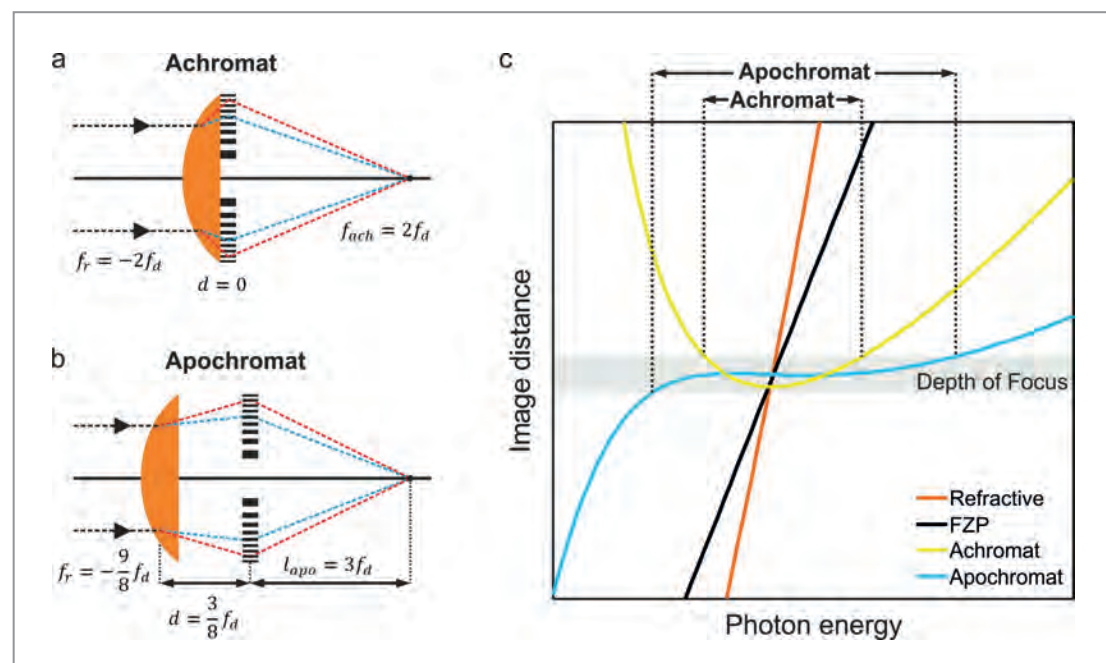


Figure 1
Conceptual design for a) an X-ray achromat and b) an X-ray apochromat by combining a refractive lens and a Fresnel zone plate. c) Conceptual energy-dependent image distance curves (dispersion) are compared for an achromat (yellow) and apochromat (blue) as well as a Fresnel zone plate (black) and refractive lens (orange). The ranges of the chromatic aberration correction for the achromat and apochromat are qualitatively shown on the top axis of the plot.

References

1. J. Ramsden, 'Some observations on the invention of achromatic telescopes', R. Soc. Lett. Pap. decade IX, 138 (1789).
2. Y. Wang, W. Yun and C. Jacobsen, 'Achromatic Fresnel optics for wideband extreme-ultraviolet and X-ray imaging', Nature 424, 50–53 (2003).
3. A. Kubec, M.-C. Zdora, U. T. Sanli, A. Diaz, J. Vila-Comamala and C. David, 'An achromatic X-ray lens', Nat. Commun. 13, 1305 (2022).
4. H. N. Chapman and S. Bajt, 'High-resolution achromatic X-ray optical systems for broad-band imaging and for focusing attosecond pulses', Proc. R. Soc. A 477, 20210334 (2021).

Original publication

'Apochromatic X-ray focusing', Light: Science & Applications 12, 107 (2023). DOI: 10.1038/s41377-023-01157-8



Umut T. Sanli¹, Griffin Rodgers², Marie-Christine Zdora¹, Qi Peng⁴, Jan Garrevoet³, Ken Vidar Falch³, Bert Müller², Christian David² and Joan Vila-Comamala¹

1. Paul Scherrer Institut, Villigen-PSI, Switzerland
2. University of Basel, Basel, Switzerland
3. Deutsches Elektronen-Synchrotron DESY, Hamburg, Germany

Artificial intelligence for self-supervised tomographic image reconstruction

Reconstructing high quality images from sinograms containing limited number of projections

X-ray chemical tomography methods are non-destructive methods that yield images corresponding to a sample's cross-section. In these 'chemical' images, each pixel is associated with a local spectrum or scattering pattern containing unique physicochemical information regarding the sample's properties. These techniques, however, typically suffer from long data acquisition times, and often sparse data are acquired which lead to artefacts in the reconstructed images. Here, we leverage deep learning methods using artificial neural networks to improve the quality of the reconstructed images and suppress the formation of such artefacts.

X-ray chemical tomography methods combine a scattering or spectroscopic technique with the tomographic data acquisition approach [1]. These methods are most often implemented using a so-called 'pencil' beam (i.e. a narrowly focused beam) and are associated with long data acquisition times, as the sample needs to be both translated and rotated during the computed tomography (CT) scan. The CT measurement typically involves a series of line scans performed at different tomographic angles (projections) covering an angular range of 0–180°. In practice, in order to acquire the experimental data at reasonable timescales, the number of projections used is usually significantly smaller than the ideal number suggested by the Nyquist

sampling theorem. This applies to both lower spatial resolution dynamic experiments and high spatial resolution static measurements. Unfortunately, this approach of using sparse sinograms and fewer projections can create images with angular undersampling artefacts.

Over the last decade, artificial intelligence-based methods have significantly advanced image processing tasks, often outperforming traditional algorithms. Traditionally, supervised learning has been the main approach to train artificial neural networks. This method requires artefact and artefact-free image pairs for training. However, obtaining such pairs from experimental data is challenging, if not impossible. Recently, the focus has shifted to self-supervised approaches. These methods allow neural networks to learn directly from the experimental data without needing predefined artefact-free images.

In this work, we have developed a scalable lightweight neural network architecture that reconstructs an image from a given sinogram using a self-supervised approach (Fig. 1). In our method, a generator network, which we term 'SingleDigit2Image' (SD2I), creates an image, that is then forward projected, e.g. by using a 2D Radon transform, to yield a corresponding sinogram. Subsequently, this

Figure 1

The flowchart of the SD2I training algorithm and its architecture. SD2I generates an image based on a random constant input; this image ($m \times m$ pixels large) is then converted into a sinogram which is compared with the experimental sinogram. SD2I's architecture consists of four dense (red) layers followed by a series of upsampling (blue) and 2D convolutional (yellow) layers.

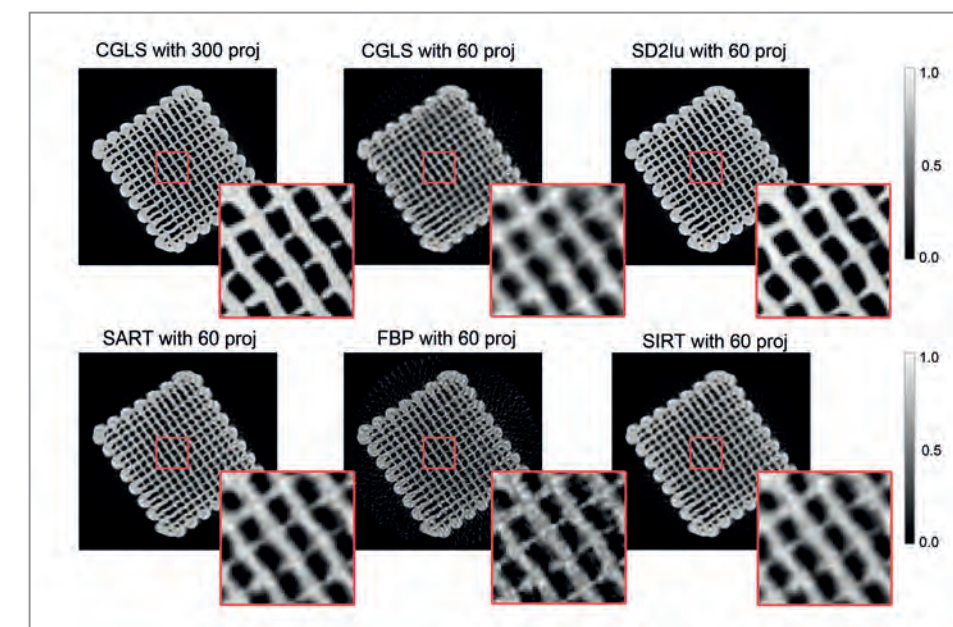
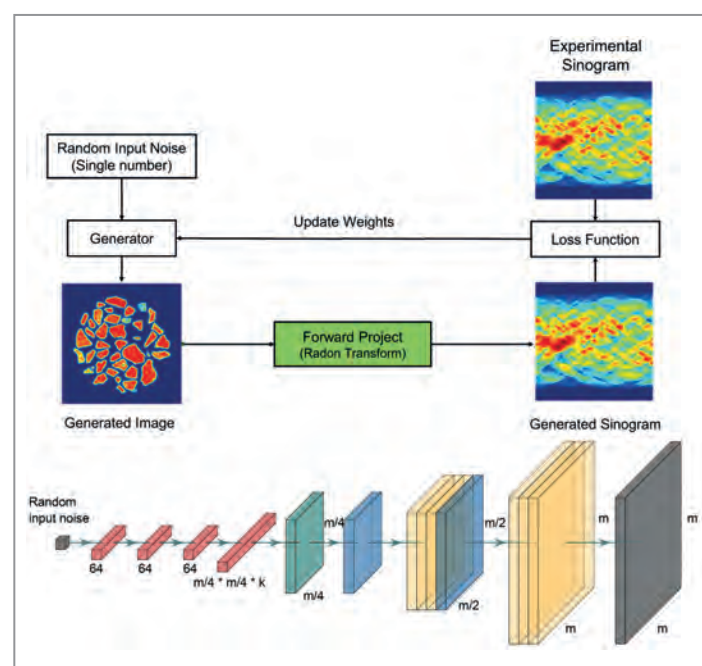


Figure 2

Comparison of reconstructed images from a photocatalyst XRD-CT sinogram using various reconstruction approaches. The SD2I network is able to yield high quality images from this sinogram which has limited numbers of projections.

simulated sinogram is compared with the experimental sinogram through the loss function, and the weights of the SD2I are updated accordingly. The process is repeated until a convergence criterion is reached. The SD2I architecture consists of a series of four dense layers, i.e. three small layers of 64 neurons and a large dense layer, followed by a series of upsampling and 2D convolutional layers. Two new concepts have been introduced in this architecture compared to previous implementations [2]: First, the input to the network is not an image but a single number and second, the large dense layer is 4 times smaller compared to final image in each dimension, i.e. 16 times smaller in terms of numbers of pixels/neurons and is followed by a decoder part using 2D convolutional layers. This architecture allowed us to radically decrease the number of network parameters and employ it even for very large datasets.

Specifically, we have tested the efficacy of the method, using simulated data as well as experimental synchrotron X-ray micro-CT and X-ray diffraction-computed tomography (XRD-CT) data. The largest images that the network was able to reconstruct were larger than 1024×1024 pixels. Importantly, it was shown that the network is able to reconstruct high quality images even from sinogram data that have limited numbers of projections (Fig. 2). Last but not least, the network does not normalise the reconstructed images, which is an important feature, if information regarding the absolute intensities is required for quantitative analysis of the reconstructed data.

The network could be potentially applied to other tomographic methods and modalities, such as neutron tomography and X-ray fluorescence tomography. The network was originally developed for tomographic image reconstruction

using 2D parallel/pencil beam geometries. However, it is possible to extend it for other inverse problems in imaging if the appropriate forward model is known, such as the parallax problem in XRD-CT [3].

Author contact: Antonis Vamvakeros, antony@finden.co.uk

References

1. A.M. Beale et al., 'Progress towards five dimensional diffraction imaging of functional materials under process conditions', *Coord. Chem. Rev.* 277, 208–223 (2014).
2. X. Yang et al., 'Tomographic reconstruction with a generative adversarial network', *J. Synchrotron Radiat.* 27, 486–493 (2020).
3. H. Dong et al., 'A neural network reconstruction approach for obtaining parallax-free X-ray powder diffraction computed tomography data from large samples', *ChemRxiv preprint*, DOI: 10.26434/chemrxiv-2023-wgjmf (2023).

Original publication

'A scalable neural network architecture for self-supervised tomographic image reconstruction', *RSC Digital Discovery* 2, 967–980 (2023). DOI: 10.1039/D2DD00105E



H. Dong¹, S. D. M. Jacques², W. Kockelmann³, S. W. T. Price², R. Emberson⁴, D. Matras^{5,6}, Y. Odarchenko², V. Middelkoop⁷, A. Giokaris², O. Gutowski⁸, A.-C. Dippel⁹, M. von Zimmermann⁹, A. M. Beale^{1,2,9}, K. T. Butler^{10,11} and A. Vamvakeros^{2,12}

1. Department of Chemistry, University College London, London, United Kingdom
2. Finden Ltd, Rutherford Appleton Laboratory, Harwell, Oxford, United Kingdom
3. STFC, Rutherford Appleton Laboratory, ISIS Facility, Harwell, United Kingdom
4. Depart. of Mathematics & Statistics, Lancaster Univ. Lancaster, United Kingdom
5. Diamond Light Source, Harwell Science and Innovation Campus, Didcot, United Kingdom
6. The Faraday Institution, Quad One, Harwell Campus, Didcot, United Kingdom
7. Flemish Institute for Technological Research (VITO), Mol, Belgium.
8. Deutsches Elektronen-Synchrotron DESY, Hamburg, Germany
9. Research Complex at Harwell, Rutherford Appleton Laboratory, Didcot, United Kingdom
10. SciML, Scientific Computing Depart. STFC Rutherford Appleton Lab., Didcot, United Kingdom
11. School of Engineering and Materials Science, Queen Mary University of London, London, United Kingdom
12. Dyson School of Design Engineering, Imperial College London, London, United Kingdom

Imaging out of incoherence

Intensity interferometry with atomic fluorescence radiation is possible

To determine the structure of condensed matter, coherent X-ray diffraction has been an indispensable method for more than a hundred years. Today, accelerator-based X-ray sources such as synchrotron radiation sources and X-ray lasers are used for a plethora of imaging applications employing coherent light. In contrast, an experiment at the European XFEL has recently succeeded in using incoherent X-ray fluorescence photons for imaging - an approach that dates back to Max von Laue and the beginnings of X-ray crystallography in 1912.

In the search for interference phenomena of atomic lattices, the researchers Walter Friedrich, Paul Knipping and Max von Laue initially set up their photographic plates sideways to copper sulphate crystals so that they could detect as much as possible of the fluorescence radiation excited by the X-ray tube. However, these efforts remained unsuccessful until Arnold Sommerfeld remarked that the fluorescence radiation could not produce an interference pattern since the independent spontaneous emissions of the atoms in the crystal have no well-defined phase relationships with each other [1]. The breakthrough came only when the researchers placed their photographic plates behind the crystals. Characteristic patterns appeared on the photographic plates which could be explained by the coherent superposition of the incident X-ray waves scattered by the atoms. This was the birth of X-ray crystallography, for which Max von Laue received the Nobel Prize in Physics two years later in 1914.

Since then, fluorescence radiation has been considered unsuitable for coherent imaging methods. However, this view is only true as long as the detection or integration time of the detectors is significantly longer than the emission time of the atomic fluorescence and thus averages over many independent emission processes. If, on the other hand, the detection time is comparable to the emission time, the emission processes occurring within this time are phase-coherent and capable of giving rise to an interference pattern.

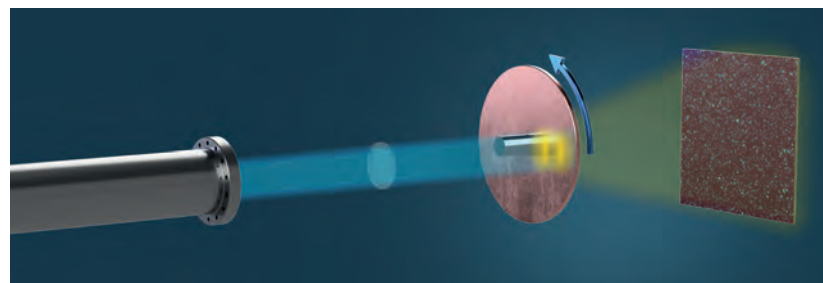


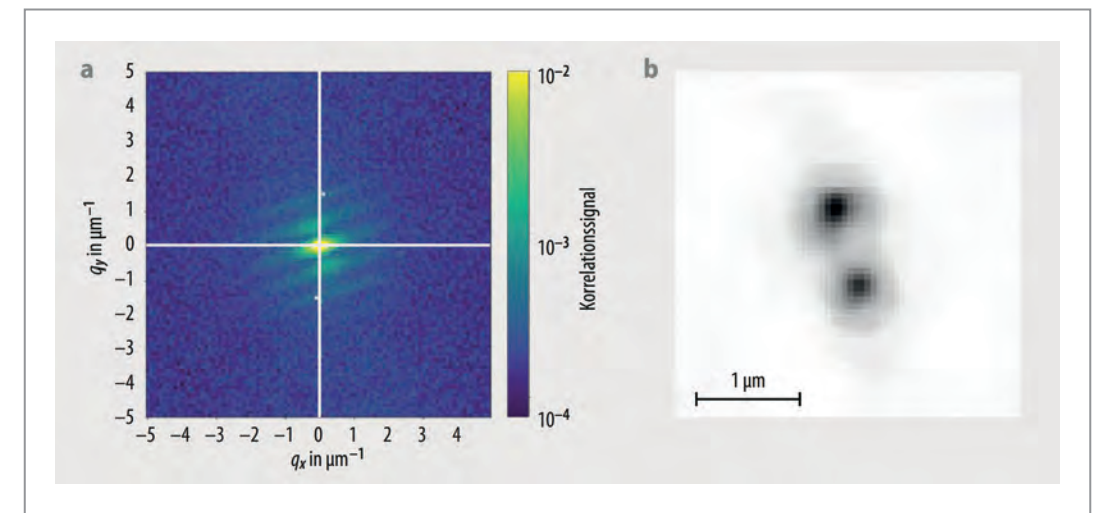
Figure 1

In the experimental setup at the European XFEL, a phase grating focuses the X-ray beam on two points (yellow) on a thin copper foil. The resulting fluorescence radiation produces a speckle pattern in the far field which is recorded by a spatially resolving detector. The copper foil rotates continuously so that the intense X-ray pulse does not destroy it.

From measurement to measurement, the pattern will fluctuate in its structure. It is possible to create a stationary distribution by evaluating the so-called spatial correlation function of each pattern. In the 1950s, this insight prompted two British astronomers, Robert Hanbury Brown and Richard Q. Twiss (HBT), to apply this principle to the light of stars whose images were washed out by atmospheric fluctuations. By reducing the detection time to below the typical fluctuation time of the atmosphere and by evaluating the spatial correlations of the intensities recorded by two separate detectors, HBT were able to determine structural information such as the diameters and distances of stars [2,3].

This revolutionary method of HBT, called intensity interferometry, is a two-photon interference phenomenon that occurs when two indistinguishable photons emitted from different positions within a source reach two different detectors simultaneously. Applications of intensity interferometry with atomic fluorescence radiation and thus its extension into the X-ray domain have so far been ruled out because in this case, the coherence time is given by the extremely short lifetime of the atomic fluorescence states. For example, the lifetime of the electronic state of a copper atom with a vacancy in the K shell is less than 1 fs. However, the photons of the copper atoms indeed do become indistinguishable if the atoms are excited within this time interval. Such fast excitation has only recently become possible with the development of X-ray lasers

Figure 2
a) More than 58 million correlations of X-ray fluorescence snapshots yield a map of the spatial frequency distribution of the sources or q-vectors in reciprocal space.
b) An analysis of the interference pattern using conventional coherent diffractive imaging methods produces a high-resolution image of the two illuminated spots on the copper disk. (Copyright: 2023 by the APS, adapted from the original publication.)



with pulse durations of femtoseconds or less. They allow intensity interferometry to be transferred to diffractive imaging with X-ray fluorescence photons [4].

Recently, an important experimental step in this direction was made in an experiment at the European XFEL. A refractive lens combined with a phase grating focused the X-ray beam with 109 photons per pulse, a photon energy of 9 keV, and a pulse length of 6.2 fs into two points impinging on a thin copper foil, forcing the illuminated copper atoms to emit K-fluorescence radiation at 8.9 keV (Fig. 1). An 'Adaptive Gain Integrating Pixel detector' with one million pixels recorded the light from this luminous source (the two fluorescing spots), giving the opportunity to compute up to 1012 correlations between pixel pairs within a single laser pulse. The calculated correlation signal clearly shows the two-photon interference, with maxima up to the third order (Fig. 2a). To reconstruct the image of the source, the obtained fringe pattern was analysed by employing iterative algorithms to determine the phase of the field to then create the image through Fourier synthesis. This allowed the size and spacing of the two fluorescent spots on the copper foil to be determined directly (Fig. 2b).

The experiment returns to Max von Laue's original approach and provides evidence that fluorescence radiation can indeed be used for diffractive imaging - thanks to femtosecond X-ray sources and spatially resolving pixel detectors that were obviously not available in 1912. With further improvements, the method can in principle be used to determine structures down to atomic resolution. With the European XFEL providing even shorter pulses in the future, significantly smaller numbers of fluorescence images will be required. Ultimately, the scheme could allow the imaging of single molecules in combination with coherent X-ray diffraction. Using ultrashort X-ray pulses, it would then be possible to obtain element-specific and time-resolved reaction processes with atomic resolution.

Author contact: Fabian Trost, fabian.trost@desy.de
Ralf Röhlsberger ralf.roehlsberger@desy.de
Joachim von Zanthier, joachim.vonzanthier@physik.uni-erlangen.de
Henry Chapman, henry.chapman@desy.de

References

1. M. Eckert, 'Max von Laue and the discovery of X-ray diffraction in 1912', *Ann. Phys.* 524, A83 – A85 (2012).
2. R. Hanbury Brown and R. Q. Twiss, 'Correlation between Photons in two Coherent Beams of Light', *Nature* 177, 27 – 29 (1956).
3. R. Hanbury Brown and R. Q. Twiss, 'A Test of a New Type of Stellar Interferometer on Sirius', *Nature* 178, 1046 – 1048 (1956).
4. A. Classen, K. Ayyer, H. N. Chapman, R. Röhlsberger and J. von Zanthier, 'Incoherent Diffractive Imaging via Intensity Correlations of Hard X Rays', *Phys. Rev. Lett.* 119, 053401 (2017)

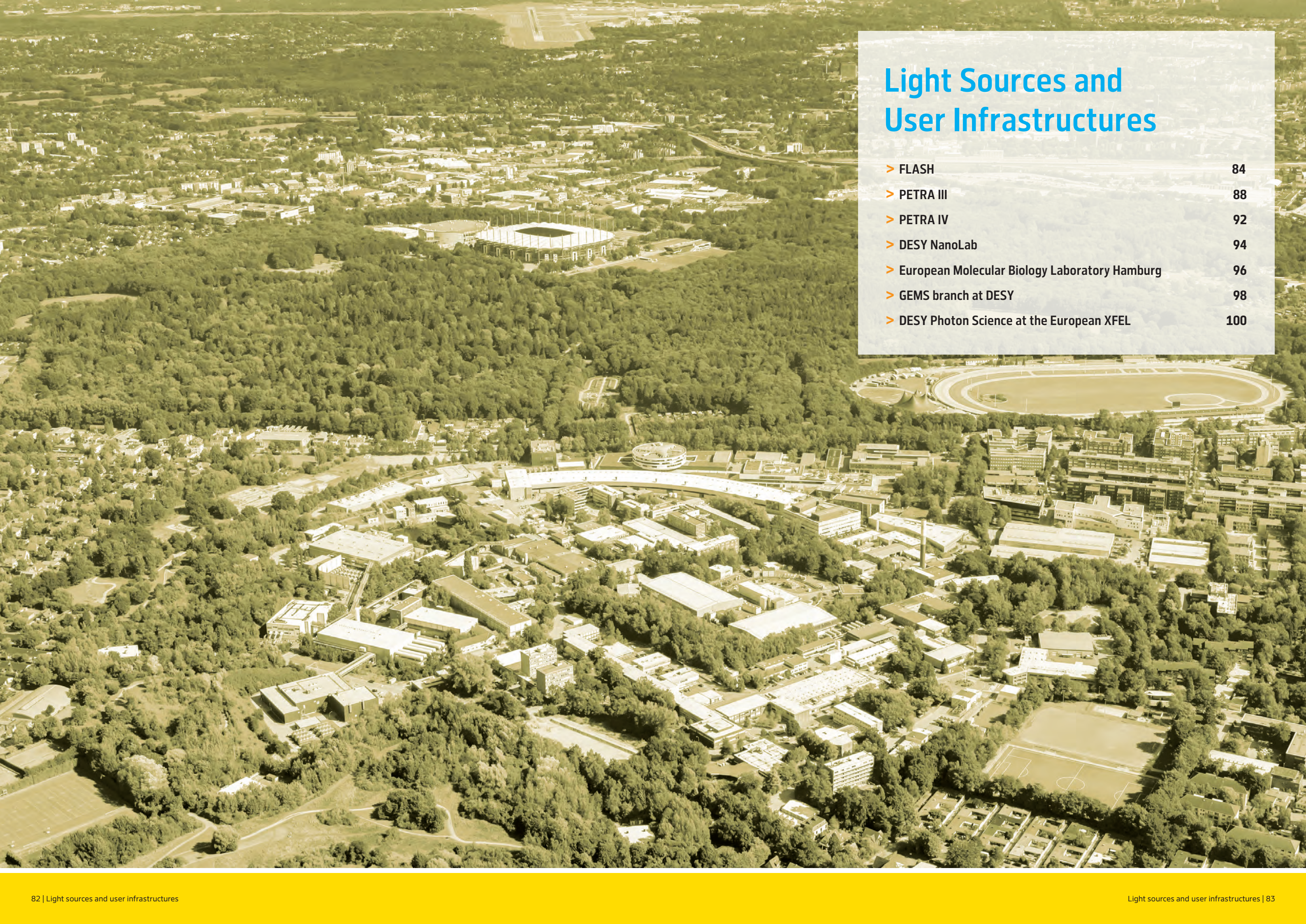
Original publication

'Imaging via Correlation of X-Ray Fluorescence Photons', *Physical Review Letters* 130, 173201 (2023).
DOI: 10.1103/PhysRevLett.130.173201



Fabian Trost¹, Kartik Ayyer^{2,3}, Mauro Prasciolu¹, Holger Fleckenstein¹, Miriam Barthelmess¹, Oleksandr Yefanov¹, J. L. Dresselhaus³, Chufeng Li¹, Saša Bajt^{1,3}, Jerome Carnis¹, Tamme Wollweber^{2,3}, Abhishek Mall², Zhou Shen², Yulong Zhuang², Stefan Richter^{4,5}, Sebastian Karl⁴, Sebastian Cardoch⁶, Kajwal Kumar Patra⁶, Johannes Möller⁷, Alexey Zozulya⁷, Roman Shayduk⁷, Wei Lu⁷, Felix Brauße⁷, Bertram Friedrich⁷, Ulrike Boesenberg⁷, Ilia Petrov⁷, Sergey Tomin⁸, Marc Guetg⁸, Anders Madsen⁷, Nicusor Timneanu⁶, Carl Coleman^{4,6}, Ralf Röhlsberger^{3,9,10,11,8}, Joachim von Zanthier^{4,5} and Henry N. Chapman^{1,3,6,12}

1. Center for Free-Electron Laser Science CFEL, DESY, Hamburg, Germany
2. Max Planck Institute for the Structure and Dynamics of Matter, Hamburg, Germany
3. The Hamburg Centre for Ultrafast Imaging, Universität Hamburg, Hamburg, Germany
4. Dept. of Physics, Friedrich-Alexander-Univ. Erlangen-Nürnberg, Erlangen, Germany
5. Erlangen Graduate School in Advanced Optical Technologies (SAOT), Erlangen, Germany
6. Department of Physics and Astronomy, Uppsala, Sweden
7. European XFEL, Schenefeld, Germany
8. Deutsches Elektronen-Synchrotron DESY, Hamburg, Germany
9. Helmholtz-Institut Jena, Jena, Germany
10. GSI Helmholtzzentrum für Schwerionenforschung, Darmstadt, Germany
11. Friedrich-Schiller Universität Jena, Institut für Optik und Quantenelektronik, Jena, Germany
12. Department of Physics, Universität Hamburg, Hamburg, Germany



Light Sources and User Infrastructures

> FLASH	84
> PETRA III	88
> PETRA IV	92
> DESY NanoLab	94
> European Molecular Biology Laboratory Hamburg	96
> GEMS branch at DESY	98
> DESY Photon Science at the European XFEL	100

FLASH – on its way towards FLASH2020+

A buzz of activity and the next upgrades

The year 2023, positioned in between the two FLASH2020+ upgrade-related shutdowns, was quite intense for the whole FLASH team. It was characterised by a very high fraction of 24/7 operation with the intention to partially make up for the longer shutdowns, in particular by providing 5000 hours of machine operation for user experiments in 30 weeks instead of the usual about 4500 hours in 27 weeks.

At FLASH2 the new pulse-length preserving monochromator beamline FL23 [1,2] saw first light at the beginning of 2023 and has since been commissioned using the FEL beam in several FLASH study shifts. The beamline optics alignment has been performed and optimised for the full operation wavelength range from 2 to 25 nm. Moreover, the performance in single- and double-grating monochromator operation mode has been validated experimentally for the resolving power, efficiency and dispersion. Well-known absorption resonances in neon and krypton were used to calibrate the monochromator (Fig. 1), and a microfocus below $8\ \mu\text{m} \times 8\ \mu\text{m}$ FWHM has been achieved so far (Fig. 2 depicts an intermediate result) – all close to specifications. A first FLASH in-house user experiment on

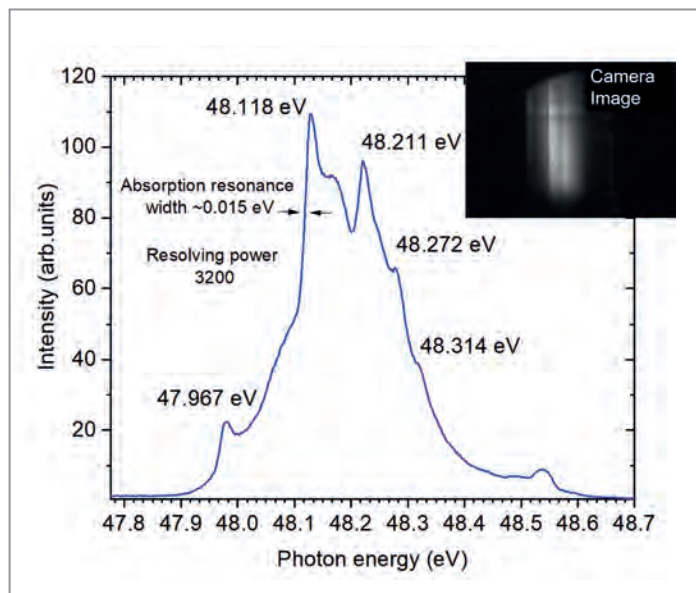


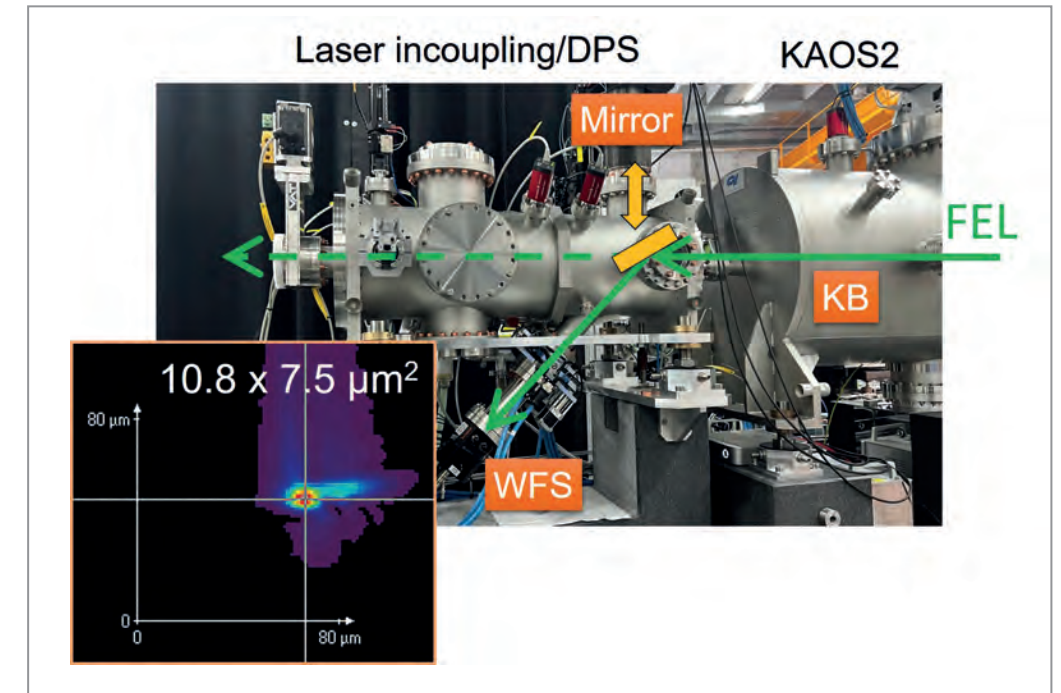
Figure 1
SASE spectrum (averaged over a pulse train with 20 pulses) with sharp neon gas absorption resonances, visible as superimposed dips, for calibration of energy and resolving power. This spectrum was taken at the intermediate ('exit') slit plane behind the first grating of FL23. It yields a resolving power of 3200, fitting to specs.

single-shot ptychography together with colleagues from European XFEL and the DESY Photon Science detector group has been successfully conducted. In parallel, the FLASH2 optical laser connection to FL23 has been realised, and a pilot experiment using FEL and pump-probe laser for a time-resolved study and characterisation of the pulse-length preserving double monochromator scheme is planned for the beginning of 2024. Furthermore, three more user experiments, one with a liquid jet setup and two employing the afterburner undulator for variable polarisation, are currently planned at FL23 before the next shutdown starting mid 2024 (see below).

First steps of the FLASH2020+ pump-probe laser design plans were implemented by the laser science and technology group from DESY Photon Science: The FLASH pump-probe lasers will be utilising a novel laser pulse post-compression technique to reduce the duration of the 1030 nm high-repetition rate Yb pump laser pulses from about 1 ps to below 70 fs and deliver them to the experiment. This technique was already successfully implemented at the PG beamlines in 2021 [3] and is now also rolled out at FL23. The new pulse-shortening technique based on multi-pass cells (MPC) is about ten times more energy-efficient than the previously established optical parametric chirped-pulse amplification (OPCPA) approach, and, additionally, cost and maintenance demands are lower. Now, the 1 ps pump pulses run through a gas-filled MPC for spectral broadening, followed by an efficient pulse compressor close to the instrument end station [4,5] (Fig. 3). By implementing a second MPC stage we expect to reach sub-20 fs duration at $> 1\ \text{mJ}$ energy per pulse and 100 kHz intra-burst repetition rate ($> 100\ \mu\text{J}$ at 1 MHz) at the FLASH experiments. The MPC technology was developed to its current mature level in cooperation between our laser science and technology group, the University of Lund and Helmholtz Institute Jena. Once established at FL23, it will also be implemented at the other FLASH beamlines in the near future.

In late September 2023, as planned, the afterburner-undulator was mounted at the end of the FLASH2 undulator line (Fig. 4). The electrical and network connections for remote gap and polarisation control have meanwhile been installed as well, and the afterburner performance will be characterised by determining the polarisation state of the generated FEL pulses. To accomplish this, a setup of circularly arranged time-of-flight photoelectron spectrometers, simi-

Figure 2
Focus measured with a wavefront sensor (WFS) behind the Kirkpatrick-Baez (KB) Active Optical System ('KAOS2' from FERMI, see photo) after some optimisation. The outcoupling mirror towards the WFS is integrated into the differential pumping stage (DPS) which separates the focusing optics from the experiment behind.



lar to the 'cookie-box' instrument developed by Viefhaus et al. [6], will be used. In spring 2024, two magnetism experiments utilising X-ray circular dichroism at the 3d transition metal L-edges at FL23 will make use of the high degree of circular polarisation of the FEL pulses generated by the afterburner undulator. In the near future, the afterburner also allows for studies of chiral molecules. Here, the handedness of stereoisomers is particularly relevant for the therapeutic properties of pharmaceuticals.

Outlook towards 2024:

In the first half of 2024, another twelve weeks (~2000 hours) of user operation are planned, of which about ten weeks

are reserved for the remaining scientific proposals that have already been approved by our project review panel (PRP). In the last two user weeks end of May, a test of a new 'Standardised Access Mode' (SAM) for users is planned. Similar to the corresponding access schemes at other facilities, the operation parameters of the FLASH facility, the optical lasers, as well as instrumental setups will be kept within 'routinely' achievable predefined boundary conditions, communicated to potential users in a corresponding call. The goal is to run a set of similar experiments in a fast sequence with a few days per experiment only. We strive for further enhancing the productivity in terms of publication output at FLASH, at reduced effort

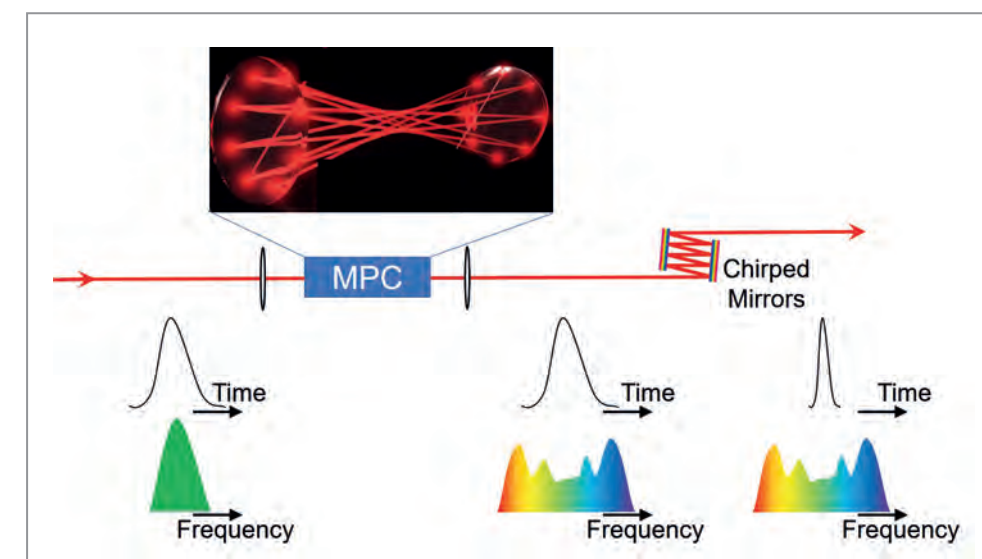


Figure 3
Sketch of the temporal and spectral properties of the optical laser pulses along their path. Left: before entering the multi-pass cell, middle: exiting the multi-pass cell, right: behind a chirped mirror compressor close to the experiment.



Figure 4

Afterburner undulator mounted in the FLASH2 tunnel. The few hundred individually mounted and fine-adjusted permanent magnets (above and below the filigree vacuum tube for the electrons held by the black adjustment stages) are still protected by wooden boards against potential damage.



Figure 5

Impressions from a commissioning shift at the FLASH beamline FL23.

for users and staff. This first SAM test will happen in the well-suited facility-owned instrument URSA-PQ [7] which employs a magnetic bottle spectrometer for atomic, molecular and optical physics (AMO) and gas-phase chemistry experiments. After this test we will evaluate how and if SAM can be combined with other instruments and/or other machine or laser parameter configurations.

From June 2024 to August 2025, FLASH will be in the next upgrade shutdown within the FLASH2020+ programme [8], with this time in particular the FLASH1 FEL branch undergoing a complete makeover:

- External seeding will be installed, i.e. new undulators with variable gap and polarisation control and a high repetition rate (MHz) seed laser. The latter imprints its longitudinal coherence properties onto the electron bunches which results in FEL pulses with an almost full degree of longitudinal coherence at defined wavelength and very small spectral bandwidth. In addition, the energy fluctuations of the generated pulses will be at the percent level only. In many science areas this is a major step forward compared to strongly fluctuating SASE pulse parameters. The combination of synchrotron-like stability and optical laser-like coherence at FLASH1 is supposed to attract also new users which have been mostly working at their own lab sources or with synchrotron radiation before.

FLASH1 will then provide them with up to 5000 extremely intense (μJ -level) and short (a few 10 fs) pulses per second in the XUV to soft X-ray range, which is unique worldwide.

- A new photon transport beamline with pulse-resolved diagnostics will be installed behind the undulators. It will be based on the latest diagnostics developments for FLASH2 while adding new components especially required for characterisation of the seeded FEL pulses. The state-of-the-art diagnostics for pulse intensity, beam position and spectral distribution developed at FLASH [9] will be complemented by established diagnostic concepts for pulse length and polarisation [6] which are presently further developed for the specific needs at the seeded FLASH1. Those diagnostics will not only allow to characterise all pulses comprehensively but also to steer the seeding process towards best parameter output.

Even in difficult times like now, the transition of FLASH1 to an externally seeded FEL has always been seen as the priority within the FLASH2020+ project. The extremely tight financial and temporal framework imposed the challenging task to find the most scientifically beneficial upgrade plan. This required strong modifications to the original project timeline as initially described in the conceptual design report (CDR) of FLASH 2020+ [9]. Especially components

not requiring installation inside the accelerator tunnel were postponed to a future realisation. We implemented cost adjustments, resulting in a reduced parameter range for SASE as well as limitations regarding other surrounding instrumentation, which we plan to resolve as soon as the central seeding project is close to accomplishment and the financial situation allows.

After the next shutdown, in the period between the commissioning and the regular competitive access, we plan for 'community proposals' at the seeded FLASH1. These proposals are thought as first demonstrations of a specific capability of the new source which, is essential for a particular science community. A workshop on developing these proposals with the international user community and the FLASH team will take place end of January 2024 in the week of the Photon Science Users' Meeting. The goal of the workshop is to assemble the communities to work on these key experiments together. We are looking for 1-2 community proposals per science area (chemistry, materials science, AMO, biology), also accounting for the local expertise and available instrumentation at FLASH.

Contact (FLASH and FLASH2020+):
 Markus Gühr, markus.guehr@desy.de
 Rolf Treusch, rolf.treusch@desy.de
 Lucas Schaper, lucas.schaper@desy.de

References

1. L. Poletto, F. Frassetto, G. Brenner, M. Kuhlmann and E. Plönjes, 'Double-grating monochromatic beamline with ultrafast response for FLASH2' at DESY, *J. Synchrotron Rad.* 25, 131-137 (2018).
2. M. Ruiz-Lopez, L. Samoylova, G. Brenner, M. Mehrjoo, B. Faatz, M. Kuhlmann, L. Poletto and E. Plönjes, 'Wavefront-propagation simulations supporting the design of a time-delay compensating monochromator beamline' at FLASH2, *J. Synchrotron Rad.* 26, 899-905 (2019).
3. M. Seidel, F. Pressacco, O. Akcaalan, T. Binhammer, J. Darvill, N. Ekanayake, M. Frede, U. Grosse-Wortmann, M. Heber, C. M. Heyl, D. Kutnyakhov, C. Li, C. Mohr, J. Müller, O. Puncken, H. Redlin, N. Schirmel, S. Schulz, A. Swiderski, H. Tavakol, H. Tünnermann, C. Vidoli, L. Wenthaus, N. Wind, L. Winkelmann, B. Manschwetus, I. Hartl, 'Ultrafast MHz-Rate Burst-Mode Pump-Probe Laser for the FLASH FEL Facility Based on Nonlinear Compression of ps-Level Pulses from an Yb-Amplifier Chain', *Laser Photonics Rev.* 16, 2100268 (2022).
4. A.-L. Viotti, S. Alisauskas, M. Seidel, A. Tajalli, B. Manschwetus, H. Cankaya, K. Jurkus, V. Sinkus and I. Hartl, 'FLASH free electron laser pump-probe laser concept based on spectral broadening of high-power ytterbium picosecond systems in multi-pass cells', *Rev. Sci. Instrum.* 94, 023002 (2023).
5. A.-L. Viotti, M. Seidel, E. Escoto, S. Rajhans, W. P. Leemans, I. Hartl and C. M. Heyl, 'Multi-pass cells for post-compression of ultrashort laser pulses', *Optica* 9, 197-216 (2022).
6. G. Hartmann, A. O. Lindahl, A. Knie, N. Hartmann, A. A. Lutman, J. P. MacArthur, I. Shevchuk, J. Buck, A. Galler, J. M. Glowina, W. Helml, Z. Huang, N. M. Kabachnik, A. K. Kazansky, J. Liu, A. Marinelli, T. Mazza, H.-D. Nuhn, P. Walter, J. Viehhaus, M. Meyer, S. Moeller, R. N. Coffee and M. Ilchen, 'Circular dichroism measurements at an x-ray free-electron laser with polarization control', *Rev. Sci. Instrum.* 87, 083113 (2016).
7. J. Metje, F. Lever, D. Mayer, R. J. Squibb, M. S. Robinson, M. Niebuhr, R. Feifel, S. Düsterer, M. Gühr, 'URSA-PQ: A Mobile and Flexible Pump-Probe Instrument for Gas Phase Samples at the FLASH Free Electron Laser', *Appl. Sci.* 10, 7882 (2020).
8. M. Beye, M. Gühr, I. Hartl, E. Plönjes, L. Schaper, S. Schreiber, K. Tiedtke and R. Treusch, 'FLASH and the FLASH2020+ project - current status and upgrades for the free-electron laser in Hamburg at DESY', *Eur. Phys. J. Plus* 138, 193 (2023)
9. FLASH2020+ CDR (2020), chapter 8, <https://bib-pubdb1.desy.de/record/434950/files/FLASH2020pCDR.pdf>.

PETRA III

Last two PETRA III beamlines in planning or under construction



Figure 1
View into the PETRA III experimental hall 'Max-von-Laue' hosting 15 beamlines.

In the year 2023 about 3500 individual users, including mail-in and remote access, performed experiments at PETRA III beamlines. Two periods of PETRA III user operation were scheduled in 2023. The first period was from mid of February until mid of July, the second period was from mid of August until end of December. During the first run 2573 hours of user operation were provided, in the second run 2326 hours. In the year 2023, 25 beamlines were operating and open for users: P01-P14 in the PETRA III experimental hall 'Max von Laue' (see Fig. 1), P21.1-P24 in the hall 'Ada Yonath', P61-P62 and P64-P65 in the hall 'Paul Peter Ewald' and at P66 in building 47K. Therefore, in 2023 at each of the 25 beamlines 4822 hours of X-ray user beamtime were provided. In 2023, users submitted 1345 proposals, thereof 9 Block Allocation Group (BAG) proposals and 28 Long Term Proposals (LTP). In addition, 115 proposals, including 58 BAG proposals, have been collected for the EMBL beamlines P12-P14 at PETRA III.

PETRA III - machine operation

In 2023, the availability of the PETRA III storage ring for synchrotron radiation users was very good at 98.4%. As in recent years, the largest fraction of failures is related to power interruptions, overall 27 events, mainly caused by glitches in the external electricity grid. Since DESY has no facility to compensate sudden power drops of a few percent, such as batteries or flywheels, power glitches almost always cause a beam dump. The PETRA III storage usually recovers within 15-45 minutes from a beam loss caused by a power glitch, depending on the respective equipment failures. An extraordinary source of failures was related to the master clock of PETRA III, which produced 15 dumps, most of them in one single week, before the source of the error was found and the system could be successfully repaired. Due to this single cause alone and the associated high number of dumps within one week, the mean time between failure averaged over the year went down by 6 h, leading to a final value of 50 h and 30 min.

As usual, two different bunch filling modes were offered in the PETRA III storage ring: a mode for 'time resolved' experiments with 40 bunches and a 'multi bunch' mode with 480 bunches, both with approximately the same share. This bunch mode distribution has proven to be an optimal scenario to provide a maximum number of 'timing mode' shifts while minimising the radioactive activation of ring components as well as radiation damage of undulators.

With regard to the upgrade plan for PETRA IV and the planned extensive construction work during the operation of PETRA III, it was investigated how this could influence the stability of the electron beam. Evidently, construction machines like compactors have the highest impact on the beam stability. The compaction induces vibrations in the ground, which can couple to sensitive components of the electron optics of the PETRA III machine, such as quadrupoles and beam position monitors. If the orbit feedback cannot compensate these excitations, the displaced electron beam causes displacements of the X-rays beam position at the beamlines. The compactors can additionally induce vibrations to the X-ray optics at the beamlines, leading to the same effect. The general effect is already known from previous construction areas close to the PETRA III experimental hall 'Max von Laue'.

To study the effect of ground vibrations on the electron beam stability in more detail, a compactor was used on the opposite side of the campus close to the PETRA III experimental hall 'Paul Peter Ewald'. Ground excitations were induced only a few meters away from the PETRA III accelerator, but around 400 m away from the experimental hall 'Max von Laue'. The shifts in the position of the

X-ray beam are clearly visible in the Fourier spectrum of the PETRA III beamline P04 (see Fig. 2), which means that the orbit feedback cannot fully compensate the induced ground vibrations. More studies are necessary to quantify the vibration effect at all beamlines and to study possible schemes of compensation. In the case that construction work on the DESY site significantly affects the position of the X-ray beam, it is planned to coordinate PETRA III user operations with construction works accordingly.

PETRA III - new beamlines and end stations in design and automation project funded

Two more new beamlines — P25 in the PETRA III experimental hall 'Ada Yonath' and P63 PETRA III experimental hall 'Paul Peter Ewald' — are under construction and in the planning phase, respectively. The first beam for P25 is expected in late 2024 or early 2025, in addition, one end station for imaging (HIKA) at P23 is almost finalised and has seen the first X-ray beam.

Beamline P25 is a cooperation project of PETRA III and the DESY group for Innovation and Technology Transfer (ITT) with main funding from ITT. It will serve customers from industry and academic partners with imaging and powder diffraction applications located in the experimental hutch EH1 for monochromatic X-ray beams. The powder diffraction end station will be designed for fully automated user operation and is expected to serve many industrial clients, e.g. from pharmaceutical industry using 'mail-in operation'. The imaging end station will provide element-specific X-ray fluorescence microscopy with focus on biomedical applications in collaboration with the

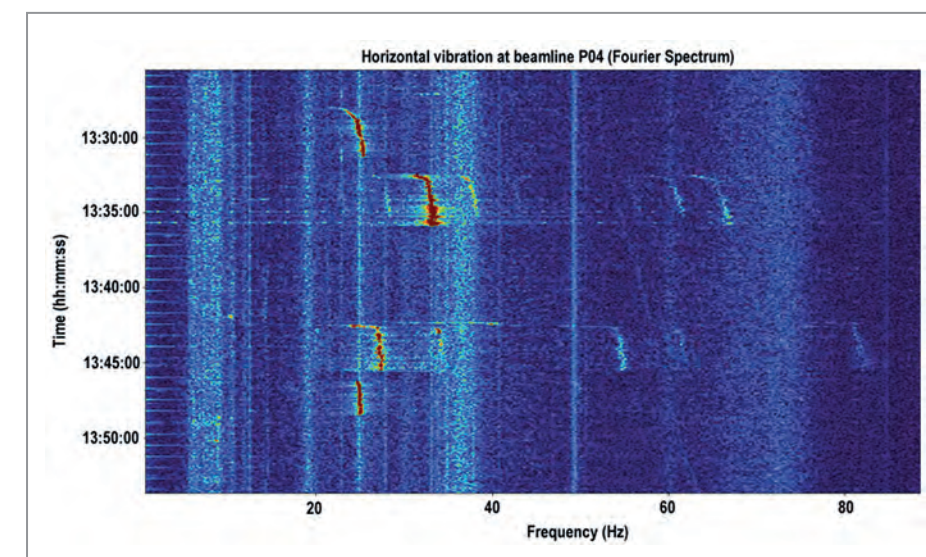


Figure 2
Fourier spectrum of the horizontal beam position, here at the PETRA III beamline P04, when using the compactor four times with different gears. The X-ray beam excitations are clearly visible in the range between 25 Hz and 45 Hz as red lines in the spectrum.



Figure 3
Experimental hutches EH1 for powder diffraction and the imaging end station at the PETRA III beamline P25.



Figure 4
Monochromator for the PETRA III beamline P25 in the setup phase under a laminar flow box.

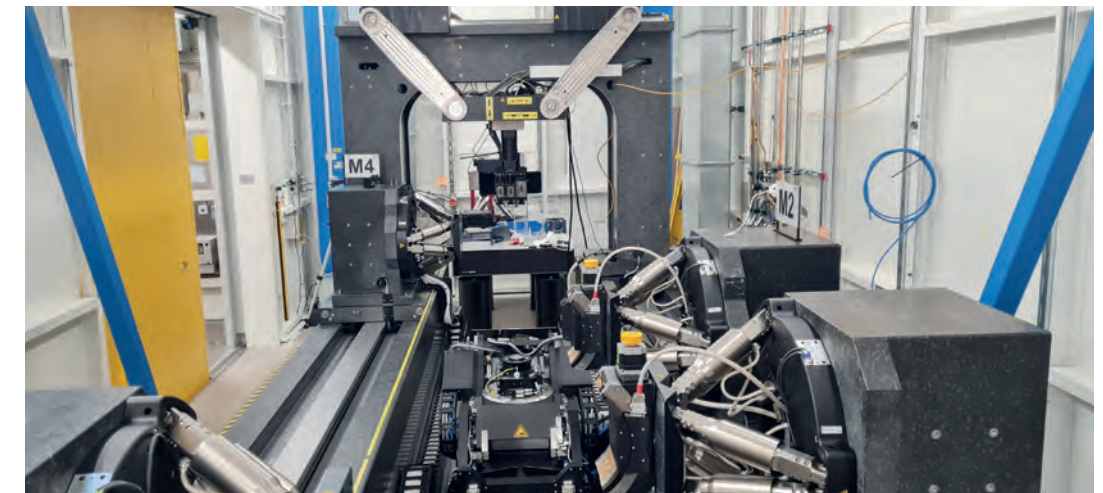


Figure 6
The HIKA end station at the PETRA III beamline P23. In the background the detector portal can be seen. In the foreground, the sample goniometer is mounted.



Figure 7
Image of some random insect in ethanol obtained at HIKA. Left: absorption contrast, middle: differential phase contrast, right: dark field contrast.

University Medical Center Hamburg-Eppendorf (UKE). In addition, an end station for white and pink beam applications will be constructed in a separate optics hutches (see Fig. 3).

This hutches will be used to test and commission components related to PETRA IV. The hutches design has been finished in 2022, and both hutches have been successfully installed in summer 2023. This required a shutdown of beamline P24 from beginning of July 2023 until end of August 2023. The monochromator (Fig. 4) and the undulator have already been delivered.

Plans for the PETRA III beamline P63 have been detailed in 2023. This beamline is a cooperative effort of the Fritz Haber Institute Berlin, the Max Planck Institute for Chemical Energy Conversion in Mülheim and DESY, with investments from the Max-Planck-Gesellschaft. P63 will be dedicated to combined X-ray absorption spectroscopy (XAS)/small angle scattering (SAXS) and powder diffraction studies. It complements the XAS capabilities already available at the highly requested XAS beamlines P64 and P65 and the SAXS experiments at P62 and P03. First components such as dedicated detectors have already arrived, the design of the experimental hutches is finalised and construction of the beamline is expected to start in 2024 (see Fig. 5). The hutches of beamline P63 will be constructed in a way that they can stay unmodified when PETRA IV is commissioned.

In 2023, the construction and implementation of the end station for Hierarchical Imaging Karlsruhe (HIKA) at the In Situ Diffraction and Scattering beamline P23 (see Fig. 6) has been finalised and first successful test experiments have been performed. Beamline P23 was ideally suited for this end station due to the versatile optics with up to 10^{13} ph/sec flux at a photon energy range of 5 keV to 35 keV and the capability to focus down to approx. 500 nm vertically.

The P23 end station HIKA is funded by the Karlsruhe Institute of Technology (KIT) and is built and operated in close cooperation with DESY. The end station is optimised for *in situ* and *operando* full field X-ray imaging of biological materials and hard condensed materials, e.g. batteries or catalysts. In particular, plate-like samples such as semiconductor devices can be imaged via laminography which is optimally suited for flat or elongated samples. First test

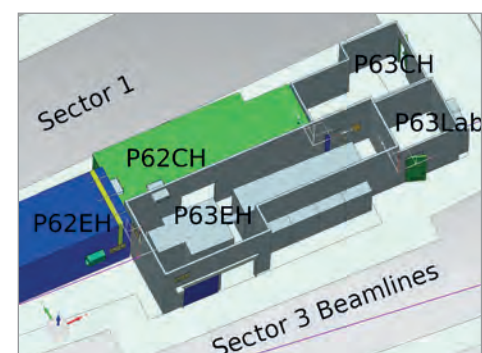


Figure 5
Drawing of the experimental hutches at the PETRA III beamline P63.

imaging measurements have been done with an insect stored in ethanol using different X-ray contrast variations (Fig. 7). The results are very promising. It is expected, that HIKA will be open for user beamtime applications from March 2024 on.

In fall 2023, a so-called 'Dewar hotel' was inaugurated. It is an infrastructure for storing and handling samples in cryogenic storage containers. DESY and the European Molecular Biology Laboratory (EMBL) operate it as a shared infrastructure for the molecular crystallography (MX) beamlines P11 at DESY, P13 and P14 at the EMBL, in particular for remote or mail-in experiments, where the experiments are executed by remote access or by the beamline teams, respectively.

Sample shipment in specially designed transport dewars became a standard part of operation at the three MX beamlines at PETRA III. The logistics of the sample delivery and tracking becomes challenging in terms of handling over 600 dewar shipments annually with each shipment containing 5–7 sample holders with 10–16 samples each. In particular, the effective and error-free deliveries, the storage and the reliable refills of the cooling agent into the dewars is routinely needed.

Therefore, as a common effort of DESY and EMBL a Dewar hotel with eight shelves for four dewars each was installed at the EMBL sector in the 'Max von Laue' hall



Figure 8
The DESY-EMBL Dewar hotel: One of the four shelves containing dewars in transport boxes ready for handling. On the right the controller panel is visible which is used to register and check-out the dewars.

(see Fig. 8). Additionally, in cooperation with the Hamburg University of Applied Sciences (HAW), a software for cooling agent and sample handling has been developed and installed. This software has also an interface to the information system for protein crystallography beamlines (ISPyB).

Contact: Oliver Seeck, oliver.seeck@desy.de
Hans-Christian Wille, hans.christian.wille@desy.de

PETRA IV – The Ultimate 3D-X-Ray Microscope

Plans for the new light source PETRA IV are taking concrete shape

PETRA IV is the planned ultra-low-emittance upgrade of the existing PETRA III storage ring. DESY's flagship project will be the brightest synchrotron light source in the world for decades to come. Academic and industrial users will benefit from the enormous increase in coherent X-ray flux, the planned cutting-edge beamlines, the novel experimental possibilities, as well as from the new business model in preparation for the facility. It will provide easy on-demand access, extended services and support for non-expert synchrotron radiation users, especially in processing and analysis of their data. PETRA IV will be a cornerstone of the Science City Hamburg Bahrenfeld and a central component of DESY's vision of a data- and information-driven solution ecosystem for academia and industry.

In 2023, the PETRA IV project team has made progress on the planning for civil construction, the accelerator complex and the photon beamlines. In particular, the team has completed the comprehensive project proposal, comprised of the scientific case, a technical description, the business model, a data management plan, the project budget and the future operation costs for the facility. The largest part of the project proposal is the technical description of PETRA IV itself. Due to its level of detail, this part also serves as a Technical Design Report (TDR).

For the accelerators, a new design aspect has been introduced. A second injector branch for the storage ring is now included, based on a laser plasma accelerator (LPA). This LPA will be located in the area of the former DORIS complex. Here, KALDERA, a high-power laser system for the next generation of laser-plasma accelerators, is currently being set up and commissioned. From there, a new transfer line will be built, allowing to switch between the conventional RF cavity booster synchrotron DESY IV and the new LPA injector.

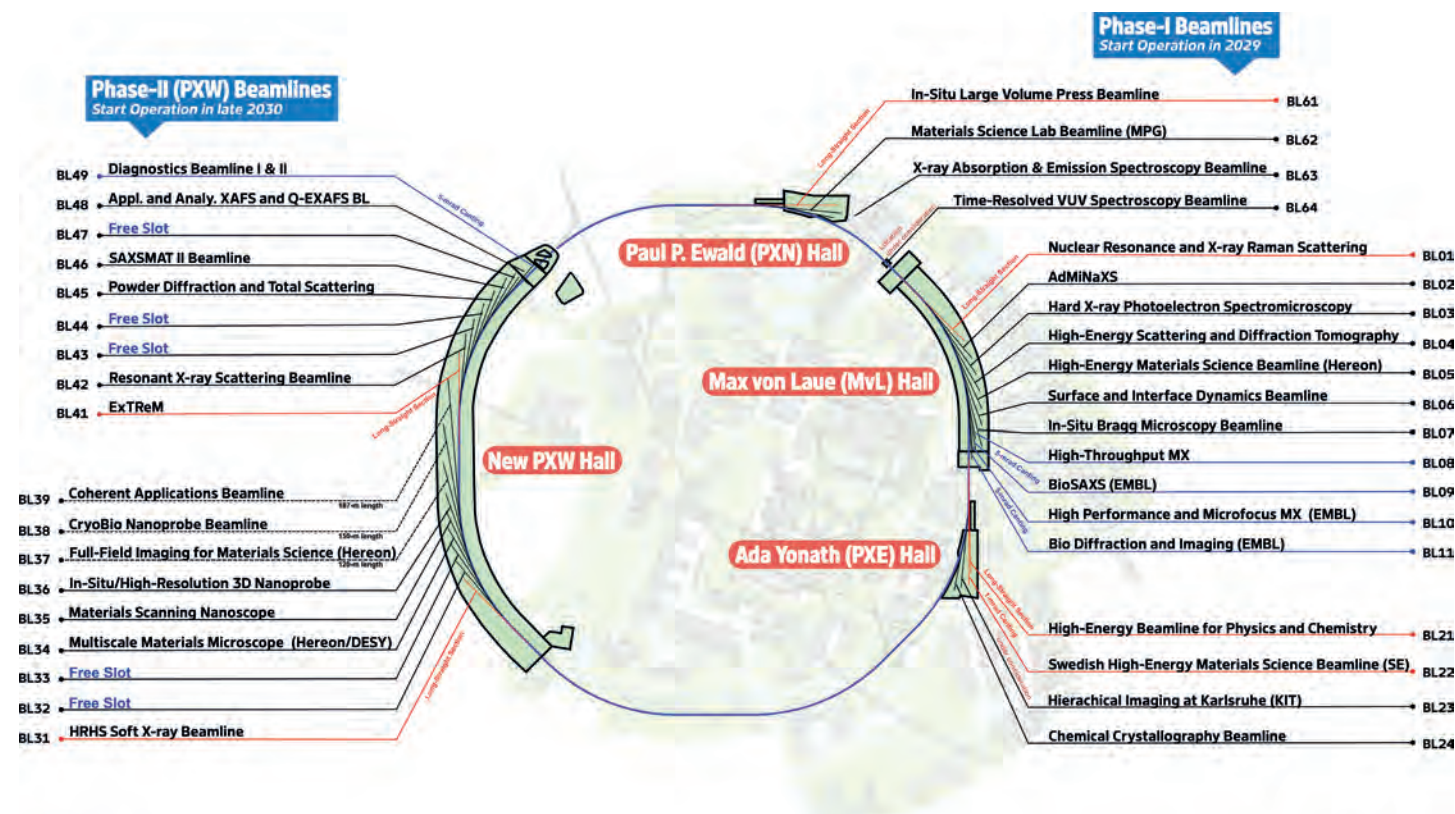


Figure 1 Current distribution of planned PETRA IV beamlines in the existing experimental halls (right) and the planned new hall in the West.

For the photon science experiments exploiting the brilliant beams of PETRA IV, strategic priorities have been identified from the multitude of scientific possibilities and applications, to which PETRA IV could contribute significantly. These include the development of novel materials for a sustainable future, tools to foster bio-preparedness and instruments to secure technological sovereignty in areas such as nanoelectronics.

As part of the new business model for PETRA IV, the classical access model will be replaced by a modern rolling access approach. This includes a new service concept provided by a user support group. Applications for projects, including request for beamtime and/or requests for other analytical services, can be submitted by prospective users to DESY at any time and will be reviewed directly upon submission. The goal is to provide access to the PETRA IV facility within weeks instead of months. With the same application, users can also apply for multiple visits and access to multiple instruments. This new access model will soon be tested at PETRA III. Five beamlines were selected for this purpose: P08, P11, P22, P23 and P24. Submission for the rolling access will be launched in spring 2024.

The current PETRA IV beamline portfolio of 31 beamlines (of a total of 36 beamlines + 1 VUV) was further developed in 2023 (see Fig. 1). Two new imaging beamlines have been added to the portfolio: the 'Hierarchical Imaging and Serial Tomography Karlsruhe' (HIKA) beamline and the 'Multiscale Materials Microscope' (MMM) beamline. This beamline portfolio offers a broad spectrum of experimental possibilities and analytical techniques with a wide range of contrasts and sensitivities, as well as the flexibility to tackle future scientific and technological challenges for scientific and industrial users.

The individual optical layouts for the beamlines and their conceptual designs were intensively discussed and further optimised in 2023. Based on the spectral requirements of the beamlines, an initial insertion device portfolio has been elaborated. In-house developments for beamline optics could further enhance beamline capabilities. The next step will be the formal acceptance of the collected requirements and the finalisation of the beamline conceptual designs in 2024.

An essential part of the work on the PETRA IV project proposal was the compilation of the project costs and the required future operation budget. The latter will be evaluated separately by the Helmholtz Association (HGF) as part of the program-oriented funding (POF V) process which is due to start in 2024. The total costs of the project are estimated at 1.5 billion Euro in 2022 prices, including in-kind contributions from DESY and the HGF. All cost estimates were subject to a thorough internal and external cost review focusing on civil construction and infrastructure, the accelerator complex and the experimental facilities of PETRA IV. Both cost reviews were successfully passed and the committees recommended the implementation of PETRA IV as soon as possible.



Figure 2 PETRA IV exhibition at the summer festival of the 'Landesvertretung' of the City of Hamburg in Berlin (Credit: G. Harms, DESY)

The technical design and the cost estimates were also presented to all pertaining advisory committees at DESY, the Machine Advisory Committee (MAC), the Photon Science Committee (PSC) and in particular the Scientific Council and the Foundation Council. In an extraordinary meeting at the end of March 2023, the Foundation Council approved the submission of the project proposal to the appropriate funding agencies. In September 2023, the Hamburg City Parliament unanimously decided that the City of Hamburg will provide its share of ten percent of the requested funds and continues to advocate for the remaining share of 90 percent from federal funds.

The campaign for PETRA IV was launched at a Senate Reception in Hamburg's City Hall in September 2022. Its aim is to convince funding agencies and decision makers of the importance of PETRA IV for Germany and the national economy. Numerous visits and events were organised at DESY and elsewhere in the course of 2023, the most prominent being the summer festival of the 'Landesvertretung' Hamburg in Berlin, where many stakeholders on the federal and state level visited the PETRA IV exhibition (see Fig. 2).

Parallel to the preparation of the project proposal, an impact study for the light sources PETRA III and PETRA IV was carried out by the Fraunhofer Institute for Systems and Innovation Research ISI in Karlsruhe and published in October [1]. DESY and the PETRA IV project team are now ready to submit the package comprised of the project proposal, this study and the external cost review report.

[1] Kroll et al., 'Impact-Studie Synchrotronstrahlungsquelle PETRA III im Kontext des Forschungs- und Innovationsökosystems DESY', Fraunhofer (2023), DOI: 10.24406/publica-1929

Contact: Harald Reichert, harald.reichert@desy.de
 Karolin Baev, karolin.baev@desy.de
 Kai Bagschik, kai.bagschik@desy.de
 Stephan Klumpp, stephan.klumpp@desy.de

Since the beginning of 2023, the DESY NanoLab is fully back to high-level user support, around half a year after the labs and offices have been moved to the new Centre for X-ray and Nanoscience (CXNS) building.

The DESY NanoLab offers on-site methods for nanoscience that complement techniques and experiments at the DESY light sources and the European XFEL, including nanocharacterisation, nanostructuring and nanosynthesis techniques for investigation of atomic scale structure, chemistry and magnetism. Access is also offered to the electrochemistry lab and e-beam lithography in cooperation with the Centre for Hybrid Nanostructures (CHyN) of the Universität Hamburg.

A further specific offer for users is the 'nanotransfer protocol' that assists in the re-localisation of preselected microscopic regions of interest in focussed PETRA III X-rays. The scanning Auger microscope with chemical resolution at the nanoscale is operational and now part of the regular DESY NanoLab offer.

The establishment of a laser laboratory for the investigation of dynamics at the nanoscale in cooperation with the Leibniz-Institut für Kristallzüchtung (IKZ), also a partner of the CXNS, is underway. The lab will be used for ultrafast pump-probe experiments which complement the existing portfolio. A detailed overview on the current DESY NanoLab instrumentation can be found in the 'Facts and Numbers' section of this DESY Photon Science annual report.

The research has already profited from the new spacious state-of-the-art laboratories in the CXNS building. One example deals with oleyl phosphate ligand-stabilised iron oxide nanocubes used as building blocks to assemble 2D supercrystalline mono- and multilayers on flat YSZ substrates by a simple spin-coating process [1]. As a bottom-up process, the growth takes place in a layer-by-layer mode. Microscopy in combination with X-ray reflectivity showed that the monolayers are ordering in a square or hexagonal lattice depending on which solvent is used, i.e. toluene or chloroform, a crucial step for building the materials in 3D.

Another recent publication on how refractive X-ray lenses can be tailor-made by focused ion-beam (FIB) milling shows how the neighbouring laboratories of the DESY research groups in the CXNS building can boost collaborations. Using the FIB at the DESY NanoLab a residual lens aberration was directly inserted into the silicon material as corrective optical element [2]. Already in 2022, the FIB was equipped with an EDX system that permits an additional 3D chemical analysis by the slicing capabilities of the Ga ions.

A more detailed insight into the research activities and user collaborations at the DESY NanoLab is provided in the Science Highlights Section of this report (Larsson et al., Wagstaffe et al., Kohantorabi et al. and Dey et al.).

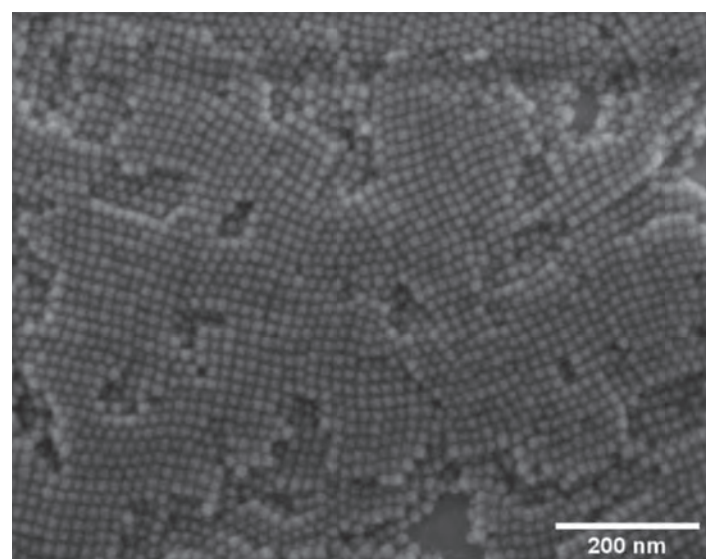
Contact: *Andreas Stierle*, andreas.stierle@desy.de

References

1. E. Erik Beck, A. Weimer, A. Feld, V. Vonk, H. Noei, D. Lott, A. Jeromin, S. Kulkarni, D. Giuntini, A. Plunkett, B. Domènech, G. A. Schneider, T. Vossmeier, H. Weller, T. F. Keller and A. Stierle, 'Solvent controlled 2D structures of bottom-up fabricated nanoparticle superlattices', *Nanoscale* 15, 4506–4514 (2023).
2. F. Seiboth, A. Schropp, M. Lyubomirskiy, W. Wang, A. Jahn, S. Kulkarni, T. F. Keller and C. G. Schroer, 'On-chip aberration correction for planar nanofocusing x-ray lenses by focused ion-beam milling', *Appl. Phys. Lett.* 122 (2023).

Figure 1

Scanning electron microscopy image of self-assembled oleyl phosphate ligand-stabilised iron oxide nanocubes.



The European Molecular Biology Laboratory Hamburg Unit

Research and infrastructures for applications in the life sciences

The European Molecular Biology Laboratory (EMBL) unit in Hamburg carries out research with a focus on infection biology using structural biology and imaging tools at various scales. EMBL Hamburg provides access to three beamlines at PETRA III and a Sample Preparation and Characterisation (SPC) Facility for users from academia and industry as well as training. During the reporting period, EMBL Hamburg served 675 individual users at its facilities. External access to EMBL's facilities is supported by several European consortia: INSTRUCT, iNEXT-Discovery, MOSBRI, ISIDORE and canSERV.

EMBL's Sample Preparation and Characterisation (SPC) Facility offers a pipeline from the lab bench to the EMBL beamlines, helping optimise and prepare samples for further studies. During the reporting period, the facility served 190 individual users and introduced new technologies to its portfolio: Nanotemper Panta Prometheus nanoDSF, incorporating Differential Scanning Fluorimetry (DSF), Dynamic Light Scattering (DLS) and Static Light Scattering (SLS); Malvern Panalytical Creoptix WAVESystem for studying binding kinetics and Refeyn MP2 combined with a MassFluidix HC microfluidic system (Fig 1.) for studying weak protein-protein interaction by mass photometry. The facility has added a tool for analysing DLS data to their eSPC online platform [1] and plans to release more online tools in the future. The platform was accessed 3728 times during the reporting period.

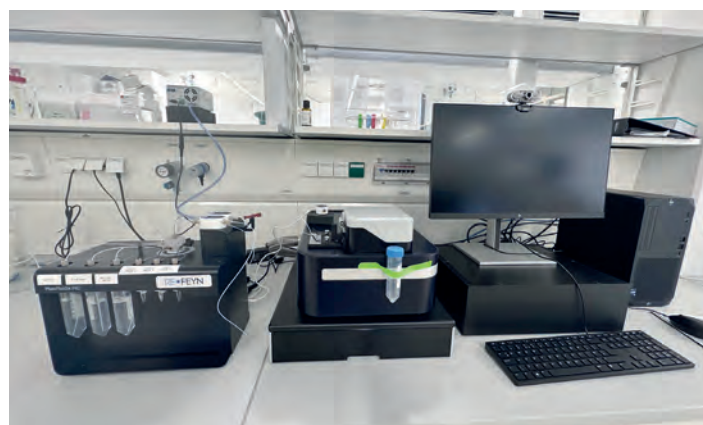


Figure 1
Refeyn MP2 with MassFluidix HC is a recent technology from Refeyn that allows measurements of low-affinity binding in micromolar concentration.

Beamline P12 for biological small-angle X-ray scattering (BioSAXS) is dedicated to the measurement of weakly-scattering and low-contrast biological macromolecular samples and bio-composites. The role of BioSAXS team leader has been assumed by Clément Blanchet, succeeding Dmitri Svergun who retired in 2022. Under his leadership, the team continues their work on advancing the SAXS technology, offering essential services and training to the scientific community.

Collaborating with Johannes Gutenberg University Mainz, Postnova Analytics GmbH and BioNTech SE, EMBL Hamburg has pioneered a novel sample delivery method based on asymmetrical-flow field-flow fractionation (Fig. 2) [2] (see article in Science Highlights section of this report). This innovative approach separates solutes based on their size before subjecting them to SAXS analysis. Using this technique, the team has characterised diverse samples from proteins to nanoplastics. The method allows developing a quantitative approach for characterising lipid nanoparticles (LNPs) based on their size.

Beamlines P13 and P14 for macromolecular crystallography (MX) enable collecting static and time-resolved diffraction data using single/multiple/serial approaches. Time-resolved serial crystallography is developed in close collaboration with HARBOR (Hamburg Advanced Research Centre for Bioorganic Chemistry).

EMBL scientists as well as P13 and P14 played an essential role in the development of the 'spitrobot' [3] for 'cryo-trapping', i.e. stopping chemical reactions taking place inside protein crystals by quickly freezing them at precisely defined timepoints, so that the structural models from different timepoints can be combined into a movie of the proceeding reaction. The device can be used in conjunction with various reaction triggering methods and is available to beamline users at HARBOR.

X-ray Imaging is an additional functionality on P14 that makes use of technologies originally developed for MX. 2023 brought significant progress in establishing High



Figure 2
Asymmetrical-flow field-flow fractionation (AF4), available now at P12, sorts nanoparticles and macromolecules according to their size (Credit: Melissa Graewert/EMBL).

Throughput Tomography (HiTT) for acquiring X-ray tomograms from biological samples. Samples imaged using HiTT range from heavy metal-stained, resin-embedded samples, which can be imaged with both X-rays and volume electron microscopy, through formalin-fixed paraffin-embedded tissue samples to fixed and either hydrated or dehydrated samples mounted in liquid [4].

An upgraded camera with three objective lenses allows data collection with both a 10x lens (FOV 1.3 mm × 1.3 mm; pixel size 660 nm) and a 20x lens (FOV 650 μm × 650 μm; pixel size 330 nm) (Fig. 3). The 1.3 mm Field of View (FOV) is convenient for 1mm punch biopsy tissue samples, as the entire sample width fits into the field of view. Data acquisitions are automatically tiled together which enables easy acquisition of samples larger than the field of view – particularly useful for long cylindrical samples. High-speed data acquisition and the automated data processing pipeline allow users to view the reconstructed 3D volume within 3.5 minutes. This, in combination with the routine use of the robotic sample changer, enables high-throughput data collection and processing.

AI in structural biology

During the last years the EMBL Hamburg Unit has expanded its portfolio by combining experimental structural biology approaches with computational methods which allow integrative modelling of heterogeneous experimental data. Along these lines, the Kosinski Group has released AlphaPulldown [5], a freely available Python package for protein-protein interaction screens and high-throughput modelling of higher-order oligomers using AlphaFold-Multimer. Another tool, checkMySequence, developed in the Wilmanns group, enables quantitative

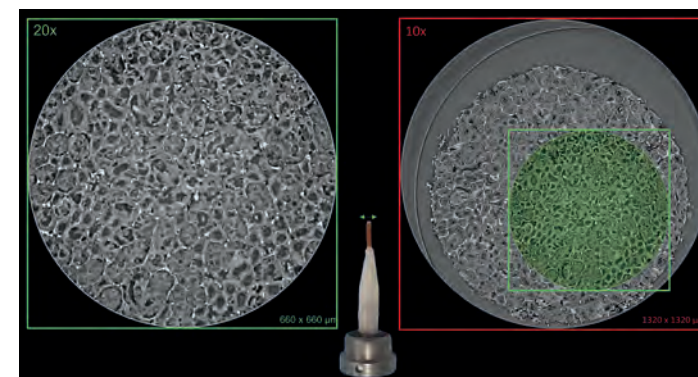


Figure 3
Image of a 1mm punch biopsy of an FFPE mouse kidney scanned with a 20x lens and a 10x lens showing the impact of the different fields of view on the data.

sequence-assignment validation in experimental structure models determined at various resolutions [6].

Plans for EMBL @ PETRA IV

In collaboration with DESY, EMBL has further developed its plans for providing integrated services in structural biology and imaging at PETRA IV. This was reflected in the Memorandum of Understanding signed by EMBL and DESY in February.

ERC grants for two EMBL Hamburg group leaders

Visiting group leader Meytal Landau received a five-year ERC Consolidator Grant to investigate microbial amyloid proteins. The grant will allow her to build a team which will involve DESY, EMBL Hamburg, the University Hospital Hamburg-Eppendorf (UKE) and CSSB. Group leader Jan Kosinski, together with Julia Mahamid at EMBL Heidelberg and collaborators, received an ERC Synergy Grant for their project 'TransFORM', focusing on the specific composition of diverse molecular complexes that make up the protein synthesis machinery.

Contact: Dorota Badowska,
dorota.badowska@embl-hamburg.de

References

1. O. Burastero et al., *Acta Crystallogr. D* 77, 1241–1250 (2021).
2. M. A. Graewert, C. Wilhelmy, T. Bacic et al., *Sci. Rep.* 13, 15764 (2023).
3. P. Mehrabi, S. Sung, D. von Stetten et al., *Nat. Commun.* 14, 2365 (2023).
4. J. Albers et al., *J. Synchrotron Rad.* 31 (2024).
5. D. Yu, G. Chojnowski, M. Rosenthal and J. Kosinski, *Bioinformatics* 39, btac749 (2023).
6. G. Chojnowski, *Acta Crystallogr D Struct Biol.* 79, 559–568 (2023).

The GEMS branch at PETRA III - beamlines and instruments operated by Hereon

Diffraction and imaging techniques optimised for the needs of materials research

Helmholtz-Zentrum Hereon operates the German Engineering Materials Science Centre (GEMS). The experimental stations of GEMS at PETRA III are being continuously developed and upgraded for engineering materials and bio-materials science users from institutions in Germany and all over Europe. At the same time the design and specifications of the successor beamlines at PETRA IV are being developed in order to meet future user demands for cutting edge instrumentation optimised for materials science.

Diffraction

The engineering materials station P61A of the only PETRA III white-beam beamline was equipped with a large Eulerian cradle for carrying up to 20 kg load. This enables sample environments such as, e.g. a load frame to be rotated in the beam; this is essential for a full residual stress analysis. The most challenging experiment at P61A was the *in situ* experiment using an Electron Beam Melting (EBM) chamber for additive manufacturing combined with a camera system for high-speed radiography (Fig. 1). The camera tower has a mass of 600 kg, as the high radiation background in the hutch requires significant lead shielding. The experiment was built and operated at the two beamlines P21.2 and P61A within the Röntgen-Ångström-Cluster project 'Track-AM'. At P61A, energies up to 200 keV were used and the flux from the damping wigglers allows high frame rates. Up to 25 kHz could be used with the existing camera and more than 100 kHz will be feasible with a faster camera. The results have shown that good absorption contrast is still obtained with the white beam [1,2].

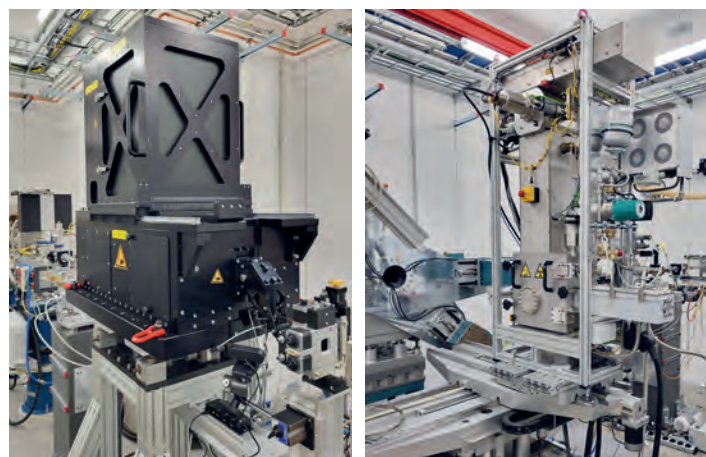


Figure 1

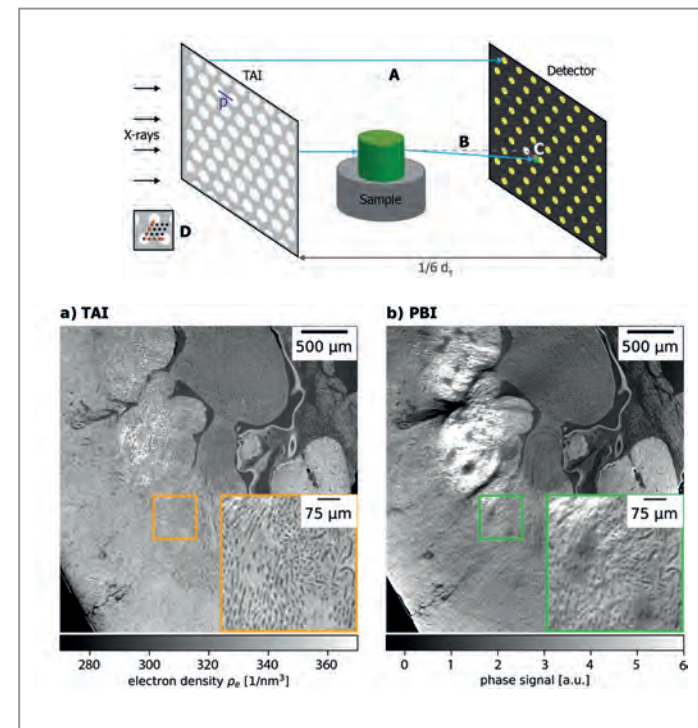
In situ experiment for the study of the EBM (Electron Beam Melting) additive manufacturing process at beamline P61A. Left: Fast camera with shielding for high-speed radiography. Right: EBM chamber from Freemelt AB, Sweden. (Images: Peter Staron, Hereon)

At P07, a new electro-mechanic load frame with up to 50 kN load was put into operation. It adds to the previous version with 20 kN load and closes a gap between the small load frame and the large hydraulic 100 kN INSTRON load frame. The setup 'FlexiStir' for *in situ* experiments on the friction stir welding process has been used again in 2023 for two beamtimes with different user groups. FlexiStir was built and used for the first time in 2008 at the HARWI beamline at DORIS III; since then FlexiStir was used for 13 beamtimes in 5 different projects while it has undergone several upgrades. The latest beamtime was used for a study of the friction extrusion process for Al alloys, with simultaneous diffraction and SAXS to study the precipitation kinetics.

Imaging

Our imaging instruments at beamlines P03, P05 and P07 are specifically optimised for materials science but are also widely applied for applications from life sciences. This is appreciated by Hereon-internal collaborations as well as external users. The unique attributes of our instruments include high X-ray energies, extended space for sample environments, phase contrast techniques as well as a broad spectrum of spatial resolutions which are being continuously improved. Significant effort was directed to enhancing phase-contrast techniques. Phase contrast is of high relevance for low-absorbing sample systems, e.g. lightweight metal alloys, biological or medical samples. In

Top: Schematic drawing of the Talbot Interferometer Imaging (TAI) setup. The hexagonal TAI with a period $p = 10 \mu\text{m}$ and a phase shift of $2\pi/3$ is placed with a fractional Talbot distance of $1/6 dT = 0.54 \text{ m}$ (at a beam energy of 20 keV) to the detector. The sample is mounted on the rotation stage in between. A marks a non-refracted beamlet. When one beamlet passes the sample as shown in B, it is refracted from its original path (grey dashed line) and the pattern on the detector is shifted as shown by the magenta arrow next to C. To record a full scan, multiple rotations are done, stepping the TAI in between rotations along the grating axes in fractions of a grating period, as shown in D. The steps are then used to determine the shift vector for each pixel using a unified modulated pattern analysis. Bottom: Comparison of TAI quantitative phase-contrast imaging a) with a propagation-based imaging (PBI) phase-retrieval in b). The picture shows a mouse kidney, stained during previous investigation with a Bismuth-based stain. Zoom-ins show a part of the outer medulla. The PBI phase-retrieval shows strong artifacts where the stain aggregated in the centre as well as towards the edges of the sample. In contrast, the phase retrieval from the TAI data only shows a slight increase in electron density in the affected areas but no artifacts [4]. (Figures adapted from [4] licensed under CC-BY 4.0)



particular in the nanoimaging regime, however, the low signal-to-noise ratio often requires relatively long scan times. In order to tackle this drawback, a LAMBDA single-photon-counting detector has been implemented at the nanotomography setup of the imaging beamline P05. Thanks to the available long sample-to-detector distance of up to 22 m, spatial resolutions of below 100 nm were achieved despite the typically large physical pixel size of these detectors. The high efficiency of these detectors allows for a significant increase in time resolution for nano imaging by a factor of 10 [3]. Another instrumental development of phase-contrast techniques has been implemented at the microtomography stations of beamlines P05 and P07. Phase contrast can also nicely visualise even low density-contrast in soft tissue samples, most commonly by using propagation-based imaging (PBI) techniques. However, these suffer from a low degree of quantitative data and phase-retrieval artefacts due to simplifying assumptions of the sample properties in the reconstruction, i.e. the grey values are more or less random. A new setup developed at P05 and P07 using a Talbot Array Illuminator (TAI) provides quantitative tomography data with a resolution comparable to PBI techniques but with grey values proportional to the local electron density [4] as shown in Fig. 2.

Other ongoing in-house collaborations target the development of novel biodegradable magnesium implants for use in fractured bones. One focus lies in finding the appropriate magnesium alloy (see also the article in the Science Highlights Section of this report [5]). Within another study, much smaller structural features of magnesium implants were studied by means of nanotomography at P05 to determine the influence of plasma electrolytic oxidation (PEO) coatings on the regeneration process. These coatings can be used to specifically slow down the degradation

properties of magnesium implants, and the nanotomography data indicates that the slower degradation of coated implants promotes healthier structures in the lacunacicular network. However, uncoated implants lead to more interconnected bone microstructure which is a better outcome in terms of bone disturbance [6].

Our in-house software development activities include a new application for the automatic reduction and analysis of large sets of X-ray diffraction data. The PYDIDAS project (PYthon Diffraction Data Analysis Suite) aims at making the analysis of X-ray diffraction data more accessible to non-experts through automated analysis, e.g. for mapping residual stresses or visualising scanning nanodiffraction data recorded from our nanofocus setup at P03 and P07. PYDIDAS is in continuous development to extend its feature range. More information is available on the project website [7].

Author contact:

Christina Krywka, christina.krywka@hereon.de

Peter Staron, peter.staron@hereon.de

Martin Müller, martin.mueller@hereon.de

References

1. H.-H. König et al., 'MiniMelt: An instrument for real-time tracking of electron beam additive manufacturing using synchrotron X-ray techniques', *Rev. Sci. Instrum.* **94**, 125103 (2023)
2. P. Bidola et al., *Proceedings of SPIE*, 1269402 (2023)
3. S. Flenner et al., *Journal of Synchrotron Radiation* **30**, 390 (2023)
4. M. Riedel et al., *Scientific Reports* **13**, 6996 (2023)
5. S. Bruns et al., *Bioactive Materials* **28**, 155 (2023)
6. J. Espiritu et al., *Bioactive Materials* **26**, 14 (2023)
7. M. Storm, <https://pydidas.hereon.de>

DESY Photon Science at the European XFEL

User consortia

DESY is not only responsible for the construction and the operation of the European XFEL linear accelerator but also plays an important role as part of the user community. Moreover, DESY scientists develop lasers and detectors for use at the European XFEL. DESY is involved in several user consortia including three of the largest: SFX, HIBEF and hRIXS.

Serial Femtosecond Crystallography (SFX)

The SFX Consortium provides instrumentation and methodology in serial femtosecond crystallography and solution scattering at the 'Single Particles, Clusters and Biomolecules and Serial Femtosecond Crystallography' (SPB/SFX) instrument of the European XFEL. By outrunning radiation damage with femtosecond X-ray pulses, high-quality diffraction data can be acquired at ambient temperatures, allowing the study of macromolecular systems undergoing reactions with temporal resolution ranging from femtoseconds to minutes. This capability, combined with rapid data collection achievable at the European XFEL, may also be far-reaching for drug discovery. To date, large-scale

structure-based screening of compounds binding to (and thus inhibiting) macromolecular drug targets is carried out by X-ray crystallography at synchrotron facilities, requiring cryogenic cooling of the sample and slow sample exchange. Recent experiments show that measurements at physiological temperatures reveal different binding compounds and other binding sites to those observed under cooling, likely due to the dynamic nature of protein structures. Funded by a Röntgen-Ångström Cluster proposal and building upon screening capabilities developed in response to the Corona pandemic, high-throughput room-temperature serial-crystallography screening will be deployed at SPB/SFX.

A recent experiment from the Consortium partnering with new XFEL users produced the molecular structures of naturally-occurring insecticides from bacteria by serial crystallography of nanocrystals. Due to the sub-micrometer crystal size, high concentrations could be flowed in a liquid jet, giving data collection rates of over 3000 indexable patterns per second. The nano-focus at SPB/SFX enabled diffraction information to be recorded to 1.6 Å resolution. Some of the structures were novel, giving no suitable reference structure to use for molecular replacement phasing. Instead, the AI-based prediction software AlphaFold was used to generate a starting model for refinement, thereby overcoming the need to employ additional experimental phasing methodologies. These structures give new insights into the mode of action of these toxins and how to design effective and specific mosquitocides. The structure of one component of a toxin, Tpp49Aa1, is depicted in Fig. 1 [1].

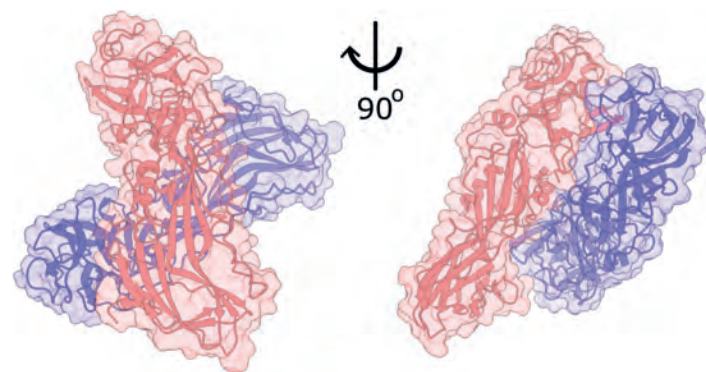


Figure 1

Two views of the Tpp49Aa1 macromolecular dimer, solved by serial femtosecond crystallography from natural protein crystals isolated from *B. thuringiensis* bacteria. The crystal only dissolves under the pH conditions of the mosquito gut, leading to toxicity for that insect. The structure reveals the mechanism of the dissolution and insights into developing novel and specific insecticides.



Figure 2

The new DiPOLE laser at the HED experiment station (Copyright: HZDR)

Helmholtz International Beamline for Extreme Fields (HIBEF)

The HIBEF user consortium is founded by the Helmholtz-Zentrum Dresden-Rossendorf (HZDR), DESY and the Central Laser Facility (CLF) from Rutherford Appleton Laboratory in the UK. It contributes some of the main experimental drivers, scientific and technical personnel, and scientific input for experiments at the High Energy Density (HED) instrument of European XFEL.

Two of the main drivers are now in successful user operation for several years: the High Intensity Relativistic Laser at XFEL (ReLaX) for investigations of relativistic plasmas with various X-ray based diagnostics like scattering, mainly SAXS, spectroscopy and imaging. Interaction chamber 2 is dedicated to diffraction experiments using diamond anvil cells combined with X-ray and pulsed laser-heating studies at static compression, dynamic compression in piezo-driven dynamic diamond anvil cells, and dynamic laser compression using the 'Diode Pumped Optical Laser for Experiments' (DiPOLE) (Fig. 2).

In Spring 2023, an international group of more than 80 scientists gathered for the first community-assisted dynamic laser compression experiment using the DiPOLE 100-X laser contributed to HIBEF through CLF. For the diagnostics, the campaign focused on diffraction in interaction chamber 2 and the velocity interferometry system for any reflector (VISAR) which was constructed with significant contributions by the French HIBEF partner CNRS and the Los Alamos National Laboratories. Since autumn, the system is open to general users and was already used by several single investigator groups.

The design of the pulsed magnetic field setup, generating fields up to 58 T in diffraction experiments was completed and the diffractometer and pulsed power supply have already been installed at European XFEL. The magnetic field pulse duration adapted to the time structure of the European XFEL pulse train in combination with a MHz time-resolved 'Sparta' AGIPD single module detector procured from X-Spectrum make the setup at this station unique. A first commissioning experiment of the full system is scheduled for early 2024, and a user community experiment is planned for the second half of 2024.

Heisenberg Resonant Inelastic X-ray Scattering (hRIXS)

The hRIXS consortium includes partners from Germany, Switzerland, Finland, France, Sweden, Italy and the UK. The project is coordinated by Potsdam University in close collaboration with DESY and European XFEL.

Contact:

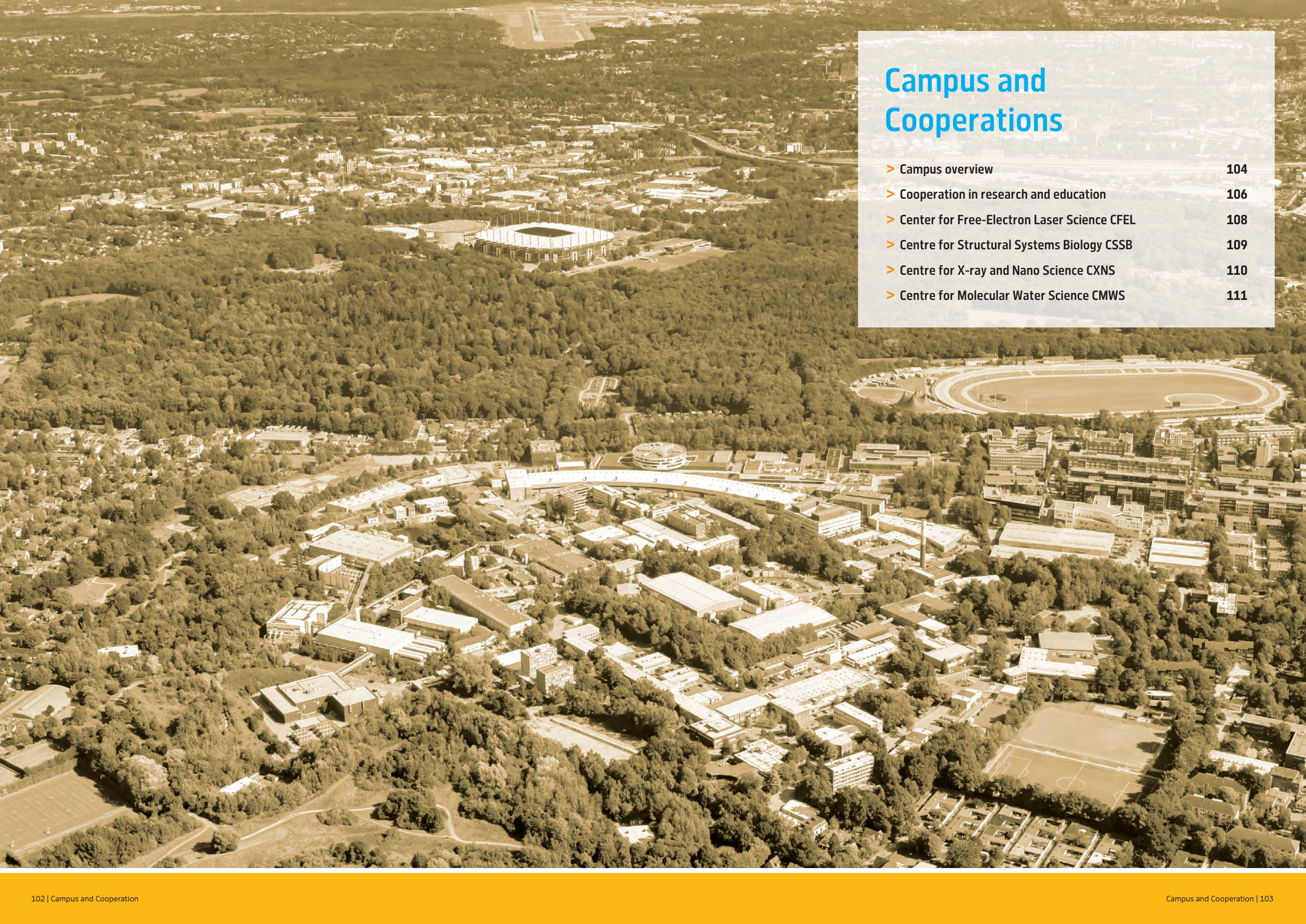
SFX: Henry Chapman, CFEL/DESY and Universität Hamburg, henry.chapman@desy.de

HIBEF: Thomas Cowan, HZDR, t.cowan@hzdr.de

hRIXS: Alexander Föhlisch, Potsdam University and HZB, alexander.foehlich@helmholtz-berlin.de

References

1. L. J. Williamson et al., 'Structure of the *Lysinibacillus sphaericus* Tpp49Aa1 pesticidal protein elucidated from natural crystals using MHz-SFX', PNAS 120, e2203241120 (2023).



Campus and Cooperations

- > Campus overview 104
- > Cooperation in research and education 106
- > Center for Free-Electron Laser Science CFEL 108
- > Centre for Structural Systems Biology CSSB 109
- > Centre for X-ray and Nano Science CXNS 110
- > Centre for Molecular Water Science CMWS 111

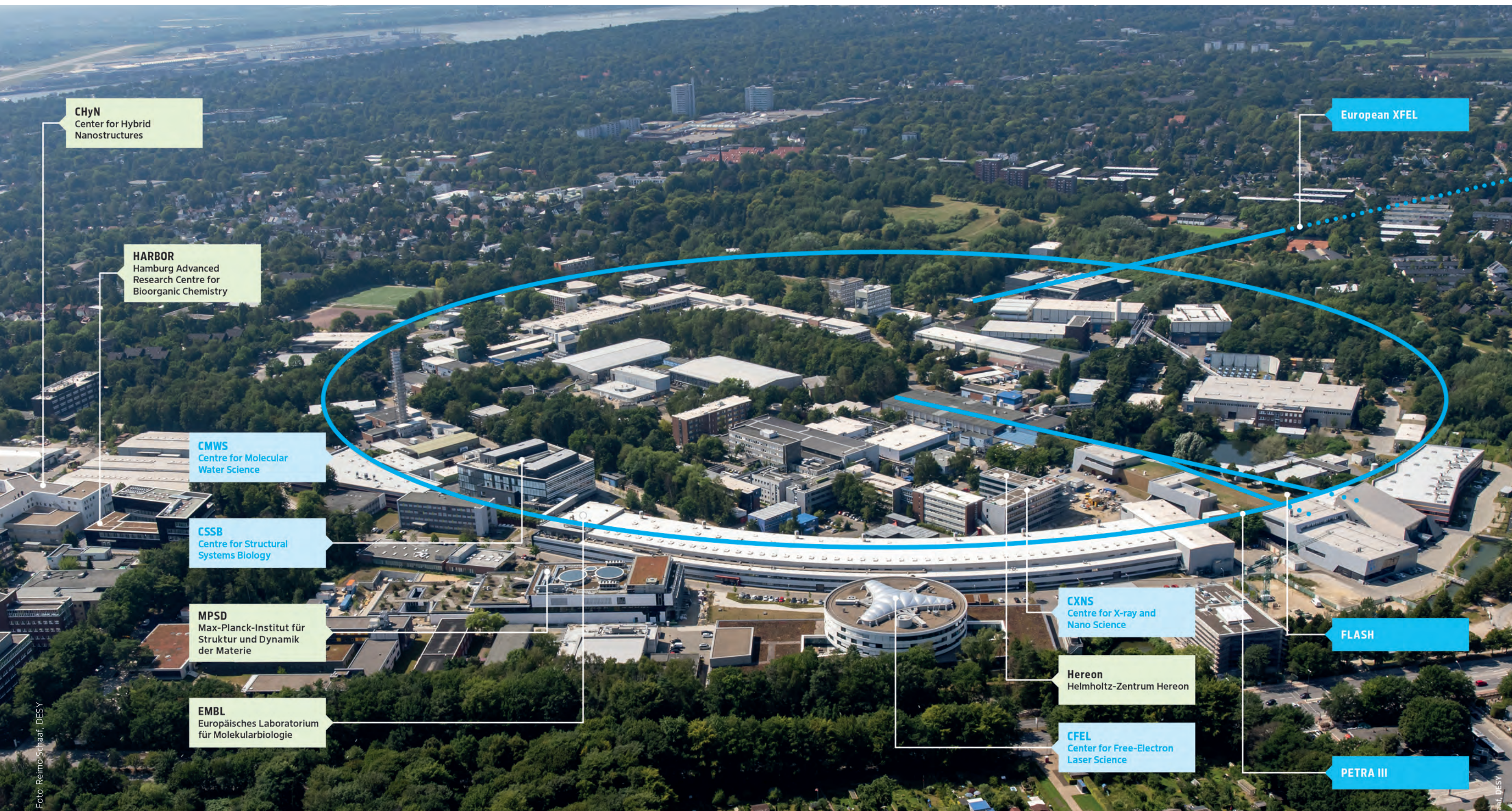
Campus overview

Research centres and cooperations

The research and cooperation landscape at DESY Photon Science involves local, national and international partners with a number of research centres as nuclei for cooperation. All benefit from the excellent scientific environment and research facilities on the Research Campus Bahrenfeld. The image below highlights the light sources, the four research centres in which DESY Photon Science is involved as well as the outstations of EMBL and HEREON and the research centres of the Universität Hamburg. Some major coopera-

tion activities with universities and the interdisciplinary research platforms on campus are reported on within this chapter.

German universities are also closely involved in developments at PETRA III and FLASH, for example through collaborative research projects funded via the BMBF programme ErUM-Pro. Major developments in connection to PETRA III, FLASH and European XFEL are described in the chapter 'Light Sources and User Infrastructures'.



Cooperation in research and education

Universities and networks overview

Graduate Schools

• PIER Helmholtz Graduate School (PHGS)

PHGS is a graduate education programme at DESY in cooperation with Universität Hamburg. In 2023, about 270 doctoral researchers have been members of the PHGS. The PhD students benefit from outstanding research in particle and astroparticle physics, nanoscience, photon science, infection and structural biology as well as accelerators and theoretical physics and –very new– in the PIER emerging topic artefact profiling.

PHGS offers numerous scientific or career development courses but also supervision and a buddy programme. The annual PIER Graduate Week includes interdisciplinary lectures and workshops to introduce doctoral researchers to the various science fields within PIER. During the 2023 PIER PhD Reception on 5 July at DESY, about 150 doctoral researchers, supervisors, friends, relatives and staff met to welcome all new doctoral researchers and to honour this year's 64 graduates, twenty of whom attended the event in person.

graduateschool.pier-hamburg.de



PHGS graduates participating in the PIER reception on 5 July at DESY. (Photo: PHGS, K. Winkler)



HELIOS doctoral researchers and PIs at the HELIOS training retreat in April 2023. (Photo: HELIOS, S. Tille)

• The Helmholtz-Lund International Graduate School (HELIOS)

HELIOS has been launched in October 2020 and focuses on instrumentation development in the fields of particle physics, molecular physics, nano(bio) science and ultrafast photon science. A major aim is to prepare young scientists for the next generation of instrumentation. The involved partners are Universität Hamburg, Lund University, City of Hamburg and DESY. Twenty doctoral candidates are currently enrolled in HELIOS.

In 2023, HELIOS focused its training efforts on data science and artificial intelligence (AI). A training retreat was held in Hamburg from 24 to 28 April, with lectures on machine learning and AI theory and applications. The final day was dedicated to career development and orientation, with presentations from the companies Philips and Nexperia on working in industry as well as on private sector recruitment processes. In addition, the doctoral candidates gained an insight into legal aspects of intellectual property and patents and participated in a lively panel discussion on start-up companies. www.heliosgraduateschool.org

• Data Science in Hamburg – Helmholtz Graduate School for the Structure of Matter (DASHH)

DASHH is a joint project of DESY, Universität Hamburg, Hamburg University of Technology, Helmut-Schmidt-Universität, Helmholtz-Zentrum Hereon, Helmholtz Centre for Infection Research, Max Planck Institute for the Structure and Dynamics of Matter, European XFEL and Hamburg University of Applied Sciences.

DASHH's goal is to train the next generation of data and information scientists in the field of novel data acquisition and analysis techniques to meet the challenges posed by the huge data sets generated by experiments at large-scale facilities. After the successful evaluation by the Helmholtz Association in 2023, funding for another five years was granted.

At present, 31 interdisciplinary PhD projects are funded by DASHH, mainly in the fields of photon science, particle physics, accelerator science but also structural biology, materials science and ultrafast X-ray science. Five DASHH doctoral researchers graduated in 2023. DASHH regularly organises a PhD Seminar, a Data Science Colloquium and PhD get-togethers as well as an annual retreat. Applications to join DASHH as associated doctoral researcher are welcome.

www.dashh.org



Participants of the 2023 DASHH retreat in Gifhorn. (Photo: DASHH)

Strategic networks

• LEAPS

The 'League of European Accelerator-based Photon Sources' is a strategic consortium initiated by the directors of the synchrotron radiation and free-electron laser user facilities in Europe. An important project is LEAPS-INNOV which aims at the implementation of the LEAPS Technology Roadmap and at fostering a partnership with European industry through innovation.

• PIER PLUS

The 'Partnership for Innovation, Education and Research' PIER was founded as a strategic partnership between DESY and Universität Hamburg in 2011. The successor PIER PLUS acts as a Hamburg metropolitan region's scientific platform and has expanded the collaboration and networking to several universities and independent research institutes.

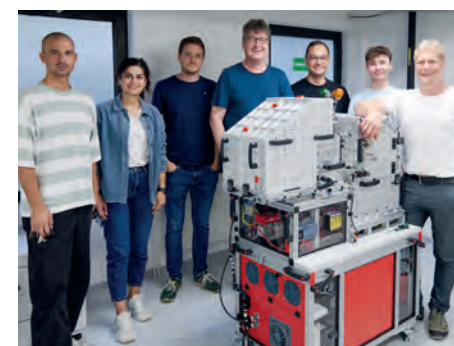
Excellence clusters

• 'CUI Advanced Imaging of Matter' (AIM)

Many of the DESY Photon Science leading scientists are strongly involved in the cluster's research programme, with Francesca Calegari and Henry Chapman acting as two of the three spokespersons. CUI also places great emphasis on education and equal opportunity programmes such as the dynaMENT Mentoring Program.

• 'Understanding Written Artefacts' (UWA)

Christian Schroer, leading scientist at DESY Photon Science, is principal investigator of the research project 'Reading Closed Cuneiform Tablets Using High-Resolution Computed Tomography'. The team has developed a portable tomography scanner that can be used to read ancient cuneiform tablets directly in museums. The first destinations for the device are the Louvre in Paris and several museums in Turkey.



The mobile XCT scanner proudly presented by the team. From left: S. Bosch, S. Ehteram (both UHH) P. Wiljes, C. Schroer, A. Schropp (all DESY), P. Paetzold (UHH/DESY), R. Döhrmann (DESY).

Joint laboratories

• In the 'Helmholtz International Laboratory on Reliability, Repetition, Results at the most advanced X-ray Sources' (HIR3X), DESY, European XFEL and the SLAC (U.S.) have joined forces to develop techniques and procedures that enable the reliable application of X-ray lasers.

• DESY is partner of the Helmholtz Institute Jena, an outstation of the GSI Helmholtz Center for Heavy Ion Research on the campus of the Friedrich Schiller University of Jena. The institute is mainly focused on applied and fundamental research at the borderline of high-power lasers and particle accelerator facilities.

• The Ruprecht Haensel Laboratory is a joint research facility of Christians-Albrecht-Universität zu Kiel (CAU) and DESY and combines state-of-the-art instruments and methods of nano-research, makes new developments available to international cooperation partners and, with joint appointments, ensures that teaching in the field of nano and surface science is strengthened in a research-oriented manner.

Collaborative research

• Tracking the active site in heterogeneous catalysis for emission control (SFB 1441), coordinated by Karlsruhe Institute of Technology

• Tailor-made multi-scale materials systems (SFB 986), coordinated by Technische Universität Hamburg (TUHH)

• Atomic scale control of energy conversion (SFB 1073), coordinated by Georg-August-Universität Göttingen

• Quantum cooperativity of light and matter (TRR 306), coordinated by Friedrich-Alexander-Universität Erlangen-Nürnberg

• Center for Integrated Multiscale Materials Systems (CIMMS), coordinated by TUHH

• Center for Data and Computing in Natural Sciences (CDCS), coordinated by Universität Hamburg

• Extreme Light for sensing and driving molecular Chirality (ELCH) (SFB 1319), coordinated by Universität Kassel

• Data for PHoton and Neutron for a National Research Data Infrastructure (DAPHNE4NFDI), coordinated by DESY

• Basic Services for a German National Research Data Infrastructure (Base4NFD), coordinated by Technische Universität Dresden

• Sustainability-driven nano- and materials science and technology with synchrotron, a cooperation between DESY and Technische Universität Bergakademie Freiberg.

• X-ray analyses on the PETRA III synchrotron radiation source and their evaluation, a cooperation between DESY, Hereon, EMBL and Fraunhofer-Gesellschaft

Center for Free-Electron Laser Science CFEL

Three institutions working together successfully

Researchers, partly from the MPSD group of Andrea Cavalleri at CFEL and colleagues from U.S. institutions, have shown for the first time that terahertz (THz) light pulses can stabilise ferromagnetism in a crystal at temperatures more than three times its usual transition temperature (see Fig. 1). In the *Nature* article titled 'Photo-induced high-temperature ferromagnetism in YTiO_3 ' [1], the team reports how pulses just hundreds of femtoseconds long induce a ferromagnetic state at high temperature in the rare-earth titanate which persisted for many nanoseconds after the light exposure. Below the equilibrium transition temperature, the laser pulses still strengthened the existing magnetic state, increasing the magnetisation up to its theoretical limit.

How did life begin on Earth? Experts have long been fascinated by this question and over the years have come up with a variety of theories. One hypothesis is that the origin of life can be traced back to warm little ponds which are thought to have existed on Earth four billion years ago. The water in these ponds probably contained urea molecules; these were exposed to ultraviolet radiation from the sun which at that time would have penetrated to the surface of the Earth largely unimpeded. This high-energy radiation was able to convert the urea into reaction products which then formed biomolecules that later served as the building blocks of life – or so the idea goes. This theory of 'warm little ponds' was one of the ideas that led a research team from Hamburg, Zurich and Geneva to devise and carry out a novel experiment. The theoreticians around Ludger Inhester from DESY's CFEL theory group of Robin Santra successfully performed the theoretical analysis of experimental data from two Swiss groups which were reported in the *Nature* article 'Femtosecond proton transfer in urea solutions probed by X-ray spectroscopy' [2] (see also article in the

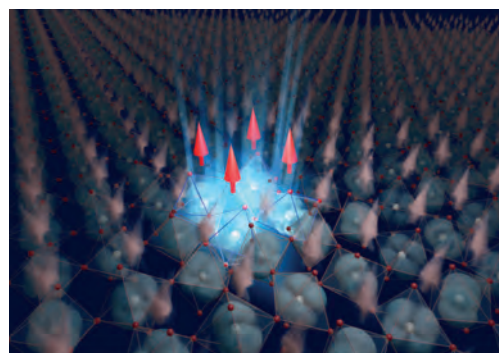


Figure 1
Magnetic spins in YTiO_3 are synchronised by THz light, leading to a stronger and higher temperature ferromagnetic phase. (Credit: Jörg Harms, MPSD)

Science Highlights Section of this report). The team, led by Hans Jakob Wörner and Jean-Pierre Wolf, used a special X-ray source to examine the first, extremely rapid steps of light-induced urea conversion (Fig. 2).

The infiltration of immune cells into sites of inflammation is one key feature of immune-mediated inflammatory diseases. A detailed assessment of the *in vivo* dynamics of relevant cell subtypes could boost the understanding of this disease and the development of novel therapies. In the *Scientific Reports* article 'Enabling X-ray fluorescence imaging for *in vivo* immune cell tracking' [3], Theresa Stauffer and colleagues from the UHH group of Florian Grüner at CFEL show in detail how advanced X-ray fluorescence imaging enables such quantitative *in vivo* cell tracking. It offers solutions that could pave the way beyond what other imaging modalities provide today. The key for this achievement is a detailed study of the spectral background contribution from multiple Compton scattering in a mouse-scaled object when this is scanned with a monochromatic pencil X-ray beam from a synchrotron. Under optimal conditions, the detection sensitivity is sufficient for observing local accumulations of the labelled immune cells, hence providing experimental demonstration of *in vivo* immune cell tracking in mice.

Contact: Ralf Köhn, ralf.koehn@cfel.de

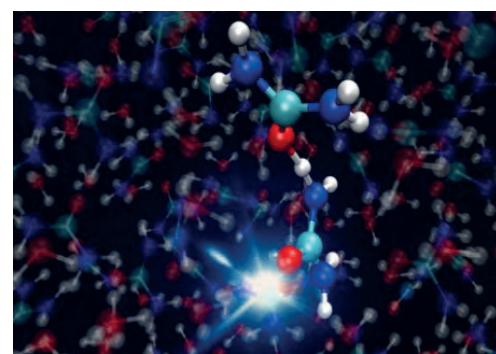


Figure 2
Two neighbouring urea molecules in aqueous solution exchange protons. (Credit: DESY, Ludger Inhester)

References

1. A. S. Disa et al., *Nature* 617, 73-78 (2023).
2. Z. Yin et al., *Nature* 619, 749-754 (2023).
3. T. Stauffer et al., *Sci Rep* 13, 11505 (2023).

CFEL Partner Institutions

- Deutsches Elektronen-Synchrotron DESY, Hamburg, Germany
 - Max Planck Institute for the Structure and Dynamics of Matter (MPSD)
 - Universität Hamburg, Hamburg, Germany (UHH)
- www.cfel.de

Centre for Structural Systems Biology CSSB

A hub for molecular infection research



Figure 1
Attendees of the third International CSSB Symposium (Credit: Tina Mavric)

Over 100 participants attended CSSB's third International Symposium 'Charting the landscape of infection: From entry to exit' held 3-5 May 2023. The symposium focused on the biology of infections and highlighted different key cellular processes leading to pathogen proliferation. In June, the second scientific evaluation of the centre with external evaluators took place, followed by a virtual Scientific Advisory Board meeting in October. The CSSB directorate is developing a 'CSSB Strategy 2023' paper which provides a clear and inspiring vision for the centre's future development.

CSSB is also involved in new collaborative training endeavours. Five PIs and two associate members are part of a new Research Training Group 'VISualization and imaging of virus Infection' (VISION). PI Charlotte Uetrecht (CSSB, DESY, LIV, Univ. Siegen) will coordinate SPIDoc's new doctoral network funded within the Marie Skłodowska-Curie Actions (MSCA). Six CSSB PIs and one facility head are involved in the 'Integrative Analysis of pathogen-induced compartments programme' (InterAct), which received 1.2 million Euro in funding for another four years.

Research highlights

CSSB scientists used high-resolution imaging techniques to analyse the molecular skeleton of four cell forms of the malaria parasite *Plasmodium falciparum* [1]; revealed the cryo-EM structure of a transporter and adaptor proteins in a signalling pathway known to be involved in the pathogenesis of lupus [2]; presented the first comprehensive method for live-cell imaging of cellular and viral nucleic acids using a two-step labelling approach [3]; engineered a new molecule, darobactin 22, with superior antibiotic activity [4] (see also Science Highlights Section of this report) and characterised the structure and function of the Sin Nombre virus L protein [5]. Our scientists are also involved in the development of new tools and technologies for the infection and structural biology community, such as

a biophysical pipeline to characterise membrane proteins [6]; a programme for identifying 'sub-interfaces' in protein-protein complexes using distance clustering [7]; an ultrafast particle finder for cryo-EM tomograms [8] and a guided-deconvolution for correlative light and electron microscopy [9].

New group leader

In September Professor Caroline Barisch joined CSSB with an appointment from the Research Centre Borstel. Her group focuses on deciphering the molecular mechanisms by which pathogenic mycobacteria remodel, acquire, import and utilise lipids from their host to support infection.

Awards

CSSB PI Meytal Landau (DESY, UKE) was awarded a two million Euro ERC Consolidator Grant from the European Research Council to investigate microbial amyloid proteins. Catalin Bunduc from the Marlovits group received a Veni Grant for his research on tuberculosis. Dorte Stalling from the Bosse group received the Gesellschaft für Biochemie und Molekularbiologie e.V. (GBM) prize for best master's thesis in Biochemistry at Hannover Medical School. Sarah Nentwich from the Utrecht group received the Wolfgang-Paul Study Prize of the DGMS for best master's thesis. Emily Machala from the Grünwald group received a MSCA Postdoctoral Fellowship funded under the Horizon Europe Programme.

Contact: Kay Grünwald, kay.gruenewald@cssb-hamburg.de

References

1. J. L. Ferreira et al., *Nat Commun.* 14, 1216 (2023).
2. T. F. Custódio et al., *Nat Commun.* 14, 5696 (2023).
3. V. T. Sterrenberg et al., *Angew. Chem. Int. Ed.* 62, 38 (2023).
4. C. E. Seyfert et al., *Angew. Chem. Int. Ed.* 62, 2 (2023).
5. K. Meier et al., *PLoS Pathog.* 19, 8 (2023).
6. S. Niebling et al., *MIMB*, 2652 (2023).
7. L. R. Genz et al., *Bioinformatics*, btad629 (2023).
8. E. Genthe et al., *J Struct Biol.* 215, 107990 (2023).
9. F. Ma et al., *PLoS One.* 18(3), e0282803 (2023).

CSSB Partner Institutions

- Bernhard Nocht Institute for Tropical Medicine (BNITM)
- Deutsches Elektronen-Synchrotron DESY
- European Molecular Biology Laboratory (EMBL)
- Hannover Medical School (MHH)
- Leibniz Institute of Virology (LIV)
- Helmholtz Centre for Infection Research (HZI)
- Research Center Borstel (FZB)
- Universität Hamburg (UHH)
- University Medical Center Hamburg-Eppendorf (UKE)

Centre for X-ray and Nano Science CXNS

Research with X-ray light in combination with materials science and nanoscience



Figure 1
Participants of the NanoMat Science Day 2023.

One and a half years after the opening of the centre for X-ray and Nanoscience (CXNS), the new research centre with its own laboratory unit has passed the practical test. It enables closer cooperation of the CXNS partners: DESY Photon Science groups, the Helmholtz-Zentrum Hereon with its German Engineering Materials Science Center (GEMS), Kiel University (CAU) with the Ruprecht-Haensel-Labor (RHL), the Leibniz-Institut für Kristallzüchtung (IKZ) and the Hamburg Technical University (TUHH).

The spacious well-equipped laboratories and short ways between them are game-changing. The CXNS' unique profile also offers instrumentation for sample preparation and characterisation for experiments at the close-by large-scale facilities such as PETRA III and FLASH. This special intertwined research environment has more than fulfilled expectations for DESY projects, for external scientific users as well as for business customers. Many projects have already used the newly developed and implemented 'nanotransfer'-protocol, the relocation of preselected interesting sample regions. This enables and supports *in situ* nano experiments at the large-scale facilities. In cooperation with the IKZ, a laserlab for time-resolved ultrafast spectroscopy will start operation at the CXNS in 2024.

In 2023, the NanoMat Science Day has taken place again as an on-site event with more than 120 participants from 20 countries. It has been created as an internal forum for young scientists in nano and materials sciences. This work-

shop is promoting networking of young scientists. It enables connections and further developments of new scientific research and projects and helps to develop a deeper exchange between young scientists and different DESY groups related to the CXNS or to the research topics.

The scientific highlights at the CXNS laboratories in 2023 also reflect the broad range of research at the CXNS either in cooperation with other teams or the inhouse research by the CXNS groups. In corrosion research, materials science, in the further development of quantum research and quantum networks as well as in catalysis and hydrogen or medical research, the participating scientists and the involved teams reached strategic milestones in 2023.

Contact: *Andreas Stierle*, andreas.stierle@desy.de

CXNS Partner Institutions

- Helmholtz-Zentrum Hereon, German Engineering Materials Science Centre (GEMS)
- Christian-Albrechts-Universität zu Kiel (CAU), Ruprecht-Haensel-Labor
- Deutsches Elektronen-Synchrotron DESY, Hamburg, Germany
- Technical University Hamburg (TUHH), Center for Integrated Multiscale Material Systems (CIMMS)
- Leibniz-Institut für Kristallzüchtung (IKZ Berlin)
photon-science.desy.de/research/centres_for_research/cxns

Centre for Molecular Water Science CMWS

Achieving a detailed molecular understanding of water

The Centre for Molecular Water Science (CMWS) brings together key experts from different areas of water-related sciences. The common goal of CMWS is delivering a detailed molecular understanding of the various structures, phenomena and dynamic processes in water and water interfaces that are relevant for green-energy technologies, health and environment. In a series of workshops and general meetings the science concept has been developed by the CMWS consortium consisting of more than 140 scientists worldwide. The research of CMWS is organised in five pillars (Fig. 1) and coordinated by DESY. The key idea is a combined theoretical and multimodal experimental approach. One important focus are the X-ray methods available at DESY and European XFEL for studying molecular structure and dynamics in different timescales and environments [1].

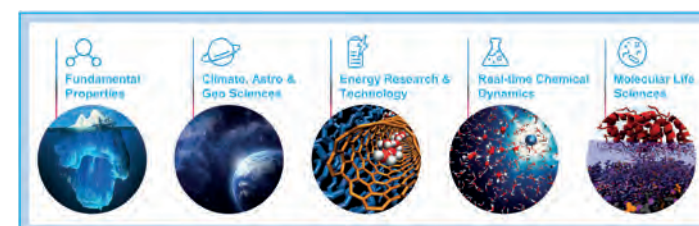


Figure 1
The five research pillars focus on different interdisciplinary aspects of molecular water research.

Driving water research forward within CMWS

In 2023, a formal declaration was drafted to take CMWS to a more formal level and build a robust and sustainable structure. More than 40 partners are about to sign this declaration and thereby joining the CMWS consortium as founding members. On the DESY campus, two CMWS laboratories offer access to high-level spectrometers, and further dedicated DESY laboratories have been expanded with specific instrumentation in 2023. The first targeted, challenge-driven calls of European XFEL and PETRA III on molecular-water science were successful with a number of experiments of the CMWS network. For instance, within this proposal call, CMWS researchers study the structure and dynamics of particular amorphous ices named amorphous solid water (ASW) and hyperquenched amorphous water (HGW) which frequently appear in outer space. They will especially investigate how these ices transform into other phases under external triggers present in outer space such as heat and UV irradiation. Currently, new challenge-driven calls on molecular-water science are announced and discussed by DESY and European XFEL.

The next DESY call specifically allows combining FLASH and PETRA III beamlines.

To extend and further strengthen the common research activities within CMWS researchers, an Early Science Program (ESP) was launched by DESY in 2019, supporting PhD projects between different CMWS partners. The programme is jointly financed by DESY and CMWS partners with equal contributions. In 2023, within the third round of the CMWS Science Program, ten new successful projects started with focus on the research agenda of the CMWS White Paper [2].

Events and activities

The CMWS Water DAYS, including the DESY Research Course with focus on Water in climate, astro- and geo-sciences, took again place in February 2023 as an in-person event with more than 120 participants. During this meeting, highlights of CMWS research were presented and the outcome, and lessons learnt from the topical calls on water research of European XFEL and PETRA III were discussed. The next DESY Water Days are planned for February 2024.

For the first time, CMWS organised the CMWS graduate workshop, addressing master and PhD students, young research fellows as well as interested scientists, taking place in November 2023. Topics covered recent developments in the field of molecular-water research with special focus on modern experimental techniques hosted in the Hamburg environment as well as connections between simulation, theory and experiment.

The CMWS Seminar continued as a series on water-related science and technology. The aim of the series is to intensify the scientific exchange within the network of CMWS and to introduce students and young scientists to the different research areas of CMWS.

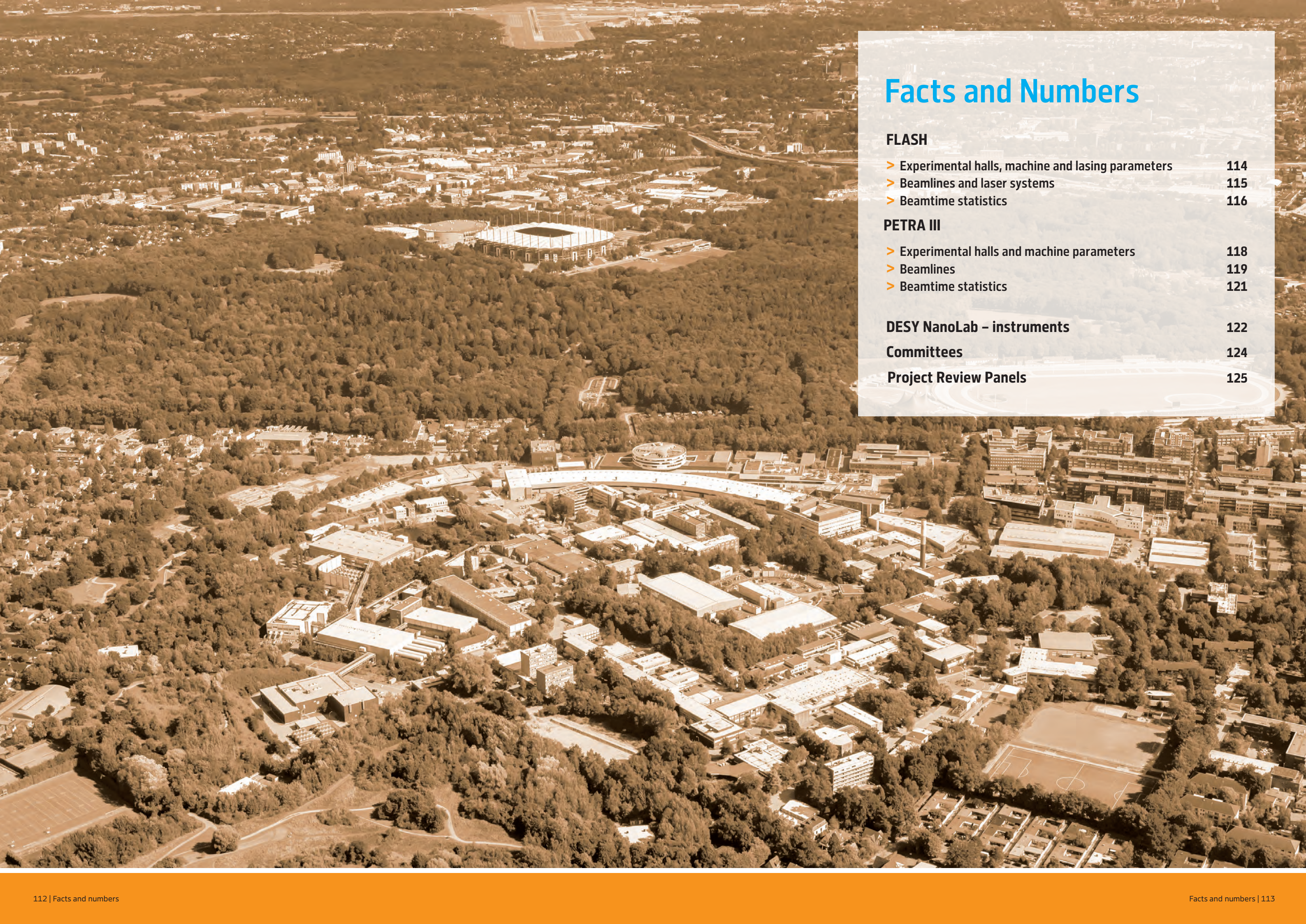
Contact: *Claudia Goy*, claudia.goy@desy.de

References

1. F. Lehmkuhler, C. Goy, R. Santra and G. Grübel, *Phys. unserer Zeit*, 52, 298-305 (2021). DOI: [10.1002/piuz.202101616](https://doi.org/10.1002/piuz.202101616)
2. G. Gruebel, M. Schnell, C. Goy, F. Lehmkuhler and S. Bari (Eds.), *CMWS - White paper*, DESY, 127 (2021) DOI: [10.3204/PUBDB-2021-01859](https://doi.org/10.3204/PUBDB-2021-01859)

CMWS Partner Institutions

60 partner institutions from 16 countries
www.cmws-hamburg.de



Facts and Numbers

FLASH

- > Experimental halls, machine and lasing parameters 114
- > Beamlines and laser systems 115
- > Beamtime statistics 116

PETRA III

- > Experimental halls and machine parameters 118
- > Beamlines 119
- > Beamtime statistics 121

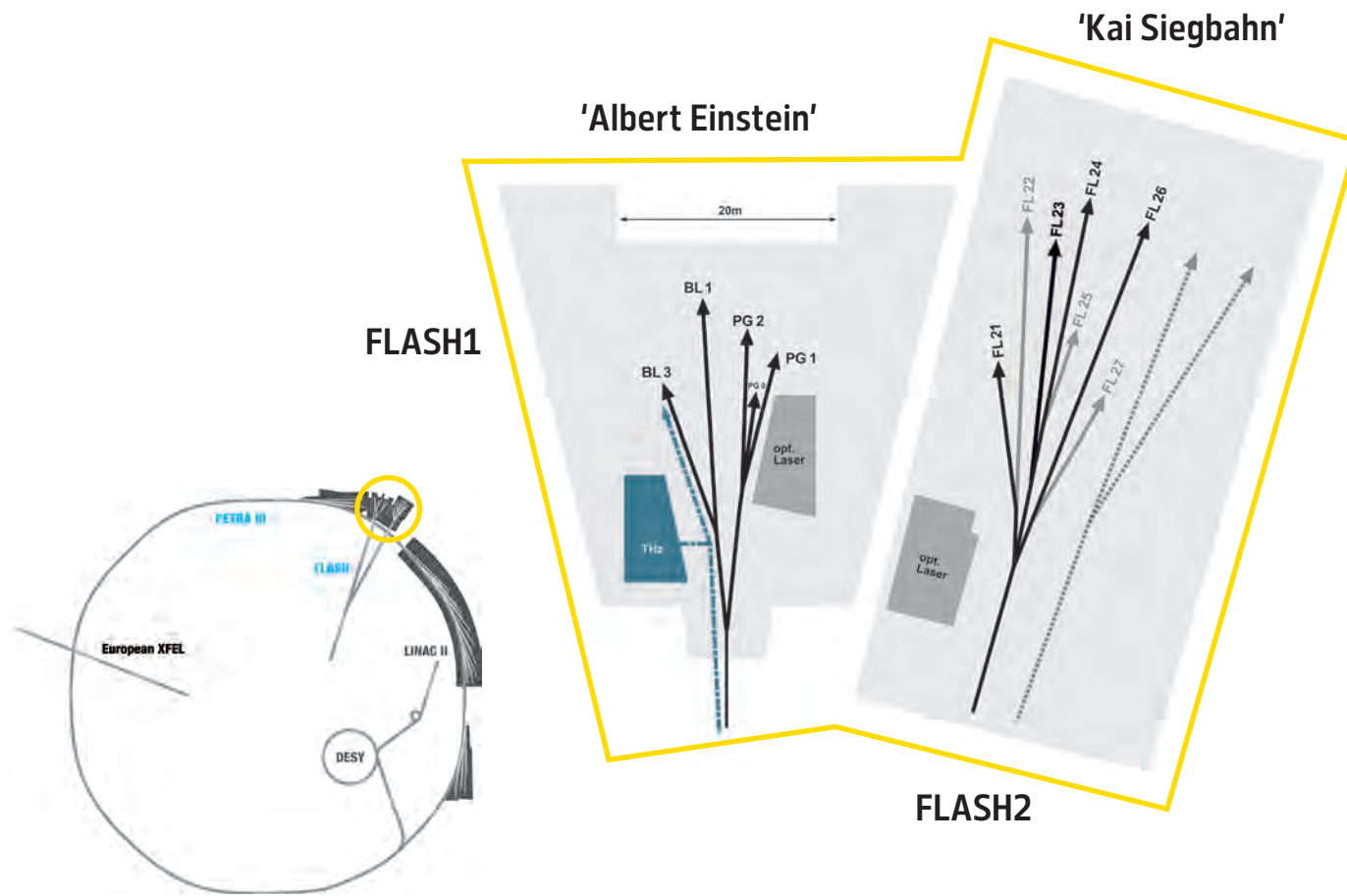
DESY NanoLab – instruments 122

Committees 124

Project Review Panels 125

FLASH

Experimental halls, machine and lasing parameters



FLASH – machine parameters

	FLASH1	FLASH2
Electron energy range	0.35–1.35 GeV	0.4–1.35 GeV
Normalised emittance at 0.4 nC (rms)	0.4 mm mrad	0.4 mm mrad
Energy spread	200 keV	500 keV
Electron bunch charge	0.01–1.2 nC	0.01–1 nC
Peak current	1–2.5 kA	1–2.5 kA
Electron bunches per second (shared between FL1 and FL2)	5000	5000

FLASH – lasing parameters

	FLASH1	FLASH2
Photon energy fundamental	24–360 eV	14–370 eV
Wavelength fundamental	51–3.4 nm	90–3.3 nm
Photon pulse duration (FWHM)	30–200 fs	10–200 fs
Peak power	1–5 GW	1–5 GW
Single photon pulse energy (average)	1–500 μ J	1–1000 μ J
Spectral width (FWHM)	0.7–2%	0.5–2%
Photons per bunch	10^{11} – 10^{14}	10^{11} – 10^{14}
Peak brilliance photons/sec/mm ² /mrad ² /0.1%	10^{28} – 10^{31}	10^{28} – 10^{31}

FLASH

Beamlines and laser systems

FLASH1 experimental hall 'Albert Einstein'

BL1	non-monochromatic FEL photons Kirkpatrick-Baez (KB) focusing optics, FEL focal spot of $\approx 7 \mu\text{m} \times 8 \mu\text{m}$ (FWHM) split-and-delay unit for XUV pump – XUV probe experiments (mirrors for 13.57 nm, -30 ps to +650 ps delay) no optical pump – probe laser available until 2025 4-mirror polariser for variable FEL polarisation from 30–70 eV permanent end station: multipurpose CAMP chamber with pnCCD detectors, electron and ion spectrometers and collinear incoupling optics for optical laser	TU Berlin
BL3	non-monochromatic FEL photons, spectral range: $> 4.5 \text{ nm}$ (carbon coated optics) focused to $\approx 20 \mu\text{m}$ / unfocused beam size ≈ 5 – 10 mm (FWHM, depending on wavelength) optional pump – probe experiments using the FLASH1 optical laser system for BL1 and BL3 4-mirror polariser for variable FEL polarisation from 30–70 eV optional pump – probe experiments using THz radiation: - tuneable: 10–230 μm ; up to 150 $\mu\text{J}/\text{pulse}$; $\approx 10\%$ bandwidth - broadband at 200 μm ; up to 10 $\mu\text{J}/\text{pulse}$; $\approx 100\%$ bandwidth - synchronised and phase stable to X-ray pulses (down to 5 fs) - delivered to the experiment via vacuum beamline as: (i) ultra-high vacuum (10^{-8} mbar), shorter delay between THz and X-ray ($\approx 4 \text{ m}$ path difference); can accommodate up to 0.3 m wide setup (ii) high vacuum ($\approx 10^{-6}$ mbar), longer delay between THz and X-ray ($\approx 7 \text{ m}$ path difference); can accommodate up to 2 m wide setup - UHV chamber with mounts for refocusing XUV optics to compensate for XUV/THz path delay about 3 x 4 m platform for user-provided end station	TU Berlin
PG1	high resolution plane grating XUV monochromator (SX 700 type, $< 10^{-4}$ bandwidth, carbon coated optics): - variable combination of photon flux and resolution (from high flux to high resolution) - controlled temporal-spectral properties at moderate resolution for pump – probe experiments - high photon flux with harmonic filtering Kirkpatrick-Baez (KB) refocusing optics, FEL focal spot down to 5 μm FWHM (vertically, monochromator exit slit size dependent) permanent end station: - XUV-Raman spectrometer TRIXS for high-resolution and time-resolved RIXS measurements on solid samples (20–400 K, resolving power ≈ 1700 , time resolution 170–300 fs FWHM) - optional pump – probe experiments (RIXS; XAS and reflectivity with angular resolution) using the FLASH1 optical laser system for PG1 and PG2	
PG2	uses the same monochromator as PG1 50 μm focus XUV beam splitter with variable time delay ($\pm 6 \text{ ps}$) for time resolved studies optional pump – probe experiments using FLASH1 optical laser system for PG1 and PG2 about 3 x 4 m platform for user-provided end station	

FLASH1 optical / NIR laser system for pump-probe experiments for beamlines BL1 and BL3

The laser will be decommissioned in 2024, new laser availability depending on further funding.	
intra-burst repetition rate	single pulse
number of pulses per burst	1
pulse duration	$< 60 \text{ fs}$ FWHM, $\approx 200 \text{ ps}$ FWHM (uncompressed)
timing jitter to FEL	$< 60 \text{ fs}$ rms
pulse energy	0–10 mJ (before coupling to chamber), 0–7 mJ (at interaction region)
polarisation	Linear (s or p)
peak intensity	$> 10^{14} \text{ W}/\text{cm}^2$
time delay to FEL	-1 ns to +1 ns, 10 fs resolution
energy stability	$< 10\%$ pulse-to-pulse peak (3% rms)
Harmonic generation conversion to 400 nm, 266 nm and 200 nm central wavelength is available with conversion efficiencies of $> 30\%$ SHG, $> 5\%$ THG at BL1	

FLASH1 optical / NIR laser system for pump-probe experiments for beamlines PG1 and PG2

central wavelength	1030 nm
spectral bandwidth	30 to 50 nm (pre-set for experiment)
intra-burst repetition rate	Up to 1 MHz
number of pulses per burst	1–800
pulse duration	60–100 fs FWHM
timing jitter to FEL	< 60 fs rms
pulse energy	0–30 μJ (at interaction point at 1030 nm)
polarisation	Linear (s or p)
peak intensity	> 10 ¹⁴ W/cm ²
time delay to FEL	-1.5 ns to +1.5 ns, larger delays optional
energy stability	< 10% pulse-to-pulse peak (3% rms)

Harmonic generation conversion to (SHG) 515 nm, (THG) 343 nm or (FHG) 257 nm central wavelength is available with conversion efficiencies of > 50% SHG, > 10% THG, > 6% FHG.

FLASH2 experimental hall 'Kai Siegbahn'

FL21	diagnostics beamline – not available for user experiments	
FL23	pulse-length preserving double grating monochromator beamline wavelength range: 2–20 nm fundamental plus 3. harmonic High transmission option (single grating) & high temporal resolution option (double grating) (effective) pulse duration <50 fs FWHM Kirkpatrick-Baez (KB) focusing optics with variable foci down to < 10 μm (FWHM)/unfocussed beam size ≈ 5–10 mm (FWHM, depending on wavelength)	
	optional pump – probe experiments using FLASH2 optical laser system grazing incidence split-and-delay unit with -5/+18 ps time delay	Univ. Münster
	about 3 × 4 m platform for user-provided end station	
FL24	non-monochromatic FEL photons wavelength range: 4–90 nm fundamental Kirkpatrick-Baez (KB) focusing optics with variable foci down to < 10 μm (FWHM)/unfocussed beam size ≈ 5–10 mm (FWHM, depending on wavelength)	
	optional pump – probe experiments using FLASH2 optical laser system grazing incidence split-and-delay unit with -5/+18 ps time delay	Univ. Münster
	about 3 × 4 m platform for user-provided end station	
FL26	non-monochromatic FEL photons wavelength range: 6–90 nm fundamental	
	optional pump – probe experiments using FLASH2 optical laser system Laser-based high harmonic generation VUV source for VUV-XUV pump-probe experiments with up to 50 eV VUV photon energy	Univ. Hannover
	permanent end station:	MPI-K Heidelberg
	- reaction microscope (REMI) for time-resolved AMO spectroscopy - grazing incidence split-and-delay unit and refocusing optics: FEL focal spot < 10 μm × 10 μm (FWHM, depending on wavelength) - ± 2.7 ps time delay range, 1 fs precision - grating spectrometer for online spectral distribution monitoring and for transient absorption spectroscopy	

FLASH2 optical / NIR laser system for pump-probe experiments for beamlines FL23

central wavelength	1030 nm
spectral bandwidth (@-10dB)	< 50 nm
intra-burst repetition rate	100 kHz
number of pulses per burst	80 (burst 800 μs flat)
pulse duration	> 70 fs (FWHM (compressed to 1.1 × bandwidth limit), >1000 fs FWHM (uncompressed))
timing jitter to FEL	t.b.d.
pulse energy	0–1.8 mJ (at interface with experimental chamber)
polarisation	Linear (s or p)
focus size (1/e ² diameter)	> 50 μm (1/e ²)
peak intensity	> 10 ¹⁵ W/cm ²
time delay to FEL	-1.5 ns to +1.5 ns, larger delays optional
energy stability	< 10% pulse-to-pulse peak (3% rms)

Harmonic generation conversion to 515, 343 and 257 nm central wavelength is available

FLASH2 optical / NIR laser system for pump-probe experiments for beamlines FL24 and FL26

central wavelength	700 to 900 nm (fast tuneable)
spectral bandwidth	30 to 140 nm (pre-set for experiment)
intra-burst repetition rate	100 kHz
number of pulses per burst	1–77
pulse duration	15–65 fs FWHM (compressed to 1.1 × bandwidth limit), ~1000 fs FWHM (uncompressed)
timing jitter to FEL	~ 30 fs rms (~ 15 fs rms with Laser Arrival Monitor [LAM])
pulse energy	0–120 μJ (at interaction region)
polarisation	Linear (s or p)
focus size (1/e ² diameter)	> 50 μm (1/e ²)
peak intensity	10 ¹³ W/cm ² (@50 μm)
time delay to FEL	-1.5 ns to +1.5 ns, larger delays optional
energy stability	< 10% pulse-to-pulse peak (3% rms)

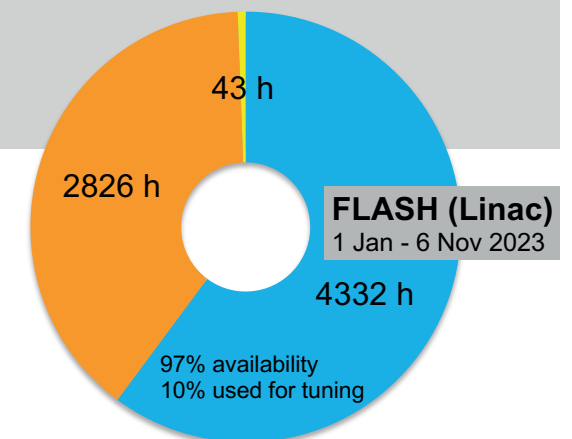
Harmonic generation conversion to 400 nm (SHG) and 266 nm (THG) central wavelength is available with conversion efficiencies of > 10% SHG, > 3% THG, pulse durations are increasing.

All FLASH beamlines provide online photon diagnostics for intensity, wavelength and beam position, fast shutter, aperture and filter sets.

FLASH beamtime statistics 2023

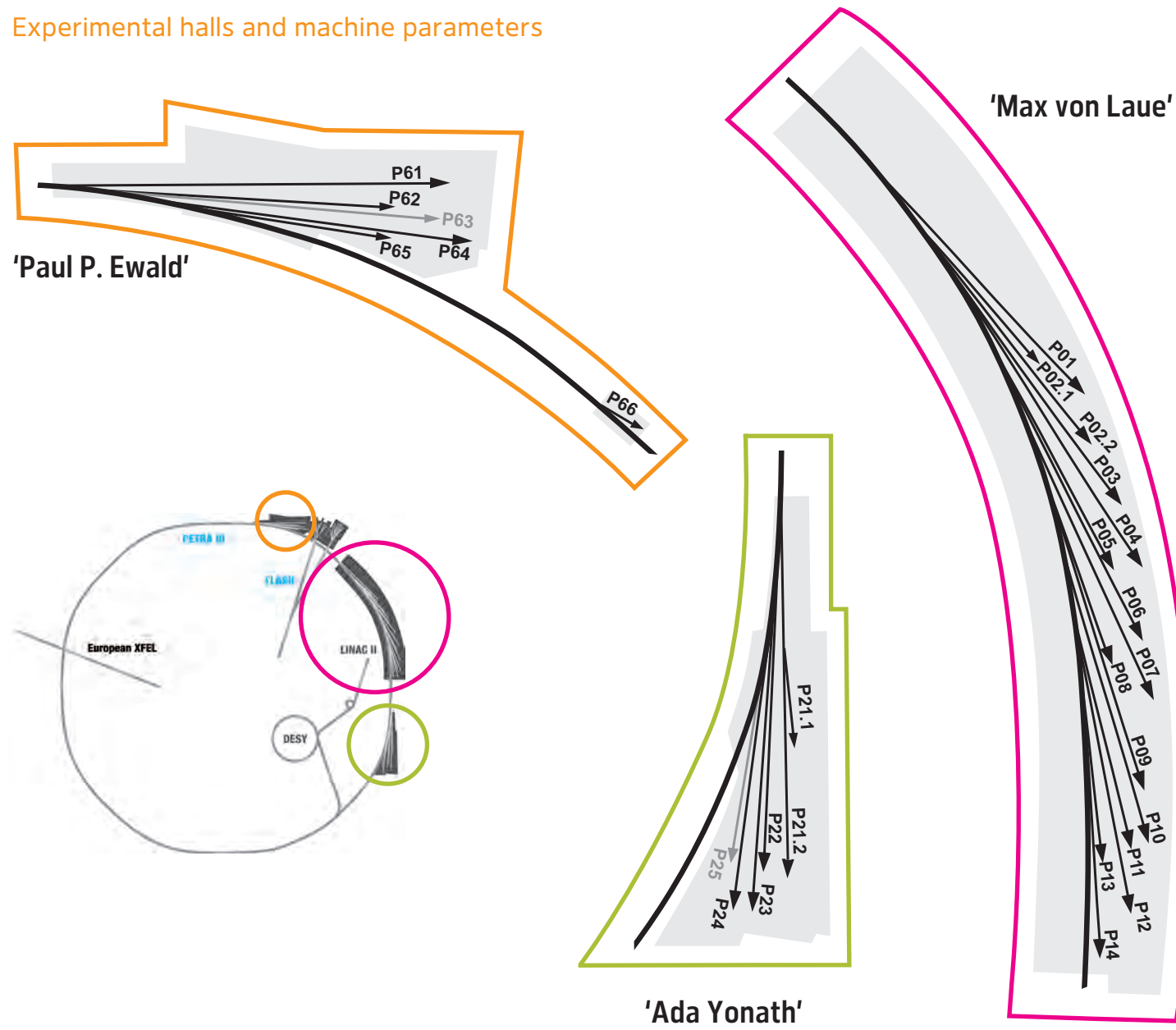
FLASH	Operation period 2023	User beamtime	Machine studies and user experiment preparation	Maintenance	Shutdown and commissioning
FLASH (Linac)	1 Jan – 6 Nov	4332 h	2826 h	43 h	246 h
	planned for 7 Nov – 31 Dec	696 h	376 h	8 h	233 h
FLASH1	1 Jan – 6 Nov	2844 h			
	planned for 7 Nov – 31 Dec	360 h			
FLASH2	1 Jan – 6 Nov	2427 h			
	planned for 7 Nov – 31 Dec	336 h			

- User beamtime
- Machine studies/User experiment preparation
- Maintenance



PETRA III

Experimental halls and machine parameters



PETRA III - machine parameters

Electron energy	6.08 GeV
Circumference of the storage ring	2304 m
Number of bunches	40 (timing mode) 480 (continuous mode)
Bunch separation	192 ns (timing mode) 16 ns (continuous mode)
Electron beam current	100 mA (timing mode) 120 mA (continuous mode)
Horizontal electron beam emittance	1.3 nmrاد
Vertical electron beam emittance	0.01 nmrاد
Electron beam energy spread (rms)	0.1%
Horizontal × vertical beam size (rms) at 5 m undulator (high β section) and 10 keV photon energy	141 μm × 5.2 μm
Horizontal × vertical beam size (rms) at 5 m undulator (low β section) and 10 keV photon energy	36 μm × 5.7 μm

PETRA III

Beamlines

PETRA III experimental hall 'Max von Laue'

Beamline and instruments	Operated by
R — option for remote user operation M — option for mail-in service	
P01 High Resolution Dynamics 10 m U36 2.5–80 keV	DESY
Nuclear resonant scattering	DESY
Resonant inelastic X-ray scattering	DESY MPI
X-ray Raman scattering	DESY MPI
P02.1 Powder Diffraction and Total Scattering 2 m U23 60 keV	DESY
M Standard and <i>in situ</i> powder diffraction	DESY
M Standard and <i>in situ</i> total scattering	DESY
P02.2 Extreme Conditions 2 m U23 25.6 keV, 42.7 keV	DESY
R Laser heated experiment for diamond anvil cells (DACs)	DESY
R General purpose experiment for high pressure DAC applications	DESY
P03 Micro- and Nano-SAXS/WAXS 2 m U29 7–21 keV	DESY
Grazing incidence & transmission micro-beam small and wide-angle scattering	DESY
Nano-beam scattering and diffraction	DESY Hereon collaborators
P04 Variable Polarisation Soft X-rays 5 m UE65 250–2800 eV	DESY
UHV diffractometer and soft X-ray spectrometer	DESY collaborators
Photon-ion spectrometer (PIPE)	DESY collaborators
Ultra-high resolution angular resolved photoelectron spectroscopy (solids & liquids)	DESY collaborators
Soft X-ray absorption holographic imaging instrument	DESY collaborators
P05 Micro- and Nano-Imaging 2 m U29 8–50 keV	Hereon
M Micro-tomography	Hereon
Nano-tomography	Hereon
P06 Hard X-ray Micro- and Nano-probe 2 m U32 5–45 keV	DESY
Micro-probe	DESY
Nano-probe	DESY
P07 High Energy X-ray Materials Science 4 m IVU21 50–200 keV	Hereon
Surface diffraction, grazing incidence total scattering, diffraction tomography	DESY
Heavy-load diffractometer	Hereon
Grain mapper	Hereon
High energy tomography	Hereon
P08 High Resolution Diffraction 2 m U29 5.4–29.4 keV	DESY
M High resolution diffractometer	DESY
Liquid surface diffractometer	DESY collaborators
Langmuir trough in-plane diffractometer	DESY
P09 Resonant Scattering and Diffraction 2 m U32 2.7–31 keV	DESY
Resonant X-ray diffraction at low temperatures (2 K < T < 750 K)	DESY
Resonant X-ray diffraction in high B-fields (2 K < T < 300 K; B < 14 T, B ⊥ Q)	DESY
Resonant X-ray diffraction at high pressure (4 K < T < 300 K; p < 30 GPa)	DESY
High-throughput Pharmaceutical X-ray screening (HiPhax)	DESY
P10 Coherence Applications 5 m U32 4–20 keV	DESY
R X-ray photon correlation spectroscopy (SAXS/WAXS geometry) (5–15 keV)	DESY
R Bragg coherent diffraction imaging (5–13 keV)	DESY
R GINIX — Nano-focusing setup (8 and 13.8 keV)	DESY collaborators
P11 High-throughput Macromolecular Crystallography 2 m U32 2.4–30 keV	DESY
R, M Macromolecular crystallography (6–26 keV)	DESY HZI Univ. Lübeck
M Serial crystallography (6–26 keV)	DESY

PETRA III experimental hall 'Max von Laue'

Beamline and instruments	Operated by
R — option for remote user operation M — option for mail-in service	
P12 Bio SAXS 2 m U29 4–20 keV	EMBL
R Small-angle and wide-angle X-ray scattering	EMBL
Time-resolved X-ray scattering	EMBL
Anomalous small-angle X-ray scattering	EMBL
P13 Macromolecular Crystallography 2 m U29 4.5–17.5 keV	EMBL
R Macromolecular crystallography	EMBL
P14 Macromolecular Crystallography and Imaging 2 m U29 6–27 keV	EMBL
R Macromolecular crystallography (7–27 keV)	EMBL
R Serial crystallography (7–18 keV)	EMBL
High throughput micro-tomography (6–20 keV)	EMBL
Time-resolved serial crystallography (12.7 keV)	EMBL U Hamburg

PETRA III experimental hall 'Ada Yonath'

Beamline and instruments	Operated by
R — option for remote user operation M — option for mail-in service	
P21.1 High-Energy Diffraction for Physics & Chemistry at the Swedish Materials Science Beamline side branch: 2 m U29 54 keV, 88 keV, 102 keV	Center for X-rays in Swedish Materials Science (CeXS) DESY
Single crystal diffuse scattering & 3d-ΔPDF	CeXS DESY
Total scattering (transmission & grazing incidence)	CeXS DESY
P21.2 Swedish Materials Science Beamline 4 m IVU21 40–150 keV	Center for X-rays in Swedish Materials Science (CeXS) DESY
Multi-purpose triple-axis diffractometer	CeXS DESY
Small-angle scattering	CeXS DESY
Grain mapper	CeXS DESY
P22 Hard X-ray Photoelectron Spectroscopy 2 m U33 2.4–15 keV	DESY
R Hard X-ray photoelectron spectrometer (HAXPES)	DESY
Ambient pressure XPS (POLARIS)	DESY collaborators
Hard X-ray photoemission electron microscope (HAXPEEM)	DESY collaborators
R Hard X-Ray momentum microscope (HarMoMic)	DESY
P23 <i>In situ</i> Nano-Diffraction Beamline 2 m U32 5–35 keV	DESY
XRD and secondary processes, <i>in situ</i> and complex environments	DESY
Hierarchical X-ray imaging	KIT DESY
P24 Chemical Crystallography 2 m U29 8 keV, 15–44 keV	DESY
Single crystal diffraction in complex sample environments	DESY
Small molecule crystallography	DESY
P25 Beamline for applied bio-medical imaging, powder diffraction and innovation 2m U32 8–60 keV	DESY
Start of operation planned for 2024	
X-ray fluorescence imaging (milliprobe) (XFI)	DESY
Scanning X-ray microscopy (SAXRM)	DESY
High throughput powder diffraction (15–35 keV)	DESY
PETRA IV test station (white beam)	DESY

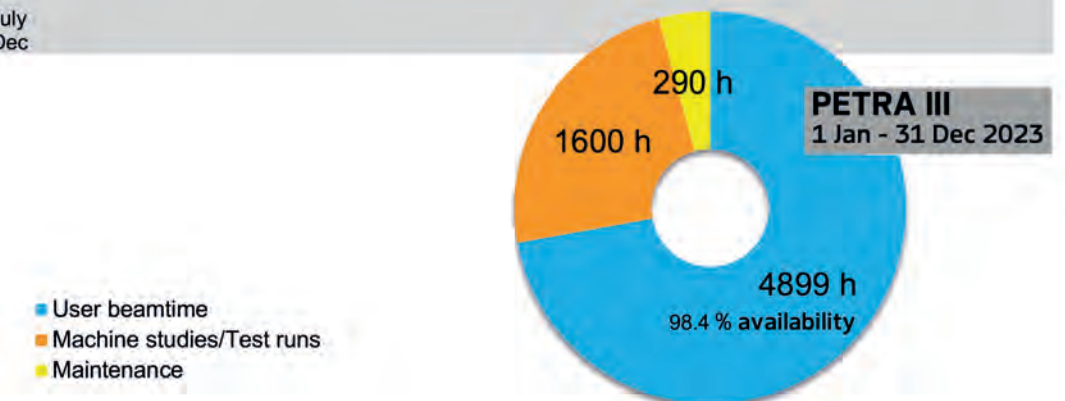
PETRA III experimental hall 'Paul P. Ewald'

Beamline and instruments	Operated by
R — option for remote user operation M — option for mail-in service	
P61 High Energy Wiggler Beamline 10 × 4 m damping wigglers white beam btw. 30–250 keV	DESY
High energy engineering materials science	Hereon
Large volume press — extreme conditions	DESY
P62 Anomalous Small-Angle X-ray Scattering 2 m U32 3.5–35 keV	DESY
Anomalous small-angle X-ray scattering	DESY
SAXS tomography	DESY
P63 Material Science Beamline	DESY MPI
Start of operation: not yet defined	
<i>Ex situ</i> and <i>in situ</i> XAFS with simultaneous scattering & diffraction	
P64 Advanced X-ray Absorption Spectroscopy 2 m U33 4–44 keV	DESY
<i>Ex situ</i> and <i>in-situ</i> XAFS	DESY
High-resolution X-ray emission spectroscopy (non-resonant and resonant)	DESY
QEXAFS	DESY
P65 Applied X-ray Absorption Spectroscopy 41 cm U33 4–44 keV	DESY
<i>Ex situ</i> and <i>in situ</i> XAFS of bulk samples	DESY
P66 Superlumi (between PETRA III halls 'Paul P. Ewald' and 'Max von Laue')	DESY
Bending magnet 4–40 eV	
Time-resolved luminescence spectroscopy	DESY

PETRA III beamtime statistics 2023

PETRA III Operation period 2023				
	User beamtime	Machine studies and test runs	Maintenance	Shutdown
1 Jan – 31 Dec	4899 h	1600 h	290 h	1971 h

run periods:
22 Feb – 17 July
10 Aug – 20 Dec



Instruments	Operated by
Sample preparation (CXNS, ground floor, laboratory 006a and 006b)	DESY
2 UHV sample preparation chambers	DESY
Low energy electron diffraction	DESY
Zn evaporation chamber	DESY
Auger electron spectroscopy	DESY
UHV multi flange tunnel chamber	DESY
Surface spectroscopy (CXNS, ground floor, laboratory 006a and 006b)	DESY
UHV Infrared reflection absorption spectroscopy (IRRAS)	DESY
X-ray photoelectron spectroscopy (XPS)	DESY
Ultraviolet photoelectron spectroscopy (UPS)	DESY
X-ray diffraction (building 25, laboratory 023)	DESY
UFO chamber, 2 mini reactors, 2 gas mixer	DESY
2 <i>in situ</i> UHV chambers	DESY
Reflectometer	DESY
2 six-circle diffractometers	DESY
Microscopy and nanomanipulation (CXNS, ground floor, laboratories 001-004, 006a PETRA III experimental hall 'Max von Laue', 47c, laboratory L096)	DESY
Scanning Auger microscope (SAM)	DESY
Dual-beam focused ion beam (FIB-SEM)	DESY Univ. Bayreuth
High-resolution scanning electron microscope (HR-SEM)	DESY
Versatile high-resolution atomic force microscope (AFM)	DESY
UHV scanning tunnelling / atomic force microscope (UHV-STM/AFM)	DESY
Optical polarisation microscope	DESY
Sputter coater	DESY
Physical and magnetic sample characterisation (CXNS, ground floor, laboratories 014 and 015)	DESY
Superconducting magnet	DESY
Sample cryostat	DESY
Vibrating sample magnetometer	DESY
AC Susceptibility	DESY
AC and DC resistivity and Hall effect	DESY
AC calorimetry	DESY
Thermal transport	DESY
Magnetic microscopy	DESY
Electrocatalysis and electrochemistry (building 25b, laboratory 027)	DESY
Rotating disc electrode surface X-ray diffraction setup	DESY
Combined infrared X-ray diffraction setup	DESY FAU Erlangen-Nürnberg
Hanging meniscus cell, flow cell	DESY
Langmuir trough	DESY CAU Kiel

Acknowledgement

We would like to acknowledge all contributions to the development and operation of FLASH and PETRA III beamlines and instruments provided within the framework of 'Verbundforschung/ErUM-Pro' of the Federal Ministry of Education and Research (BMBF), and as part of collaborations with the Department of Science and Technology (Government of India) 'India@DESY'.



DESY campus with the preaccelerators LINAC II, PIA and DESY II for the operation of the storage ring PETRA III, the FLASH FEL beamlines FLASH1 and FLASH2 as well as the first section of the linear accelerator of the European XFEL.

Committees 2023

Photon Science Committee PSC — advises the DESY Photon Science management

Christian David (Chair)	Paul Scherrer Institut, Villigen, CH
Stefan Eisebitt (Vice Chair)	MBI and Technische Universität Berlin, DE
Serena DeBeer	MPI-CEC, Mülheim an der Ruhr, DE
Kristina Djinovic-Carugo	Universität Wien, AT
Jan-Dierk Grunwaldt	Karlsruher Institut für Technologie, Karlsruhe, DE
Mark Heron	Diamond Light Source Ltd, Didcot, UK
Simo Huotari	University of Helsinki, FI
Oxana Klementieva	Lund University, SE
Sarah Köster	Georg-August-Universität Göttingen, DE
Michael Krisch	ESRF, Grenoble, F
Jan Lüning	Helmholtz-Zentrum Berlin, DE
Edvin Lundgren	Lund University, SE
Thomas Pfeifer	MPI for Nuclear Physics, Heidelberg, DE
Daniela Rupp	Eidgenössische Technische Hochschule Zürich, CH
Bernd Schmitt	Paul Scherrer Institut, Villigen, CH
Thomas Schröder	Humboldt-Universität zu Berlin and IKZ, Berlin, DE
Andrea Somogyi	Synchrotron SOLEIL, Saint-Aubin, FR
Stefan Vogt	Argonne National Laboratory, Lemont, US
Olga Vybornova, Hermann Franz (PSC Secretaries)	DESY, Hamburg, DE

Laser Advisory Committee LAC — advises DESY and European XFEL

Thomas Dekorsy (Chair)	Deutsches Zentrum für Luft- und Raumfahrt e.V., Stuttgart, DE
Jonathan Zuegel	Laboratory for Laser Energetics, Rochester, US
Miltcho Danailov	Elettra-Sincrotrone, Trieste, IT
Alan Fry	SLAC, Menlo Park, US
Catherine Le Blanc	Ecole Polytechnique, Laboratoire LULI, FR
Emma Springate	STFC Rutherford Appleton Laboratory, US
Clara Saraceno	Ruhr Uni Bochum, DE
Jörg Hallmann (LAC Secretary)	European XFEL, Schenefeld, DE
Karolin Baev (LAC Secretary)	DESY, Hamburg, DE

DESY Photon Science User Committee DPS-UC — represents the user community

Peter Müller-Buschbaum (Chair)	Technische Universität München, DE
Natalia Dubrovinskaia	Universität Bayreuth, DE
Hermann Duerr	Uppsala Universität, SE
Julia Herzen	Technische Universität München, DE
Gregor Witte	Ludwig-Maximilians-Universität München, DE

Komitee Forschung mit Synchrotronstrahlung KFS — representative body of the German SR and FEL user community (election in autumn 2023)

Christian Gutt (Chair)	Universität Siegen, DE
Birgit Kanngießer (Vice Chair)	Technische Universität Berlin, DE
Jan-Dierk Grunwaldt	Karlsruher Institut für Technologie, Karlsruhe, DE
Sarah Köster (until autumn 2023)	Georg-August-Universität Göttingen, DE
Dorota Kozej	Universität Hamburg, DE
Taisia Gorkhover	Universität Hamburg, DE
Christian Gutt	Universität Siegen, DE
Dirk Lützenkirchen-Hecht	Bergische Universität Wuppertal, DE
Martina Müller	Universität Konstanz, DE
Bridget Murphy	Christian-Albrechts-Universität zu Kiel, DE
Andrea Thorn	Universität Hamburg, DE
Max Wilke	Universität Potsdam, DE

The European Synchrotron and FEL User Organisation ESUO (Executive Board)

Cormac McGuinness (ESUO President)	Trinity College Dublin, IRL
Carla Bittencourt	Université de Mons, BE
Wojciech Gawelda	Universidad Autónoma de Madrid, ES
Tom P. Hase	University of Warwick, UK
Rainer Lechner	Montanuniversität Leoben, AT
Derek Logan	Lund University, SE
Bridget Murphy	Christian-Albrechts-Universität zu Kiel, DE
Moniek Tromp	Rijksuniversiteit Groningen, NL

For national delegates please see: www.esuo.eu/user-representation/user-delegates-representatives/

Project Review Panels 2023

Bulk and surface diffraction

P08 | P23 | P24

Wuge Briscoe	University of Bristol, UK
Jan Ingo Flege	Brandenburgische Tech. Univ. Cottbus-Senftenberg, DE
Michael Hanke	Paul-Drude-Institut für Festkörperelektronik, Berlin, DE
Richard Harvey	Universität Wien, AT
Fouad Maroun	Ecole Polytechnique Palaiseau, FR
Reinhard Neder	Friedrich-Alexander-Universität Erlangen-Nürnberg, DE
Oliver Oeckler	Universität Leipzig, DE
SoHyun Park	Ludwig-Maximilians-Universität München, DE
Sander van Smaalen	Universität Bayreuth, DE
Hans-Georg Steinrück	Universität Paderborn, DE
Chandan Upadhyay	Indian Institute of Technology, Varanasi, IN
Matthias Zschornak	Technische Universität, Bergakademie Freiberg, DE
Florian Bertram, Dimitri Novikov, Martin Tolkehn (PRP Secretaries)	DESY, Hamburg, DE

Coherent applications

P10

Giacomo Baldi	Università di Trento, IT
Sylvain Bohic	Research Centre INSERM, Grenoble, FR
Ralf Busch	Universität des Saarlandes, Saarbrücken, DE
Birgit Hankiewicz	Universität Hamburg, DE
Michael Paulus	Universität Dortmund, DE
Ullrich Pietsch	Universität Siegen, DE
Barbara Ruzicka	Institute for Complex Systems, Roma, IT
Dina Sheyfer	Argonne National Laboratory, Lemont, US
Olivier Thomas	Aix-Marseille Université, Marseille, FR
Michael Sprung (PRP Secretary)	DESY, Hamburg, DE

EXAFS

P64 | P65

Dmitry Doronkin	Karlsruher Institut für Technologie, Karlsruhe, DE
Stephan Klemme	Westfälische Wilhelms-Universität, Münster, DE
Dorota Kozej	Universität Hamburg, DE
Aleksej Kuzmin	University of Latvia, Riga, LV
Katherine Mazzi	Helmholtz-Zentrum Berlin, Berlin, DE
Dooshaye Moonshiram	Materials Science Institute of Madrid, ES
Christina Roth	Universität Bayreuth, DE
Karel Saks	Slovak Academy of Sciences, Kosice, SK
Claudia Schnorr	Universität Leipzig, DE
Roland Schoch	Universität Paderborn, DE
Kajsa Sigfridsson Clauss	MAX IV Laboratory, Lund, SE
Case van Genuchten	Geological Survey of Denmark and Greenland, København, DK
Andrea Zitolo	Synchrotron SOLEIL, Gif-sur-Yvette, FR
Wolfgang Caliebe, Edmund Welter (PRP Secretaries)	DESY, Hamburg, DE

Extreme conditions

P02.2 | P61 LVP

Eglantine Boulard	Sorbonne Université, Paris, FR
Martin Bremholm	Aarhus University, DK
Lars Ehm	Stony Brook University, Stony Brook, US
Holger Kohlmann	Universität Leipzig, DE
Sergey Lobanov	Helmholtz-Zentrum Potsdam, GFZ, Potsdam, DE
Paolo Lotti	Università degli Studi di Milano Statale, Milano, IT
Sergey Medvedev	MPI für Chemische Physik fester Stoffe, Dresden, DE
Hauke Marquardt	University of Oxford, UK
Bjoern Winkler	Goethe-Universität Frankfurt am Main, DE
Tony Withers	Universität Bayreuth, DE
Hanns-Peter Liermann, Robert Farla (PRP Secretaries)	DESY, Hamburg, DE

HAXPES

P22

Felix Gunkel	Forschungszentrum Jülich GmbH, Jülich, DE
Maria Hahlin	Uppsala Universität, Uppsala, SE
Martina Müller	Universität Konstanz, DE
Christian Papp	Friedrich-Alexander-Universität Erlangen-Nürnberg, DE
Christoph Rameshan	Montanuniversität Leoben, AT
Anna Regoutz	University College London, GB
Michael Sing	Universität Würzburg, DE
Vladimir N. Strocov	Paul Scherrer Institut, Villigen, CH
Christoph Schlüter (PRP Secretary)	DESY, Hamburg, DE

Project Review Panels 2023

High energy diffraction P07 (DESY) | P21.1 | P21.2

Frauke Alves William Brant Olaf Borkiewicz Peter Broekmann Per-Anders Carlsson Magnus Colliander Margit Fabian Jens Gibmeier Julia Herzen Nina Lock Matt Miller Tobias Ritschel Larissa Veiga Joachim Wollschläger Ann-Christin Dippel, Martin von Zimmermann, Ulrich Lienert (PRP Secretaries)	Georg-August-Universität, Göttingen, DE Uppsala Universitet, SE Argonne National Laboratory, Lemont, US Universität Bern, CH Chalmers Tekniska Högskola, Gothenborg, SE Chalmers Tekniska Högskola, Gothenborg, SE Centre for Energy Research, MTA, Budapest, HU Karlsruher Institut für Technologie, Karlsruhe, DE Technische Universität München, Garching, DE Aarhus Universitet, Aarhus, DK Cornell University, Ithaca, US Technische Universität Dresden, DE Diamond Light Source, Didcot, UK Universität Osnabrück, DE DESY, Hamburg, DE
--	--

Imaging P05 | P06

Matthias Alfeld Martin Bech Ulrike Boesenberg Asuncion Carmona Fabien Chauveau David Fenning Frank Friedrich Sebastian Kalbfleisch Andrew Kiss Florian Meier Bert Mueller Guillermo Requena Roberto Terzano Jürgen Thieme Katarina Vogel-Mikus Ulrich Vogt Benjamin Wipfler Fabian Wilde; Gerald Falkenberg (PRP Secretaries)	Delft University of Technology, NL Lund University, SE European XFEL, Schenefeld, DE Centre d'Etudes Nucléaires de Bordeaux Gradignan, FR Lyon Neuroscience Research Center, Bron, FR University of California, San Diego, US Universität Hamburg, DE MAX IV Laboratory, Lund, SE Brookhaven National Laboratory, Upton, US University of Utrecht, NL Universität Basel, Allschwil, CH Rheinisch-Westfälische Technische Hochschule (RWTH) Aachen, DE Università degli studi di Bari, IT Brookhaven National Laboratory, Upton, US University of Ljubljana, SI Royal Institute of Technology, Stockholm, SE Zool. Forschungsmuseum Alexander Koenig, Bonn, DE Helmholtz-Zentrum Hereon, Geesthacht; DESY, Hamburg, DE
--	--

Inelastic, magnetic and resonant scattering P01 | P09

Manuel Angst Elizabeth Blackburn Kristina Kvashnina Catherine McCammon Daniel Merkel Matteo Minola Volker Schünemann Joachim von Zanthier Jonathan White Ilya Sergeev, Sonia Francoual (PRP Secretaries)	Forschungszentrum Jülich GmbH, DE Lund University, SE Helmholtz-Zentrum Dresden-Rossendorf (HZDR), DE Universität Bayreuth, DE Wigner Research Centre for Physics, Budapest, HU Max Planck Institute for Solid State Research, Stuttgart, DE Technische Universität Kaiserslautern, DE Friedrich-Alexander-Universität Erlangen-Nürnberg, DE Paul Scherrer Institut, Villigen, CH DESY, Hamburg, DE
---	--

Materials science (Hereon) P07 (Hereon) | P61 (Hereon)

Jeremy Epp Guillaume Geandier Astrid Haibel Julia Herzen Christian Krempaszky Ingo Manke Thomas Niendorf Wolfgang Pantleon Walter Reimers Georg Schulz Carsten Siemers Dieter Lott (PRP Secretary)	Leibniz-IWT, Bremen, DE Institut Jean Lamour, Nancy, FR Beuth Hochschule für Technik, Berlin, DE Technische Universität München, DE Technische Universität München, DE Helmholtz Zentrum Berlin für Materialien und Energie, Berlin, DE Universität Kassel, DE Technical University of Denmark, Lyngby, DK Technische Universität Berlin, DE Universität Basel, CH Technische Universität Braunschweig, DE Helmholtz-Zentrum Hereon, Geesthacht, DE
---	--

Powder diffraction P02.1

Dorthe Bomholdt Ravnsbæk Bernd Hinrichsen Gregor Kieslich Michael Knapp Daria Mikhailova Martin Sahlberg Anatoliy Senyshyn Florian Spieckermann Claudia Weidenthaler Mirijam Zobel Martin Etter (PRP Secretary)	Aarhus Universitet, Aarhus, DK BASF SE, Ludwigshafen, DE Technische Universität München, Garching, DE Karlsruher Institut für Technologie, Karlsruhe, DE Leibniz-Institut f. Festkörper- und Werkstoffforschung Dresden, DE Uppsala Universitet, Uppsala, SE Technische Universität München, Garching, DE Montanuniversität Leoben, AT MPI fuer Kohlenforschung, Mülheim a.d. Ruhr, DE Rheinisch-Westfälische Technische Hochschule (RWTH) Aachen, DE DESY, Hamburg, DE
---	---

SAXS/WAXS/GISAXS P03 | P62

Jens Wenzel Andreasen Sabrina Disch Eva Herzig Rainer T. Lechner Eva Malmstroem Peter Šiffalovič Qi Zhong Sarathlal Koyiloth Vayalil, Sylvio Haas (PRP Secretaries)	Danmarks Tekniske Universit, Roskilde, DK Universität Duisburg-Essen, DE Universität Bayreuth, DE Montanuniversität Leoben, AT KTH Royal Institute of Technology, Stockholm, SE Institute of Physics, Bratislava, SK Zhejiang Sci-Tech University, Hangzhou, CN DESY, Hamburg, DE
---	--

Soft X-ray and VUV P04 | P66

Yves Acremann Paola Bolognesi Arno Ehresmann Mark Golden Aleksandr Luštšik Jan-Erik Rubensson Yasmine Sassa Emma Sokell Anna Vedda Moritz Hoesch, Aleksei Kotlov (PRP secretaries)	ETH Zürich, CH CNR-ISM, Istituto di Struttura della Materia, Roma, IT Universität Kassel, DE Universiteit van Amsterdam, NL University of Tartu, EE Uppsala Universitet, SE Chalmers Tekniska Högskola, Gothenborg, SE University College Dublin, IE Università di Milano-Bicocca, Milano, IT DESY, Hamburg, DE
---	--

Soft X-ray FEL experiments FLASH

Majed Chergui Hermann Dürr Irene Groot Marion Harmand Michael Meyer Christian Schüssler-Langeheine Marc Simon Julia Stähler Elke Plönjes-Palm, Rolf Treusch (PRP Secretaries)	École Polytechnique Fédérale de Lausanne, CH Uppsala Universitet, Uppsala, SE Universiteit Leiden, NL Sorbonne Université, Paris, FR European XFEL, Schenefeld, DE Helmholtz-Zentrum Berlin, DE Sorbonne Université, Paris, FR Humboldt-Universität zu Berlin, DE DESY, Hamburg, DE
---	---

PEC: EMBL Life Science beamlines P12-P14 / PRP Bio-crystallography at P11

Savvas Savvides Pau Bernadó Gwyndaf Evans Robert Fischetti Mariusz Jaskolski Gergely Katona Annette E. Langkilde Javier Pérez Teresa Santos-Silva Zehra Sayers Joel L. Sussman Maria A. Vanoni Mark J. van Raaij Gregor Witte Christian Schroer (DESY observer)	Ghent University CBS/CNRS, Montpellier, FR Diamond Light Source, Didcot, GB Argonne National Laboratory, US Adam Mickiewicz University of Poznan, PL University of Gothenburg, SE University of Copenhagen, DK Synchrotron SOLEIL, Saint-Aubin, FR Universidade NOVA de Lisboa, PT Sabanci University, Istanbul, TR Weizmann Institute of Sciences, Rehovot, IL Università degli Studi di Milano, IT Centro Nacional de Biotecnología, Madrid, ES Ludwig-Maximilians-Universität München, DE DESY, Hamburg, DE
---	--

Photographs and Graphics

Axel Heimken, Kiel
Britta Liebaug, DESY
CFEL
Christian-Albrechts-Universität zu Kiel
CMWS
Cristina Lopez-Gonzalez, DESY
CSSB
DASHH
DESY
Diana von Ilsemann, DESY
DPG / Lösel
EMBL

Esmerando Escoto, DESY
European XFEL
Florian Grüner, Univ. Hamburg
Georg Wendt, DESY
Gesine Born / DESY
HALRIC
Heiner Müller-Elsner, Hamburg
Helmholtz-Zentrum Hereon
HPP Architekten, Hamburg
Irmgard Flick, Univ. Hamburg
Jörg Harms, MPSD
Joseph Piergrossi, DESY

Ludger Inhester, DESY
Marta Mayer, DESY
Matthias Piplak
Miaoqi Chu / Jin Wang, APS Argonne
MPG
PIER, Hamburg
Reimo Schaaf, Hamburg
Tina Mavric, CSSB
UNIPRENEURS, Berlin
Universität Hamburg

Acknowledgement

We would like to thank all authors and all who have contributed to the realisation of this Annual Report

Imprint

Publishing and Contact:

Deutsches Elektronen-Synchrotron DESY
A Research Centre of the Helmholtz Association

Hamburg location:

Notkestr. 85, 22607 Hamburg, Germany
Tel.: +49 40 8998-0, Fax: +49 40 8998-3282
desyinfo@desy.de

Zeuthen location:

Platanenallee 6, 15738 Zeuthen, Germany
Tel.: +49 33762 7-70, Fax: +49 33762 7-7413

Photon Science at DESY

Tel.: +49 40 8998-2304, Fax: +49 40 8998-4475
photon-science@desy.de
photon-science.desy.de

www.desy.de

ISBN 978-3-945931-49-3
DOI 10.3204/PUBDB-2023-07365

Online version:

photon-science.desy.de/annual_report



Realisation:

Wiebke Laasch, Daniela Unger

Editing:

Sadia Bari, Krishnayan Basuroy, Lars Bocklage, Christina Bömer, Günter Brenner, Ulrike Frühling, Thomas Keller, Dmytro Kutnyakhov, Wiebke Laasch, Britta Niemann, Christoph Schlüter, Markus Scholz, Sang-Kil Son, Sebastian Trippel, Daniela Unger, Olga Vybornova

Layout: Sabine Kuhls-Dawideit, Büro für Grafik und Design, Halstenbek

Printing and image processing: EHS Druck GmbH, Schenefeld

Copy deadline: December 2023

Reproduction including extracts is permitted subject to crediting the source.

HELMHOLTZ

Deutsches Elektronen-Synchrotron DESY
A Research Centre of the Helmholtz Association

Helmholtz contributes to solving major challenges facing society, science and the economy through top-level scientific achievements in six research fields: Energy, Earth and Environment, Health, Information, Matter as well as Aeronautics, Space and Transport. With about 45 000 employees at 18 research centres and an annual budget of more than 5 billion euros, Helmholtz is Germany's largest scientific organisation. Its work is rooted in the tradition of the great natural scientist Hermann von Helmholtz (1821-1894).

www.helmholtz.de